HIGH EFFICIENCY RCCI COMBUSTION

By

Derek A. Splitter

A dissertation submitted in partial fulfillment
of the requirements for the degree of

Doctor of Philosophy
(Mechanical Engineering)

at the
University of Wisconsin – Madison

2012

Date of Final Oral Examination: Sept 24, 2012

The dissertation is approved by the members of the Final Oral Committee:
Rolf Reitz, Professor, Mechanical Engineering
Jaal Ghandhi, Professor, Mechanical Engineering
David Foster, Professor, Mechanical Engineering
David Rothamer, Assistant Professor, Mechanical Engineering
James Schauer, Professor, Civil and Environmental Engineering

Abstract

An experimental investigation of the pragmatic limits of Reactivity Controlled Compression Ignition (RCCI) engine efficiency was performed. The study utilized engine experiments combined with zero-dimensional modeling. Initially, simulations were used to suggest conditions of high engine efficiency with RCCI. Preliminary simulations suggested that high efficiency could be obtained by using a very dilute charge with a high compression ratio. Moreover, the preliminary simulations further suggested that with simultaneous 50 % reductions in heat transfer and incomplete combustion, 60% gross thermal efficiency may be achievable with RCCI.

Following the initial simulations, experiments to investigate the combustion process, fuel effects, and methods to reduce heat transfer and incomplete combustion reduction were conducted. The results demonstrated that the engine cycle and combustion process are linked, and if high efficiency is to be had, then the combustion event must be tailored to the initial cycle conditions. It was found that reductions to engine heat transfer are a key enabler to increasing engine efficiency. In addition, it was found that the piston oil jet gallery cooling in RCCI may be unnecessary, as it had a negative impact on efficiency. Without piston oil gallery cooling, it was found that RCCI was nearly adiabatic, achieving 95% of the theoretical maximum cycle efficiency (air standard Otto cycle efficiency).

Acknowledgements

This research would not have been possible without the support and guidance of many individuals. Foremost I would like to thank Professor Rolf Reitz for extending the opportunity to work in his laboratory as his student.

Within the Engine Research Center there are several other individuals who have also been responsible for the success of this research. In particular the fellow graduate students and staff at the ERC have been instrumental in conducting and understanding of this research and general laboratory procedures. I would also like to thank the Department of Energy and Sandia National Lab for funding this research and Caterpillar for supply of specialty parts and support of the SCOTE laboratory at ERC.

Most of all I would like to thank my wife Jessica for her guidance and support both in my research and life, and our sons Max and Jack. They are my sources of motivation.

Table of Contents

Abstract ..... **i**

Acknowledgements ..... **ii**

Table of Contents ..... **iii**

Chapter 1 Introduction **1**

1.1 Background 1

1.2 Research Objectives 2

1.3 Research Method and Tools 3

Chapter 2 Literature Review **4**

2.1 Conventional Diesel Emissions Dilemma 4

2.2 Low Temperature Combustion (LTC) 7

2.2.1 Homogeneous Charge Compression Ignition (HCCI) 7

2.2.2 HCCI Research on Control Through Stratification and Fuels 8

2.3 Chemical Kinetics 12

2.3.1 General Effects of Pressure, Temperature, and Fuel Properties on Combustion Kinetics 12

2.3.2 Cylinder Gas Composition Effects 25

2.3.2.1 EGR Influence on Cycle Thermodynamics 25

2.3.2.2 EGR Influence on Fuel Kinetics 27

2.3.3 Kinetic Literature Review Conclusions 32

2.4 Cetane Improvers 32

2.5 Engine Energy and Exergy Flows. Where are the Losses? 37
2.6 Availability Destruction with LTC 37
2.6.1 Availability Flow with Low Heat Rejection 40
2.6.2 Availability Flow with Nontraditional Engine Strategies 42
2.7 Low Heat Rejection Strategies 43
2.7.1 Engine Coolant Temperature Strategies 43
2.7.2 Thermal Barrier Coatings 45
2.7.3 Piston Oil Gallery Spray Cooling Modulation 48
2.8 Knock Effects on Heat Transfer 51
2.9 Literature Review Conclusions 54
CHAPTER 3 Modeling Details 55
3.1 Zero Dimensional Engine Modeling for High Efficiency 56
3.2 Air Handling in Dilute Combustion Strategies 59
3.3 Application to RCCI 61
3.4 Preliminary Computational Study Results 64
Chapter 4 Experimental Details 70
4.1 Engine 70
4.2 Pistons 71
4.3 Fueling strategy 73
4.4 Fuel Properties 74
4.5 Injection Systems 75
4.5.1 Low-Reactivity Fuel System Hardware and Plumbing 76

4.5.2 High Pressure Injection Hardware and Plumbing....79
4.6 Engine Out Emissions....83
4.7 Data Acquisition and Processing....85
4.8 Determining Losses and Efficiencies....87
4.8.1 Determining Efficiencies....87
4.8.2 Determining Losses....90
4.8.3 Determining Uncertainties....93
Chapter 5 Results....98
5.1 Addressing Incomplete Combustion in RCCI....99
5.1.1 Hydrocarbon Sources and Solutions....99
5.1.2 Sources and Solutions to CO in RCCI....102
5.2 Effects of Engine Operating Conditions on Engine Efficiency....112
5.2.1 Fuel Effects on RCCI....113
5.2.2 3% EHN Gasoline Behavior in Mixing Controlled Combustion....115
5.2.3 RCCI with 3% EHN Gasoline....119
5.2.4 Operable Limits of E85 Fuels....122
5.2.5 Comparisons of Constant Φ, Temperature, and PPRR in Φ-T Space....124
5.2.5.1 Constant Φ Sweeping Intake Temperature....125
5.2.5.2 Constant Temperature Sweeping Φ....130
5.2.5.3 Constant PPRR by Simultaneously Sweeping Φ and Temperature....134
5.2.6 Fuel Composition Effects on Reactivity....138
5.2.7 Gas Composition Effects on Reactivity....142
5.2.8 Gas Composition Effects on Φ-T Matrix Results....144

5.3 Charge Preparation Effects 151
5.4 High Compression Ratio, and Efficiency Experiments 162
5.4.1 RCCI Piston Temperatures 162
5.4.2 High Cr RCCI with and Without Piston Oil Gallery Cooling 166
5.4.2.1 Piston Oil Gallery Cooling Emissions Analysis 168
5.4.2.2 Piston Oil Gallery Cooling Efficiency Analysis 173
5.4.2.2.1 Efficiency with 0% EGR 173
5.4.2.2.2 Efficiency with 40% EGR 176
5.4.3 PPRR Effects with Piston Oil Gallery Cooling Modulation 179
5.4.4 Overall GTE Trends With Piston Oil Gallery Cooling Modulation 181
5.4.4.1 Lean Limit Extension and Efficiency Effects 183
5.4.5 Volumetric Efficiency Effects of Piston Oil Gallery Cooling Modulation 186
5.4.6 Minimization of Losses for Maximum Efficiency 191
CHAPTER 6 Discussion, Maximum Cycle Efficiency Limits 194
6.1 Simulation Results and Model Validation with Experiments 195
6.2 Simulation with Adiabatic and 100% Combustion Efficiency Operation .. 199
6.3 Cylinder Gas Composition Effects on Efficiency 203
6.4 Combustion Duration Effects on Efficiency 208
6.4 Turbocharger Effects on Efficiencies 210
CHAPTER 7 Conclusions and Suggestions for Future Research 213
7.1 Study Findings and Conclusions 213
7.2 Suggestions for Future Research 215

References 217

Appendix A, Data 231

Φ-T Matrix Conditions 231

Oil Matrix Conditions 249

Appendix B - Impingement 261

A.B.1 GTE and Losses of Tested E85 Fuels 261

A.B.2 Effects of Volatility for Direct Injected Fuel 264

Appendix C – Combustion Phasing Effects 271

A.C.1 GTE and Losses of Tested E85 Fuels 271

Appendix D – Codes 277

A.D.1 AFR Calculation 277

A.D.2 AFR, GTE, and Efficiency Uncertainty Calculation 281

Appendix F – Fuel Properties 286

A.E.1 Fuel Lubricity Additive 286

A.E.2 Gasoline Fuel Properties 287

A.E.3 ULSD Fuel Properties 288

A.E.4 Ethanol Fuel Properties 289

List of Figures

Figure 1 The three distinct regimes of ignition delay. Note that regime 2 is opposite of regimes 1 and 3, which are positively affected by temperature. Figure adopted from Vandersickel et al. [41], top axis (T (K)) added for clarity.....13

Figure 2 Ignition delay times of n-heptane/air mixtures for different equivalence ratios at 50 bar. [42] Note that when the mixtures are very lean NTC behavior is not observed, where at richer mixtures NTC is observed. The grey symbols depict the pre-ignition delay times.....14

Figure 3 Simulation results of 1.9L engine operation at 2300 rev/min 0% EGR, 1.58 bar IVC pressure and 81°C IVC temperature, DI -60°CA ATDC, global PRF number of 88. The results demonstrate the effects of Φ only stratification (top) Φ+reactivity stratification (bottom), where reactivity plus Φ stratification spread the combustion event significantly more, as chemical dependency (reactivity) is added to the charge. Figure reproduced from Kokjohn and Reitz [47].....16

Figure 4 Effect of pressure on n-heptane fuel kinetics at representative CI engine conditions. Note that as pressure increases ignition delay decreases significantly, as the vertical axis is plotted on a log scale. Figure reproduced form Vandersickel et al. [41].....17

Figure 5 Shock tube data of n-heptane isooctane mixtures with ethanol (PRF 82 base with 20% ethanol added) [48].....18

Figure 6 Ignition delay of n-heptane and kerosene surrogates at CI engine-like conditions. Note that the higher pressure conditions (right) exhibit decreased ignition delay. Of interest is that the lighter fuel (Fuel B) has over a 50% cycloalkanes content, demonstrating that chemical composition has a marked interaction on ignition delay pressure dependency. Figure reproduced from [41]. 19

Figure 7 Intermediate temperature heat release behavior of gasoline (right) and neat ethanol (left) at matched conditions while sweeping intake pressure. Note that neat ethanol expresses no pressure dependency, while gasoline exhibits increased ITHR with pressure. Figures reproduced from Sjöberg and Dec [51] (left) and Dec et al. [21] (right). 20

Figure 8 HCCI Intermediate temperature heat resale behavior of pump gasoline at various initial conditions. Engine is simulated to be an identical match of Dec [21] with a compression ratio of14:1, at 1200 rev/min. The results show that reduced intake temperature and increased boost increase the reactivity of pump gasoline to be more like diesel fuel. Figure reproduced from [52]. 21

Figure 9 Three-dimensional surface of ignition delay of stoichiometric iso-octane and air. Figure reproduced from [53]. 22

Figure 10 Stoichiometric ignition delays for different fuel molecules. Note that for all but aromatics and oxygenated fuel, intermediate temperature dependency exists, but at varying degrees. Figure reproduced from [53] 23

Figure 11 Effects of different diluent strategies on the ratio of specific heats (γ). Figure reproduced from Lavoie et al [58], where gas properties were evaluated as noted. 26

Figure 12 Effects of charge dilution on Ignition delay. (b) effect of equivalence ratio (air dilution) on ignition delay. (c) effect of EGR on ignition delay. EGR increases ignition delay more than air dilution (even in the presence of 30% EGR). Open markers denote first stage ignition delay, figure reproduced from Vandersickel et al. [41] 28

Figure 13 High temperature gasoline shock tube experiments with and without EGR. The findings demonstrate that EGR suppress ignition delay of high temperature gasoline kinetics. Figure reproduced from Gauthier et al. [62] 30

Figure 14 Gasoline and surrogate gasoline HCCI ignition delay as a function of equivalence ratio with varied EGR. In general as EGR or leaner conditions are encountered the crank angle of HTHR is phased later, and in the leanest operating conditions, only LTHR is observed. Figure reproduced form Machrafi and Cavadias [63] 31

Figure 15 Cetane improver effectiveness in #2 diesel fuel as a function of volume addition. Figure reproduced from [69] 35

Figure 16 Simulated ignition delay times of EHN doped n-heptane as a function of EHN concentration. Figure reproduced from Hartman et al [70]. 36

Figure 17 Combustion availability destruction as a function of equivalence ratio, and corresponding temperature, reproduced from [72] 38

Figure 18 Fuel availability flow for standard and LHR engines. Note the shift in availability to the exhaust and increased work with the LHR design, reproduced from [74]. 40

Figure 19 Distribution of fuel availability for the Otto cycle with stoichiometric propane. Note the increase in work relative to losses as compression ratio is increased, reproduced from [82] 43

Figure 20 MEP values for CDC operation at low load (Operating Point 1) and higher load (Operating Point 2). Coolant temperature was swept, and observed MEP trends are shown. It was found that reduced coolant temps. may actually increase engine efficiency, as it simultaneously reduced EGR temps.. Figure adopted from Burke and Brace [85]. 44

Figure 21 Various Piston cooling strategies and the relative distribution of heat loss associated with each. Figure adopted from [97]. 49

Figure 22 Transient piston surface temperature-time response to eliminating piston oil gallery cooling at a mid-load and speed LD CDC engine. Figure reproduced from Luff et al. [98] 50

Figure 23 Transient cylinder liner surface temperature-time response to eliminating piston oil gallery cooling at a mid-load and speed LD CDC engine, cooling turned off at time of 900 (s). Figure reproduced from Luff et al. [98] 50

Figure 24 Peak heat flux as a function of knock intensity for stoichiometric SI combustion. Figure from Grandin et al. [103]. 53

Figure 25 Figure reproduced from Caton [107] where zero-dimensional simulation work was conducted to determine pathways for increased engine efficiency; base condition is a simulated SI engine with 8:1 Cr, 0.71 L/cyl, 9 bar BMEP 2000 rev/min. Note that the largest gains were offered through increased compression ratio, and dilute operation. 56

Figure 26 Lean operation is observed to have a significant effect on gross efficiency, with very lean operation negatively effecting brake efficiency through increased pumping work. Figure reproduced from Lavoie et al. [58]. 57

Figure 27 Curve of optimal brake efficiency for 50% combined turbocharger operation. Note that higher loads require charge enrichment and tend to deviate from LTC operation to conventional combustion strategies. The richer operation is required to mitigate increases in pumping losses associated with LTC strategies at high engine loads. Figure reproduced from Lavoie et al. [58]. 58

Figure 28 Zero-dimensional cycle simulations from Mamalis et al. [108]. The findings show that the higher IMEPn (right) associated with supercharging is more than offset by additional FMEP, resulting in reduced BMEP and thus efficiency. Figure reproduced from [108].....60

Figure 29 Relative effect of “perfect” boosting on gross and brake efficiencies. Note that “perfect” boosting has a greater effect on brake than gross efficiencies, as it affects both the pumping and heat transfer losses in brake, and only heat transfer in gross. Figure reproduced from Lavoie et al. [58].....61

Figure 30 Generalization of performance and trends required to achieve DOE goal of +50% BTE. Assumptions: No waste heat recovery PMEP=0.4, FMEP=1.0, GIE=54.5 (constant over sweep). Note, GIE is equivalent terminology to GTE 63

Figure 31 Comparison of GT Power simulations (red) and experimental results (black) at 9 bar IMEPg high efficiency conditions. The results show that a convection coefficient of 0.4 in the simulations produces a close match on the compression and expansion pressures (default convection coefficient is 1.5, 0 is adiabatic). 66

Figure 32 GTPower RCCI simulations of high compression ratio operation (18.6:1). Note that the simulations assume the same heat release profile as lower compression ratio experimental operation (black). At the simulated conditions (right) an increase in trapped mass, and a simultaneous 50% reduction in heat transfer and incomplete combustion suggested that 60% GTE and 50% BTE may be possible.....68

Figure 33 Diagram of the engine lab 71

Figure 34 Cross sectional view of the stock CDC 16.1:1 Cr (black), 14.88:1Cr optimized RCCI bathtub (green), and 18.7:1 Cr pancake (blue) pistons. The grey line atop the pistons represents the cylinder fire deck at TDC spacing. Note the undercutting of the top ringland in the 14.88 and 18.7 Cr pistons relative to the stock piston. 72

Figure 35 Experimental fuel injection locations and strategy 73

Figure 36 low pressure fuel system, diagram courtesy of DelVescovo [117] 77

Figure 37 installed port injector in intake elbow 78

Figure 38 Common rail fuel delivery system diagram courtesy of DelVescovo [117] 80

Figure 39 Common rail adaptor insert assembly for use with HEUI 315 inserts . 81

Figure 40 Bosch Common rail injector installed into HEUI 315B head with custom insert (purple) and clamps (orange and green) 82

Figure 41 GTE as calculated from different AFR and direct mass based measurements. Note that AFR_{LAMBDA} measurements are consistently low and have the highest uncertainty. 95

Figure 42 Flow Chart of Results Section for operation towards high efficiency .. 98

Figure 43 Engine out HC emission sources in SI combustion. Note that engine crevices are observed to be the major contribution factor. An equally significant contribution was found in the combination of oil and fuel films. Data from Alkidis [130] 99

Figure 44 RCCI Φ-T test matrix, at constant combustion phasing and load. Thus Φ is analogous to constant IVC density (charge mass), obtained by sweeping pressure at constant density with several IVC temperatures. 104

Figure 45 Contours of CO at fixed combustion timing and load. The engine was fueled with ULSD and E85 at a 8.45 bar IMEPn condition 1300 rev/min. The trends show that the highest CO emissions are generated at the leanest conditions with the lowest premixed fuel fractions. This suggests that overly lean areas (premixed) significantly contribute to RCCI CO emissions. 106

Figure 46 Contours of RCCI CO with EGR at fixed combustion timing and load, Φ/Φ′ based analysis left, and intake pressure analysis right. The engine was fueled with ULSD and 91 PON gasoline at a 8.45 bar $IMEP_n$ condition 1300 rev/min. The trends show that CO occurs at both globally lean and near-rich conditions with the lowest premixed fuel fractions. This suggests that locally lean or rich areas (possible with EGR operation) can both contribute to RCCI CO emissions. 108

Figure 47 CO emissions associated with sweeping intake temperature at constant phasing and load, see Table 19, with the single injection strategy at -50°CA ATDC injection timing. Note that as the premixed fuel equivalence ratio increases, CO losses decrease. When the premixed fuel mixture is richer than the lean limit, a sharp reduction in CO is observed. Figure reproduced from Splitter et al. [38] 110

Figure 48 Apparent heat release rates of the PRF/Temperature sweep at constant load and phasing. Note that the long tail observed in the heat release of PRF values below 69, indicate poor combustion, with higher CO levels as seen in Figure 47. Cases without tails demonstrate good combustion efficiency. Figure reproduced from Splitter et al. [38]. 111

Figure 49 Sweep of combustion phasing to determine the location of highest efficiencies. The engine was operated lean at Φ=0.29 and 1300 rev/min speed ~9 bar IMEPg. Engine efficiency defined as gross, net, and brake, as calculated using Equations 10, 11, and 21 in Chapter 4. 114

Figure 50 #2 ULSD mixing controlled operation (black) and EHN gasoline mixing controlled operation (dashed red). Blue traces show injection current, where a pilot and main injection strategy was used (see Table 22). Single injections

resulted in high premixed burn fractions as EHN gasoline was found to have lower cetane number than ULSD. 117

Figure 51 Key emissions and performance metrics of ULSD and 3% EHN in 91 PON gasoline as a function of rail pressure. 118

Figure 52 RCCI heat release at matched conditions in Φ-T space (matrix point #20) with 3% EHN gasoline and ULSD DI and E85 PFI fueling. Operation with EHN gasoline demonstrates reduced reactivity stratification as the onset of HTHR is more abrupt, and the peak heat release rate is higher. 120

Figure 53 Pressure and Heat release behavior at matched Φ-T conditions (matrix point #28) for ULSD/E85 (red) and EHN Gas/E85 (dashed red). Also plotted for reference is the AHRR of matched fueling ratios for EHN gas/E85 (dashed red) and ULSD/E85 (blue, matrix point #20). The results demonstrate that at matched Φ-T conditions of fuel delivery ratios. EHN gasoline displays a reduced reactivity gradient as compared to ULSD/E85, with matched fueling ratios exhibiting a larger difference. 122

Figure 54 Operable space of Φ-T matrix with the tested E85 based fuels. Note that the larger reactivity gradient of ULSD/E85 offers a larger operable window than the reduced reactivity gradient of EHN gasoline/E85. 124

Figure 55 AFR_c based GTE contours and associated AHRR for fixed Φ, varied T operation. 126

Figure 56 Losses associated with sweeping intake temperature at constant Φ, the operating conditions are in Table 16 with the Φ-T matrix data in marked for reference in Appendix A. The dashed lines with open markers denote richer operation at Φ=0.31 demonstrating a tradeoff in reduced combustion efficiency for increased HX+EXH losses 128

Figure 57 Incomplete combustion species at constant Φ conditions, the operating conditions are in Table 16 with the Φ-T matrix data in marked for reference in Appendix A, Table A. 2. Note that CO is the dominant emission for all but the highest temperatures, with richer operation exhibiting lower CO. 129

Figure 58 AFR_c based GTE contours and associated AHRR for constant T varied Φ operation. The operating conditions are in Table 16 with the tested operating point data provided as in Appendix A, Table A. 2. 130

Figure 59 Losses associated with sweeping Φ (boost) at constant temperature, the operating conditions are in Table 16 with the Φ-T matrix data in marked for reference in Appendix A, Table A. 2. The dashed lines with open markers denote cooler operation at T_{in}=42°C. The results demonstrate a tradeoff in combustion efficiency and increased HX+EXH losses. 132

Figure 60 Incomplete combustion species at constant temperature varied Φ conditions, the operating conditions are in Table 16 with the Φ-T matrix data in marked for reference in Appendix A, Table A. 2. Note that CO is the dominant emission for all but the highest Φ, with hotter operation exhibiting lower CO. .. 133

Figure 61 AFR_c based GTE contours and associated AHRR for constant PPRR with simultaneously varied Φ and T operation, with the Φ-T matrix data in marked for reference in Appendix A, Table A. 2. 134

Figure 62 Losses associated with sweeping Φ (boost) at constant PPRR. The dashed lines with open markers denote constant temperature operation at T_{in}=57°C. The constant PPRR results (closed markers solid lines) demonstrate a nearly constant combustion efficiency with increased HX+EXH losses as Φ is swept. This demonstrates that losses can be optimized through modulation of initial conditions. Φ-T matrix data in marked for reference to Appendix A, Table A. 2. 136

Figure 63 CO and HC emissions at constant temperature, varied Φ conditions (dashed) and at constant PPRR condition (solid). At the constant combustion process condition (PPRR), combustion efficiency is constant, suggesting that initial conditions can be used to control engine incomplete combustion species (primarily CO) in RCCI. Φ-T matrix data in marked for reference to Appendix A, Table A. 2. 137

Figure 64 Operable space of Φ-T matrix with the tested E85 based fuels (left), 91 PON gasoline (right). With gasoline base fuel (port) no conditions satisfied the constraints. 139

Figure 65 RCCI and HCCI operation at matched phasing. As intake pressure is increased from 1.5 to 2 bar absolute, RCCI operation was not possible as 91 PON gasoline exhibited HCCI. 141

Figure 66 Matched Φ′ operation with and without EGR at lean conditions. Note that with EGR (red) the intake temperaurre is higher and the heat relase rate is longer, while operation without EGR (black) is shorter even when operated at cooler temperatures. 143

Figure 67 Operable areas of E85 based fuels with 0% EGR (right) and gasoline based fueling with EGR (right). (With 0% EGR gasoline HCCI is encountered, prohibiting RCCI at the tested conditions). When 45% EGR is introduced the operable area expands enabling RCCI operation at select points within the Φ-T space. 145

Figure 68 Φ-T matrix points and operation with 91 PON gasoline with and without EGR 146

Figure 69 Energy budget of HCCI with and without EGR, and RCCI with EGR at matched conditions. It is seen that operation with 45% EGR reduces incomplete combustion by approximately half. Additionally, RCCI exhibits reduced HX and HX+Exh losses as compared to HCCI operation. 148

Figure 70 Incomplete combustion species emissions concentrations of RCCI bounded by HCCI 149

Figure 71 Incomplete combustion by emission type of RCCI bounded by HCCI 150

Figure 72 Matched phasing, intake pressure, speed, and load operation of RCCI and HCCI. Pressure traces are unfiltered to display knocking intensity. 152

Figure 73 Losses and performance of different charge preparation strategies. The results demonstrate the HX + EXH losses are the most dominant if efficiency is to be maximized. These losses were generally observed to trend proportional to PPRR and inverse effects with incomplete combustion. 154

Figure 74 Unfiltered Cylinder Pressure and AHRR for select charge preparation strategies. Note that only the intermediate (highest gross efficiency) strategies exhibit low pressure oscillatory behavior. As fuel is introduced early into the cycle (red and traces in top sub-figure), the charge is over stratified and the entire charge knocks. This condition is effectively lower octane fuel HCCI. Likewise, as fuel is introduced late into the cycle (as in the cyan traces in bottom sub-figure) the charge is over stratified and end gas knock is encountered. 156

Figure 75 Exhaust and unaccounted for (HX) losses as functions of charge preparation strategy (see Chapter 4 for discussion of the unaccounted for losses). The exhaust losses (EXH) were observed to be relatively constant, while HX losses were observed to be dependent on charge preparation, with the lowest losses observed at intermediate RCCI injection timings with single or double injections. 157

Figure 76 Unaccounted for losses (HX) plotted as a function of PPRR. The trends suggest that a proportional relation between PPRR and HX, with higher values of PPRR increasing HX. 158

Figure 77 Box plot statistical analysis of PPRR in HCCI and RCCI operation at matched load, intake density, and phasing. 160

Figure 78 Steady state average piston surface temperature reduction for ULSD/E85 RCCI relative to matched CDC ~0.34 Φ operation at ~9 bar IMEPg 1300 (rev/min). 164

Figure 79 Steady state piston oil gallery surface temperatures vs. load for CDC and RCCI. The trends show that engine speed effects are minimal, while charge dilution and combustion processes with RCCI exhibit almost a 3-fold-reduction in ΔT at low loads compared to 0.6 Φ CDC operation, and a 2-fold-reduction compared to matched Φ CDC (Φ=0.4). 165

Figure 80 Conditions of with oil galley cooling tests, 102 total data points, as described in Table A. 10 to Table A. 13. 168

Figure 81 Incomplete combustion and emissions as function of Φ/Φ′ for operation with (black squares) and without (red circles) piston oil gallery cooling. Open or closed markers denote conditions with (closed) or without EGR (open). The

results show that without piston oil cooling the lean limit is extended, and that without EGR, incomplete combustion is lower at a given Φ. 169

Figure 82 NO_X emissions as a function of charge dilution with or without EGR and with and without the use of the piston oil cooling jet. With lean operation and EGR, NO_X emissions with EHN/gasoline were below EPA 2010 regulations in-cylinder. 171

Figure 83 AVL 415S smoke emissions for EHN gasoline/gasoline RCCI. For all conditions near zero smoke was observed, suggesting that fuel-liner impingement was minimal. 172

Figure 84 Cylinder pressure, temperature, and AHRR of 0% EGR RCCI with (black) and without (red) piston oil gallery cooling. Note, pressure and corresponding temperature traces are unfiltered. The IVC temperature of the cases were 314 K and 321 K for operation with and without oil cooling respectively. 175

Figure 85 Cylinder pressure, temperature, and AHRR of 40% EGR RCCI operation with (black) and without (red) piston oil gallery cooling. Note, pressure and corresponding temperature traces are unfiltered. The IVC temperature of the cases were 333 and 347 K for operation with and without oil cooling, respectively. 178

Figure 86 Box plots of PPRR for operation with EGR (left two points) and without EGR (right two points). Operation with the piston cooling jet off is in red and with the cooling jet on is in black. Conditions without piston oil gallery cooling exhibit higher PPRR values, and demonstrated similar temperature dependency to that of HCCI as previously observed 180

Figure 87 PPRR for tests with (red) and without (black) piston oil cooling. Open markers denote 0% EGR operation and closed markers denote 40% EGR operation. Generally operation without piston oil cooling exhibited higher PPRR for a given Φ′ 181

Figure 88 GTE measurements of high compression ratio RCCI with and without piston oil gallery cooling. Data points are the average GTE determined from AFC_C and direct mass (AFR_{MASS}); whiskers denote the range of GTE determined by the respective AFR approaches. 182

Figure 89 Energy budget with and without piston oil cooling for 40% EGR operation. The combustion efficiency for operation without oil cooling is actually worse that with cooling. However, the heat and exhaust losses are much lower, which dominate the efficiency advantage. 183

Figure 90 Φ/Φ′ of maximum efficiency operation. Without oil cooling the charge can be further leaned without GTE penalty, thereby further reducing heat losses. 184

Figure 91 matched Φ′ operation with and without piston oil cooling. Without oil cooling the losses at the lean condition are reduced, increasing efficiency. 185

Figure 92 GTE plotted versus VE and HX for the 14.88 Cr piston data of Appendix A, Table A. 2. Contours of PPRR of 12 bar/°CA or greater are plotted in blue, and combustion efficiencies of 98% or less are plotted in black. The original Φ-T constraints of 12 bar/°CA and 97% combustion efficiency are bolded contours. The results demonstrate that good breathing and low losses are critical for high engine efficiency. 187

Figure 93 GTE versus HX and VE. Note that without piston oil gallery cooling, the lowest VE and HX conditions correspond to the lowest HX and associated GTE. Both 18.7 Cr conditions are with EGR operation. Note, conditions are with combustion efficiency greater than 95.5%. Data in Appendix A, Table A. 2, Table A. 12, and Table A. 13 188

Figure 94 GTE results with 40% EGR and 18.7 Cr plotted in VE and HX space. Contour lines of PPRR of 12 bar/°CA or greater are overlaid in blue, and combustion efficiencies of 98% or less are overlaid in black. The original Φ-T constraints of 12 bar/°CA and 97% combustion efficiency are bolded contours. The results demonstrate that without piston oil cooling mediocre engine breathing exists, but that heat losses and high efficiency are simultaneously achieved. Data in Appendix A Table A. 13 189

Figure 95 Simulated required overall turbocharger efficiency for the tested conditions. The simulated conditions are optimistic. Data in Appendix A Table A. 13 191

Figure 96 Combustion and heat transfer losses as function of Φ without piston oil cooling and with 40% EGR. Note that as the charge approaches the richer air based Φ, incomplete combustion increase, suggesting overly rich areas. Data in Appendix A Table A. 13 192

Figure 97 GT Power convection coefficient tuning for 18.7:1 Cr RCCI. With piston oil gallery cooling, the model convection coefficient needed to be reduced to 0.2 196

Figure 98 Comparison of convection coefficients for operation with piston oil cooling, and 18.7:1 Cr. The results suggest that the reduced surface area and smooth surface finish of the high compression ratio piston may in-and-of-itself reduce heat transfer somewhat as compared to the 14.88:1 bathtub profile, which required a convection coefficient of 0.4..... 198

Figure 99 Experimental operation without piston oil gallery cooling (black) and GT Power simulation of matched initial condition operation with 100% combustion efficiency and adiabatic operation (dashed magenta). The results demonstrate that very lean RCCI operation without piston oil cooling is nearly adiabatic 200

Figure 100 Experimental operation with piston oil gallery cooling (black) and GT Power simulation of matched initial condition operation with 100% combustion efficiency and adiabatic operation (dashed magenta). The results demonstrate that very lean RCCI operation with piston oil cooling is not quite as close to adiabatic as operation without piston oil gallery cooling. This is seen by the increased difference in expansion pressure of the above case. 202

Figure 101 Experimental operation without piston oil gallery cooling (black) and GT Power simulation of matched initial conditions, combustion efficiency, and expansion pressure (red), and GT Power simulations with 0% EGR assumed with matched conditions (cyan). The results demonstrate that if 0% EGR could be used with matched AHRR and combustion efficiency, greater expansion work and thus efficiency could be realized. 205

Figure 102 Experimental operation without piston oil gallery cooling (black) and GT Power simulation of matched initial conditions, but with 100% combustion efficiency and adiabatic operation (magenta), and GT Power simulations with 0% EGR and assumed adiabatic 100% combustion efficiency operation (cyan). The

results demonstrate that if 0% EGR and no losses even greater expansion work and thus efficiency could be realized. 207

Figure 103 Experimental operation without piston oil gallery cooling (black), GT Power simulations with 0% EGR and assumed adiabatic 100% combustion efficiency operation (cyan), and GT Power simulation of the Otto cycle (air standard) (orange). The results demonstrate that if 0% EGR and no losses even greater expansion work and thus efficiency could be realized. 208

Figure 104 GTE and NTE for cases 1-5 of Table 49.....211

List of Tables

Table 1 Stock 3401 SCOTE geometry 70

Table 2. Diesel fuel properties 75

Table 3. Gasoline fuel properties 75

Table 4. Ethanol fuel properties 75

Table 5. 2-Ethylhexyl-Nitrate fuel properties 75

Table 6 Low Pressure Fuel System Hardware 77

Table 7 Port fuel injector specifications 79

Table 8 Common Rail System Hardware 79

Table 9 Common rail injector nozzle specifications 83

Table 10 Emissions Analyzers 84

Table 11 Production tuned RCCI FMEP coefficients used in the present study . 89

Table 12 measurement uncertainty values 94

Table 13 Average GTE, GTE uncertainty and relative GTE uncertainty of oil points 72-102, Appendix A, Table A. 13 95

Table 14 Energy budget using AFR_C and AFR_{mass} averaged fuel flow. Energy use, uncertainty, and relative uncertainty of GTE shown, data are average of oil points 72-102, Appendix A, Table A. 13 96

Table 15 Top two sources of uncertainty of oil point 83, Appendix A, Table A. 13 97

Table 16 Engine operating parameters and hardware for Φ-T matrix 103

Table 17 Fuel combinations used in Φ-T test matrix, specifics of the fuel delivery are given in Table 16 and Appendix A 105

Table 18 Engine operating parameters and hardware for CO sources with EGR 107

Table 19 Engine operating parameters and hardware low load CO investigation [38] 110

Table 20 Engine operating parameters and hardware for efficiency vs. CA50 sweep 113

Table 21 Engine operating parameters and hardware for mixing controlled combustion 116

Table 22 Mixing controlled injection schedule for ULSD and 3% EHN + 91 PON gasoline 116

Table 23 Φ-T matrix constraint satisfaction color key 123

Table 24 key losses and parameters of constant Φ varied T operation 127

Table 25 Losses and parameters of constant T varied Φ operation 131

Table 26 Losses and parameters of constant PPRR operation through simultaneous variation of Φ and T, the Φ-T matrix data in marked for reference in Appendix A, Table A. 2. 135

Table 27 Engine operating parameters for gasoline reactivity sensitivity 141

Table 28 Engine operating parameters for EGR dilution effects 142

Table 29 Φ-T operating parameters with 45% EGR 145

Table 30 Intake temperature sweep (0% EGR load is slightly low, as higher load operation was not possible without excessive knock). 147

Table 31 Operating parameters for charge preparation tests 153

Table 32 Injection strategies for charge preparation tests 153

Table 33 RCCI and HCCI cumulative distribution function (CDF) statistics, 9 bar IMEPg operation CA50 5°CA ATDC, where all units are in bar/°CA. 161

Table 34 Operating parameters for piston temperature tests [111] 163

Table 35 Operating parameters for oil gallery temperature comparison tests ... 165

Table 36 Conditions of with oil galley cooling tests, (see Appendix A, Table A. 10 to Table A. 13) 167

Table 37 Performance metrics of 0% EGR operation with and without oil gallery cooling 174

Table 38 Efficiencies for operation in Figure 84 176

Table 39 Performance metrics of EGR operation with and without oil gallery cooling 177

Table 40 Efficiencies for operation in Figure 85 179

Table 41 Inputs for GT Power simulations of high efficiency operation.....194

Table 42 Operating and efficiency parameters from the experiment without piston oil cooling and GT Power with various convection coefficients. 197

Table 43 Operating and efficiency parameters from the experiment with piston oil cooling and GT Power with various convection coefficients. 198

Table 44 Operating and efficiency parameters from the experiment without piston oil cooling and GT Power with adiabatic 100% combustion efficiency operation assumed. 200

Table 45 Key operating and efficiency parameters from the experiment with piston oil cooling and GT Power with adiabatic 100% combustion efficiency operation assumed. 203

Table 46 Operating and efficiency parameters from the experiment and GT Power simulations. GT Power simulations with air demonstrates higher efficiency potential than with EGR (assuming that matched combustion efficiency and AHRR are possible) 205

Table 47 Operating and efficiency parameters from the experiment and adiabatic 100% combustion efficiency GT Power simulations. GT Power simulations with air demonstrates higher efficiency potential than with EGR. 207

Table 48 Operating and efficiency parameters from the experiment, adiabatic 100% combustion efficiency GT Power simulations with air, and GT Power Otto cycle (air standard) simulation. 209

Table 49 to GT Power overall turbocharger efficiency simulation input modifications to Table 41 to oil matrix data point 83 210

Nomenclature

AHRR	Apparent Heat Release Rate
AFR	Air Fuel Ratio
AFR_C	Air Fuel Ratio based on emissions bench carbon
AFR_{LAMBDA}	Air Fuel Ratio based on exhaust Lambda meter
AFR_{MASS}	Air Fuel Ratio based on directly measured masses
ATDC	After Top Dead Center
BMEP	Brake Mean Effective Pressure
C	Degrees Celsius
C_1	Atomic Carbon
CA	Crank Angle
CDC	Conventional Diesel Combustion
CI	Compression Ignition
cm	Centimeter
CO	Carbon Monoxide
CO_2	Carbon Dioxide
Cr	Compression Ratio
DEF	Diesel Exhaust Fluid
deg	Degree
DI	Direct Injected
DOC	Diesel Oxidation Catalyst
DOE	Department of Energy
DPF	Diesel Particulate Trap
E85	85% Ethanol and 15% Gasoline by volume
EGR	Exhaust Gas Recirculation
EHN	2-Exhylhethyl-Nitrate
EPA	Environmental Protection Agency
ERC	Engine Research Center
FID	Flame Ionization Detector
FMEP	Friction Mean Effective Pressure
FSN	Filer Smoke Number
g	Gram
GTE	Gross Thermal Efficiency
H-to-C	Atomic Hydrogen to Carbon Ratio
HC	Unburned Hydrocarbons
HCCI	Homogeneous Charge Compression Ignition
HD	Heavy Duty
H_2O	Water
H_2O_2	Hydrogen Peroxide
HO_2	Hydroperoxyl Radical
hp	Horse Power
HTHR	High Temperature Heat Release
HX	Heat Transfer
Hz	Hertz
ICE	Internal Combustion Engine

IMEP	Indicated Mean Effective Pressure
IMEPg	Indicated Mean Effective Pressure, Gross
IMEPn	Indicated Mean Effective Pressure, Net
ITHR	Intermediate Temperature Heat Release
IVC	Intake Valve Closure
K	Degrees Kelvin
kg	Kilo-gram
kWh	Kilo-Watt Hour
kPa	Kilopascal
J	Joule
L	Liter
LHR	Low Heat Rejection
LHV	Lower Heating Value
LNT	Lean NO_x Trap
LTC	Low Temperature Combustion
LTHR	Low Temperature Heat Release
MEP	Mean Effective Pressure
min	Minute
N_2	Nitrogen
NASA	National Aeronautical and Space Administration
NiCrAlY	Nickel Chromium Aluminum Yttrium
NO_x	Nitrogen Oxides
NTE	Net Thermal Efficiency
NTC	Negative Temperature Coefficient
NVH	Noise Vibration and Harshness
O-to-C	Atomic Oxygen to Carbon ratio
O_2	Oxygen
ON	Octane Number
OH	Hydroxyl Radical
P	Pressure
PCCI	Premixed Charge Compression Ignition
PID	Proportional Integral Derivative
PLIF	Planar Laser Induced Fluorescence
PM	Particulate Matter
PON	Pump Octane Number
PP	Peak Pressure
PPRR	Peak Pressure Rise Rate
PRF	Primary Reference Fuel
$\dot{R}$	Fuel Radical
RCCI	Reactivity Controlled Compression Ignition
rev	Revolution
SCOTE	Single Cylinder Oil Test Engine
SCR	Selective Catalytic Reduction
SEM	Scanning Electron Microscope
SG	Savitzky-Golay
SI	Spark Ignition

SOI	Start of Injection
T	Temperature
TBC	Thermal Barrier Coating
TDC	Top Dead Center
TACOM	U.S. Army Tank Automotive Command
U.S.	United States
ULSD	Ultra Low Sulfur Diesel
VE	Volumetric Efficiency
°	Degree
Φ	Equivalence Ratio (fresh air based)
Φ′	Equivalence Ratio (fresh air based)
λ	Lambda
γ	Gamma

Chapter 1 Introduction

1.1 Background

As an energy conversion device, the internal combustion engine (ICE) has become invaluable to society. The ability of the ICE to provide economically viable and reliable power for both stationary and mobile applications has resulted in mass production of the ICE in a variety of displacement and design platforms [1]. Primarily, engines have been operated with non-renewable petroleum-based fuel sources. The depletion of fuel stocks has raised both historical and recent concerns over improving the fuel efficiency of engines. Secondly, because of the widespread engine usage, emission production has been and continues to be a major area of both concern and improvement.

Regardless of the engine design or the type of hydrocarbon-based fuel feedstock, the engine is an energy conversion device that converts chemical potential into useful work through combustion. Ideally, the products of hydrocarbon combustion with air would be carbon dioxide (CO_2) water (H_2O) and nitrogen (N_2). Unfortunately, this is almost never the case. Typical engine operation produces incomplete combustion products that results in inefficiency and anthropogenic-derived atmospheric pollution. Government mandated regulation of pollutants such as carbon monoxide (CO), unburned hydrocarbon (HC), oxides of nitrogen (NO_X), and particulate matter (PM) have been aggressively increased since their implementation, as summarized in reference [2]. To combat these emissions and fuel consumption issues, advanced

combustion strategies have been investigated, which are often referred to as low temperature combustion (LTC) strategies.

1.2 Research Objectives

To address the efficiency and emissions issues associated with conventional engine designs, research on the Reactivity Controlled Compression Ignition (RCCI) low temperature combustion (LTC) strategy is proposed. Like many LTC strategies, RCCI employs increased fuel-air mixing time from early fuel injection and diluent control, thus reducing NO_X and PM emissions. However, although these conditions are possible, it is of interest to explore the pragmatic efficiency potential of RCCI as a LTC strategy. The primary proposed research objectives are:

1. Use computational simulations to explore operating conditions that may provide high efficiency. (Chapter 3)
2. Conduct single cylinder engine experiments to improve the understanding between the engine thermodynamic conditions and the combustion event such as to increase engine efficiency (Chapters 5).
3. Explore the maximum practical engine efficiency of RCCI (Chapter 5) through adoption of engine architecture from the initial simulation studies in Chapter 3, coupled to the experimentally based relations on the combustion process developed in Chapters 5.

4. Investigate the cycle efficiency limits using computational simulations (chapter 6) and relate these limits to the maximum efficiency obtained in the experiments of Chapter 5.

1.3 Research Method and Tools

The primary research tool used in this study was a single-cylinder, heavy-duty (HD), metal research engine. Single-cylinder engine experiments are able to provide a highly controlled research environment for pressure based combustion analysis. However, design variations to single-cylinder engine internals, such as compression ratio, are time consuming and are difficult to quantify a-priori. Therefore, closed cycle zero-dimensional computational tools were combined with single-cylinder engine results to better understand the physical phenomena observed in the experiments. These tools were used to develop engine conditions by simulating conditions that may improve engine efficiency, and then conducting experiments to better understand the potential influence that the conditions had on the combustion process.

The research goals are to: 1, expand on zero-dimensional simulation results using single-cylinder engine experiments to explore RCCI operation over a wide range of engine thermodynamic conditions; 2, determine sources of additional efficiency gains; 3, investigate the maximum practical efficiency of 4-stroke engines.

Chapter 2 Literature Review

2.1 Conventional Diesel Emissions Dilemma

It is well known that compression ignition (CI) engines offer improved efficiency potential compared to spark ignition (SI) engine. However, to meet current emissions mandates, the conventional CI engine has become reliant on exhaust after-treatment devices. For a SI engine, these devices can be as simple as a conventional three-way catalyst [3]. However, for sufficient emissions reductions with the lean operation of conventional CI engines, different and less mature aftertreatment systems are being implemented. These devices are used to mitigate tailpipe emissions of NO_X and PM (also referred to as soot). Although effective, these devices can be expensive to install and operate, and can decrease engine efficiency. Moreover, recent legislation has been passed [4] which will mandate fuel consumption reductions from vocational class heavy duty vehicles. This legislation will effectively add another exhaust gas to be mitigated, viz., CO_2. This recent legislation couples an increase in fuel economy with current reductions in exhaust emissions. These new regulations may require a rethinking of the traditional and independent ways in which engine emissions and efficiency have been classified, and will require a uniform approach for simultaneous reductions.

The environmental protection agency (EPA) 2010 heavy-duty (HD) emissions mandates have pushed engine emissions to very low levels. To mitigate NO_X emissions, aftertreatment devices such as a Lean NO_X Trap (LNT) [5] or NO_X absorber [6] have become necessary, as traditional in-cylinder

reductions techniques have not proved sufficiently effective. Unfortunately, these aftertreatment devices are made using large amounts of expensive, high purity precious metals, like platinum, adding cost to their installation. Moreover, their operating principle requires frequent combustion enrichment which can degrade fuel economy. Alternatively, a lower first-cost catalyst approach called selective catalytic reduction (SCR) can be used, but it requires consumption of a secondary fluid, urea, which is dosed at a rate of approximately 1 g of urea per g/kW-h of engine-out NO_X [7]. This means that typical conventional diesel operation at 4-10g/kW-h of engine out NO_X requires significant urea dosing. Lastly, urea is not a low cost fluid, and it is nearly comparable to current (2012) diesel fuel cost. So, although NO_X can be controlled, it can have an undesirable effect on operating cost and efficiency.

Similar to NO_X emissions, soot emissions from diesel engines are also problematic. Diesel particulate filters (DPF) have been introduced to reduce soot in the exhaust stream. A DPF loads with soot as the engine operates, and after some level of soot loading, must be regenerated. This regeneration process can be passive or active, which depends on the inlet temperature of the gas into the filter. Passive regeneration requires no additional thermal assistance to clean the filter, where active regeneration does, typically catalyzing diesel fuel with a diesel oxidation catalyst (DOC) [8]. This requires additional fuel to be injected either directly into the exhaust system or with late in-cylinder post injections, which both increase fuel consumption. This process is a major detriment from both an

economic perspective, and in light of the recent CO_2 mandates, from an emissions standpoint.

The additional use of fuel in PM-or-LNT based NO_X emissions aftertreatment systems could cause a given vehicle to not meet the proposed CO_2 targets. Combustion research for the reduction of these emissions in-cylinder has led to the development of several non-traditional or advanced combustion strategies. Many of these alternative strategies can simultaneously reduce emissions and increase fuel efficiency.

Typically these advanced strategies rely on long ignition delays to increase fuel-air mixing, reducing local equivalence ratios or temperature or both [9-13]. To avoid thermal NO_X formation and heat transfer losses, the strategies have focused on decreasing peak combustion temperatures, and thus have been termed LTC strategies. Although LTC strategies can reduce NO_X and soot while maintaining diesel-like or higher efficiencies; often HC, CO, and, with some strategies, combustion control and peak pressure rise rate (PPRR), are often sacrificed [14,15]. Moreover, the reduced combustion temperatures often reduce exhaust temperatures, thus requiring highly efficient and optimized exhaust energy recovery devices, such as advanced turbochargers. Without careful consideration, high levels of pumping work can be incurred in LTC strategies, as pointed out by Chadwell et al. [16]. These added losses can offset potential efficiency gains from reduced temperatures. Ideally, an advanced combustion strategy would minimize the impacts of negative emissions or control effects, while optimizing the NO_X, soot, and fuel efficiency gains.

2.2 Low Temperature Combustion (LTC)

2.2.1 Homogeneous Charge Compression Ignition (HCCI)

A well-researched LTC strategy, called homogeneous charge compression ignition (HCCI), can best be described as a melding of the SI and CI engine combustion strategies. In HCCI, the fuel and air mixture is ideally prepared externally from the cylinder and is inducted as a homogeneous charge. The engine operates un-throttled and load is controlled by the equivalence ratio (Φ^*) of the charge and the thermodynamic conditions (i.e., in-cylinder gas composition temperature and pressure).

The charge has minimal compositional (i.e., Φ) and thermal gradients and the reactants rely only on chemistry to initiate combustion, not on an external means such as a spark plug. Due to the nature of the ignition process, this type of combustion is commonly referred to as kinetically controlled. The highly mixed charge auto-ignites with rapid and nearly simultaneous uniform combustion throughout the cylinder. This rapid heat release produces rapid PPRR, which at moderate to high loads, can have adverse mechanical and noise vibration and harshness (NVH) characteristics. Moreover, this can have an adverse effect on engine heat loss, since, as engine load increases, the amount of heat released increases, as well as the subsequent PPRR. This is a practical and technical

---

* $\Phi \equiv \frac{\left(\frac{M_{air}}{M_{fuel}}\right)_{Stoichometric}}{\left(\frac{M_{air}}{M_{fuel}}\right)_{Actual}}$

hurdle that HCCI combustion must still address and solve prior to its mainstream adaptation.

HCCI operation was initially researched by Onishi et al. [17] in gasoline-fueled two-stroke engines. In 1983, Najt and Foster [18] and later Thring [19] demonstrated HCCI operation in four-stroke engines. Since these initial studies several researches have explored HCCI to further understand its operation, while discovering several benefits and limitations. HCCI has been demonstrated to be operable on many fuels, with several demonstrated by Christensen et al. [20].

Recent focus of much HCCI research has been on methods of low noise (knock free) load extension. Although some more recent researchers have demonstrated high load HCCI operation with either diesel [6] or gasoline fuels [21, and 22], typical engine structural, NVH, or control strategy requirements prohibit practical and commercial HD HCCI operation beyond that of low/mid load operation.

2.2.2 HCCI Research on Control Through Stratification and Fuels

Efforts to address the control issues of HCCI have been numerous. To minimize the excessive pressure rise rates, either the combustion duration must be increased, or combustion must be phased appropriately. Research on methods of increasing combustion duration or phasing through compositional [23-25] or thermal stratification [26, and 27] have demonstrated potential means of controlling and extending the operational range of HCCI combustion. However, interesting work by Herold et al. [28] demonstrated that both compositional and

thermal effects can compete during the ignition process of HCCI operation and careful management of both thermal and reactant composition distributions are needed for successful stratified combustion control.

An alternative approach to gaining control of HCCI is through manipulation of fuel properties. Research by Shibata [23, 24], which studied fuel effects on HCCI, showed many interesting trends. Key finding of these works were that both high temperature and low temperature chemistry needed to be studied, and that the timing of the low temperature reactions was critical to the phasing of the high temperature heat release event. Similar to this work, Kalghatgi [29, and 30] and Bessonette et al. [25] studied fuel reactivity and load limits of HCCI. Although Bessonette was able to achieve loads of 16 (bar) indicated mean effective pressure (IMEP) with HCCI operation, significant pressure rise rates (up to 30 [bar/°CA]) were also obtained. Both Kalghatgi and Bessonette demonstrated that at higher load conditions, the best fuel reactivity for optimal combustion phasing and lower PPRR is that of a low cetane number fuel, between that of ultra-low sulfur diesel (ULSD) and gasoline.

Although these results are promising, commercially available low cetane fuels are not standard. Moreover, fuel composition and reactivity also change according to climate (winter/summer) and market conditions. To avoid the need for designer fuels, similar research was performed by Inagaki et al. [31] where multiple reference fuels were blended to simulate real fuels, and was found to extend the heat release rate event. However, in that study the fuels were internally blended within the combustion chamber through the use of separate

fuel delivery systems. The results of Inagaki et al. [31] were very promising, and although the fuel delivery strategy was not true HCCI, it was near-fully premixed. This research demonstrated that through the use of appropriate fuels with proper mixing, a significant increase in load with low-pressure rise rates could be realized while operating in a fully premixed combustion regime.

Optimization of the work of Inagaki has been demonstrated computationally by Kokjohn et al. [32], and experimentally by Hanson et al. [33, and 34]. Unlike the work by Inagaki, Hanson used commercial pump fuels instead of reference fuels. The fuels selected were United States (U.S.) pump #2 ULSD and premium grade pump gasoline 91 pump octane number (PON). More recent in-cylinder planer laser induced florescence (PLIF) measurements by Kokjohn et al. [35] supported earlier emissions spectroscopy work by Splitter et al. [36], these studies demonstrated that the combustion event is controlled by zones of reactivity sequentially igniting from the most to least reactive. The studies also demonstrated that although the charge was very premixed, the dual-fuel in-cylinder blended process established gradients in composition responsible for controlling the combustion process. This technique has correspondingly been called reactivity controlled compression ignition (RCCI).

Recent RCCI experiments by Splitter et al. [37] have demonstrated that full-load (20 bar brake mean effective pressure (BMEP)) RCCI operation is possible with simultaneous low PPRR and meeting EPA 2010 NO_X and soot emissions mandates in-cylinder. Similar experiments by Splitter et al. [38] also

demonstrated at low load, that the use of multiple injections offers a benefit to expanding the low emission high efficiency capability of RCCI.

Although these RCCI results were promising, the strategy required the use of two separate fuel stocks, thus requiring two fuel systems for operation in an application. Both fuel tanks require regular refueling, which could result in decreased market acceptance due to the requirement to refuel two systems. An alternative strategy might be to use a single fuel stock with the same delivery system as that proposed by Hanson et al. [33, 34], but with the introduction of a small concentration of a highly reactive chemical to the direct injection fuel, as demonstrated by Splitter et al. [39]. In that work Splitter demonstrated that identical, near zero levels of NO_X and PM were realized.

Moreover, because the magnitude of the low temperature heat release was reduced with cetane improvers, the compression pressure and thus negative work were reduced, potentially yielding about a 1% point increase in net and gross efficiency. It was demonstrated in Splitter et al. [39] that the system could be properly sized to allow the reactivity enhancer to be replenished at oil change-like intervals while necessitating a much smaller tank size than previous HCCI studies, such as that of Eng et al. [40], thereby aiding in packaging and use of the system. Similar systems have been designed and implemented into current market products for the storage and injection of diesel exhaust fluid (DEF) for use with SCR catalysts for NO_X aftertreatment control.

2.3 Chemical Kinetics

The discussion of RCCI shows that it is a kinetically controlled LTC strategy. The distinction of RCCI vs. other strategies is that it uses fuel chemistry stratification to control combustion. To better understand the fundamentals of the processes controlling RCCI heat release, a literature review on fuel kinetics and ignition process was performed. Specifically, literature on kinetics of fuel composition, temperature, pressure, and EGR were addressed, such that their independent and dependent relationships can be utilized for increasing efficiency.

2.3.1 General Effects of Pressure, Temperature, and Fuel Properties on Combustion Kinetics

The previously cited RCCI works have shown that EGR, intake pressure and temperature, and fuel properties can all affect the ignition delay of the mixture. Based on the bulk gas temperature from RCCI experiments, ignition delays are determined by temperatures in the 700-1100K range, typically referred to as the intermediate temperature region. Unlike most of the kinetics literature, which considers shock tube rapid compression machine or HCCI experiments, gradients in mixture and composition exist in RCCI which complicate the effects of composition on ignition delay. Figure 1 summarizes characteristics of the ignition process typically observed in shock tube studies [41].

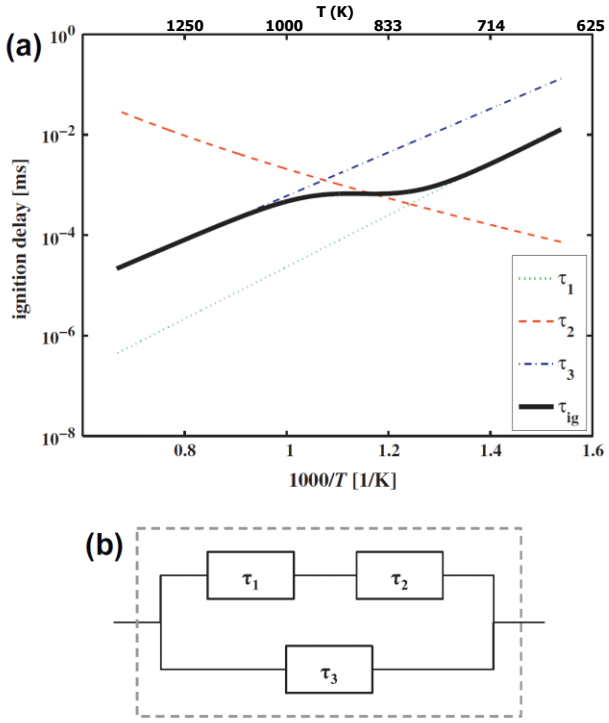

Figure 1 The three distinct regimes of ignition delay. Note that regime 2 is opposite of regimes 1 and 3, which are positively affected by temperature. Figure adopted from Vandersickel et al. [41], top axis (T (K)) added for clarity

Figure 1 shows that there are distinct regions which are important for fuel auto-ignition. In particular, the region within the 700-1200 K temperature space appears to have multiple interactions present. Due to the flat or opposite trend in ignition delay with respect to temperature, this region is typically called the negative temperature coefficient (NTC) region, as the ignition delay can actually increase with increasing temperature. However, in general it is observed that as temperature increases, ignition delay decreases. Figure 1 indicates that in the high (T > 1000 K) and low temperature (T < 600 K) ranges ignition delay trends exhibit linear behavior. Only in the intermediate temperature range is significant deviation observed.

Like temperature, Φ has been shown to influence where the intermediate temperature range, with reduced a dependency in the low and high temperature regimes. For example, Figure 2 from research by Herzler et al. [42] demonstrates the effect of Φ on n-heptane air mixtures at a pressure of 50 bar.

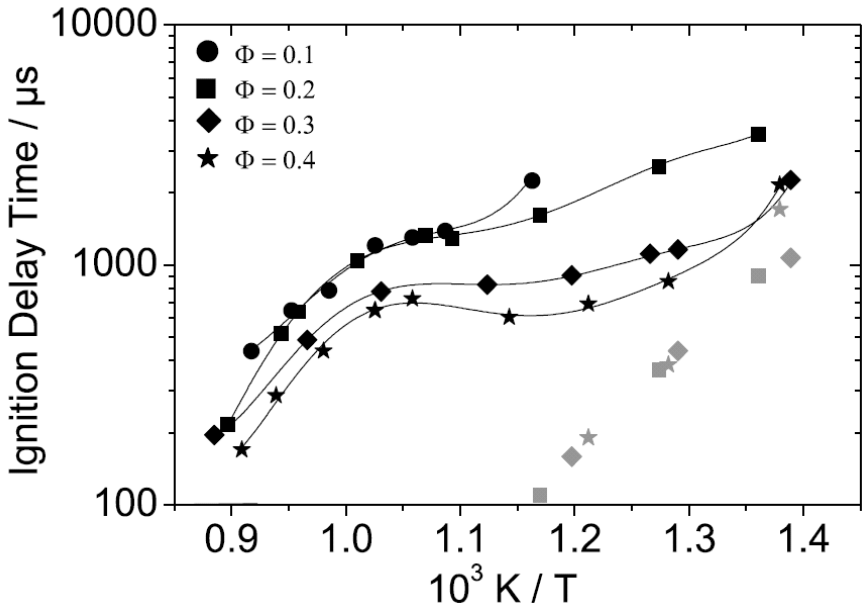

Figure 2 Ignition delay times of n-heptane/air mixtures for different equivalence ratios at 50 bar. [42] Note that when the mixtures are very lean NTC behavior is not observed, where at richer mixtures NTC is observed. The grey symbols depict the pre-ignition delay times.

Figure 2 illustrate that with richer (Φ=0.4) mixtures, NTC behavior is observed, while leaner mixtures, NTC is not. Also of interest is that the pre-ignition delay times shown in gray marks in Figure 2 (T<900K) show no Φ dependence. Similar findings by Ciezki and Adomeit [43], have shown that outside of the intermediate temperature range ignition delays of n-heptane/air mixtures showed only weak dependence on equivalence ratio. Although the cited study trends were observed in n-heptane mixtures, Vandersickel et al. [41]

observed similar trends in multi-component surrogate mixtures of kerosene-like fuels. Thus, the most important aspect of fuel chemistry is often prior to hot ignition, where conditions and composition dominate, with a reduced influence on the high and low temperature kinetics.

In engine experiments, Φ sensitivity can be exploited to increase the local ignition delay through compositional gradient in the charge. Select findings of Sjöberg and Dec [44] and later by Yang et al. [45] and at high loads by Dec et al. [46] have all demonstrated that Φ stratification in auto-ignition combustion can enable higher load and more advanced phasing of HCCI. This effect can be compounded by introducing simultaneous reactivity and Φ stratification. Kokjohn and Reitz [47] have demonstrated this though modeling stratification with both Φ and Φ together with reactivity stratification ΦRCCI). Key findings from that study are presented in Figure 3.

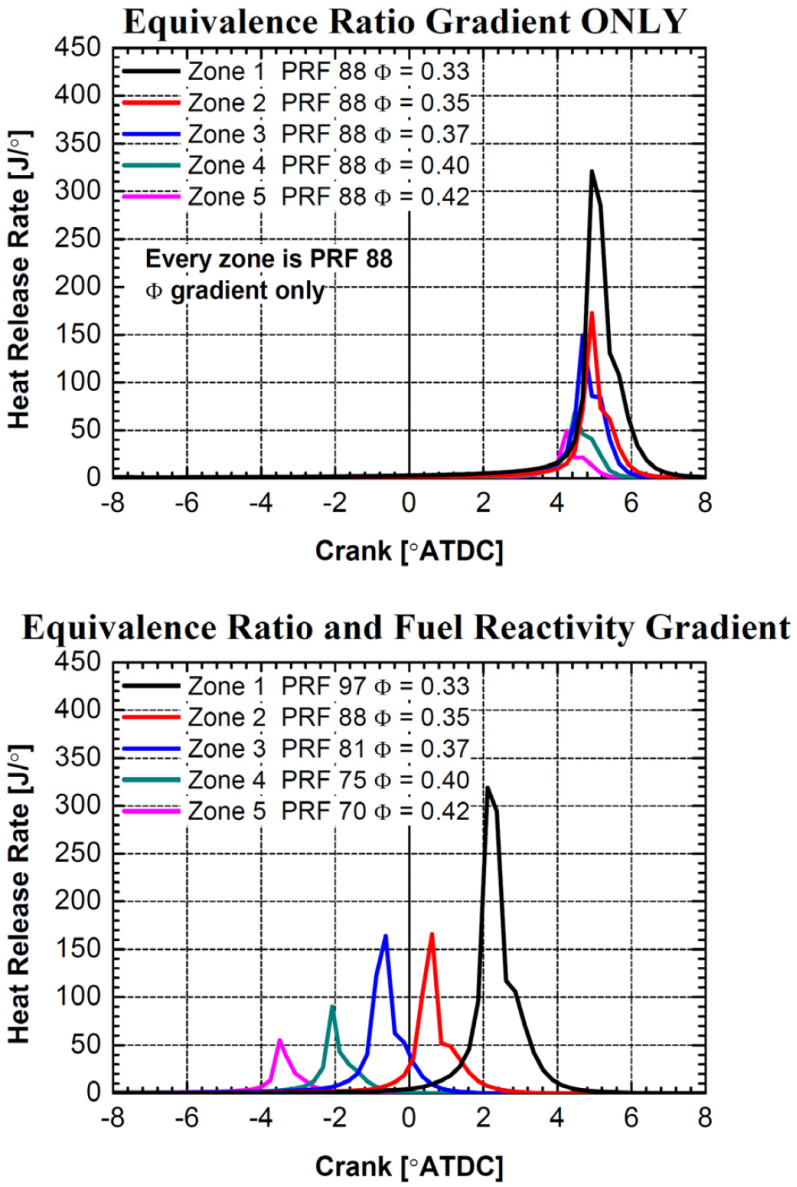

Figure 3 Simulation results of 1.9L engine operation at 2300 rev/min 0% EGR, 1.58 bar IVC pressure and 81°C IVC temperature, DI -60°CA ATDC, global PRF number of 88. The results demonstrate the effects of Φ only stratification (top) Φ+reactivity stratification (bottom), where reactivity plus Φ stratification spread the combustion event significantly more, as chemical dependency (reactivity) is added to the charge. Figure reproduced from Kokjohn and Reitz [47]

The findings displayed in Figure 3 demonstrate that Φ sensitivity can be important, as ignition delay can vary with Φ. However, the study also demonstrates that simultaneous composition and Φ changes can offer significant control over the combustion process. As demonstrated by Kokjohn and Reitz

[47], stratifying the composition offers the potential for varied ignition properties throughout the charge. Therefore, in RCCI, effects of fuel composition and reactivity must simultaneously be addressed.

An additional essential parameter is pressure, which can affect fuel reactivity. It is well known that the ignition process in many fuels is pressure sensitive. For instance, long chain (fully saturated) alkanes, like n-heptane can be highly pressure dependent. Figure 4 from a shock tube and modeling study by Vandersickel et al. [41] shows the effects of pressure on the intermediate temperature behavior with n-heptane air mixtures.

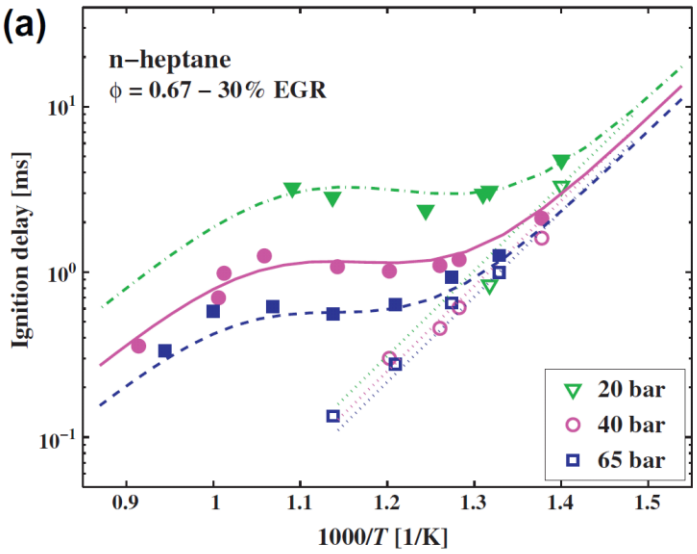

Figure 4 Effect of pressure on n-heptane fuel kinetics at representative CI engine conditions. Note that as pressure increases ignition delay decreases significantly, as the vertical axis is plotted on a log scale. Figure reproduced form Vandersickel et al. [41]

It is observed that pressure has a pronounced effect on the ignition delay in the intermediate and subsequent high temperature regimes. Additionally, Figure 4 demonstrates that the first stage reactions are primarily dependent on temperature alone and not on composition or pressure. These findings

demonstrate that for a given mixture at increased pressure, fuel reactivity is likely to increase.

Similar pressure dependency effects have been observed with several different fuel compositions. For example, shock tube research by Fikri et al. [48] demonstrated that n-heptane/isooctane/ethanol mixtures display intermediate temperature pressure dependence, at CI-engine like pressure, as shown in select results from this study, Figure 5.

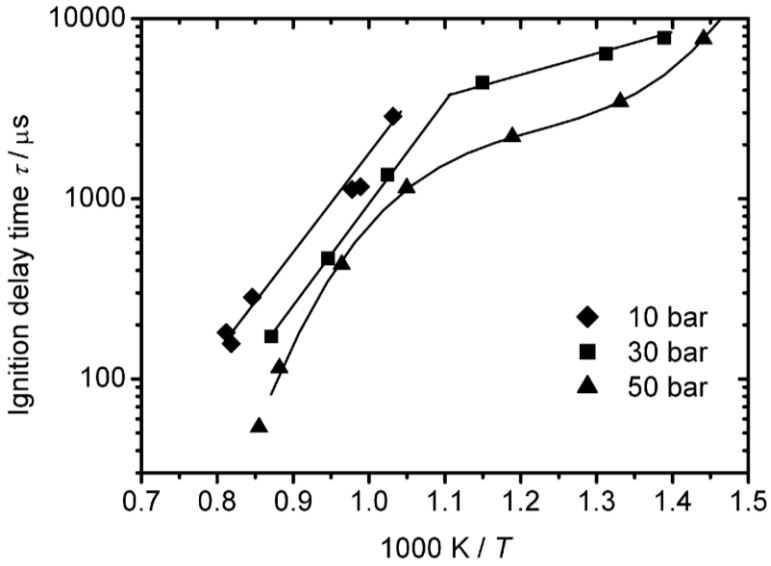

Figure 5 Shock tube data of n-heptane isooctane mixtures with ethanol (PRF 82 base with 20% ethanol added) [48]

Results in Figure 5 are of particular interest, because they are with fuels and conditions that that would correspond to experimental RCCI conditions with 14-16:1 Cr and 1-2 bar absolute intake pressure fueled with 88% port fuel injection of 91 PON gasoline + 22% ethanol, globally homogeneous in [48]. Of course, in RCCI the local composition changes, thereby stratifying reactivity.

Similarly, fuels with partial aromatic content like n-heptane/toluene mixtures have also been shown by Herzler et al. [49] to exhibit pressure dependency on high temperature ignition delay. Vandersickel et al. [41] also considered fuels with higher aerometric content. Fuel B in Figure 6, is closer to light kerosene/natural gasoline and fuel A is closer to a heavy kerosene/US #2 ULSD like fuel.

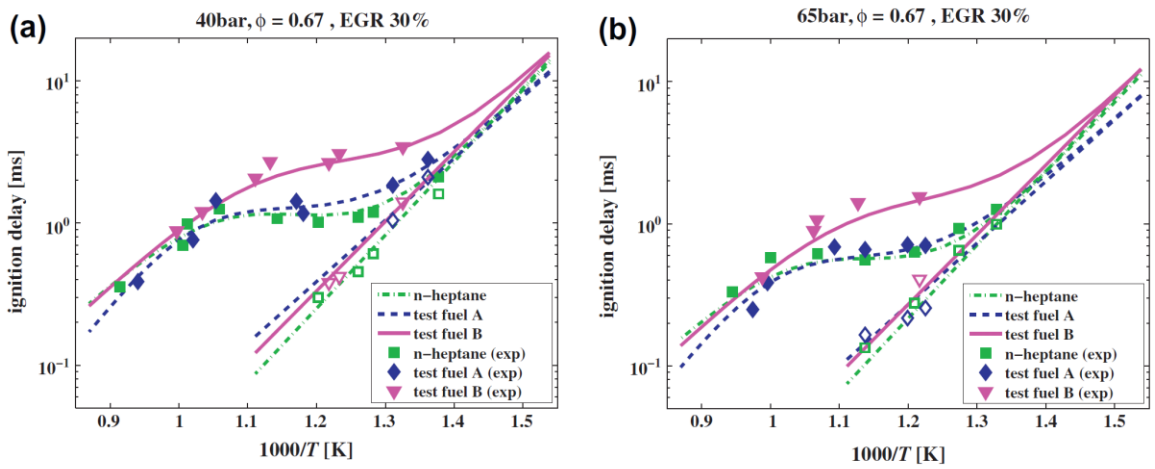

Figure 6 Ignition delay of n-heptane and kerosene surrogates at CI engine-like conditions. Note that the higher pressure conditions (right) exhibit decreased ignition delay. Of interest is that the lighter fuel (Fuel B) has over a 50% cycloalkanes content, demonstrating that chemical composition has a marked interaction on ignition delay pressure dependency. Figure reproduced from [41].

It should be noted that n-heptane is often classified as a major component of a surrogate for ULSD and kerosene kinetics. In reality ULSD and kerosene carbon chain length contain many fully saturated (normal) chain alkanes species that are often longer than C_7. Although chemically different, research by Westbrook et al. [50] demonstrated that C_7-C_{16} fully hydrogenated alkanes have no appreciable differences in ignition delay.

Although the previous studies provide examples on the behavior of higher reactivity fuels, recent research by Dec et al. [21] has demonstrated that intake pressure can have an appreciable effect on real gasoline fuels in the intermediate temperature range, while similar high octane PRF fuels and ethanol do not exhibit this dependency. Figure 7 displays the trends observed with ethanol and gasoline fuels.

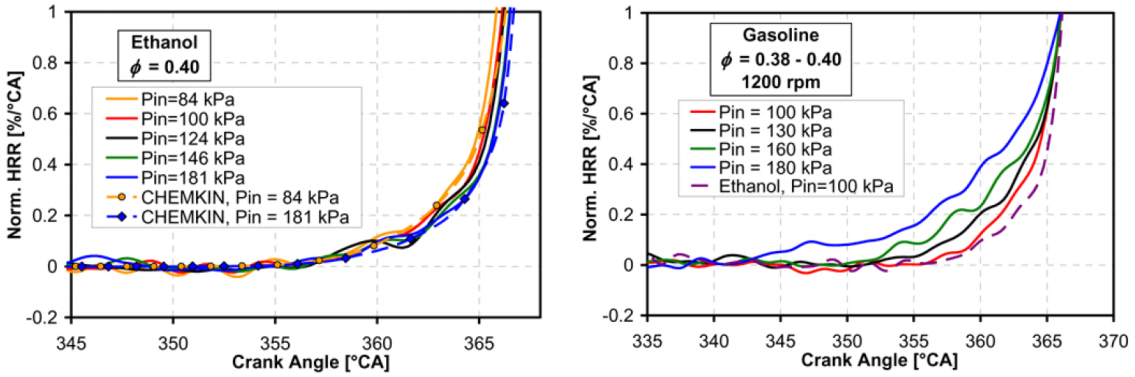

Figure 7 Intermediate temperature heat release behavior of gasoline (right) and neat ethanol (left) at matched conditions while sweeping intake pressure. Note that neat ethanol expresses no pressure dependency, while gasoline exhibits increased ITHR with pressure. Figures reproduced from Sjöberg and Dec [51] (left) and Dec et al. [21] (right).

To better understand the reasons for this, a kinetic modeling study of this effect was conducted by Mehl et al. [52]. A key finding of that study is reproduced in Figure 8.

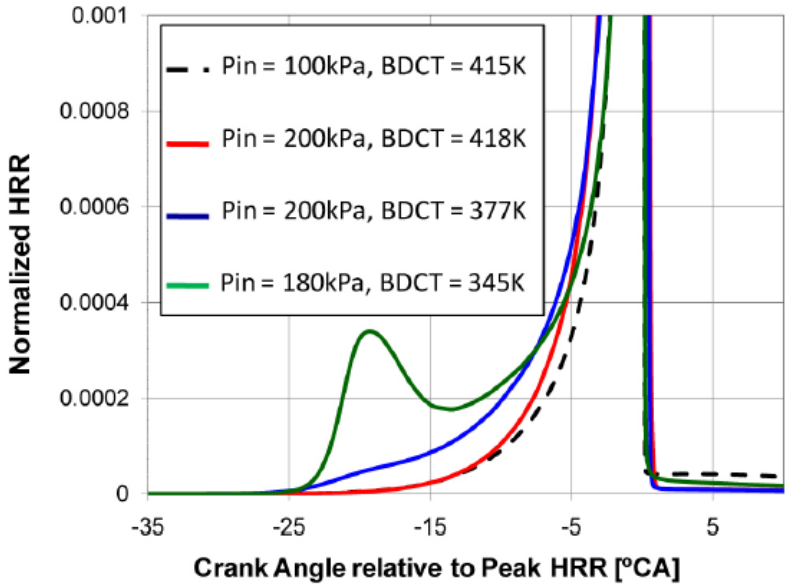

Figure 8 HCCI Intermediate temperature heat resale behavior of pump gasoline at various initial conditions. Engine is simulated to be an identical match of Dec [21] with a compression ratio of14:1, at 1200 rev/min. The results show that reduced intake temperature and increased boost increase the reactivity of pump gasoline to be more like diesel fuel. Figure reproduced from [52].

The study concluded that increased pressure was likely responsible for enhancing the formation of intermediates like the hydroproxy radical (HO_2), and with reduced temperatures, the chain branching reaction of H_2O_2 into 2OH is reduced, extending the ignition delay. If sufficiently low temperatures were used, fuel radical oxidation reactions ($\dot{R}+O_2$) became dominant, resulting in NTC behavior. Thus a fuel with low reactivity (determined by the research and motor octane tests (RON and MON respectively)), may behave more diesel-like if exposed to high pressure at lower temperatures. Figure 9 by Yates et al. [53] depicts this trend in three dimensional space of pressure temperature and ignition delay for a stoichiometric mixture of isooctane and air.

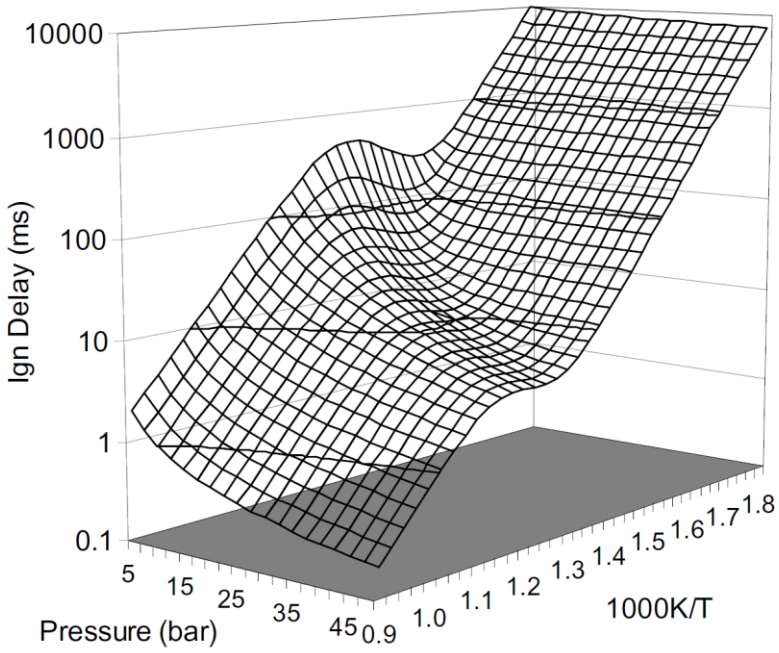

Figure 9 Three-dimensional surface of ignition delay of stoichiometric iso-octane and air. Figure reproduced from [53].

Although the experiments by Sjöberg and Dec [51] demonstrated that ITHR pressure expression was decreased or absent with neat ethanol, shock tube experiments by Curran et al. [54] demonstrated that for neat ethanol, the high temperature ignition delay was reduced with increases in pressure. These findings were supported by work by Sjöberg and Dec [51], where the transition into high temperature heat release (HTHR) was found to be faster in HCCI experiments than comparable primary reference fuels (PRF[†]) mixtures. Thus, it is possible that the kinetics of ethanol differ in pressure dependency sources. Figure 10 below from Yates et al. [53] depicts modeled ignition delay from different fuel molecule types at stoichiometric air fuel ratios and 30 bar pressure.

[†] Defined as the volumetric ratio of iso-octane (PRF=100) and n-heptane (PRF=0)

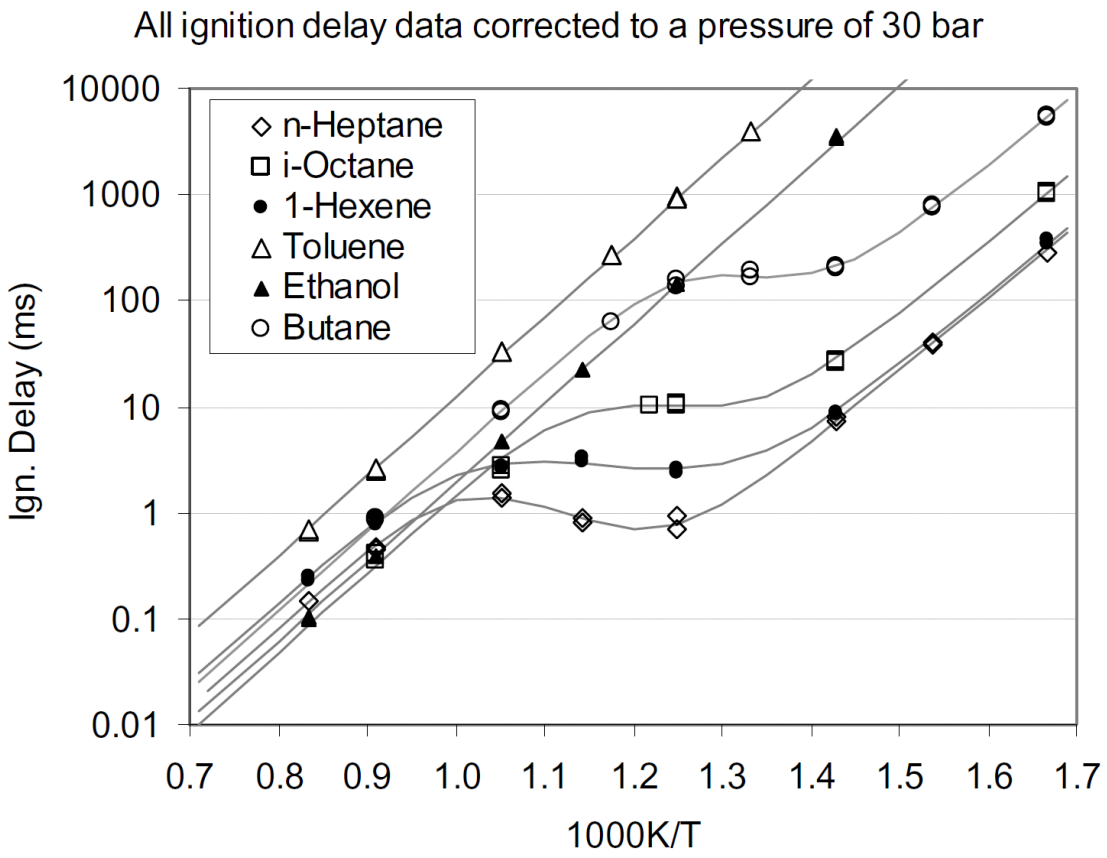

Figure 10 Stoichiometric ignition delays for different fuel molecules. Note that for all but aromatics and oxygenated fuel, intermediate temperature dependency exists, but at varying degrees. Figure reproduced from [53]

The results demonstrate a good overall synopsis of fuel decomposition: the largest least complex molecules (n-heptane in the figure) decompose the easiest and are the most reactive. These molecules also exhibit NTC behavior, and, as reviewed above, there are competing pressure sensitive reactions between intermediate and high temperature reactions. As the molecular configuration becomes more complex or smaller, the overall reactivity reduces, particularly with changes to the intermediate range and low temperature ranges. Notably aromatic and oxygenated fuels do not exhibit pressure dependency,

however it was shown in the earlier cited works that when these fuels are mixed with pressure sensitive fuels like n-heptane, their mixtures exhibit pressure dependency.

Based on these works it is seen that fuel composition and cylinder pressure can affect reactivity and combustion. In RCCI operation with moderate to high levels of ethanol/gasoline blends in-cylinder mixed with ULSD have demonstrated a reduction in NTC heat release by Splitter et al. [55]. Similar observations were previously observed by Hashimoto [56]. This study used n-heptane and ethanol blends in HCCI research to demonstrate that the low temperature heat release was reduced with the addition of ethanol. Later in [57], Hashimito used OH cemiluminescence observations to show that OH production with n-heptane/ethanol blends was reduced, suggesting that ethanol consumed OH radicals in the low and intermediate temperature reactions, thereby suppressing early heat release.

The pressure sensitivity of fuels becomes of greater importance in RCCI as higher engine loads and efficiencies are desired. For example, high pressure conditions typically exist at higher engine loads. Likewise, high pressure (dilution) is often used to suppress emissions and increase efficiency. Thus, these conditions may enhance pressure sensitive fuels reactivity more than is desired. This is not to say that operation with pressure sensitive fuels, like gasoline, is not possible at high loads and pressures, but the operable window or performance may be reduced.

Splitter et al. [37] has demonstrated that full load RCCI gasoline/ULSD operation with low emissions and brake efficiency similar to that of state of the art CDC (43%). However in those experiments, a reduced compression ratio of 12:1 was required to achieve 20 bar BMEP at rated speed (1800 rev/min). Splitter et al. [37] also demonstrated that operation with E85/ULSD enabled higher compression ratio (14.88:1) and more favorable operating conditions (higher intake temperature, lower EGR rate and turbocharger efficiency), resulting in estimated brake efficiencies as high as 48%. Based on these findings, if increased intake pressure or compression ratio is required to increase efficiency, operating conditions may be encountered where fuel reactivity is enhanced beyond that observed in the RON and MON tests. This unaccounted reactivity should be considered as it may result in altering the reactivity gradient.

2.3.2 Cylinder Gas Composition Effects

2.3.2.1 EGR Influence on Cycle Thermodynamics

In section 2.3.1 it was shown that like pressure, temperature, and fuel composition affects reactivity. Similarly cylinder gas composition can. Exhaust gas recirculation (EGR) is common in engines. EGR is a form of dilution, where excess non-participating chemicals are introduced in place of oxygen. This compositional difference has several effects. First, EGR has a notable effect on the ratio of specific heats (γ), as shown by Lavoie et al. [58].

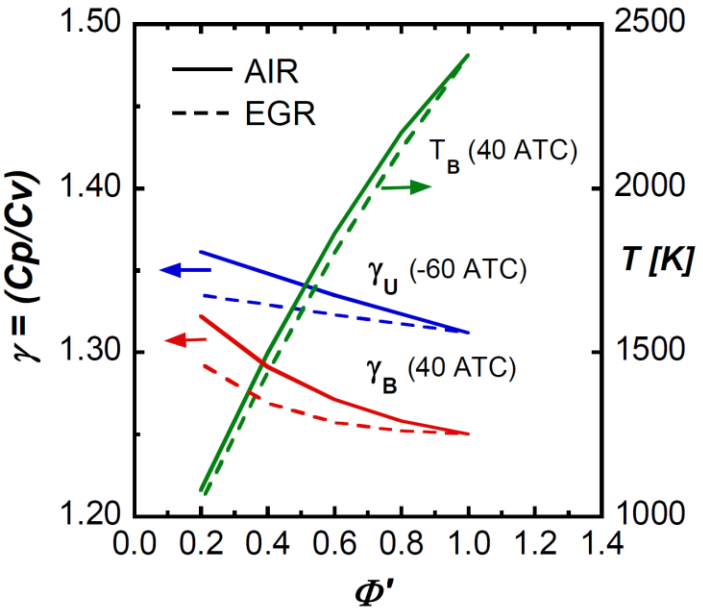

Figure 11 Effects of different diluent strategies on the ratio of specific heats (γ). Figure reproduced from Lavoie et al [58], where gas properties were evaluated as noted.

Figure 11 illustrates that the ratio of γ (γ_u/γ_b as denoted in the figure) is less favorable with EGR. This is important as the compression and expansion strokes of engines follow a polytrophic[‡] process. Thus, a reduced γ ratio leads to reduced expansion work (system work output, + work) for a given amount of compression work (system work input, - work). If high efficiency is desired, γ may provide a source.

For example, other research on the benefits of improved γ ratio by Szybist et al. [59] has shown that the higher molar product yield of ethanol may enable a more favorable γ ratio, enabling increased engine efficiency. Likewise Foster [60] has shown that reduced temperatures can increase γ, and correspondingly, efficiency. Although these two cited works examine the benefits of fuel chemistry

[‡] PV^{γ}=constant

and temperature on γ, these findings are universal to engines, as the polytrophic process is only sensitive to the magnitude of γ, not the source. Thus, when operating without EGR, the potential to increase engine efficiency is present.

2.3.2.2 EGR Influence on Fuel Kinetics

Besides the thermodynamic effects on the engine cycle, EGR has significant effects on chemical kinetics. To investigate this, fundamental relations were investigated from HCCI and shock tube data. The work by Vandersickel et al. [41], offers experiments and modeling of both air and EGR dilution on n-heptane and kerosene-like fuels. The results are presented in Figure 12, while the kerosene like fuel results are similar in trends to the work by Vandersickel et al. [41] in Figure 6, where more gasoline like fuels (Fuel B) exhibited longer ignition delay.

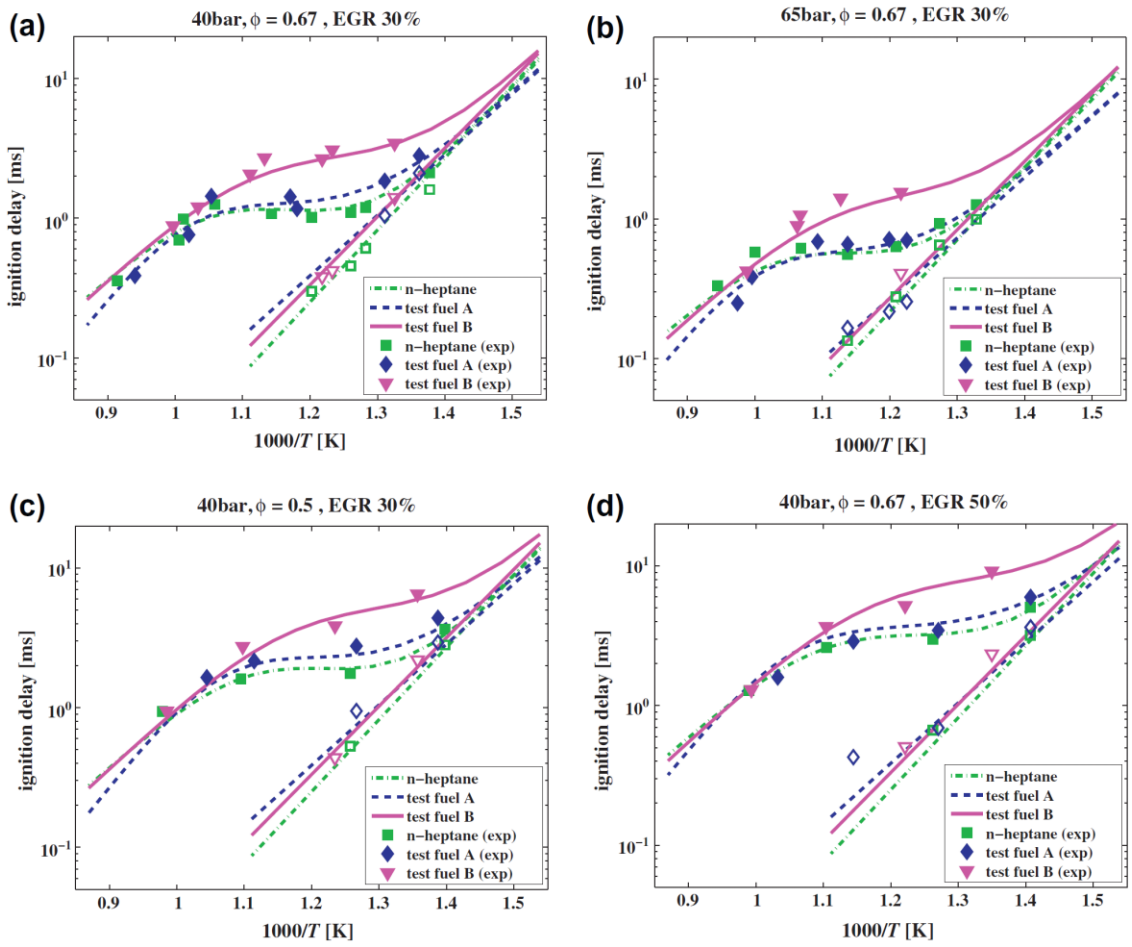

Figure 12 Effects of charge dilution on Ignition delay. (b) effect of equivalence ratio (air dilution) on ignition delay. (c) effect of EGR on ignition delay. EGR increases ignition delay more than air dilution (even in the presence of 30% EGR). Open markers denote first stage ignition delay, figure reproduced from Vandersickel et al. [41]

Figure 12 shows that for air dilution (sub-figures (a) and (c)), there is a difference in ignition delay, where leaner mixtures extend the intermediate chemistry timescale. It is seen that both air and EGR dilution (sub-figures (c) and (d)) offer increased ignition delay, with each potentially reducing the effect of NTC in the most reactive fuel, n-heptane. Vandersickel et al. [41] accounted for the effect that EGR dilution and charge dilution (Φ) has on ignition delay as seen in Equation (1)

$$\tau_i = A_i * \left(\frac{p}{p_{ref}}\right)^{\beta_i} * T^{\beta_i} * \exp\left(\frac{T_{A,i}}{T}\right) * \phi^{\gamma_i} * \left(\frac{[N_2]}{[O_2]}\right)^{d_i} * \exp\left(\frac{[N_2]}{[O_2]} * \frac{e_i}{T}\right) \; for \; i = 1,3 \quad (1)$$

This empirically derived relation shows that as the concentration of N_2[§] changes the ignition delay changes both exponentially and polynomially. Likewise, as the charge is leaned (Φ), the ignition delay is also changed, but unlike EGR, this effect is observed to only be directly proportional. The authors state that for EGR, the power term represents the effect of concentration, and the exponential term accounts for changes in the fuel temperature dependence within the intermediate temperature range. The results and correlation suggest that EGR has a magnified influence on ignition delay as opposed to Φ, thereby offering increased diluent effect.

This effect can be seen in Figure 12, sub-plot (c), (heavy EGR), in which the behavior of reactive fuels (n-heptane) is actually more gasoline like, which has less of a tendency to express NTC and more of a tendency to express intermediate temperature heat release (ITHR). Although the work by Vandersickel et al. [41] did not use physical EGR, similar findings were observed in engine tests in HCCI with real and simulated EGR. For example work by Söjberg and Dec [61] demonstrated that the chemical differences of EGR affect different types of fuel independently. In general, their work has consistently demonstrated that EGR is a key enabler of higher loads in HCCI.

Additionally, the findings of Vandersickel et al. [41] are applicable to fuels besides kerosene and diesel like fuels. Gasoline and gasoline-like fuels have

---

[§] In a shock tube environment, EGR is typically represented by nitrogen (N_2), thus this relation is only a function of the ratios of N_2 and O_2, since N_2 is the only diluent species (CSP not used)

been shown to exhibit increased ignition delay in the presence of EGR. Shock tube experiments by Gauthier et al. [62] demonstrated that high temperature kinetics are slowed in the presence of EGR. However, it is unclear if this effect was due to EGR having a more pronounced effect on intermediate temperature reactions, which, in-turn, may have affected the high temperature reactions. Figure 13 displays that for temperatures above 1000K, operation with EGR displays increased ignition delay.

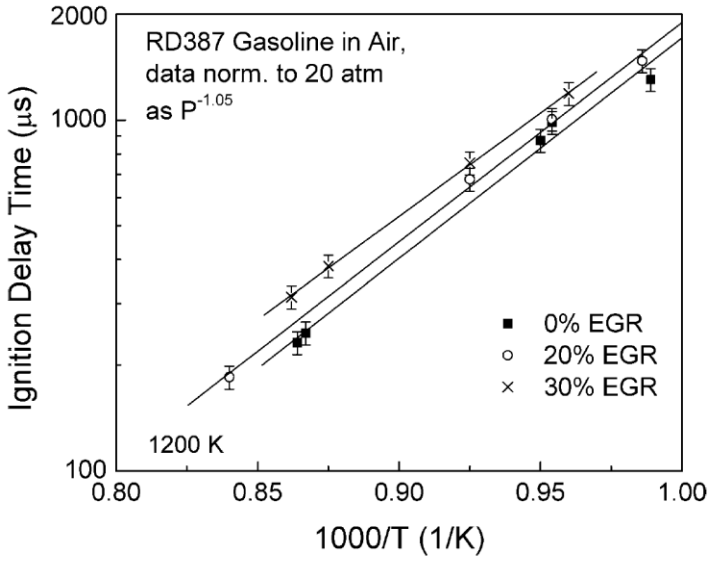

Figure 13 High temperature gasoline shock tube experiments with and without EGR. The findings demonstrate that EGR suppress ignition delay of high temperature gasoline kinetics. Figure reproduced from Gauthier et al. [62]

Although shock tube experiments are well suited for kinetic studies, they are not entirely representative of engine experiments. To explore fuel kinetics in engines, HCCI is a common strategy. HCCI engine experiments by Machrafi and Cavadias [63], demonstrated that with gasoline and n-heptane/isooctane/toluene gasoline surrogate fuels, EGR and Φ have a strong effect on the crank angle

delay between low and high temperature reactions (ignition delay). Thus, interpreting their data in Figure 14, the delay between low and high temperature reactions is increased with lean operation. This effect is exacerbated when EGR is added, in which levels of simulated EGR (N_2) above 21% vol. preventing HTHR from occurring.

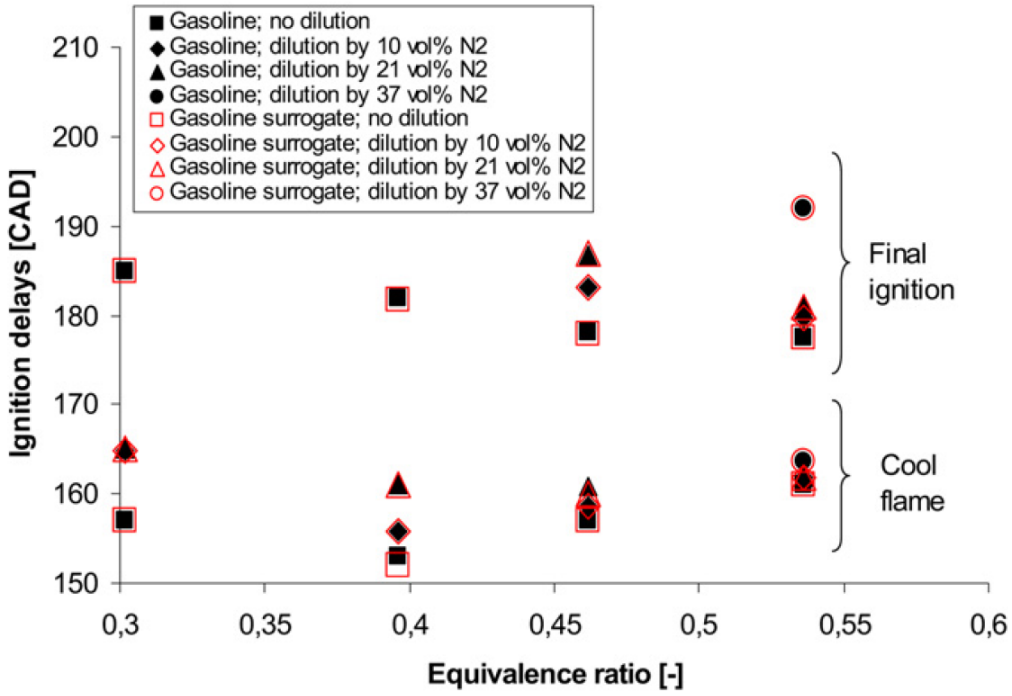

Figure 14 Gasoline and surrogate gasoline HCCI ignition delay as a function of equivalence ratio with varied EGR. In general as EGR or leaner conditions are encountered the crank angle of HTHR is phased later, and in the leanest operating conditions, only LTHR is observed. Figure reproduced form Machrafi and Cavadias [63]

These studies demonstrated that both air, and to a greater extent EGR dilution, have a noticeable effect on intermediate temperature reactions. These findings demonstrate a pathway to increasing the reactivity gradient in RCCI beyond that of pressure and temperature alone. When reactant gradients exist,

the presence of EGR and excessive dilution amplify the ignition delay of both the high and low reactivity fuels. This creates a modified gradient which, in turn, enables further staging of the ignition event. The longer ignition delay provides potential further control inputs for increases in load, speed, and efficiency. This is the reasoning behind introducing EGR into RCCI at higher engine loads, as it enables the opportunity to increase the reactive fuel fraction as the HCCI limit is suppressed by dilution.

2.3.3 Kinetic Literature Review Conclusions

Based on the presented works, EGR, Φ, fuel properties, pressure, and temperature have measurable effects on fuel decomposition, with particular importance in the intermediate reaction region. Additionally, gasoline and diesel-like fuels can behave similarly when exposed to higher pressure and/or EGR. However, with ethanol, or ethanol added to mixtures of these fuels, low and intermediate temperature chemistry heat release tendency was reduced. This suggests a pathway for tailoring the combustion event towards high efficiency operation.

2.4 Cetane Improvers

The previous section has discussed fuel reactivity. In CI engines, a common metric to define reactivity is cetane number (CN). This term is a measure of the ignition quality of a fuel. The definition of the cetane number is based on the behavior of the fuel relative to that of two reference fuels, n-hexadecane

(CN=100) and heptamethylnonane (HMN) (CN=15). Where the CN is defined as [64]

$$CN = (\%n\_hexadecane) + (.15 * \%HMN) \quad (2)$$

Although all fuels have a CN, fuels that resist auto ignition have lower CN (~15 typical of gasoline) while fuels that readily ignite have higher CN (~46 typical of U.S. diesel). The CN of the fuel depends on the fuel composition: the more reactive the components, the higher the CN of the fuel. Using this relation, the CN of a fuel can be synthetically modified through the addition or subtraction of highly reactive fuel species.

For example, the combustion behavior of HCCI engines has been characterized with an “HCCI index” by Shibata [65]. This relation expands on the octane (inverse of CN) relation developed by Kalghatgi [66], where Shibata’s modified relation accounts not only for the motor octane number (MON), but also the chemical bond structure of the constituent fuel species. The relation developed by Kalghatgi [66] is shown in Equation 3, where RON is the research Octane number, MON is the motor octane number, K is a constant that is dependent on temperature, pressure, and trapped residual, and S is the “sensitivity” of the fuel (chemical species dependent).

$$OI = (1-K)\,RON + K\,MON = RON - K \cdot S \quad (3)$$

The modified relation by Shibata in Equation 34 accounts for the individual species reactivity instead of the lumped parameter Kalghatgi classified as S.

$$\text{HCCI Index} = m \cdot MON + a[nP] + b[iP] + c[O] + d[A] + e[OX] + Y \quad (4)$$

Where m, a, b, c, d, e and Y are empirical constants, nP is the concentration of normal paraffins in the fuel, iP is the concentration of isomeric paraffins in the fuel, O is the concentration of olefins in the fuel, A is the concentration of aromatics in the fuel, OX is the concentration of oxygenates in the fuel, where the concentrations are in percent volume.

If a decrease in the HCCI index, and thus increased fuel reactivity CN, is desired, it can be accomplished through addition of fuel species that have easily broken bonds. Although normal paraffins have such qualities, chemical species with significantly weaker bond structures do exist and are often referred to as CN improvers. The weaker chemical structure of CN improvers often contain nitrate or peroxide groups. Two common CN improvers are 2-ethylhexyl nitrate (2-EHN) and di-tert butyl peroxide (DTBP). Only a small percentage of either of these chemicals is required to achieve significant increase in cetane number.

Regardless of the cetane improver used, the overall effect that CN improvers have on the overall fuel oxidation has shown to be insignificant. Higgens et al. [67] demonstrated that the addition of less than 1% (by mass or volume) of CN improver to diesel fuel dramatically shortens the ignition delay of the fuel. However, their findings also noted that, although the ignition delay decreased with the addition of CN improver, the combustion characteristics of the base fuel remained unaltered. This is important from a fuel kinetics standpoint,

and it demonstrates that the cetane improver simply lowers the activation energy of the base fuel, but does not affect other fuel chemistry.

Based on these findings it is useful to determine the reactivity enhancement provided by cetane improvers. To a specific extent, the cetane number of additized diesel fuel can be interpreted using the correlation by Thompson et al. [68], which is reproduced in Figure 15 by the EPA [69].

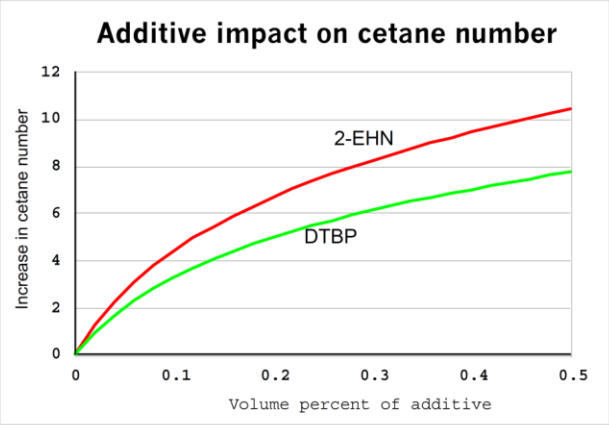

Figure 15 Cetane improver effectiveness in #2 diesel fuel as a function of volume addition. Figure reproduced from [69]

The presented correlation considers addition levels up to 0.5% by volume in diesel fuel. Shock tube research by Hartman et al. [70] shows that ignition delay of higher doping percentages of EHN in n-heptane are correlated as seen in Figure 16.

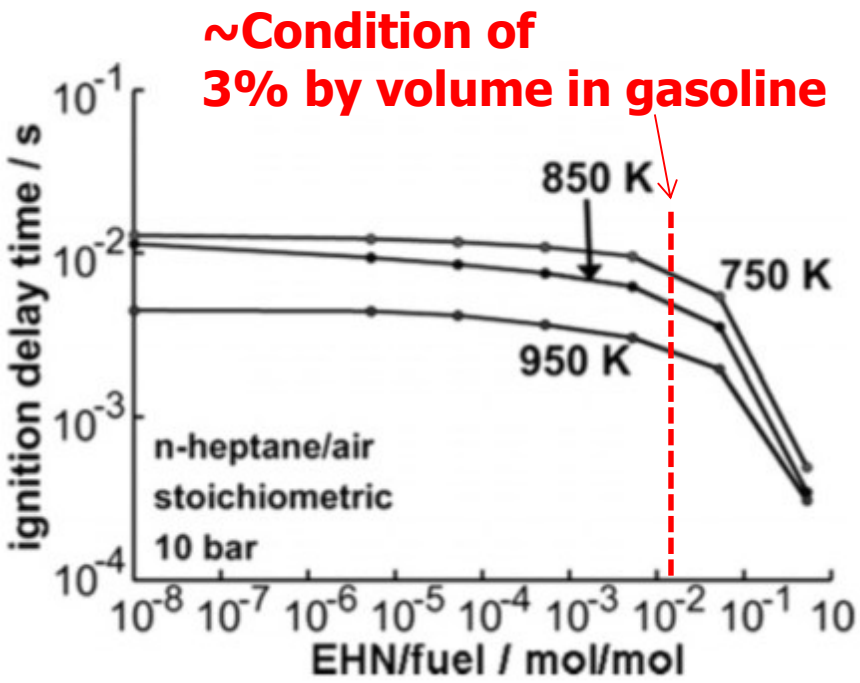

Figure 16 Simulated ignition delay times of EHN doped n-heptane as a function of EHN concentration. Figure reproduced from Hartman et al [70].

In the present research, some tests used 2-EHN doped into 91 PON gasoline at a fixed 3% by volume ratio, this addition is noted in Figure 16 by the dashed red line.

The cited studies have shown that 2-EHN is an effective cetane improver. In the present study a 3% addition by volume corresponds to a molar ratio of EHN to gasoline of 2.6% ($2.6*10^{-2}$), as indicated in Figure 16. This is near the rapid decrease in ignition delay time observed between 10^{-2} and 10^{-1}. The results of these EHN doping studies suggest that the reactivity (ignition delay) of EHN increases non-linearly, with ignition enhancement being very sensitive to EHN addition. Additionally, EHN may have un-desirable attributes to emissions. Work by Ikes et al. [71] has demonstrated that less than 1% of 2-EHN is an effective

enhancer in diesel fuels. However that research also demonstrated that the added nitrate group in 2-EHN increased NO_X emissions.

2.5 Engine Energy and Exergy Flows. Where are the Losses?

As described, engine efficiency is a major focus of present and past engine research. To analyze efficiency a first and second law approach can be used. That is, the energy or exergy flows/paths can be tracked. First and foremost, the source of energy or exergy is from the fuel itself. Fuel exergy depends on chemical composition, but for most fuels, it is roughly equal to the heating value of the fuel, a widely adopted approximation. Thus, the fuel path should be tracked to examine engine efficiency and the sources of losses. Several studies on the energy and exergy (availability) flows of internal combustion engine operation have been performed, with notable works by Caton on the availability destroyed in combustion [72] and from heat transfer [73]. In these works it was shown that the dominant losses consisted of incomplete combustion, heat losses, exhaust losses, and work losses. Remaining losses, from flows for example, were negligible compared to these other losses.

2.6 Availability Destruction with LTC

One of the most notable findings from these works, is that the availability destroyed (an inherent loss) increases at reduced combustion temperatures. Although the availability destroyed through combustion increases with leaner equivalence ratios and lower combustion temperatures, these losses compete with potential reduction in heat losses with lower temperatures. This can be

quantified either a load basis, as indicated by [74], or on a mixture (equivalence ratio) basis. This increase in inherent/unavoidable loss is in contrast with the desire to use lean mixtures to avoid NO_X and PM emissions formation in LTC. Thus, LTC strategies increase the availability destroyed associated with the combustion event itself. Caton described and presented this phenomenon as a function of equivalence ratio in [72], where, as seen in Figure 17, he calculated that approximately 15% or more of the fuel's availability was destroyed at LTC-like equivalence ratios.

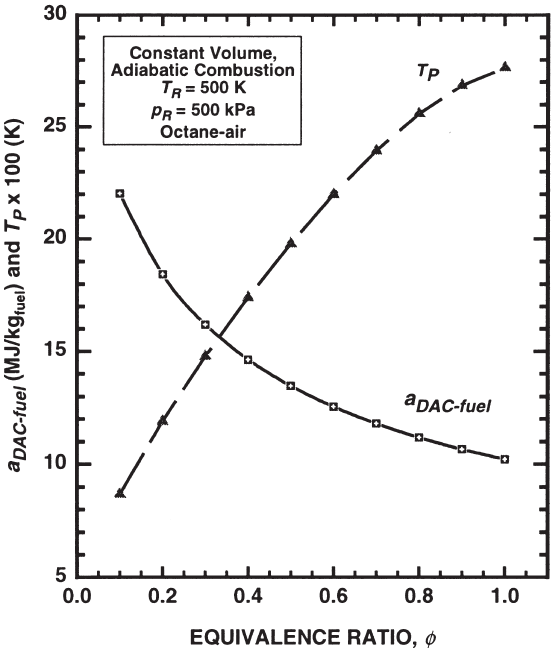

Figure 17 Combustion availability destruction as a function of equivalence ratio, and corresponding temperature, reproduced from [72]

Combustion availability losses are unavoidable and even at very high combustion temperatures a zero value is not reached (Caton [72]). Since combustion is present in the combustion engine, there are unavoidable losses. Efficiency gains

must be sought by reducing other losses. As described by Rakopoulos et al. [74], the availability of heat transfer is defined by Equation 5, where A_L is the availability lost, Q_L is the heat loss, T_O is the reference temperature, and T_{cyl} is the in-cylinder temperature (where φ is crank angle or time).

$$\frac{dA_L}{d\varphi} = \frac{dQ_L}{d\varphi} * \left(1 - \frac{T_o}{T_{cyl}}\right) \tag{5}$$

As shown by both Rakopoulos et al. [74], and Caton [73], the low temperature gradient between the cylinder internal/coolant temperatures (typically ~100-150°C) and the reference state (T_O ~25°C), for practical purposes results in 100% of this availability being destroyed.

In LTC, decreased combustion product temperatures reduce the driving potential for heat transfer, potentially offsetting the increase in availability destroyed during combustion. A study by Edo and Foster [75] has demonstrated that although the availability destruction increases at lean conditions, other losses, such as heat transfer and exhaust losses reduce, opening the potential for increased work extraction, and thus efficiency.

More recent general LTC overviews on the relations of sources of efficiency have been performed by Foster [60] and Edwards [76]. These studies have concluded that the increased availability destruction during the combustion of lean mixtures has the potential to be balanced or even offset by advantages in heat transfer and expansion work. This is the inherent relation that affords LTC strategies the ability to lend themselves to simultaneous reductions in emissions

and increases in engine efficiency. The combustion event itself has higher losses, but when constrained to the engine cycle the resulting losses tend to be lower. This demonstrates that the combustion event and the engine cycle must not be decoupled in the quest for high efficiency, and should be addressed in unison to obtain maximum benefit.

2.6.1 Availability Flow with Low Heat Rejection

Similar to operating with low temperatures, the overall availability destruction can be reduced by operating with internal engine insulation. These concepts are typically classified as low heat rejection (LHR) engines. Although effective in turbine engines, historically their durability in piston cylinder engines has been unacceptable for production environments. Regardless of their present merit on longevity, their concept provides an alternative approach to increase engine efficiency. Previous research and second law analysis of insulated engine operation was performed by Primus [77] and Rakopoulos et al. [74], as seen in Figure 18.

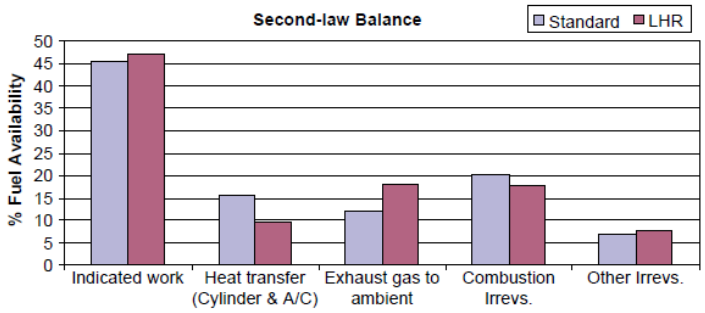

Figure 18 Fuel availability flow for standard and LHR engines. Note the shift in availability to the exhaust and increased work with the LHR design, reproduced from [74].

As seen by the figure, the LHR engine demonstrated that not only can the work output be increased, but also that the availability flow can be shifted from heat loss within the engine (availability destroyed) to heat loss in the exhaust stream. If there must be exergy flows that are not work, then exergy in the exhaust is much more preferable because there are available extraction technologies like turbochargers or even bottoming cycles [78, 79] that could be used to further extract work from the fuel external to the cylinder. This shift in losses is particularly useful for LTC strategies, as their dilute operation often requires high levels of boost, where use of internal engine insulation may improve exhaust work extraction and expand engine power density.

Also, Primus et al. [77] noted that insulating the engine results in reductions in the exhaust manifold pressure, and thus the turbine pressure ratio. Therefore, for a given trapped mass the required backpressure is reduced with an insulated engine, decreasing the pumping losses. Primus noted that this effect more than offsets the potential of reduced volumetric efficiency (VE) that can be present with an insulated engine [74, 77]. Since pumping losses could be significant in low temperature combustion regimes, as suggested by Chadwell et al. [16], insulating the internals of the engine combustion chamber may be of interest. Moreover, the potential of increased internal gas temperature with an insulated engine can decrease the availability destroyed [73]. However if NO_X emissions are to be minimized, temperatures should remain below approximately 2000 K [12, 80]. Therefore, the insulated engine may increase NO_X emissions in

LTC thereby defeating some of the emissions benefits, but may still avoid the formation of soot due to the overall lean equivalence ratios.

2.6.2 Availability Flow with Nontraditional Engine Strategies

To simultaneously combat the dilemma of availability destruction from combustion and heat transfer, non-traditional engine architectures have been proposed. Teh et al. [81] focused on engine concepts that are not constrained by a traditional slider crank mechanism and noted that optimizing engine efficiency can be addressed through minimizing the exergy destruction in combustion. It was shown that combustion availability destruction could be tracked and minimized by examining only the start and end states of the combustion process. This means that the more complex kinetic path taken (combustion thermodynamics) need not be solved for. The highest efficiencies were found to be at elevated internal energy states (high temperature). Furthermore, this work suggested that cycles like the Otto/ideal cycle, which are separated into non interacting compression, reaction, and expansion processes, maximize the engine efficiency potential.

More recent fired engine follow up work by Miller et al. [82], suggested that engines with extreme compression ratio may provide increased efficiency because the ratio of work availability to combustion destroyed availability increases, as indicated in Figure 19.

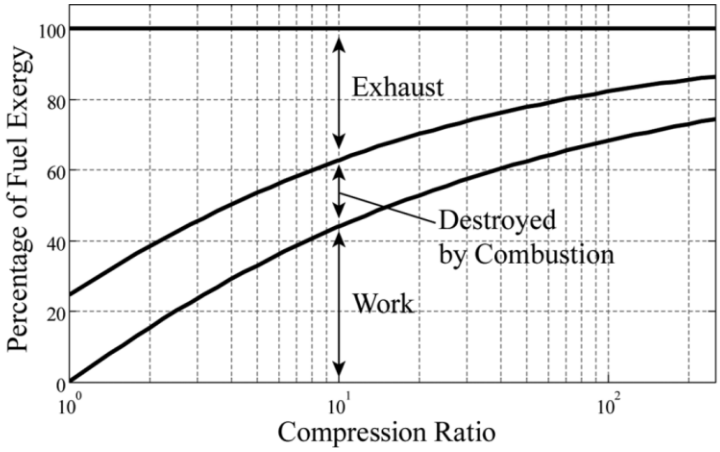

Figure 19 Distribution of fuel availability for the Otto cycle with stoichiometric propane. Note the increase in work relative to losses as compression ratio is increased, reproduced from [82]

In the above work, a free piston engine was examined because that design reduces the time for heat transfer as the rate of compression and expansion are increased. Although the proposed engine concept ass mathematically and thermodynamically eloquent, practical application is more challenging, requiring significant development with unknown potential issues. Blarigan [83], computationally investigated HCCI in a free piston engine and more recently attempted to experimentally demonstrate free piston engine techniques [84]. This work demonstrated that significant technical hurdles must be addressed in the implementation of such non-conventional engine architectures.

2.7 Low Heat Rejection Strategies

2.7.1 Engine Coolant Temperature Strategies

In practice, there are several strategies to reduce heat transfer; however each has strengths and weaknesses. Strategies may be as simple as increasing

coolant and oil operational temperatures; however any gain is typically limited by longevity concerns and practical working pressures. Although coolant temperature changes are a relatively practical approach, the net gains are low, as suggested by Edwards [76]. These are supported by conventional diesel experiments by Burke and Brace [85], which have demonstrated the trends observed in Figure 20.

	Operating Point 1			Operating Point 2		
Coolant temperature	**Gross IMEP**	**PMEP**	**FMEP**	**Gross IMEP**	**PMEP**	**FMEP**
50	3.97	0.34	1.94	N/A	N/A	N/A
70	3.83	0.32	1.91	11.24	0.12	2.02
86	3.90	0.29	1.91	11.18	0.14	1.94
98	3.88	0.31	1.87	11.18	0.12	1.96

Figure 20 MEP values for CDC operation at low load (Operating Point 1) and higher load (Operating Point 2). Coolant temperature was swept, and observed MEP trends are shown. It was found that reduced coolant temps. may actually increase engine efficiency, as it simultaneously reduced EGR temps.. Figure adopted from Burke and Brace [85].

The findings indicate that the engine system as a whole must be considered. In practice, the coolant system is integrated into the engine and EGR loop, thus coolant temperature changes affect the engine and EGR conditions. The results in Figure 20 depict that the coupling of engine and EGR conditions creates a more complex system to optimize than the engine alone, where at some conditions colder coolant conditions can improve gross IMEP (i.e. efficiency). Based on these results in combination with the kinetically controlled combustion process, such as RCCI, added complexity will likely exist if coolant temperatures are adaptively changed for reducing heat transfer.

2.7.2 Thermal Barrier Coatings

Another method to reduce engine heat loss is to apply thermal barrier coatings to the combustion chamber. Thermal barrier coatings (TBC) have been a topic of much scientific and engineering interest worldwide for several decades [86-88]. These coatings are typically ceramic powders that are plasma sprayed or deposited over metal substrates. The coating properties offer a high thermal resistance and diffusivity, low density, similar thermal expansion to the base material, and are easy to apply to complex geometries. Initially developed for the aviation industries, these lightweight robust coatings enable an increase in combustor and turbine fan exhaust gas temperatures, thus increasing turbine engine efficiency, and engine longevity for aircraft and stationary applications [89].

Although thermal barrier coatings have been vital to the advancement of internal combustion turbine engines, the environment of piston cylinder engines is quite different. Specifically, the piston cylinder engine has a much higher frequency of cyclic loading. Turbine engines are only cyclically loaded upon cold startup, but piston cylinder engines are thermally and barometrically loaded every or every-other cycle (2 or 4 stroke cycles, respectively). These less steady conditions require different coating properties. Interesting work by Hoag et al. [87] demonstrated that a 1.5 mm total coating thickness consisting of a 0.1mm bond coat of NiCrAlY with a 1.4 mm thick yttrium-stabilized zirconia (YSZ) top layer, was insufficient to survive short-duration tests in a high-output diesel engine at 13.8 bar BMEP. Moreover, extensive trial-and-error development

efforts using plasma- sprayed zirconia coatings did not result in acceptable or reproducible coating lives [90].

To investigate and improve upon these findings, research sponsored by the Department of Energy/National Aeronautics and Space Administration (DOE/NASA), and U.S. Army Tank Automotive Command (TACOM) was awarded to Cummins in the mid-1980s [91]. The goal of this research was centered on improving coating lifetime by understanding the stresses in the TBC, ultimately improving the lifespan of these coating in diesel engines [90].

It was found through both experimental and computational efforts that although the internal stresses of the zirconia based coatings were below the failure/fracture level under sustained operation, the transient response of these coatings was not. Failures occurred because of the much lower thermal diffusivity[**] of the zirconia material than the base metal, increasing surface temperatures by up to a calculated 225°C greater than uncoated operation. Furthermore, the thermal wave was calculated to penetrate only 0.13mm into the material, which, with thick coatings, results in high temperature gradients within the coating, potentially causing tensile-based failure upon repeated use.

These findings have more recently been experimentally validated engine experiments on select materials by Ramaswamy et al. [92]. That work scanning electron microscope (SEM) images of the surface and cross sections of cyclically loaded coated pistons showed that the cyclic environment of piston cylinder engines can grow micro cracks in the coating. It was found that this failure

[**] $\alpha = \frac{K}{\rho * C}$ where α is thermal diffusivity, K is thermal conductivity, C is capatance, ρ is density

mechanism does not result in a de-lamination of the coating, but it does deteriorate the performance. The formation of crack is attributed to the relaxation stress difference between the coating and the base material.

These tests have shown some promise for coating use in conventional diesel combustion where fuel and air are heavily stratified and no fuel is premixed in the chamber prior to ignition. However, the benefits of thermal barrier coatings in premixed environments have been shown to not necessarily be positive. Thermal barrier coatings were investigated in HCCI engine operation by Hulquit et al. [93] where various thermal barrier coatings and thicknesses were tested. The work showed that the coatings were effective at increasing in-cylinder temperatures, but, except for thin coatings of aluminum oxide, the porosity of thermal barrier coatings can increase the emissions of HC and CO, with all coatings underperforming in efficiency as compared to the uncoated piston.

In contrast, it has been demonstrated that deposits in HCCI engines by [94 and 95], behave similar to TBC coatings. The findings of these works were that the thermal conductivity of deposits, measured using the findings in-situ method described by Hopwood et al. [96], were similar to that of TBCs. In the work [94], an increase in HC and CO was not observed, where chamber deposits were actually seen to decrease HC emissions. The works show that even if thermal barrier coatings offer a similar insulating effect as combustion chamber deposits, they can result in efficiency reductions. These are likely due to porosity in the coating, as suggested by SEM images by Ramaswamy et al. [92], effectively offsetting potential thermal insulation gains.

Based on a review of these works it has been shown that thermal barrier coatings offer potential to reduce engine coolant heat losses. However, the selection of a coating for a piston engine has different criteria than that required in a turbine engine. Additionally, coating porosity may be an important factor in premixed combustion regimes, wherein the potential for increased incomplete combustion may offset efficiency gains from heat transfer. These factors make selection and the performance of a coating somewhat ambiguous, opening the potential for decreased engine performance. An alternative approach is to increase in-cylinder temperatures through reducing in-cylinder cooling.

2.7.3 Piston Oil Gallery Spray Cooling Modulation

In modern diesel engines, particularly in HD applications, one of the major sources of in-cylinder cooling is through piston oil gallery cooling. In CDC, high local temperatures are present at or near the piston surface. This leads to significant piston heat input. The piston can only transfer heat away through the oil, which without direct spray cooling, is through the piston rings accelerating engine wear. To increase the engine lifespan, most modern CDC applications have employed oil spray gallery cooling, where a jet of pressurized oil is directed into a channel inside the piston. The oil is used to cool the piston crown and remove heat from the ring-linear interface, a wear point. Piston heat flow with different cooling strategies has been shown by Kajiwara et al. [97], with key findings form the work in Figure 21.

Piston Cooling Structure		Spray Cooled Type	Oil Jet Type	Cooling Gallery Type
		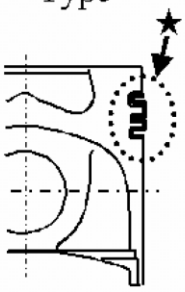	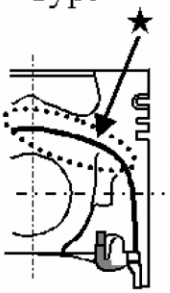	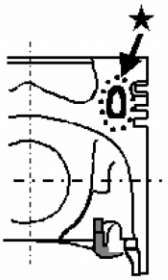
Heat Input	Combustion Bowl	100%	100%	100%
Heat Dissi-pation	Ring Belt	★ **60～70%**	30～40%	10～20%
	Backside of Crown	20～30%	★ **40～50%**	～10%
	Skirt	10～20%	～10%	～10%
	Cooling Gallery	—	—	★ **60～70%**

Figure 21 Various Piston cooling strategies and the relative distribution of heat loss associated with each. Figure adopted from [97].

The results show that by jet gallery oil cooling, approximately 2/3 of the piston crown heat is rejected directly to the oil. This cooling extends the engine lifespan by reducing ring and linear wear, an important factor for engines that are designed to operate over one million miles. Additionally, it enables higher engine loads and BMEP through reduced surface ring/linear interface temperatures.

Compared to spray cooled pistons (indirect oil mist in crankcase), direct oil gallery cooling is quite effective at removing heat. Recent in-cylinder work by Luff et al. [98] showed that piston surface temperature increases dramatically when the oil gallery jet is turned off. For instance Figure 22 below depicts an average of ~50°C rise in piston surface temperature for a light-duty CDC engine operated at a mid-load and speed point.

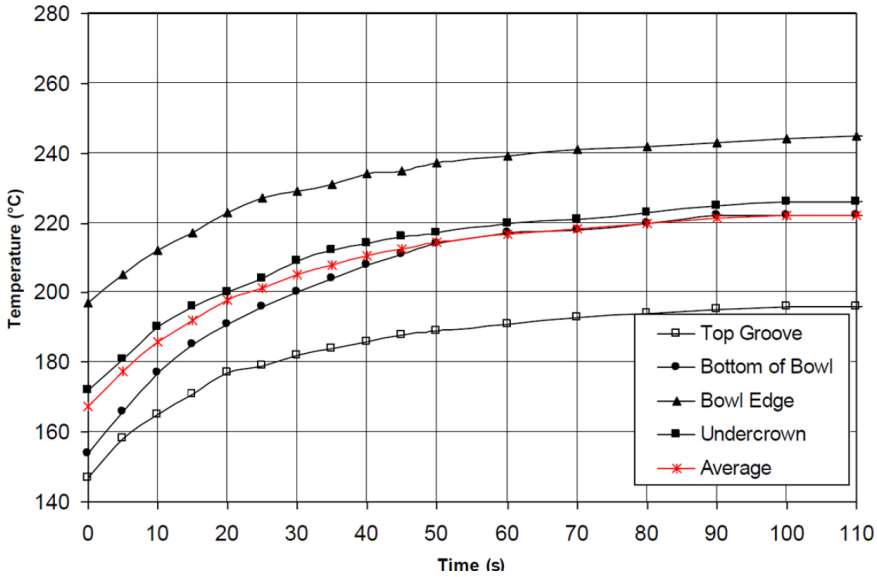

Figure 22 Transient piston surface temperature-time response to eliminating piston oil gallery cooling at a mid-load and speed LD CDC engine. Figure reproduced from Luff et al. [98]

Luff et al. [98] also showed that when the piston oil gallery cooling was turned off, the cylinder liner temperature correspondingly increased, although the increase was only a few degrees centigrade. Figure 23 illustrates the measured liner temperature trends.

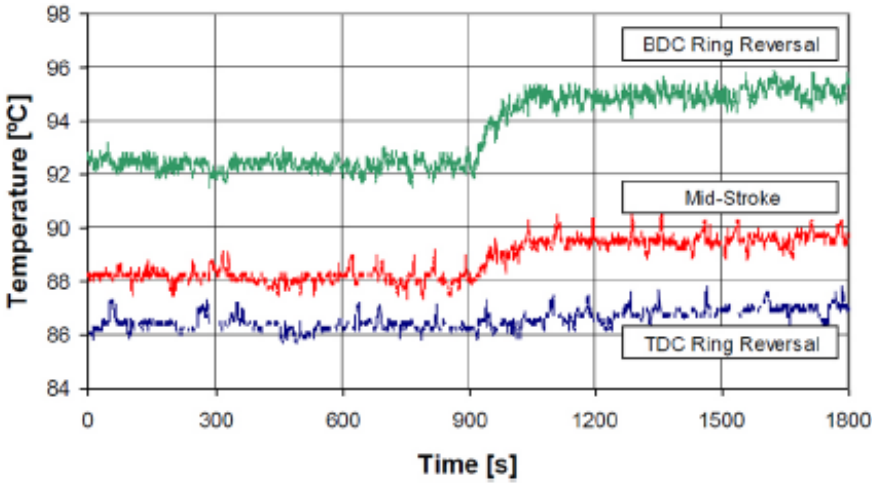

Figure 23 Transient cylinder liner surface temperature-time response to eliminating piston oil gallery cooling at a mid-load and speed LD CDC engine, cooling turned off at time of 900 (s). Figure reproduced from Luff et al. [98]

This study clearly demonstrated that the piston surface temperature significantly increases with a minimal increase in piston-liner interface temperature when there is not piston oil gallery cooling. Additionally, the study also showed that the emissions of CO reduced 5-10% and NO_X increased 3% when cooling was turned off, suggesting higher in-cylinder temperatures. These trends provide evidence that the piston oil galley cooling may be excessive, and effectively be over-cooling the piston at loads below that of full-load. The result is that below full-load operation, oil galley cooling increases losses from incomplete combustion and heat transfer.

One additional note was that the gross efficiency gains realized in the work by Luff et al. [98] were not without realized without increases in oil pump work. As the piston oil cooling was turned off, oil temperatures decreased increasing viscous losses, effectively offsetting gross and net efficiency gains. It was suggested that these additional friction losses may be eliminated through a variable displacement oil pump, which is much simpler and practical to implement and operate than a TBC or variable coolant control strategy.

2.8 Knock Effects on Heat Transfer

Similar to the oil gallery cooling results, knock can affect engine heat transfer. Schlieren experiments such as those by Lyforde and Heywood [99] have demonstrated that in SI engines there typically exists a ~1mm thermal boundary layer which insulates that engine from heat transfer. More advanced laser based measurements have also been made in non-combusting HCCI by Dec et al.

[100], where a similar finding has been found. This insulating layer provides reduced heat transfer. However, when post-combustion pressure oscillations exist, the effectiveness of this insulation can be compromised.

For example Lu et al. [101] saw that in-cylinder heat flux linearly increased with pressure oscillation amplitude, starting at values as low as 5 bar. Further, the increase in heat transfer was confined to knocking regions (peripheral chamber areas). Similar findings by Syrimis et al. [102] demonstrated that heat flux from knocking zones is often double that of non-knocking zones.

In-cylinder diagnostics techniques have been used to understand the sources of these increases such as the use of Coherent Anti-Stokes Ramen Spectroscopy (CARS) by Grandin et al. [103]. Their results supported the previous researchers findings and suggested that in knocking conditions, the thermal boundary layer may be as thin as 0.5 mm. This demonstrates that with knocking conditions boundary layer thinning occurs, simultaneously resulting in increased local near wall temperatures. They also found that the corresponding heat flux was proportional to knocking intensity (amplitude of pressure oscillation), where their findings are seen in Figure 24.

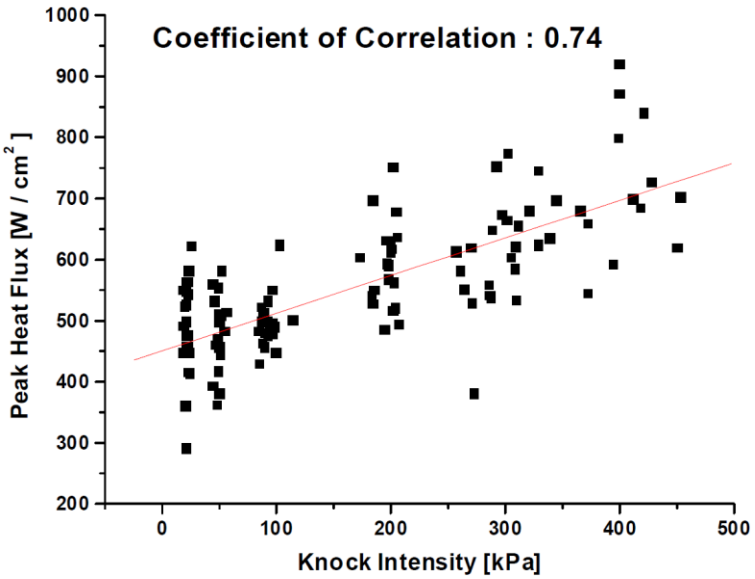

Figure 24 Peak heat flux as a function of knock intensity for stoichiometric SI combustion. Figure from Grandin et al. [103].

These experiments on knocking were investigated in near stoichiometric mixtures. However, Grandin and Denbratt [104] conducted similar CARS experiments from slightly leaner mixtures (λ=1.3, Φ=0.77) to slightly richer mixtures (λ=0.84, Φ=1.19) showed that at equal knock intensities, the mixtures adiabatic flame temperature tracks with peak heat flux rate. That is, leaner charges demonstrated reduced peak heat flux rates. This demonstrates that local temperatures play a key role in reducing engine heat transfer, even in knocking conditions.

The authors elaborate that reduced gas temperatures are only part of the reason for heat transfer losses. Heat transfer is reliant on a difference in temperature combined with the ability to transport thermal energy from hot to cold. In gasses this transport relies on convection, which is a function of the gas properties and motion. The influence of gas properties is likely to be minimal as

the gasses from knock are similar in composition and temperature to gasses from non-knocking conditions. Therefore, charge motion combined with a difference in gas-to-wall temperature is key to understanding and controlling engine heat transfer.

The higher charge motion present in higher intensity knocking and oscillatory pressure behavior can sufficiently increase local convection resulting in a measurable effect on engine heat transfer. For HCCI and RCCI, the effects of knock become more global, as knock occurs throughout more of the chamber than in knocking SI. However, if conditions are sufficiently lean, reduced in-cylinder gas temperatures mitigates the driving potential of heat transfer, potentially offsetting increases in convection from knock.

2.9 Literature Review Conclusions

These reviewed works demonstrate that LTC strategies offer a pathway for simultaneous emissions and efficiency improvements. LTC concepts are likely to have more production possible than LHR and free piston designs, as these designs require unique unproven hardware/technology. However, LTC strategies face hurdles of their own; the present study aims to build on the reviewed historical works by investigating the pragmatic limits of the LTC strategy RCCI through engine experiments coupled to zero-dimensional cycle simulations. The goal is to demonstrate the highest possible gross efficiency and to better understand the sources and sinks of gross efficiency in RCCI.

CHAPTER 3 Modeling Details

Prior to engine experiments, computational tools were used to explore the conditions that may provide increased engine efficiency. Their ease of use and reduced search time can be helpful in quickly establishing operating conditions and limits. Although state of the art multi-dimensional computational fluid dynamics (CFD) codes coupled to chemical kinetic solvers are generally the best for simulating engine operation, as they solve for both the chemical reaction and thermodynamic cycle, they introduce the complexity of solving the mixture properties in conjunction with correct local kinetics. If there are errors in either, or their combination, the simulation results can be inaccurate. Thus, the use of multi-dimensional simulation tools as an a-priori guidance tool introduces the potential for misleading results.

To improve both the generation speed and overall trends of the computational results, less complex zero-dimensional codes can be, coupled to experimental data. This approach provides useful guidance in solving the thermodynamics of the engine cycle, which can easily suggest conditions that may increase engine efficiency. However, it is critical to understand that the assumption of a combustion profile from an experiment at one condition is only valid at that condition. Changes to the heat release are not accounted for when decoupling the combustion event from the engine cycle initial conditions. Thus, the solution generated by the code should only be used as a tool for guiding a pathway only, and not as an absolute accurate solution.

3.1 Zero Dimensional Engine Modeling for High Efficiency

Several past researchers have shown that cycle simulation can be as simple as a wireframe heat release, as demonstrated by Paterson and Hampson [105]. However, in practice it is more common to use a first principles approach, such as that cited by Herold et al. [106], in their work on opposed compression ignition engines. Recent zero-D simulation work by Caton [107] has also demonstrated that a combination of factors must be used to advance engine efficiency, and that the primary factors are burn duration, phasing (represented by EGR), dilution, and compression ratio. Figure 25 was reproduced from this study.

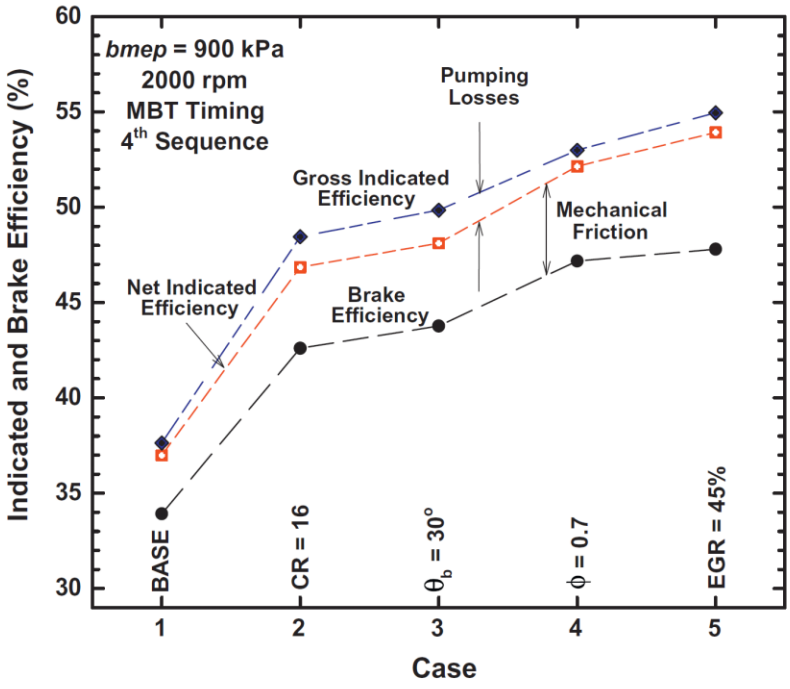

Figure 25 Figure reproduced from Caton [107] where zero-dimensional simulation work was conducted to determine pathways for increased engine efficiency; base condition is a simulated SI engine with 8:1 Cr, 0.71 L/cyl, 9 bar BMEP 2000 rev/min. Note that the largest gains were offered through increased compression ratio, and dilute operation.

In the present study, the zero dimensional commercial code GT Power by gamma technologies was used to suggest conditions for increasing RCCI engine efficiency. The pathway and logic used in the simulation exercise was suggested by literature. For example, a recent advanced combustion GT Power study by Lavoie et al. [58] has suggested that lean operation without EGR could offer the highest improvements to gross efficiency. Results from that study are depicted in Figure 26 where the trends are plotted as a function of Φ′. When operating with EGR it is useful to use a common axis. A common way to do so is to redefine Φ to be charge based as in Equation 6.

$$\Phi' = \Phi * \left(1 - \frac{EGR\ (\%)}{100}\right) \tag{6}$$

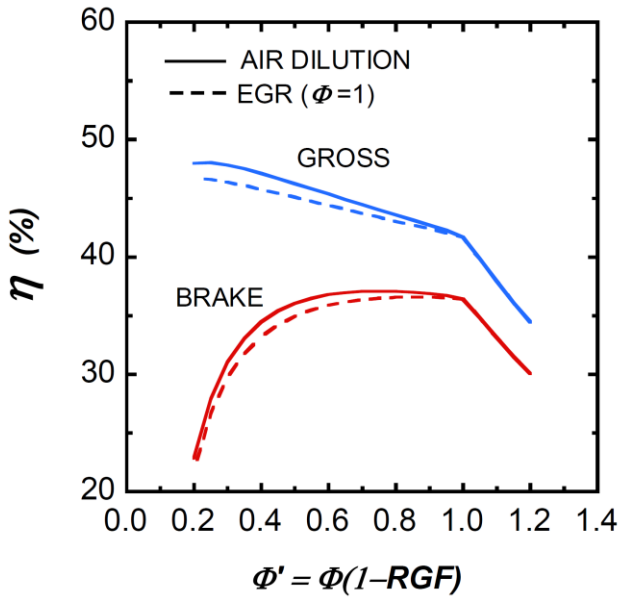

Figure 26 Lean operation is observed to have a significant effect on gross efficiency, with very lean operation negatively effecting brake efficiency through increased pumping work. Figure reproduced from Lavoie et al. [58].

However, as the figure displays, at the highest gross efficiencies, pumping increases work may occur, thereby decreasing brake efficiency. This presents

the efficiency paradox, where optimization of one definition may provide mutually exclusive results to others. In practice: maximum brake efficiency is desired, yet is the most complicated to optimize because it accounts for the entire suite of engine interactions. Zero-dimensional simulation predictions by Chadwell et al. [16] allude to the potential that optimized gross efficiency may produce reduced brake efficiencies.

The study by Lavoie et al. [58], also investigated brake efficiency, as shown in the reproduced results in Figure 27.

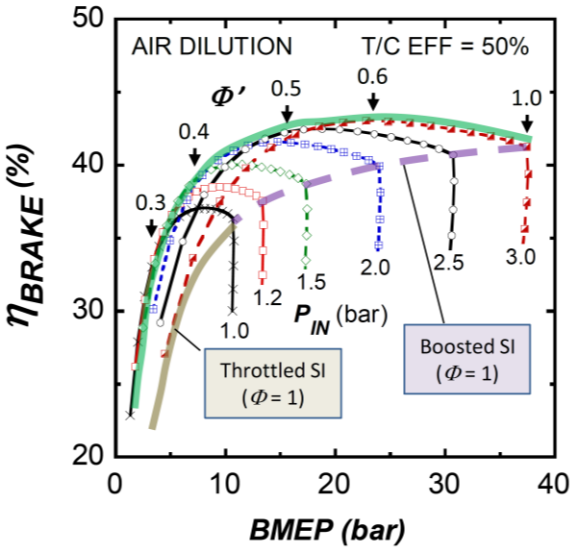

Figure 27 Curve of optimal brake efficiency for 50% combined turbocharger operation. Note that higher loads require charge enrichment and tend to deviate from LTC operation to conventional combustion strategies. The richer operation is required to mitigate increases in pumping losses associated with LTC strategies at high engine loads. Figure reproduced from Lavoie et al. [58].

This figure demonstrates that to maximize brake efficiency from low to very high loads, a shifting charge-based equivalence ratio (Φ′) may be required. If efficiency is approached in this manner, it will likely require shifting combustion regimes. For instance in the leaner conditions, auto-ignition or stratified mixture

approaches must be used, because fully homogeneous SI combustion is impractical or impossible. However, as the charge is less dilute, autoignition strategies become impractical due to high pressure rise rates, potentially requiring the necessity to shift combustion regimes. The linchpin in the contributing factors to combustion enrichment and thus, combustion regime shifting, is engine air handling.

3.2 Air Handling in Dilute Combustion Strategies

The inability of production turbocharger systems to effectively supply charge dilution at high flowrate conditions with low exhaust enthalpy increases engine pumping losses. Although superchargers can be used to provide boost, they do not operate on rejected heat (as turbochargers). In practice, even with high production-possible isentropic efficiency near 75%, a supercharger's increase in engine friction outweighs their pumping benefits at almost all engine conditions.

For example, simulation work in lean HCCI by Mamalis et al. [108] demonstrated that supercharged lean engine brake performance was worse than turbocharger performance. However, the net efficiency with supercharged performance was improved because the pumping loop was actually positive pressure, increasing IMEPn. This study demonstrates that in lean conditions it is highly unlikely that pumping losses can be offset by use of supercharging, as supercharging increases friction more than its associated reduction in pumping. Figure 28 illustrates that study's findings on fuel consumption.

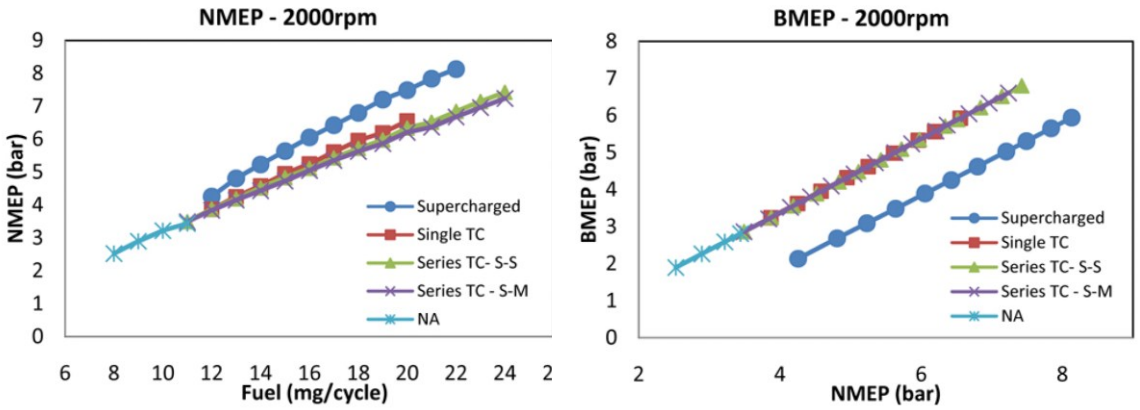

Figure 28 Zero-dimensional cycle simulations from Mamalis et al. [108]. The findings show that the higher IMEPn (right) associated with supercharging is more than offset by additional FMEP, resulting in reduced BMEP and thus efficiency. Figure reproduced from [108].

A potential optimum may exist by augmenting turbocharger operation with a supercharger. By clutching a supercharger or using an electrically driven process such as that suggested by George et al. [109], an improved brake efficiency may be possible. However, these strategies require detailed optimization to avoid potential increases to losses.

Although the air handling system is the key to high brake efficiencies, it has a reduced effect on gross efficiency. Figure 29, illustrates this through the assumption of perfect boosting (i.e., exhaust pressure=intake pressure).

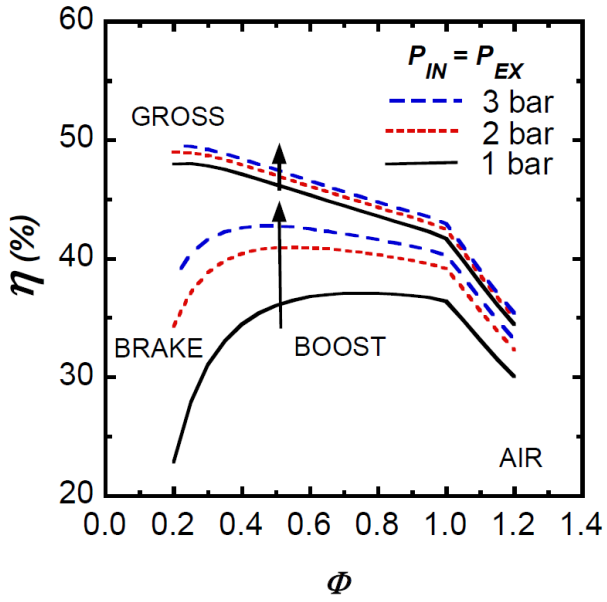

Figure 29 Relative effect of "perfect" boosting on gross and brake efficiencies. Note that "perfect" boosting has a greater effect on brake than gross efficiencies, as it affects both the pumping and heat transfer losses in brake, and only heat transfer in gross. Figure reproduced from Lavoie et al. [58]

The figure shows that the magnitude and equivalence ratio of gross and brake efficiencies become more similar with both occurring at very lean conditions. Thus, an approach of optimizing for the highest possible gross efficiency enables a pathway for improved brake efficiency with future technological advances in air handling.

3.3 Application to RCCI

The presented works show that a maximum in efficiency requires the selection of a definition of efficiency. In practice, maximum engine efficiency conditions of gross, net, and brake are often mutually exclusive. For actual engine operation, brake efficiency is of utmost importance as it is the result that is desired from the engine. However, in maximizing brake efficiency net and gross results hold

importance, as their results ultimately lead to the brake performance. In the present study, experiments on a single-cylinder research engine are performed. This tool is best suited for net and gross efficiency measurements, thus presenting a choice that must be made in defining a method for maximizing efficiency.

As shown in the cited works, the air handling system becomes important particularly as the charge is leaned out. However, if gross efficiency is used, efficiency is only a function of the combustion event and its associated losses. Thus, if one assumes that the charge can be delivered to the engine at a given condition (i.e., the turbocharger efficiency is fixed), the corresponding tradeoffs in gross efficiency become more evident. Therefore, from a fundamental approach, it is most useful to begin with gross efficiency, and to apply an assumed air handing system that can deliver the charge to the engine. This approach is used for defining efficiency in the present research.

For instance, one can achieve a certain gross efficiency, assume the associated losses, and see the effect that this would have on brake results. This was performed using Equation 7 in the results shown in Figure 30. For the department of energy (DOE) goal of +50% brake thermal efficiency (BTE), the gross efficiency and associated loss requirements are evident.

$$BTE = GIE * \left(1 - \frac{PMEP + FMEP}{IMEP_g}\right) \tag{7}$$

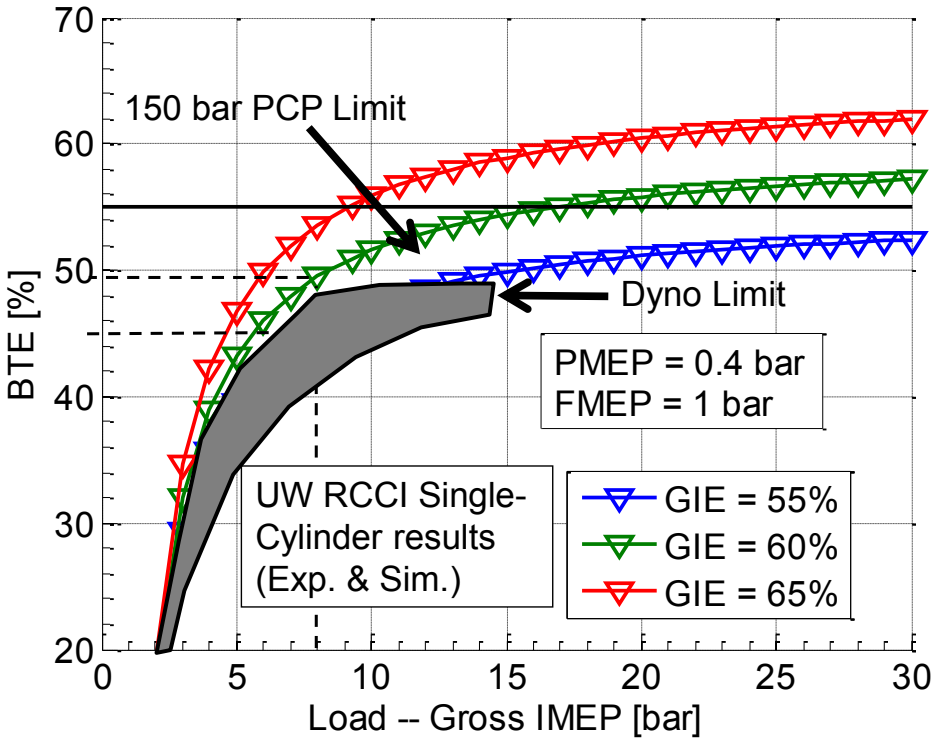

Figure 30 Generalization of performance and trends required to achieve DOE goal of +50% BTE. Assumptions: No waste heat recovery PMEP=0.4, FMEP=1.0, GIE=54.5 (constant over sweep). Note, GIE is equivalent terminology to GTE

The results suggest that a load of ~15 bar IMEPg ~55% gross thermal efficiency (GTE) is required to meet 50% BTE. If the load is reduced, the assumed frictional loss of 1 bar becomes a larger fraction of the total load and efficiency is reduced, resulting in a GTE of ~60% being required at a 10 bar IMEPg condition.

Previous RCCI GTE results by Splitter et al. [37 and 134] and Hanson et al. [136] are overlaid in the grey shaded region. These results have demonstrated that the maximum RCCI efficiency observed in the laboratory was in the vicinity of ~9 bar IMEPg. At the tested equivalence ratios of Φ'=~0.4, these results were in agreement with the simulation of Lavoie et al. [58] in Figure 30. However, in Lavoie et al. [58], a fixed heat release was assumed at all

equivalence ratios. This may or may not be possible with most advanced combustion strategies, as temperature, pressure, and equivalence ratio all can affect the combustion event. Thus, it is of interest to computationally explore the thermodynamic cycle parameters that offer high efficiency, and then use experiments to explore their effect on the combustion process. The overall goal of this method is to identify the conditions that offer high gross efficiency and the effect that the conditions have on the combustion process, and then use the combination of experiments and modeling to explore the potential for further increasing efficiency.

3.4 Preliminary Computational Study Results

An initial multi-dimensional study by Kokjohn et al. [110] was performed to explore the potential of maximizing RCCI efficiency. This study compared conventional diesel combustion (CDC) and RCCI at a mid-load point. The results suggested that if the heat transfer of either strategy was reduced (engine operated adiabatically), then engine efficiency could be increased. However, with RCCI the benefit of reduced heat transfer also increased combustion efficiency, further increasing RCCI engine efficiency. This study further suggested that reductions in engine heat transfer may be extremely important to increasing engine efficiency.

Recently, an experimental campaign by Hendricks et al. [111] experimentally demonstrated that for a given equivalence ratio, RCCI combustion had reduced engine piston heat transfer by over 40% compared to CDC. These

two studies suggest that RCCI engine heat transfer is low and that further reductions in heat transfer may be beneficial.

To explore the potential that these effects have on GTE, the GT Power code was used to simulate heavy duty RCCI combustion. A high efficiency experimental RCCI heat release was input to the code as an assumed combustion profile, and the code was validated against the corresponding experimental case. The results of this procedure are seen in Figure 31, where satisfactory agreement is seen in the pressure data and key performance parameters.

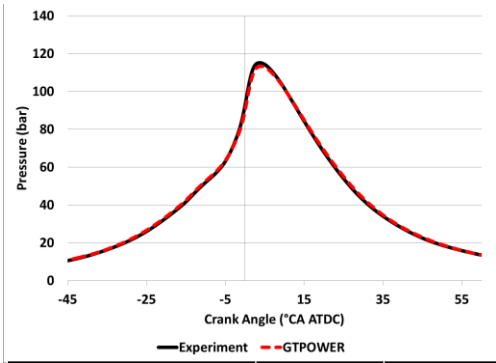

	Experiment	GTPOWER
Cr	14.88	14.88
IMEPn (bar)	8.00	7.86
Fueling (mg/cyc)	87.13	87.13
Gross Therm Eff. (%)	54.3	54.5
Net Therm Eff. (%)	52.0	52.1
BTE (%)	45.3	45.1
FMEP (bar)	1.03	1.0
Convection HX	N/A	0.4
Comb. Eff. (%)	98	98
EGR (%)	28	28
PHI (charge/air)	.320/.433	.320/.433
Intake Temp (°C)	32	37
IVC/EVO (°CA ATDC)	-143/130	-143/130
Intake Pressure (bar)	1.5	1.5
Exhaust Pressure (bar)	1.625	1.625
PPRR (bar/°CA)	11.4	11.4
Turbo eff. (no losses)	48.4	44.8
Turbo eff. (air filter + DOC)	67.5	62.3

Figure 31 Comparison of GT Power simulations (red) and experimental results (black) at 9 bar IMEPg high efficiency conditions. The results show that a convection coefficient of 0.4 in the simulations produces a close match on the compression and expansion pressures (default convection coefficient is 1.5, 0 is adiabatic).

After this validation, combinations of intake pressure, assumed reductions in heat transfer and incomplete combustion, and increases in compression ratio were simulated. The goal of the study was to determine what conditions would be necessary to achieve ~60% GTE at an ~9 bar IMEP condition. The load and efficiency suggested in Figure 31 corresponds to the DOE goal of 50% BTE. The results displayed in Figure 32 illustrate that the DOE goal may be achievable

through an increase in compression ratio (Cr) from 14.88:1 to 18.7:1, an increase in intake pressure of ~.2 bar, and simultaneous reductions in heat transfer and incomplete combustion of 50% as compared to the initial RCCI condition. These conditions are in agreement with the previous works by Caton [107], which suggested higher Cr and leaner conditions, and Lavoie et al. [58], which demonstrated reduced heat transfer from leaner conditions. Of note is that the BTE estimates from the simulation and single cylinder engine experiments are reliant on a Friction Mean Effective Pressure (FMEP) correlation. In the present work, the correlation uses production tuned RCCI constants, as described in Chapter 2 and Splitter et al. [37].

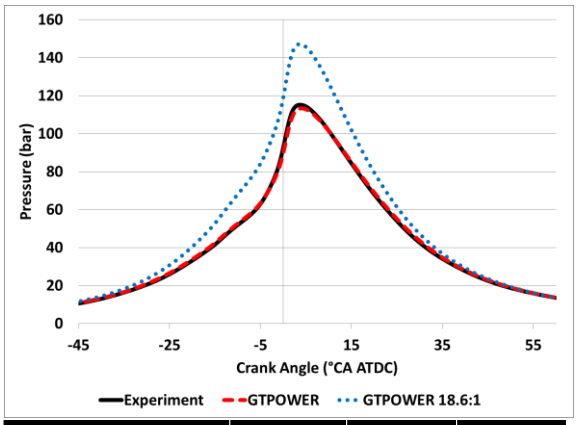

	Experiment	GTPOWER	GTPOWER
Cr	14.88	14.88	18.6
IMEPn (bar)	8.00	7.86	8.18
Fueling (mg/cyc)	87.13	87.13	87.13
Gross Therm Eff. (%)	54.3	54.5	56.7
Net Therm Eff. (%)	52.0	52.1	54.2
BTE (%)	45.3	45.1	46.4
FMEP (bar)	1.03	1.0	1.2
Convection HX	N/A	0.4	0.4
Comb. Eff. (%)	98	98	98
EGR (%)	28	28	0
PHI (charge/air)	.320/.433	.320/.433	.320/.320
Intake Temp (°C)	32	37	37
IVC/EVO (°CA ATDC)	-143/130	-143/130	-143/130
Intake Pressure (bar)	1.5	1.5	1.5
Exhaust Pressure (bar)	1.625	1.625	1.625
PPRR (bar/°CA)	11.4	11.4	14.2
Turbo eff. (no losses)	48.4	44.8	46.6
Turbo eff. (air filter + DOC)	67.5	62.3	64.9

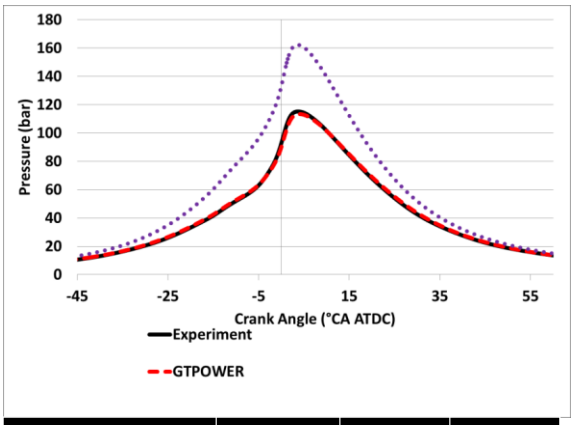

	Experiment	GTPOWER	GTPOWER
Cr	14.88	14.88	18.6
IMEPn (bar)	8.00	7.86	8.69
Fueling (mg/cyc)	87.13	87.13	87.13
Gross Therm Eff. (%)	54.3	54.5	59.7
Net Therm Eff. (%)	52.0	52.1	57.5
BTE (%)	45.3	45.1	49.1
FMEP (bar)	1.03	1.0	1.2
Convection HX	N/A	0.4	0.2
Comb. Eff. (%)	98	98	99
EGR (%)	28	28	0
PHI (charge/air)	.320/.433	.320/.433	.285/.285
Intake Temp (°C)	32	37	37
IVC/EVO (°CA ATDC)	-143/130	-143/130	-143/130
Intake Pressure (bar)	1.5	1.5	1.68
Exhaust Pressure (bar)	1.625	1.625	1.75
PPRR (bar/°CA)	11.4	11.4	14.6
Turbo eff. (no losses)	48.4	44.8	55.0
Turbo eff. (air filter + DOC)	67.5	62.3	72.8

Figure 32 GTPower RCCI simulations of high compression ratio operation (18.6:1). Note that the simulations assume the same heat release profile as lower compression ratio experimental operation (black). At the simulated conditions (right) an increase in trapped mass, and a simultaneous 50% reduction in heat transfer and incomplete combustion suggested that 60% GTE and 50% BTE may be possible.

Although the simulation results suggest that high efficiency could be achievable with RCCI, they provide no insight into the potential effects and relationships that engine conditions would have on the heat release process, or on the method to reduce heat transfer and incomplete combustion. The

subsequent sections of this work describe the pathway to achieve the performance demonstrated in these initial simulations.

Chapter 4 Experimental Details

4.1 Engine

The cited and current engine experiments utilized a heavy-duty 2.44 (L) Caterpillar 3401 Single Cylinder Oil Test Engine (SCOTE). The 3401 is a single-cylinder version of the commercially produced Caterpillar 3406E six-cylinder diesel engine. Unlike the 3406E, the SCOTE configuration is rated at 62 [kW] (83 [hp]) at a speed of 1800 revolutions per minute. The specific engine geometry and configuration are given in Table 1 and the lab setup is given in Figure 33. Details about the compression ratio and piston designs are given in the following section.

Table 1 Stock 3401 SCOTE geometry

Displacement	2.44 (L)
Bore x Stroke	13.72 x 16.51(cm)
Connecting Rod Length	21.16 (cm)
Swirl Ratio	0.7
Number of Valves	4
Intake Valve Opening	335ºCA ATDC Firing
Intake Valve Closing	-143ºCA ATDC Firing
Exhaust Valve Opening	130ºCA ATDC Firing
Exhaust valve Closing	-355ºCA ATDC Firing
Engine Cooling system	Engine Driven Pump, with Wet Liner
Engine Oiling System	External Electrically Driven Oil Pump, With Rotella T15W-40 with Advance Soot Control Oil

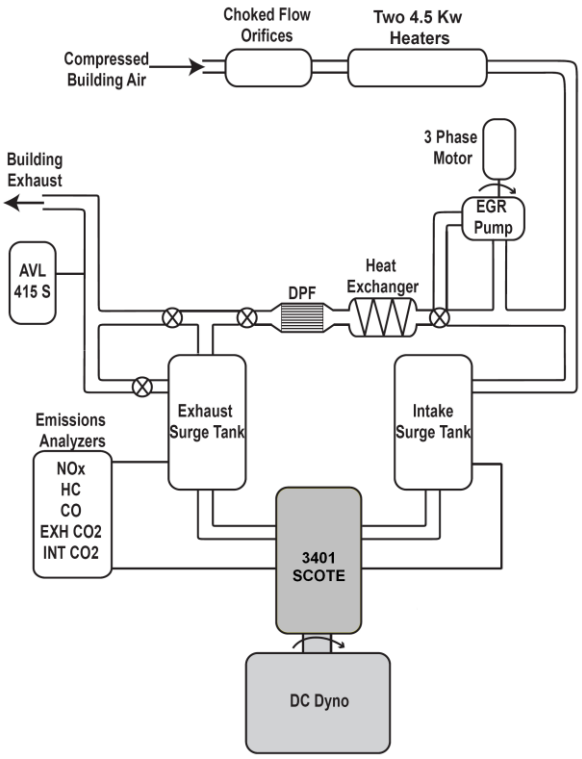

Figure 33 Diagram of the engine lab

The engine was instrumented with type K thermocouples manufactured by Omega Engineering Inc. The laboratory was also instrumented with a variety of pressure transducers. The pressure transducers were used to monitor operating conditions and to verify that steady state engine operation was achieved. The laboratory has independent simultaneously operable high and low pressure fuel systems. The details of fueling systems, temperature, and pressure transducer locations, measurement type and manufacturer can be found in Splitter [115].

4.2 Pistons

Two pistons were used, which varied in compression ratio and bowl shape. The pistons were designed based on the findings in Splitter et al. [112] for RCCI. A

section view of the pistons can be seen in Figure 34 below, where they are overlaid on the stock CDC 16.1:1 Cr pistons at TDC (firedeck indicated by gray line).

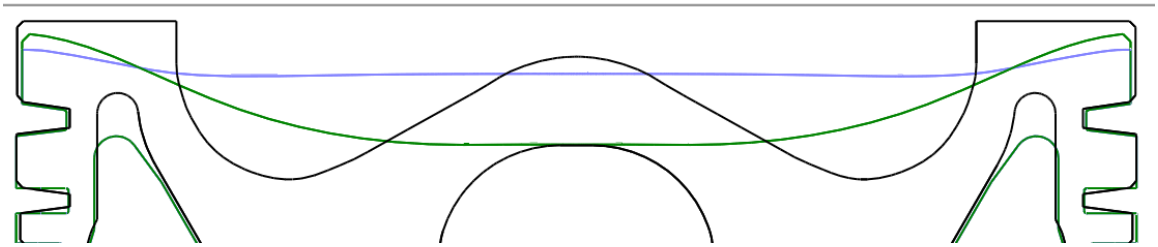

Figure 34 Cross sectional view of the stock CDC 16.1:1 Cr (black), 14.88:1Cr optimized RCCI bathtub (green), and 18.7:1 Cr pancake (blue) pistons. The grey line atop the pistons represents the cylinder fire deck at TDC spacing. Note the undercutting of the top ringland in the 14.88 and 18.7 Cr pistons relative to the stock piston.

As seen in the section view, the two pistons differed in top ring land diameter, and squish height. Details regarding these effects can be found in Splitter et al [112], where the pistons were cut from under turned research blanks. The 18.7:1 Cr piston had a reduced top ring land height (6.6 mm vs. 7.6 mm and 10.1 mm for the RCCI bathtub and stock CDC pistons respectively). The surface area of the pancake design reduced the TDC surface area of the 18.7:1 Cr piston by 1.2% relative to the 14.88:1 Cr bathtub shape (+5% relative to the CDC piston), which may have had an effect on reducing the potential for heat transfer. Also, unlike the 14.88:1 piston, the 18.7:1 piston was surface buffed to further minimize surface area for heat transfer.

4.3 Fueling strategy

RCCI experiments used port-fuel-injection of low reactivity fuel, E85 or gasoline, and direct multiple injections of high reactivity fuel, diesel or cetane improved low-reactivity fuels. The fuel delivery for this strategy is summarized in Figure 35.

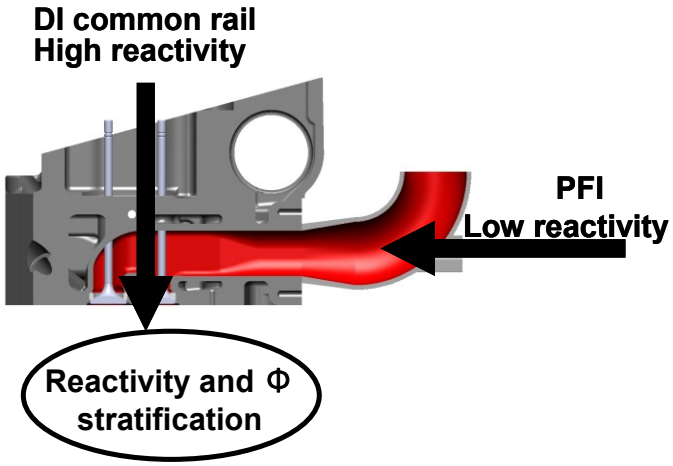

Figure 35 Experimental fuel injection locations and strategy

Engine operation in the laboratory was constrained to speeds of approximately rated torque (1300 [rev/min]) or rated speed (1700 [rev/min]), because speeds in-between resulted in laboratory harmonics that could have damaged equipment over long periods of operating time. In the present study the 1300 (rev/min) speed was used. Although the test engine is a heavy-duty engine capable of high loads, conservative maximums of peak cylinder pressure of 150 bar and PPRR of 10 (bar/°CA) were adopted, with short time excursions allowed to higher peak pressures and rise-rates.

The constraints were imposed to prolong the lifespan of the test engine and improve operator safety. Furthermore, the laboratory dynamometer was only capable of absorbing a finite torque, corresponding to an IMEP of roughly 16 bar

at 1300 [rev/min] and 18 bar at 1700 [rev/min]. For this reason, these loads were defined as full load for the laboratory. To ensure accurate cylinder pressure measurements, the peak motored cylinder pressure was set to -0.4° CA ATDC to account for thermal losses, which was the setting used by the manufacturer for internal testing ([113]). The thermodynamic conditions were deemed steady after verifying that intake and exhaust surge tank temperatures and pressures were steady for several minutes. Pressure boundary conditions were set by imposing a combined overall turbo charger efficiency. Overall turbocharger efficiency was calculated using Equation 8, as described by Wissink et al. [114].

$$\eta_{combined} = \frac{\left(\frac{\gamma_{comp}}{\gamma_{comp}-1}\right)}{\left(\frac{\gamma_{turb}}{\gamma_{turb}-1}\right)}\left(\frac{T_{comp,in}}{T_{turb,in}}\right)\frac{\left[\left(\frac{P_{comp,in}}{P_{comp,out}}\right)^{\left(\frac{\gamma_{comp}-1}{\gamma_{comp}}\right)}-1\right]}{\left(1+\frac{1}{AFR}\right)\left[1-\left(\frac{P_{turb,out}}{P_{turb,in}}\right)^{\left(\frac{\gamma_{turb}-1}{\gamma_{turb}}\right)}\right]} \quad (8)$$

The calculation used the intake and exhaust temperatures and pressures, as measured in the respective surge tanks, only after steady state operation was obtained.

4.4 Fuel Properties

A variety of fuels were studied. The fuels consisted of commercially available 91 PON gasoline, denatured ethanol directly from the distiller, the cetane improver 2-ethylhexyl-nitrate (2-EHN), and #2 ULSD. The pump available fuels properties were analyzed by an independent lab, and the current fuel properties can be found in Table 2 to Table 5, with detailed analysis in Appendix E.

Table 2. Diesel fuel properties

Grade	#2 ULSD
Lower Heating Value (MJ/kg)	42.609
Cetane Number	42
H/C ratio	1.758
Specific gravity at 60°C	0.8595

Table 3. Gasoline fuel properties

Lower Heating Value (MJ/kg)	44.301
MON	87.8
RON	94.7
AKI (RON+MON)/2	90.9
Ethanol Content (%)	0
H/C ratio	2.127
Specific gravity at 60°C	0.7009

Table 4. Ethanol fuel properties

Ethanol Lower Heating Value (MJ/kg)	26.9
Enthalpy of Vaporization (kJ/kg)	840
AKI (RON+MON)/2	99.15[††]
H/C ratio (-)	3.0
O/C ratio (-)	0.5

Table 5. 2-Ethylhexyl-Nitrate fuel properties[‡‡]

Lower Heating Value (MJ/kg)	27.364
H/C ratio	2.125
O/C ratio	0.375
Specific Gravity (@ 15.5 °C) (-)	0.96

4.5 Injection Systems

RCCI operation requires two fuel delivery systems. These systems can both be direct injection as in Wissink et al. [114], or a combination of direct and port fuel injection as in Splitter [115]. The present work uses direct injection of high

[††] PON/AKI of Ethanol has been estimated to be 99.15 by Eyidogan et al. [141].
[‡‡] EHN properties obtained from Oxley et al. [116]

reactivity fuel, and port injection of low reactivity fuel. The details of the setup are as follows.

4.5.1 Low-Reactivity Fuel System Hardware and Plumbing

In the experimental facility, the port and direct injection fuel systems are completely independent, enabling fully flexible control of each. The basic low-pressure injection system can be seen in Figure 36, with the system hardware components in Table 6. The system is capable of using either a port fuel injector, or a gasoline direct injector (GDI). To operate both a PFI and GDI injector, the low pressure boost pump is used. However, to operate the GDI, the higher pressure pump is activated though the motor controller, as described in Figure 36 and Table 6. Of note, is in its current configuration, simultaneous operation of the GDI and PFI injections results in indistinguishable respective fuel flows.

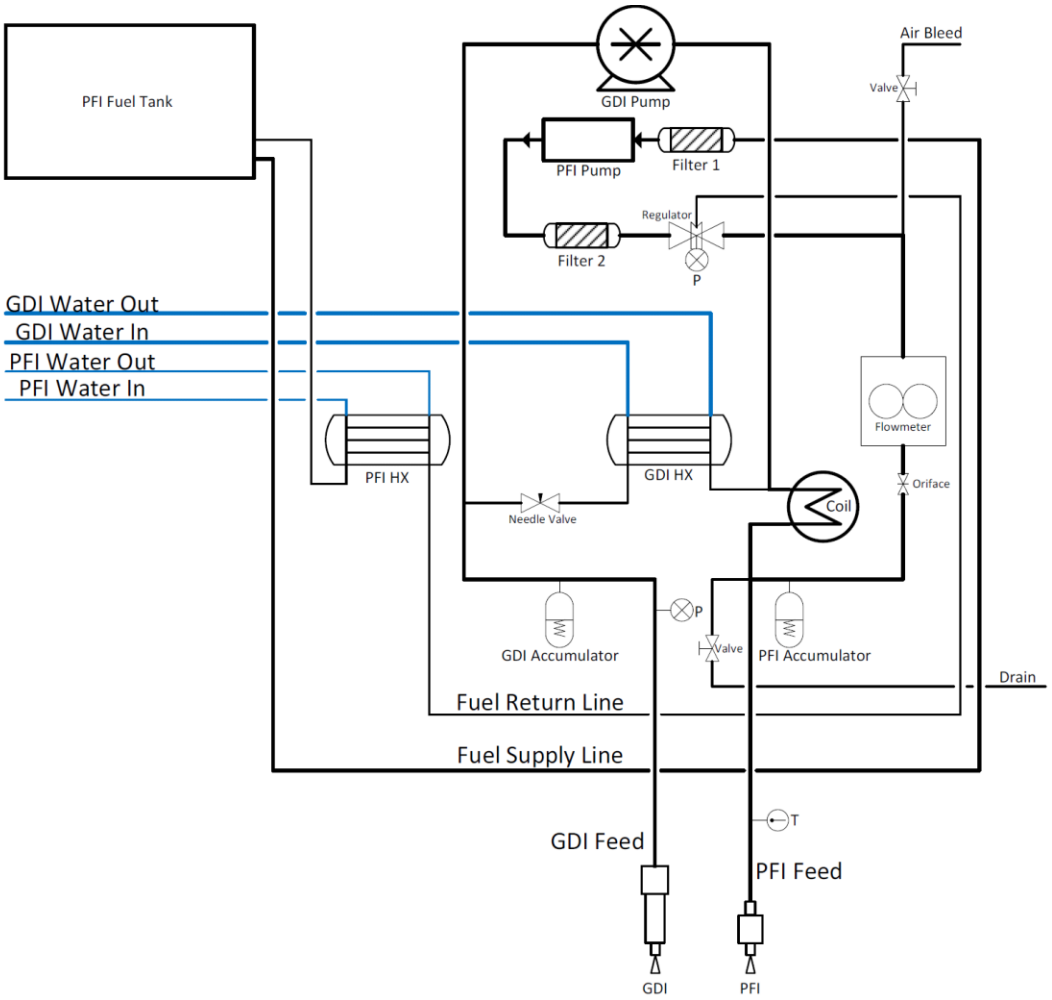

Figure 36 low pressure fuel system, diagram courtesy of DelVescovo [117]

Table 6 Low Pressure Fuel System Hardware

GDI Pump	Hydra Cell F20GASTNEMG
GDI Pump Motor	Dayton ½ HP 2M168C
GDI Motor Controller	Dayton SCR Control
PFI (Boost Pump)	Aeromotive model A1000
Pressure Regulator	Aeromotive model 13101
Filter 1	Aeromotive 12304, 100 µm
Filter 2	Aeromotive 12301, 10 µm
GDI accumulator	Parker BAC10B3U01A1
PFI accumulator	Parker BAC10B3U01A1
Oriface	None installed
PFI HX	Alfa Laval 459102 CB 14-14
GDI HX	Alfa Laval 459102 CB 14-14
Fuel Flow Meter	Endress-Hauser Promass 80A

To convert the engine to port fuel injection, the intake elbow was modified. A custom injector clamp was designed and installed. The modified and installed assembly can be seen in Figure 37.

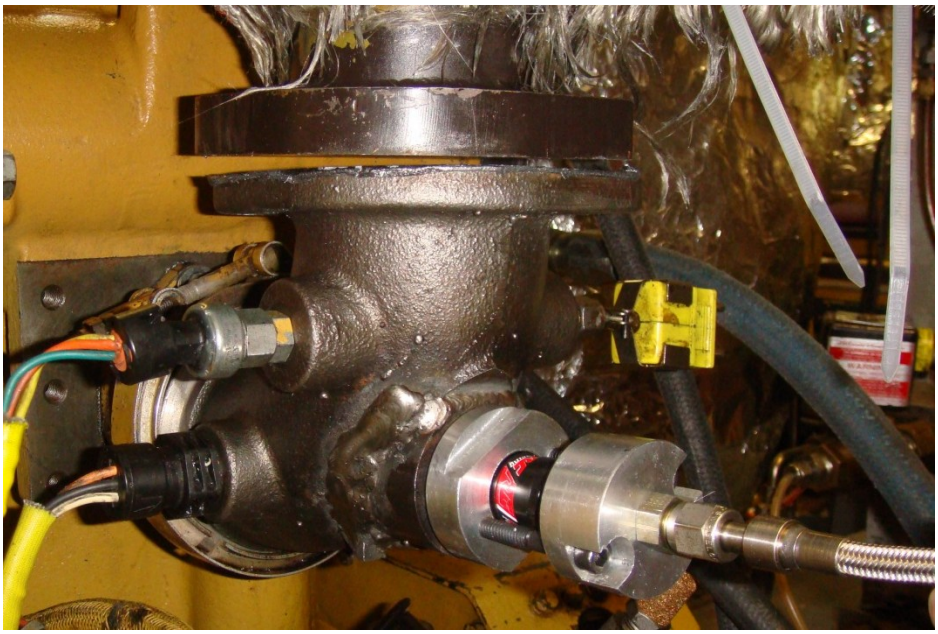

Figure 37 installed port injector in intake elbow

The figure demonstrates that the injector was placed relatively far from the cylinder head, with the injector spray directed parallel to the flow.

A common SI engine style commercially available automotive injector was used as the port-fuel-injector. To size the injector for the SCOTE, an aftermarket performance injector was selected and its specifications are in Table 7.

Table 7 Port fuel injector specifications

Manufacturer	RC Engineering
Injector Style	Lucas peak and hold
Peak and Cold Current	2 (pull in), 4(hold)
Steady flow rate @ 3 bar	750 cc/min (at 3 bar)
Included Spray Angle	15°
Fuel Pressure	5.17 bar

4.5.2 High Pressure Injection Hardware and Plumbing

To deliver high pressure fuel to the engine, a common rail system was used. A schematic of the system can be seen in Figure 38, with the system hardware listed in Table 8.

Table 8 Common Rail System Hardware

Common Rail Pump	Bosch CR/CP3S3/R110/30-789S (0 445 020 030)
Pump Motor	Emerson AD77 5 [hp] AC motor
Motor Controller	Baldor AC VFD 1D11205 - EB
Flexible Line (pump to rail)	Parker Polyflex SN: 45-13370 Hose Type: 4005ST 432307-001, 0.177”
Common Rail	Bosch A004 153 67 28 RD 000 2
Fuel HX	Alfa Laval CB14 -14
Temperature Controller	Omega CN8500 PID
Pump Coupler	Lovejoy L100 11499; 11518
Rail Pressure Control Valve	Bosch 0281002507
Fuel Flow Meter	Flowtron 10E (rosemont 1151)
Lift Pump 1	Walboro 6802
Lift Pump 2	Walboro 6802
Filter 1	Fuelman 10µm
Filter 2	Fuelman 10µm
Filter 3	Aeromotive 12301, 10 µm

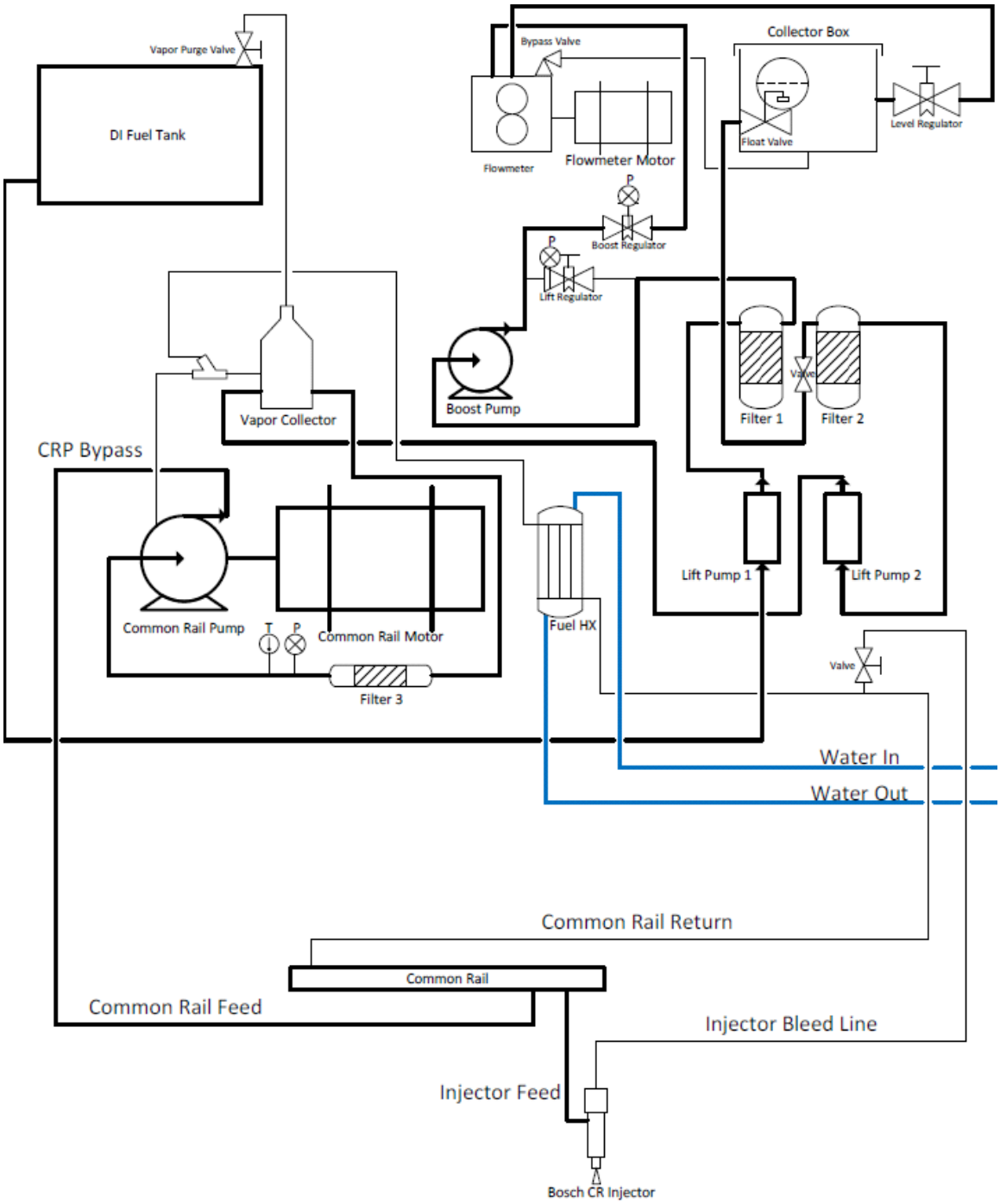

Figure 38 Common rail fuel delivery system diagram courtesy of DelVescovo [117]

To implement the common rail system in Figure 38, an adaptor was required, as described Splitter [115]. An insert and clamp system were used to install a centrally mounted injector in place of the 315B HEUI injector. The insert

was designed to mimic the exterior profile, o-ring dimensions, and brass crush insert of the 315B injector. The insert was also designed to be compatible with Bosch or Denso Common rail injectors, and Bosch or Delphi DGI injectors. An exploded view of the entire adaptor assembly with a Bosch common rail can be seen in Figure 39 and all technical drawings for the assembly can be found in Splitter [115].

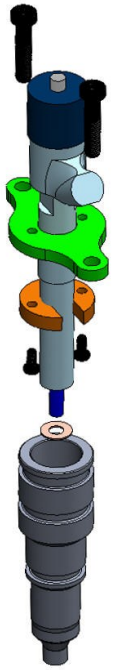

Figure 39 Common rail adaptor insert assembly for use with HEUI 315 inserts

Although the insert is designed to mimic the exterior profile of the 315 B injector, the stock Caterpillar part number 315B o-rings are toleranced to fit extremely tight, by making the insert extremely difficult to remove. To alleviate this problem, two Parker o-rings were installed on the top two o-ring lands, and a single Parker o-ring was installed on the bottom land. The installed assembly and Bosch common rail in the HEUI head can be seen in Figure 40.

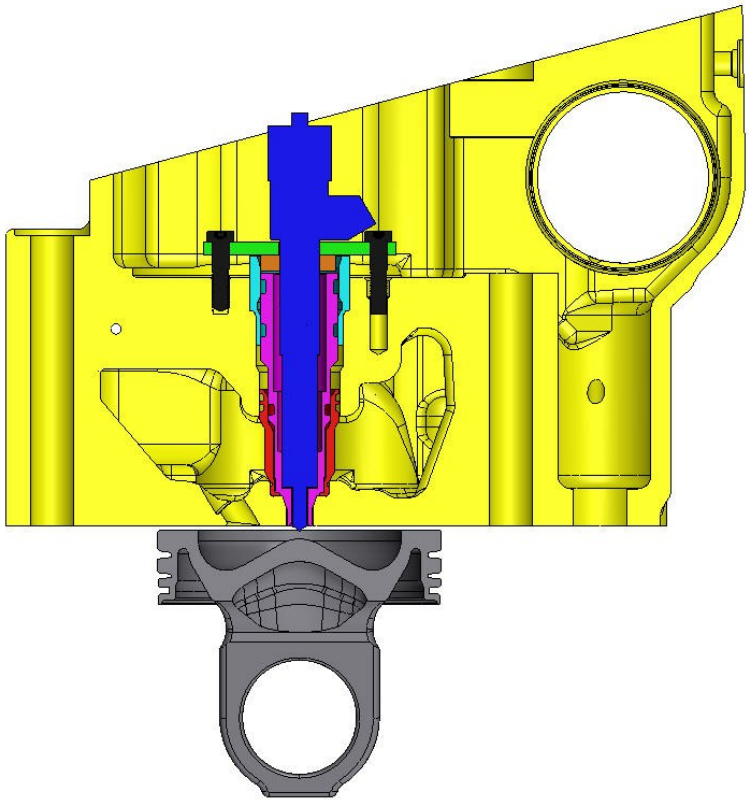

Figure 40 Bosch Common rail injector installed into HEUI 315B head with custom insert (purple) and clamps (orange and green)

Although the insert is compatible with several different injectors, a Bosch common rail system was selected for this research. The injector body was a standard OEM part on the commercially available General Motors (GM)/Fiat 1.9 (L) diesel engine used extensively throughout the Engine Research Center (ERC), with injector part number 1206097959002. The GM/Fiat engine was approximately 0.5 (L) per cylinder, while the SCOTE is 2.44 (L) for a single cylinder. The approximate 5 times per-cylinder displacement increase necessitated the need for a larger injector nozzle flow rate. An appropriate injector nozzle was selected from a commercially available 8.3 (L) high output (H.O.) Cummins QSC-600 marine engine, and installed on the GM/Fiat injector

body. The injector body and nozzle were verified to not exhibit choking by rate shaping experiments performed by Tess [118]. Details of the larger flow rate nozzle, and general information, and dimensions can be found in Table 9, and injection rate shape profiles can be found in Tess [118].

Table 9 Common rail injector nozzle specifications

Manufacturer	Bosch
Commercial Engine Design	Cummins 8.3 L QSCH.O.-600
Number of holes	6
Hole diameter	250 μm
Included spray angle	145°
K factor	0
Hydroground	yes
Sack Style	Mini-sack
Cummins part number	4993482

4.6 Engine Out Emissions

All gaseous engine-out emissions were analyzed with a five gas Horiba analyzer bench and particulates were measured with an AVL 415S smoke meter. The analyzers used in this study are displayed in Table 10. The Horiba bench was a tailpipe “bag” bench from General Motors Research, and converted to an engine bench with exhaust gas recirculation (EGR) capabilities at the engine research center (ERC).

Table 10 Emissions Analyzers

Emission Species	Instrument	Model	Measurement Method
Exhaust NO/NO2	Horiba	CLA-220	Heated Cemiluminescence Detector
Exhaust CO	Horiba	AIA-220	Non-Dispersive Infrared Light Absorption
Exhaust CO2	Horiba	AIA-220	Non-Dispersive Infrared Light Absorption
Exhaust Unburned Hydrocarbons	Horiba	FIA-236	Heated Flame Ionization Detector
Intake CO2	Horiba	AIA-220	Non-Dispersive Infrared Light Absorption
Particulate Matter	AVL	415s smoke meter	Filter Paper Opacity
Lambda Sensor	BOSCH	LSU 4.9	Nernst Concentration
Lambda Meter	ETAS	LA4	Calibrated Power Supply and Response Device for LSU Lambda Sensor

HC emissions were corrected using the Kar and Cheng correlation as stated in their 2009 SAE paper [119]. The correlation is designed to correct FID response to fuel oxygenate content, and is stated by the authors to be within 90% correction. The correlation uses a C_1 basis, where the expression is seen in Equation 9, where z is the fuels O-to-C ratio on a C_1 basis, and $HC_{FID\ C1}$ is the uncorrected FID measurement.

$$HC_{FID\ Corrected\ C1} = \frac{HC_{FID\ C1}}{\left[1 - \left\{(1 - .74) * 0.608 * \left(\frac{z}{.5}\right)^2\right\} + \left\{0.092 * \frac{z}{.5}\right\}\right]} \quad (9)$$

For the present research, the HC levels are initially quite low, the ethanol content of the total fueling is ~50%, resulting in the correction providing only minor differences (~100 PPM HC). Note that the present approach assumes that all oxygen containing fuel affects FID response the same as ethanol, which is not addressed in [119]. This assumption is minor as for the fuels in Table 2 through Table 5 the only oxygenated species other than ethanol are cetane improvers which are less than 3% by mass.

4.7 Data Acquisition and Processing

All engine data was recorded using a National Instruments LabVIEW based code. The code acquires all bench output emissions, and pressure and temperature sensor outputs, with low or high acquisition speed rates using SCXI and PXI chasses respectively. The LabVIEW code was developed by Sung [120], which is post processed using a MATLAB based code developed by Wissink [122].

Using the described cylinder pressure transducer in conjunction with a Kistler model 510 charge amplifier, the acquired cylinder pressure traces were averaged for either 200 or 500 cycles, and zero-phase filtered using a low-pass Butterworth filter with the cutoff frequency at 2200 Hz (the engine's second resonance mode, as described by Eng [121]). PPRR was calculated from the cylinder pressure ensemble averages. The apparent heat release rate (AHRR) was calculated by differentiating the ensemble average pressure using the coefficients of a Savitzky-Golay (SG) filter with first order and a window size of 9.

The AHRR calculation also used a non-constant gamma approach, where the measured constant compression gamma was used prior to top dead center (TDC) and the measured constant expansion gamma was used after TDC. Intake airflow was measured using choked flow orifices. In order to obtain choked flow for a variety of engine operating conditions, combinations of six different sized orifices were used. Intake air was heated with two immersion style heaters and proportional integral derivative (PID) control to ±1°C. Intake and exhaust gas temperatures were measured in the surge tanks with a secondary exhaust gas temperature measurement directly at the cylinder head exhaust outlet. Both the intake and exhaust surge tanks were equipped with PID pressure control to ±0.7 kPa.

PM measurements were performed with an AVL model 415s smoke meter. PM measurements of filter smoke number (FSN), mass per volume (mg/m^3) and specific emissions (g/kWh) were related with the factory AVL calibration and averaged among five samples each of a 2 L volume, taken with paper saving mode off. All gaseous emissions measurements were performed with the 5-gas Horiba emissions bench. HC emissions were measured on a wet basis using a heated sampling system. All other emissions were sampled on a dry basis. EGR rate was determined from the ratio of intake to exhaust CO_2 levels. Gaseous emissions were averaged for 30 seconds after attaining steady-state for several minutes.

4.8 Determining Losses and Efficiencies

To determine engine efficiency and losses, the following relations were used.

4.8.1 Determining Efficiencies

Gross, net, and brake thermal efficiencies were calculated using Equations 10, 11, and 21 where fuel energy was calculated using Equation 19 and 20, and the respective work terms were calculated using Equations 12-18

$$GTE = \frac{W_{gross}}{E_{fuel}} \tag{10}$$

$$NTE = \frac{W_{net}}{E_{fuel}} \tag{11}$$

$$IMEP_g = \frac{W_{gross}}{V_d} \tag{12}$$

$$IMEP_n = \frac{W_{net}}{V_d} \tag{13}$$

$$W_{gross} = \int_{\theta=-180}^{\theta=180} P\ dV \tag{14}$$

$$W_{net} = \int_{\theta=-360}^{\theta=360} P\ dV \tag{15}$$

$$V = V_{TDC} * \left[1 + 0.5 * (C_r - 1) * \left(R + 1 - \cos\theta - \sqrt{R^2 - \sin\theta^2}\right)\right] \tag{16}$$

$$R = \frac{Rod\ Length}{\left(\frac{Stroke}{2}\right)} \tag{17}$$

$$V_{TDC} = \frac{V_d}{C_r} \tag{18}$$

$$E_{fuel} = \dot{M_{Fuel}} * LHV_{Fuel} * Speed\left[\frac{sec}{cyc}\right] \tag{19}$$

A common method to determine fuel flow rate is to combine exhaust gas and direct mass measurements. By using the fuels ratio of hydrogen to carbon (H-to-C) and oxygen to carbon (O-to-C) ratio, the air fuel ratio (AFR) was determined from emission. This calculated AFR can be compared to the direct mass measured AFR, and thus two separate fuel flow rates can be determined. This approach necessitates that the fuels be compared on an atomic carbon ratio (C_1) basis, using wet based emissions (water present in exhaust gas). Using the calculation fuel flow from the emission bench (AFR_C), corresponding efficiencies and losses can be calculated (Equations 10, 11, 21 for efficiencies, and Equations 26, 28, 34, and 40 for losses). The procedure used for AFR calculation is presented in Appendix D section A.D.1, where the MATLAB processing code is shown.

$$\dot{M_{Fuel}} = \frac{\dot{M_{Fuel}}_{AFR_c} + \dot{M_{Fuel}}_{AFR_{mass}}}{2} \tag{20}$$

For most production engines, the value of brake efficiency and MEP are desired. This is calculated using Equations 21-23

$$BTE = \frac{W_{brake}}{E_{fuel}} \quad (21)$$

$$W_{brake} = BMEP * Vd \quad (22)$$

$$BMEP = IMEP_n - FMEP \quad (23)$$

However, most single-cylinder engines exhibit increased frictional loads compared to their multi-cylinder counterparts, frictional losses can be artificially increased. Therefore, an estimate of the friction mean effective pressure (FMEP) is commonly applied to assess a comparable multi-cylinder equivalent BMEP. Many commercial codes, such as GT Power, use a correlation to estimate FMEP. Such correlations often include a range of constants, and are functions of mean piston speed, and peak cylinder pressure.

The FMEP correlation used in the present work is of the same form as that used by GT Power [123], as seen in in Equation 24, where P_{max} is the peak cylinder pressure and $\overline{Sp}$ is the mean piston speed.

$$FMEP = C_1 + (C_2 * P_{max}) + \left(C_3 * \overline{S_p}\right) + \left(C_4 * \overline{S_p}^2\right) \quad (24)$$

The constants C_1 to C_4 used in the present work are listed in Table 11, and provide similar results to those observed by Hanson et al. [124] in LD multi-cylinder RCCI experiments as well as those of HD 15L sized engines [6].

Table 11 Production tuned RCCI FMEP coefficients used in the present study

Constant	**Value**	**Units**
C_1	0.3	bar
C_2	0.005	-
C_3	0.03	bar*s/m
C_4	0.0006	bar*(s/m)^2

Volumetric efficiency was calculated. This is an assessment of engine breathing. It is calculated using Equation 25, where R_u is the universal gas constant and pressure and temperature are evaluated at the intake surge tank conditions

$$VE = \frac{\dot{M}_{Intake}}{\left\{\left(\frac{P_{intake}}{R_u * T_{intake}}\right) * \frac{Speed\ \left[\frac{rev}{min}\right]}{2} * V_d\right\}} \quad (25)$$

4.8.2 Determining Losses

Pumping losses were calculated using Equations 26-27.

$$Pumping\ loss = \frac{PMEP * V_d}{E_{fuel}} \quad (26)$$

$$PMEP = IMEP_g - IMEP_n \quad (27)$$

Exhaust losses were calculated by the relation in Equations 28 – 33, where the mass flow rate of air ($\dot{M}_{Fresh\ Air}$) is from direct mass flow rate measurement. Although the specific heat of an ideal gas is a function of temperature only, the range of temperatures observed at the tested conditions is small. Therefore, a constant C_P of 1006 and 1080 J/Kg-k was assumed in the analysis for the respective intake and exhaust streams (the mass of fuel is assumed to be small and not significant in terms of the bulk gas C_P).

$$Exh.Loss = \left(\frac{\dot{E}_{Exh.} - \dot{E}_{Intake}}{\dot{E}_{fuel}}\right) \quad (28)$$

$$\dot{E}_{Intake} = \dot{M}_{Intake} * C_{p,Intake} * T_{Intake\ Tank} \quad (29)$$

$$\dot{E}_{Exh.} = \dot{M}_{Exhaust} * C_{p,Exhaust} * T_{Exhaust\ Tank} \quad (30)$$

$$\dot{M}_{Intake} = \frac{\dot{M}_{Fresh\ Air}}{\left(1 - \frac{EGR\ \%}{100}\right)} \quad (31)$$

$$\Phi\dot{M}_{Exhaust} = \dot{M}_{Intake} + \dot{M}_{fuel} \quad (32)$$

$$\dot{E}_{fuel} = \dot{M}_{Fuel} * LHV_{Fuel} \quad (33)$$

Incomplete combustion (Inc. Comb.) was calculated using Equation 34, with combustion efficiency defined in subsequent Equations 35-39. Of note is that the fuel energy and the HC energy differ. The FID was calibrated to respond 1:1 to propane, thus the heating value of HC was defined in 38 as that of propane. However, the heating value of the fuel used (E_{fuel}) was different, and was calculated using the measured values.

$$Incomplete\ Combustion = 1 - \ Comb.Efficiency \quad (34)$$

$$Comb.Efficiency = \frac{(Y_{CO} * LHV_{CO}) + (Y_{HC} * LHV_{HC}) + (Y_{PM} * LHV_{PM})}{\left(\frac{\dot{E}_{fuel}}{\dot{M}_{Fresh\ Air} + \dot{M}_{fuel}}\right)} \quad (35)$$

$$LHV_{PM} = 32.8\ \left[\frac{MJ}{Kg}\right] \quad (36)$$

$$LHV_{CO} = 10.1\ \left[\frac{MJ}{Kg}\right] \quad (37)$$

$$LHV_{HC} = 43.8\left[\frac{MJ}{Kg}\right] \tag{38}$$

$$Y_{xxx} = \frac{Emissions_{xxx}\left[\frac{g}{kg_f}\right] * \dot{M_{fuel}}\left[\frac{kg}{min}\right]}{\dot{M_{Fresh\ Air}}\left[\frac{kg}{min}\right] + \dot{M_{fuel}}\left[\frac{kg}{min}\right]} \tag{39}$$

The relation to determine the HX portion is seen in Equation 40, (denoted at HX). Of specific note, heat transfer is not directly solved in the analysis by measurement. In turn, it was solved as the left over or unaccounted for energy that remains from the input fuel energy.

$$HX\ Loss = 1 - \ GTE - Inc.Comb. - Exh.Loss \tag{40}$$

Since HX losses can result from a variety of sources, it is somewhat misleading to classify this loss entirely as heat transfer. However, heat transfer is the most likely dominant term, thus justifying the nomenclature selection.

By using multiple fuel flow rate calculation approaches, a carbon balance on the engine can be performed. The carbon flow rates can be determined from the AFR_c and AFR_{mass} measurements. This approach examines the carbon flow rate out of the engine (AFR_c) compared to the carbon flow rate into the engine (AFR_{mass}). The research approach is shown in Equations 41 and 42. Here the results can clarify potential losses and errors.

$$\frac{\dot{M}_{air}}{AFR_{xxx}} = \dot{M}_{fuel_{XXX}} \tag{41}$$

$$100 * \left(\frac{\dot{M}_{fuel_{AFRc}} - \dot{M}_{fuel_{Mass}}}{\dot{M}_{fuel_{AFRc}}}\right) = \Delta M_f \quad (42)$$

As defined in Equation 42, a negative value of ΔM_f corresponds to a higher fuel flow rate (i.e., more fuel measured into than out of the engine). Ideally, the value of ΔM_f is as close to zero as possible. However, it is a common and generally accepted practice to have ΔM_f measurements within 1-2% as the approaches in determining AFR have inherent assumptions (for example hydrogen conversion from FID measurements). It is commonly accepted that the accuracy of the technique is only sufficient to determine significant errors (greater than ~3% relative difference [125]). This value of ΔM_f was used as a metric for determining proper fuel and thus, energy measurements.

4.8.3 Determining Uncertainties

In addition to a carbon balance, measurement uncertainty and uncertainty propagation are important to investigate. Uncertainty analysis assesses the confidence of measured and calculated values. An uncertainty analysis of losses and efficiencies was performed in Engineering Equation Solver (EES) [126]. The approach used the governing equations for losses and efficacies in Equations 10-43. The measured uncertainties were determined for each device per the manufacturer's specifications, and are listed in Table 12.

Table 12 measurement uncertainty values

Measurement	Uncertainty	Type
HC	0.5% of full scale	Absolute
CO	0.5% of full scale	Absolute
NO_x	0.5% of full scale	Absolute
CO_2 Intake	0.5% of full scale	Absolute
CO_2 Exhaust	0.5% of full scale	Absolute
Lambda	3%[§§]	Relative
DI fuel	≤0.3%	Relative
PFI fuel	≤0.25%	Relative
T orifice (upstream)	.25 K	Absolute
T intake	.25 K	Absolute
T exhaust	.25 K	Absolute
P orifice (upstream)	.01 bar	Absolute
P intake	.01 bar	Absolute
P cylinder	0.5 % full scale	Absolute
Emissions Bench Suction	1 [l/min]	Absolute

Using this analysis the merit of calculated efficiency and losses can be determined. For example GTE can be calculated based on AFR_c, AFR_{mass}, or AFR_{lambda}. The procedure for calculation of GTE from the respective AFR simply uses the definition in the equation, with the fuel energy determined in Equation 19 and fuel mass flow rate from the respective AFR in Equation 41. Using these equations in EES, uncertainty analysis can be performed (the code used can be found in Appendix D, section A.D.2).

To determine the different uncertainties, a sweep of high efficiency conditions was performed (oil matrix points 71-102 in Appendix A, Table A. 13, operating conditions seen in Table 35 and Table 36). These conditions were selected because at high efficiency operation, errors in fuel flow and fuel energy

[§§] Error selected based on the findings of Regitz and Collings [129] (2%-6% error) , and ETAS User's Manual [127] (~5% AFR error of full scale)

will be magnified. Using this approach, the uncertainties of the respective AFR based GTE can be seen in Table 13.

Table 13 Average GTE, GTE uncertainty and relative GTE uncertainty of oil points 72-102, Appendix A, Table A. 13

AFR measurement	**Average GTE** (% fuel energy)	**Average Uncertainty** (% fuel energy)	**Uncertainty of GTE** (% of GTE)
Carbon	57.6	±0.5	±0.8
Mass	56.2	±0.1	±0.2
λ	55.9	±1.7	±3.0
Ave. (Mass + Carbon)	56.9	±0.2	±0.4

The data show that the average GTE and corresponding uncertainty of the λ meter based AFR is the lowest, and more importantly, the least reliable. To display this, the highest efficiency points from the sweep were selected. Figure 41 shows the GTE results from all three approaches, with whiskers indicating the respective uncertainties.

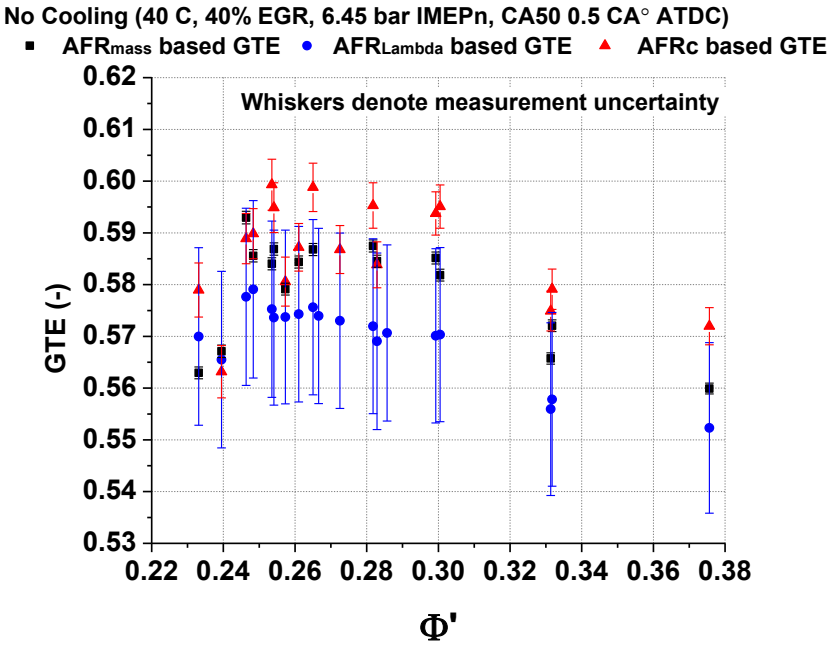

Figure 41 GTE as calculated from different AFR and direct mass based measurements. Note that AFR_{LAMBDA} measurements are consistently low and have the highest uncertainty.

The results of Table 13 and Figure 41, show that the AFR_{lambda} based measurement has the highest uncertainty and has a consistently lower GTE than the other approaches. Although wideband λ sensors are useful tools, their accuracy at lean conditions and with higher HC emissions is questionable. Indeed, Buglass et al. [128] demonstrated that λ sensors readings are strongly affected by un-burnt large hydrocarbon fuel species such as isooctane. More recent supporting results by Regitz and Collings [129] demonstrated that high HC levels and more importantly lean operation (λ≥2), resulted in over 2% and 6% respective errors in AFR_{LAMBDA} compared to AFR_C.

Based on these findings, the AFR_{lambda} based measurements were ignored throughout the analysis. Additionally, unless noted, the GTE and associated losses were determined from the average of the AFR_C and AFR_{mass} fuel flows. This approach avoids potential errors in fuel flow rate or impingement, as discussed in Appendix B.

Table 14 Energy budget using AFR_C and AFR_{mass} averaged fuel flow. Energy use, uncertainty, and relative uncertainty of GTE shown, data are average of oil points 72-102, Appendix A, Table A. 13

Energy Use	**Fuel energy** (%)	**Average Uncertainty** (% of fuel energy)
GTE	56.9	±0.2
Incomplete Combustion	2.9	±0.1
Exhaust loss (EXH)	29.5	±0.3
Heat Transfer loss (HX)	10.7	±0.5

The data shows that the HX loss and EXH losses have the highest uncertainty, but the overall value is reasonable. To determine the sources of uncertainty, a

representative case was selected, (oil test run 83 Appendix A, Table A. 13). The sources and relative contribution of uncertainty are shown in Table 15

Table 15 Top two sources of uncertainty of oil point 83, Appendix A, Table A. 13

Energy Use	**Top Contributor**	**Top Contributor** (% of uncertainty)	**Second Contributor**	**Second Contributor** (% of uncertainty)
GTE	Exhaust CO_2	78.07	Upstream Orifice Pressure	8.63
Incomplete Combustion	HC	67.78	Exhaust CO_2	27.16
Exhaust loss (EXH)	Exhaust CO_2	70.42	Intake CO_2	24.24
Heat Transfer loss (HX)	Exhaust CO_2	87.4	Intake CO_2	8.44

The results show that for accurate data, the most important measurements in the laboratory are exhaust CO_2, HC, intake CO_2, and the upstream orifice pressure (pressure into choked orifice rack). Of these sources the exhaust CO_2 analyzer introduces the largest source of error. In Table 14 it is seen that ~98% of the fuel energy, and in Table 15 there is a single source for nearly all of the associated uncertainty, namely the exhaust CO_2 measurement.

Chapter 5 Results

The current chapter will follow the format described in the flow chart in Figure 42.

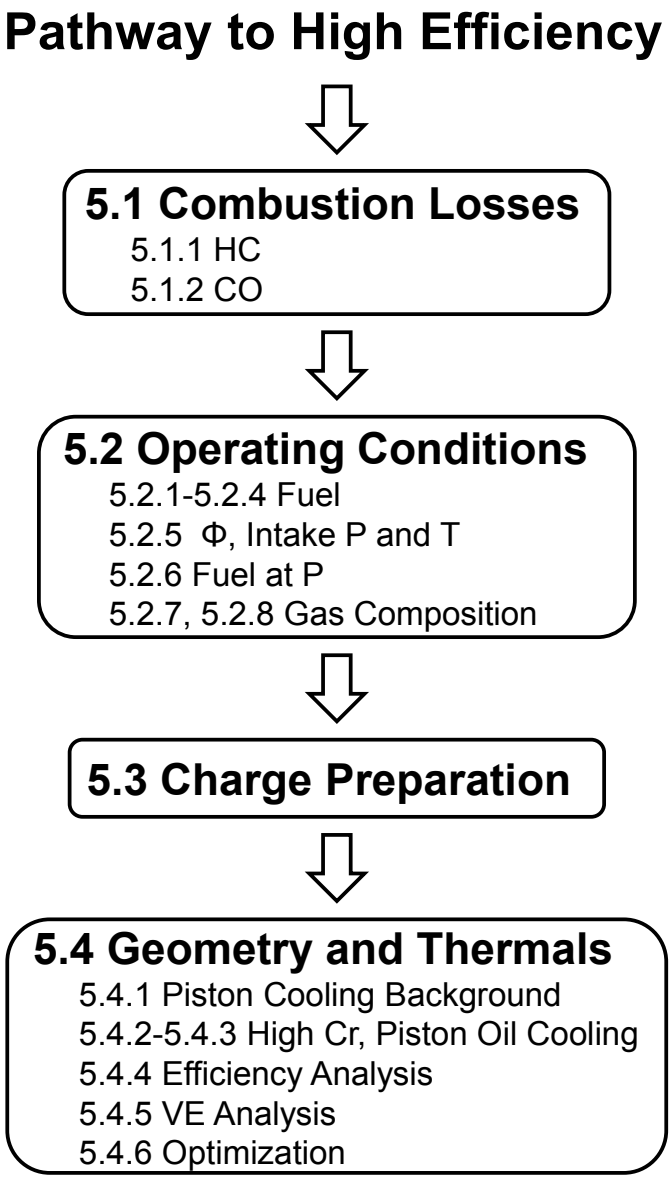

Figure 42 Flow Chart of Results Section for operation towards high efficiency

5.1 Addressing Incomplete Combustion in RCCI

5.1.1 Hydrocarbon Sources and Solutions

It is well known that SI combustion engine hydrocarbon (HC) losses stem from crevice effects. For instance, research by Alkidis [130] demonstrated that in premixed charge strategies, the inability of combustion to propagate into engine crevices is the dominant factor in engine HC emissions. Figure 43 reproduces the key findings of this study.

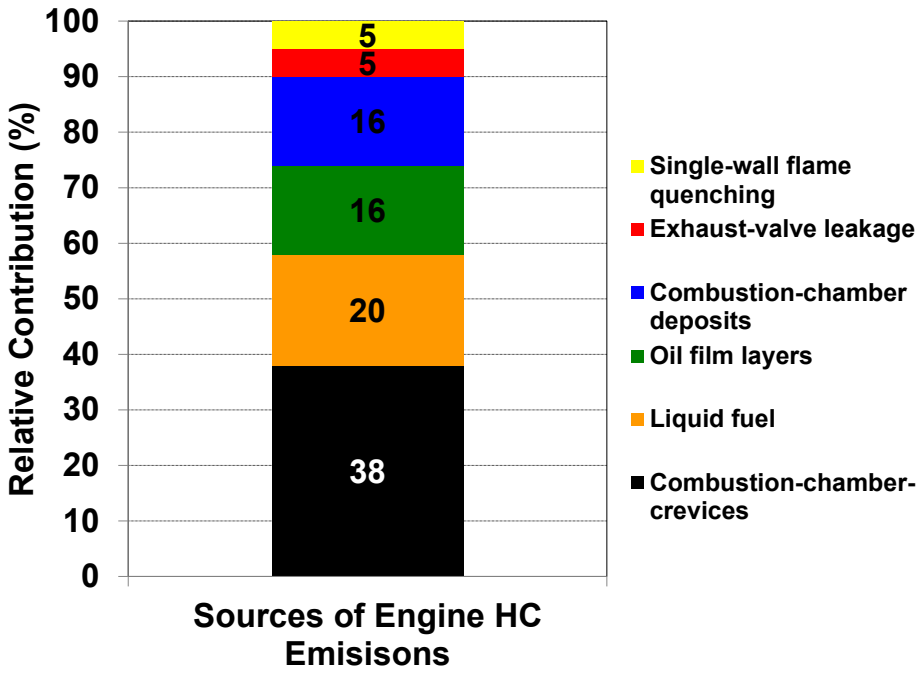

Figure 43 Engine out HC emission sources in SI combustion. Note that engine crevices are observed to be the major contribution factor. An equally significant contribution was found in the combination of oil and fuel films. Data from Alkidis [130]

This study showed that, the head gasket and piston crevices are the major contributors to combustion chamber crevices. Furthermore, the study showed that when reactions cannot propagate into piston crevices, HC emissions linearly

increase. This is especially important in dilute auto-ignited combustion because the reduced near-liner temperatures from convective cooling likely slow the combustion process.

In addition to the chamber design, HC emissions have been shown to be highly dependent on crevice flows by Salizar et al. [131] and Vera et al. [132], including post combustion gas oxidation. If combustion is fairly incomplete, (i.e., 95-90% combustion efficiency), this is a major source of inefficiency. For instance, if the combustion efficiency is 94% and the engine is operating at approximately 50% gross indicated efficiency, there are three theoretically recoverable efficiency percentage points. However, because of crevice flows and in-cylinder flows, complete combustion is difficult to obtain even with non-premixed mixing-controlled combustion. In general, 98% combustion efficiency is considered to be “acceptable” from an efficiency basis, meaning there is about a 1% loss in engine efficiency potential. Taking these trends and metrics into account, there is significant potential to increase engine efficiency with increases in combustion efficiency. Using these initial works as evidence for RCCI engine architecture optimization, analysis of effect of piston geometry on incomplete combustion and efficiency was conducted through simulations and experiments of Splitter et al. [112].

The findings suggested that efficiency gains can be made from changes to the piston geometry. In the study, five different pistons were tested, with three unique bowl designs cut in materials identical to production parts. The results demonstrated that increased ring top land crevice size increased HC emissions

correspondingly, supporting the findings of Alkidias [130]. Additionally, Splitter et al. [112] showed that piston squish and bowl geometry were equally important as piston crevices. Specifically, when the squish height and piston bowl radius were increased, HC emissions decreased. The results demonstrated that HC emissions could be reduced by decreasing storage mechanisms (reduce crevice size), and to increase near-liner oxidation (increased squish height and bowl radius).

The results of Splitter et al. [112] are critical for both optimizing engine efficiency and regulated emissions standpoints. Similar to utility engines [131 and 132], exhaust catalysis of HC and CO with highly dilute low temperature combustion strategies may be challenging. However, unlike utility engines which cannot catalyze HC due to oxygen lean operation, LTC strategies operate excessively oxygen rich. This reduces exhaust temperatures, bordering on the lower limits of present production catalyst technologies. These challenges have been demonstrated in RCCI by Prikhodko et al. [133], where a diesel oxidation catalyst (DOC) was shown to be effective at reducing tailpipe HC and CO emissions and, the conversion efficiency was significantly reduced from that required for production applications. Thus, minimizing catalyst requirements by reducing the feed gas levels of HC and CO will aid in both reducing exhaust system requirements and increasing engine efficiency.

5.1.2 Sources and Solutions to CO in RCCI

The previous sections have discussed sources and minimization techniques for RCCI HC emissions. The present section addresses conditions and solutions to CO emissions in RCCI. For “good operating” RCCI conditions, CO emissions are typically higher in concentration than HC emissions. Although zero levels of each emissions would be best from an emissions and combustion efficiency standpoint, increased CO emission relative to HC emission is more favorable. The reasoning behind this is that the heating value of HC is typically four times higher than CO (~40 MJ/kg vs. 10.8 MJ/Kg). This energy discrepancy provides a four-to-one tradeoff, where approximately four times the CO emissions are required to affect combustion efficiency the same as HC. Secondly, Prinkhodko et al. [133] demonstrated that in RCCI, CO is much more readily catalyzed in a DOC than HC, which is of particular importance in RCCI. Based on these relations, CO emissions in RCCI are important, but their reduction tends to be of less merit than HC reductions from an efficiency and practicality basis.

To investigate the sources and solutions to CO emissions in RCCI, engine experiments were conducted through an experimental matrix of varied intake conditions. The test matrix considered the effects of intake temperature and pressure, at fixed combustion phasing (0.5°CA ATDC) IMEPn (8.45 bar) engine speed (1300 rev/min) and an overall turbocharger efficiency (65%). Since the load and combustion timing are fixed, the test matrix considered variations in Φ and intake temperature at constant net power. This test matrix would not be

possible with HCCI combustion, as variations in intake pressure, temperature, and composition all determine a unique combustion phasing.

A graphical representation of the RCCI test matrix is show Figure 44, with corresponding general conditions in Table 16.

Table 16 Engine operating parameters and hardware for Φ-T matrix

Load (IMEPn)	8.45±.05
CA50 (°CA ATDC)	0.5±.5
Speed (rev/min)	1300
Piston Bowl Shape	Bathtub
Cr (-)	14.88:1
DI Timing (°CA ATDC)	-60/-35
DI Dwell Bias (%SOI1, % SOI2)	~60/40
PFI Timing (°CA ATDC)	-320
EGR (%)	0
Intake Temperature (°C)	32-66 (varied)
Intake Pressure (bar)	1.31-2.18 (varied)
Exhaust Pressure (bar)	Varied to fix turbo. η
Overall Turbocharger η (%)	~65
Low Reactivity Fuel (PFI)	See Table 17
High Reactivity Fuel (DI)	See Table 17
PFI Fuel Fraction (-) (by energy)	See Appendix A
DI Fuel Fraction (-) (by energy)	See Appendix A

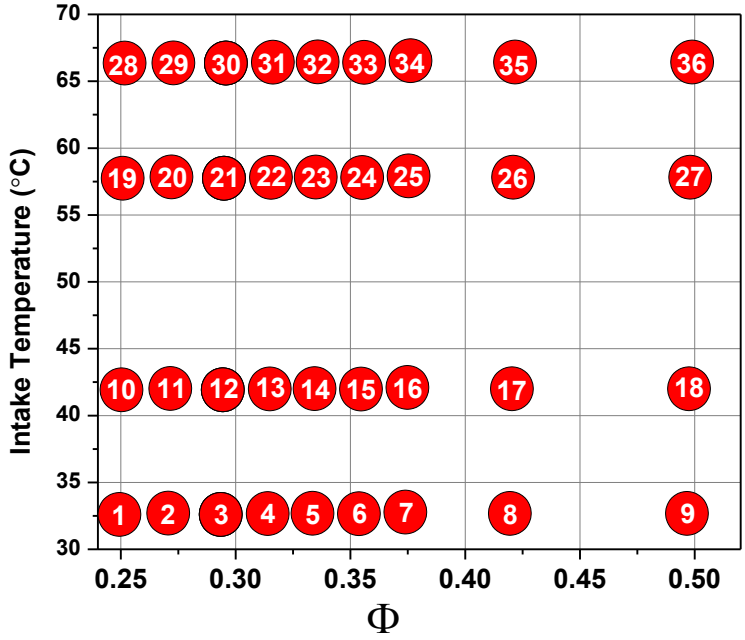

Figure 44 RCCI Φ-T test matrix, at constant combustion phasing and load. Thus Φ is analogous to constant IVC density (charge mass), obtained by sweeping pressure at constant density with several IVC temperatures.

The matrix of test points consists of nine equivalence ratios at four intake temperatures, for a total of thirty six test points. The range of intake temperatures and equivalence ratios is typical for RCCI combustion, as demonstrated by Splitter et al. [38 and 134], Curran et al. [135], Kokjohn et al. [32], and Hanson et al. [33 and 136].

In the test matrix, three fuel combinations were used. The fuels used are presented in Table 17 below, with fuel properties described previously in Chapter 4.

Table 17 Fuel combinations used in Φ-T test matrix, specifics of the fuel delivery are given in Table 16 and Appendix A

Fuel combination	DI Injector	PFI Injector
1	#2 ULSD	E85
2	3% EHN in 91 PON gasoline***	E85
3	#2 ULSD	91 PON gasoline

The direct injected fuel was delivered at fixed double injection start of command timings of -60 and -35 °CA ATDC for the respective first and second injection events. As fuel trimming was performed to maintain load and phasing at the various Φ-T conditions, a greater proportion of fuel was removed from the second injection (-35 °CA ATDC). This was implemented because when fuel from the first injection was removed, it was observed that HC and CO emissions increased (an efficiency loss). The fueling requirements for each fuel combination and Φ-T condition are listed in Appendix A. It is notable that in the initial CA50 sweep of Figure 49, these injection timings provided the minimum CO and HC emissions. However, at all tested conditions direct injection timings may not be optimal and are also fuel dependent, as shown in Appendix B.

As noted in the Table 16, intake pressure and temperature were swept independently and the ratios of more-to-less reactive fuel were trimmed to maintain phasing and load. The CO results of this study with fuel combination 1 in Table 17 (ULSD/E85) are plotted in Figure 45 below, as function premixed fuel fraction (E85) and Φ (equivalent to intake pressure at the constant phasing and load condition). The dots in the figure correspond to the operating conditions as summarized in Figure 44, and the specific data can be found in Appendix A,

*** To prevent HP pump failure, 500 ppm of the lubricity agent Infinium 655 was added, see Appendix E, Section A.E.1 for details on the additive properties.

Table A. 3 (CO of all Φ–T data points with ULSD/E85 listed in Appendix A, Table A. 3 are plotted in the figure).

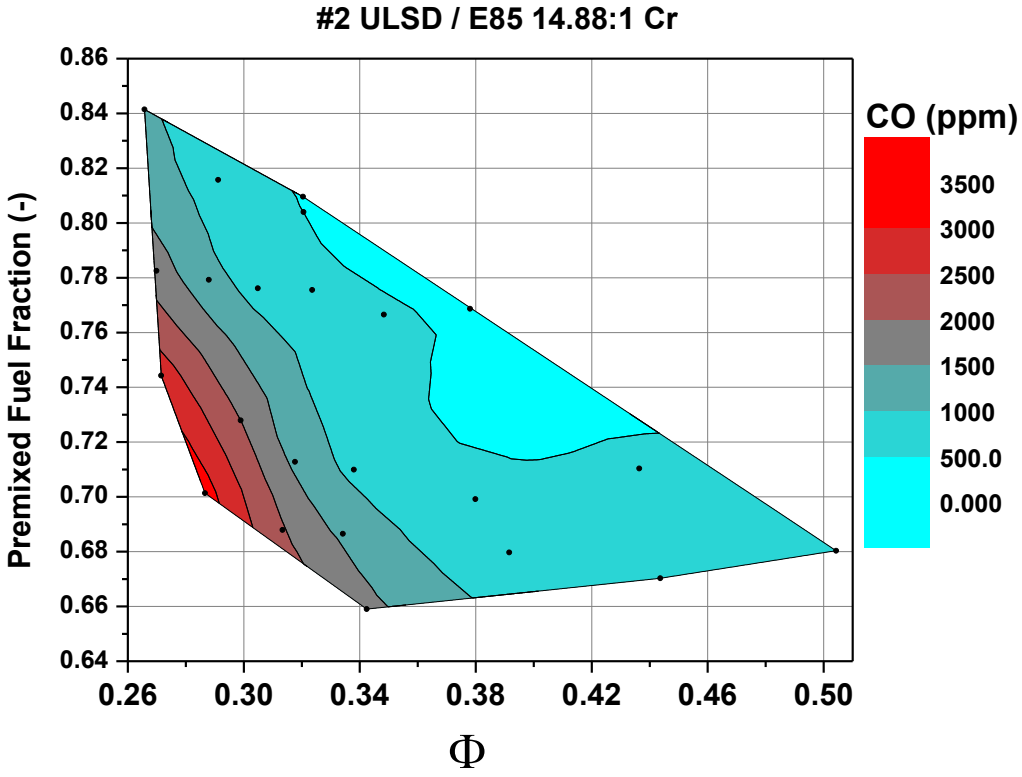

Figure 45 Contours of CO at fixed combustion timing and load. The engine was fueled with ULSD and E85 at a 8.45 bar IMEPn condition 1300 rev/min. The trends show that the highest CO emissions are generated at the leanest conditions with the lowest premixed fuel fractions. This suggests that overly lean areas (premixed) significantly contribute to RCCI CO emissions.

As observed in Figure 45, CO increases at globally lean conditions. As the charge becomes more stratified (less premixed), leaner regions are likely to exist, magnifying CO emissions. These findings are in agreement with those of Ekoto et al. [137], where in LTC strategies CO was found to reside in regions that were overly under or over mixed, leading to lean or rich regions, respectively. To explore CO trends from both under mixed or rich conditions, operation with EGR was also tested.

Figure 46 demonstrates the CO trends of RCCI operated with gasoline and ULSD, at the conditions in Table 18, and the detailed results of the sweep are in Appendix A, Table A. 1 to Table A. 5.

Table 18 Engine operating parameters and hardware for CO sources with EGR

Load (IMEPn)	8.45
CA50 (°CA ATDC)	5
Speed (rev/min)	1300
Piston Bowl Shape	Bathtub
Cr (-)	14.88:1
EGR (%)	45
Intake Temperature (°C)	42-66
Intake Pressure (bar)	1-2
Overall Turbocharger Efficiency (%)	65
Low Reactivity Fuel (PFI)	91 PON gasoline
High Reactivity Fuel (DI)	ULSD

For these tests, intake temperature and pressure were again independently swept, generating a range of Φ, however, when operating with EGR, it is useful to redefine Φ to be charge based (Φ′) as shown in Equation 6 in Chapter 3. Using this definition at the stated fixed phasing and load conditions, a sweep in Φ or Φ′ becomes a sweep in intake pressure. To maintain constant phasing and load, the premixed fuel fraction was altered (i.e., port fuel %). Note that this flexibility is an inherent advantage of RCCI. However, unlike the previous 0% EGR tests, with 45% EGR, this is a sweep between 0.28 and 0.5 Φ′ (charge based), or 0.5 to 0.9 Φ (fresh air based). As shown in the contours, this generates a distinct difference in the range where engine operation and low CO emissions can be achieved.

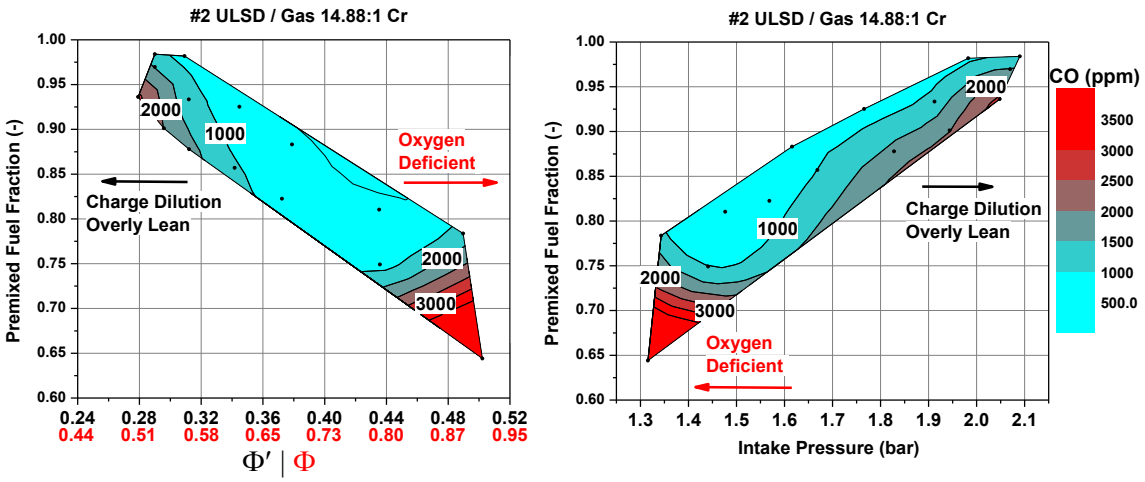

Figure 46 Contours of RCCI CO with EGR at fixed combustion timing and load, Φ/Φ′ based analysis left, and intake pressure analysis right. The engine was fueled with ULSD and 91 PON gasoline at a 8.45 bar $IMEP_n$ condition 1300 rev/min. The trends show that CO occurs at both globally lean and near-rich conditions with the lowest premixed fuel fractions. This suggests that locally lean or rich areas (possible with EGR operation) can both contribute to RCCI CO emissions.

The results depict that with EGR, the low CO (high fuel efficiency) Φ range is more limited regardless of equivalence ratio definition (Φ or Φ′). This demonstrates that total charge mass dilution (Φ′) is the better indicator of the lean condition and the fresh air fuel ratio based Φ is a better indicator of rich conditions. This is an important concept as CO can be generated from either overly rich or overly lean conditions.

For lean conditions the use of Φ′ as a metric is more logical, because the lean limit CO is not formed from an absence of oxygen or fuel, but from a mixture too kinetically slow to support combustion. Thus, with EGR, the true degree of charge dilution is only indicated by Φ′. However, CO from higher equivalence ratio conditions is generated from an absence of oxygen, which like in lean conditions, can be a local or global effect. Since Φ′ masks the lack of oxygen with EGR, it is poor at demonstrating the presence of rich conditions. Thus, to define

the rich limits Φ is a better indicator of the physical phenomena responsible. In conventional thinking, the absolute value and range of Φ or Φ′ presented in Figure 46 would not indicate both an overly lean or rich condition. However, when the two definitions of equivalence ratio are used together, it becomes more evident that both the lean and rich limits are achievable with moderate EGR levels in RCCI.

From the trends in Figure 46, it is inferred that as a larger amount of fuel is direct injected at near globally stoichiometric conditions, the possibility of increasing CO emissions also increases. Thus, in RCCI, CO emissions near both the lean and rich limits are sourced from the fuel stratification itself, with the low CO operable range tending to be narrow. Based on these findings, it is likely that mixture preparation is a key factor in reducing RCCI CO emissions.

Further results on the role of mixture preparation on RCCI CO emissions, are given in the low load study by Splitter et al. [38]. Previous work by Hanson et al. [136], demonstrated the amount of stratification in RCCI increases as the engine load is reduced. Similarly, Splitter et al. [112] demonstrated that for a given condition, the amount of stratification increases, if the compression ratio is reduced. These findings are combined in Splitter et al. [38], where a load of 4.75 bar IMEPg and 11.6:1 Cr were tested at 1200 rev/min. The metal engine study mirrored optical engine PLIF results of Kokjohn et al. [35].

The combined results of Splitter et al. [38] and Kokjohn et al. [35] demonstrated that CO can be reduced by enriching overly lean areas of the chamber. Specifically, Splitter et al. [38] demonstrated that with using multiple

injections the fuel distribution is more evenly distributed and CO emissions could be mitigated. Moreover in that study, if the stratification was high (i.e., ~65% or less premixed fuel), the premixed fuel Φ was below the auto-ignition limit. This correspondingly had a dramatic effect on CO emissions, where lean premixed Φ had very high CO emissions. Figure 47 is reproduced from that study where the trends in CO and corresponding premixed Φ are noted, with the corresponding operating conditions displayed in Table 19.

Table 19 Engine operating parameters and hardware low load CO investigation [38]

Load (IMEPn)	4.75
CA50 (°CA ATDC)	0.75
Speed (rev/min)	1200
Piston Bowl Shape	Open crater
Cr (-)	11.6:1
DI Timing (°CA ATDC)	-50
PFI Timing (°CA ATDC)	-320
EGR (%)	0
Intake Temperature (°C)	40-100
Intake flowrate (mg/cycle)	2125± 25
Fuel mass (mg/cycle)	51.5 ± 0.5
Global Φ (-)	.335± .0025
Low Reactivity Fuel (PFI)	Isooctane
High Reactivity Fuel (DI)	n-heptane

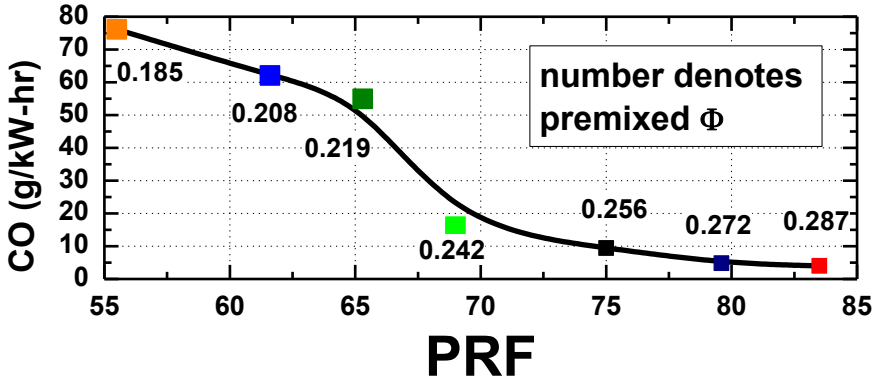

Figure 47 CO emissions associated with sweeping intake temperature at constant phasing and load, see Table 19, with the single injection strategy at -50°CA ATDC injection timing. Note that as the premixed fuel equivalence ratio increases, CO losses decrease. When the premixed fuel mixture is richer than the lean limit, a sharp reduction in CO is observed. Figure reproduced from Splitter et al. [38]

From Figure 47, a clear distinction on combustion efficiency and emissions is seen around a PRF number of 67. At these conditions the premixed fuel equivalence ratio becomes sufficiently high to promote complete combustion. The corresponding heat releases from these experiments are seen in Figure 48.

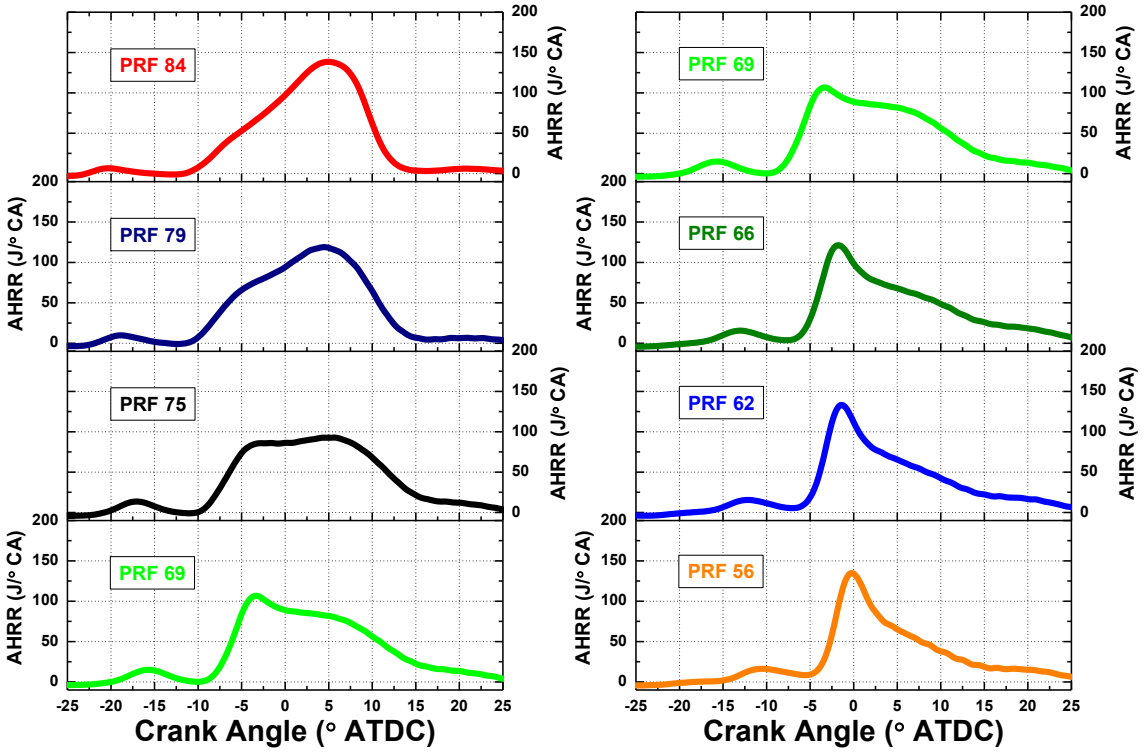

Figure 48 Apparent heat release rates of the PRF/Temperature sweep at constant load and phasing. Note that the long tail observed in the heat release of PRF values below 69, indicate poor combustion, with higher CO levels as seen in Figure 47. Cases without tails demonstrate good combustion efficiency. Figure reproduced from Splitter et al. [38].

Combining the AHRR trends of Figure 48 with the CO trends of Figure 47, when high levels of CO are encountered in RCCI, they are formed in overly lean conditions with longer combustion times. With overly lean conditions, stable rapid combustion is not supported in leaner regions, generating a drawn out combustion event, freezing the combustion process prematurely at incomplete

combustion species. To mitigate these processes sufficiently high premixed fuel Φ are required, as indicated by Figure 47.

The present and previous studies demonstrate that in RCCI, CO emissions are generated in overly lean regions and with EGR, in overly rich chamber regions. CO mitigation was possible through a combination of intake temperature or injection strategy, where the Φ of the premixed fuel was critical for reducing CO emissions. These results are critical for successfully implementing the results of the preliminary modeling study in Chapter 3, where very lean conditions were suggested to increase engine efficiency.

5.2 Effects of Engine Operating Conditions on Engine Efficiency

The previous section demonstrated that several different operating parameters and their combinations can be used to operate RCCI at similar combustion phasing. Literature was consulted as a guide for understanding the physical and chemical phenomena that is likely responsible for different factors contributing to observed RCCI trends. In the present section, these phenomena were explored experimentally to understand the relationships that chamber gas conditions and composition play on engine efficiency. The goal of these studies was to explore conditions that provide maximum efficiency for a given engine geometry so that the relationships could be applied as a pathway for achieving the conditions required to duplicate the high efficiency simulation results described in Chapter 3.

5.2.1 Fuel Effects on RCCI

To isolate the dependent variables of RCCI combustion, a prescribed load and combustion phasing was selected, as summarized in Table 20. The load selected was 8.45 bar IMEPn (~9 bar IMEPg). This load point has consistently been observed to be a maximum efficiency condition by Hanson et al. [33], and Splitter et al. [134]. After selecting the load, combustion was phased by trimming the fuel reactivity at the conditions shown in Table 20, with fixed intake pressure and temperature with no EGR. For the tests, a simulated overall turbocharger efficiency of 65%[†††] was set by adjusting the engine backpressure.

Table 20 Engine operating parameters and hardware for efficiency vs. CA50 sweep

Load (IMEPn)	8.2
CA50 (°CA ATDC)	-2 to 6
Speed (rev/min)	1300
Piston Bowl Shape	Bathtub
Cr (-)	14.88:1
DI Timing (°CA ATDC)	-60/-35
DI Dwell Bias (%SOI1, % SOI2)	~60/40
PFI Timing (°CA ATDC)	-320
EGR (%)	0
Intake Temperature (°C)	32
Intake Pressure (bar)	1.56
Exhaust Pressure (bar)	1.45
Low Reactivity Fuel (PFI)	91 PON Gasoline
High Reactivity Fuel (DI)	#2 ULSD
PFI Fuel Fraction (-) (by energy)	.77-.92
DI Fuel Fraction (-) (by energy)	.23-.08
Global Φ (-)	.298±.003

The results of the sweep are presented in Figure 49.

[†††] Simulated overall efficiency uses an air standard approach as defined in Equation 8 in Chapter 4, where it was assumed there is a 4 kPa and 16 kPa drop in intake and exhaust systems respectively, to account for piping, air filter, and DOC

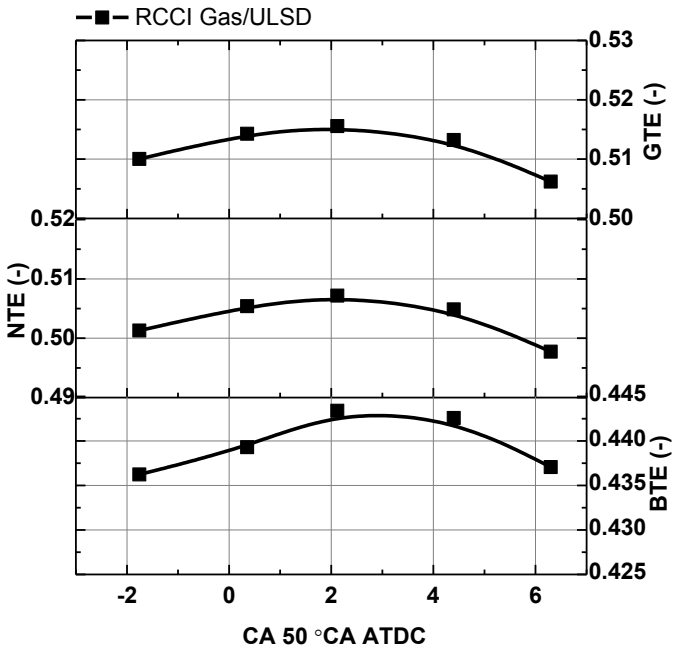

Figure 49 Sweep of combustion phasing to determine the location of highest efficiencies. The engine was operated lean at Φ=0.29 and 1300 rev/min speed ~9 bar IMEPg. Engine efficiency defined as gross, net, and brake, as calculated using Equations 10, 11, and 21 in Chapter 4.

The figure indicates that the selected maximum efficiency depends on the definition of efficiency used. That is, the highest gross efficiencies (GTE) occur at crank angles closer to TDC than the conditions of maximum brake efficiency (BTE). However, the net and brake efficiencies are dependent on air handling (turbocharger selection) and friction (materials, oil, base engine design), which are all application specific (see Chapter 4).

The above results indicate that there is a local maximum of efficiency at CA50 timings just after TDC. However, the results do not indicate that the present conditions (intake pressure and temperature) offer the condition of maximum efficiency. To explore this, the conditions described in the Φ-T matrix of Figure 44 and Table 16 were tested.

Due to the large search space of the Φ-T matrix and the multiple number of fuels tested, only select key findings will be presented, which are pertinent to the current research. Results with fuel 2 (3% EHN in 91 PON gasoline/E85) were found to offer the highest thermal efficiency. The following sections will describe their operation and behavior.

5.2.2 3% EHN Gasoline Behavior in Mixing Controlled Combustion

In the literature review in Chapter 2 it was discussed that cetane improvers can be used to enhance the reactivity of fuels. In the present study, EHN was added at 3% addition by volume to 91 PON gasoline. This has been observed by Hanson et al. [136] to offer ignition characteristics similar to that of ULSD. However, neither in the present study, nor the cited work by Hanson was detailed chemical analysis performed on the EHN doped gasoline. Indeed, Bacha and Lesnini [138] indicated that the cetane improving effects of EHN are time sensitive. Therefore, the duration associated with shipping and testing of the fuels may provide inaccurate findings. Furthermore, the exact chemistry of the fuel is less important to the present study than the observed combustion behavior. In place of fuel analysis testing, a sweep of mixing controlled combustion experiments were performed with variations in injection pressure. The results from the study are presented in Figures 51 and 52. The operating conditions are presented in Table 21 and injection schedule are given in Table 22.

Table 21 Engine operating parameters and hardware for mixing controlled combustion

Load (IMEPn)	8.45±0.05
CA50 (°CA ATDC)	3±0.5
Speed (rev/min)	1300
Piston Bowl Shape	Bathtub
Cr (-)	14.88:1
EGR (%)	0
Intake Temperature (°C)	32
Intake Pressure (bar)	1.72
Exhaust Pressure (bar)	Varied to fix turbo. η
Overall Turbocharger η (%)	65

Table 22 Mixing controlled injection schedule for ULSD and 3% EHN + 91 PON gasoline

Fuel	**Fuel Flowrate (g/s)**	**SOI Pilot (°CA ATDC)**	**Pilot Dur. (ms)**	**SOI Pilot (°CA ATDC)**	**Main Dur. (ms)**	**Rail P. (bar)**
ULSD	1.13	-30	0.35	-15	1.14	1300
ULSD	1.15	-39	0.36	-20	1.55	700
ULSD	1.15	-46	0.56	-23	1.82	500
3% EHN + 91 PON Gas	1.14	-30	0.35	-15	1.12	1300
3% EHN + 91 PON Gas	1.14	-39	0.36	-20	1.5	700
3% EHN + 91 PON Gas	1.15	-46	0.56	-23	1.82	500

In Figure 50 heat release and pressure are plotted for operation at matched conditions, with fueling of ULSD (black) and EHN doped gasoline (dashed red). The fuel was delivered in a double injection strategy at 1300 bar rail pressure. The command currents are plotted in blue.

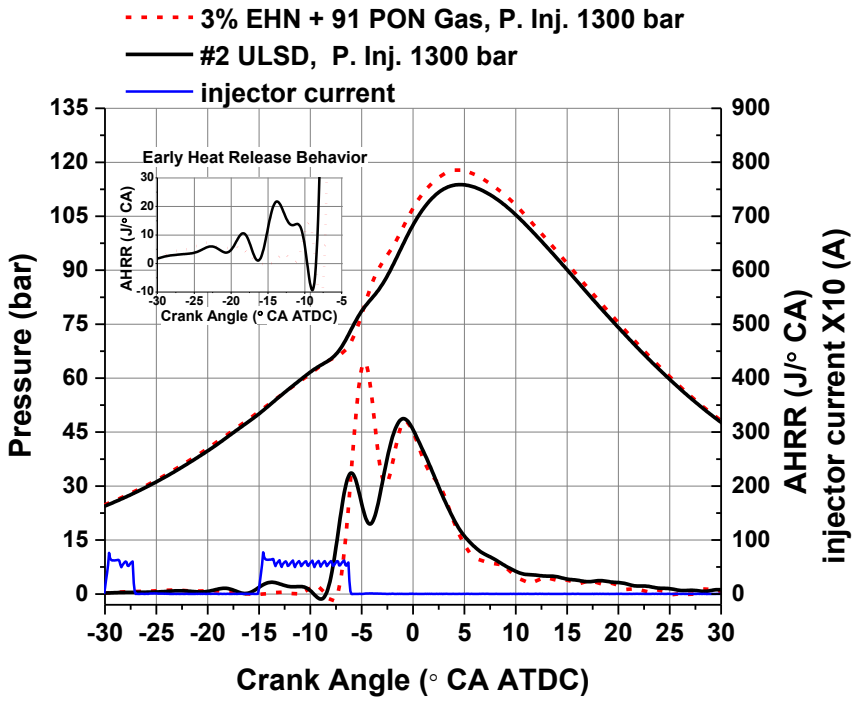

Figure 50 #2 ULSD mixing controlled operation (black) and EHN gasoline mixing controlled operation (dashed red). Blue traces show injection current, where a pilot and main injection strategy was used (see Table 22). Single injections resulted in high premixed burn fractions as EHN gasoline was found to have lower cetane number than ULSD.

The figure suggests that the cetane number of the EHN doped gasoline is lower than ULSD. It is observed that early heat release (pilot fuel combustion) is not present with EHN gasoline. This suggests that the reactivity of ULSD is higher than EHN gasoline. Additionally, the fuel analysis of ULSD in Table 2 and un-doped gasoline in Table 3 show that the volatility of the EHN doped gasoline is much higher than that of ULSD[‡‡‡]. These fuel properties affect the combustion process, in which the premixed burn spike is observed to be much larger than that of ULSD. Likewise, ULSD is observed to have a much larger fraction of fuel burnt in the lifted flame (diffusion) mode. The corresponding emissions and performance trends are shown in Figure 51.

[‡‡‡] 3% by volume addition of EHN to gasoline affects the mixture fuel volatility minimally

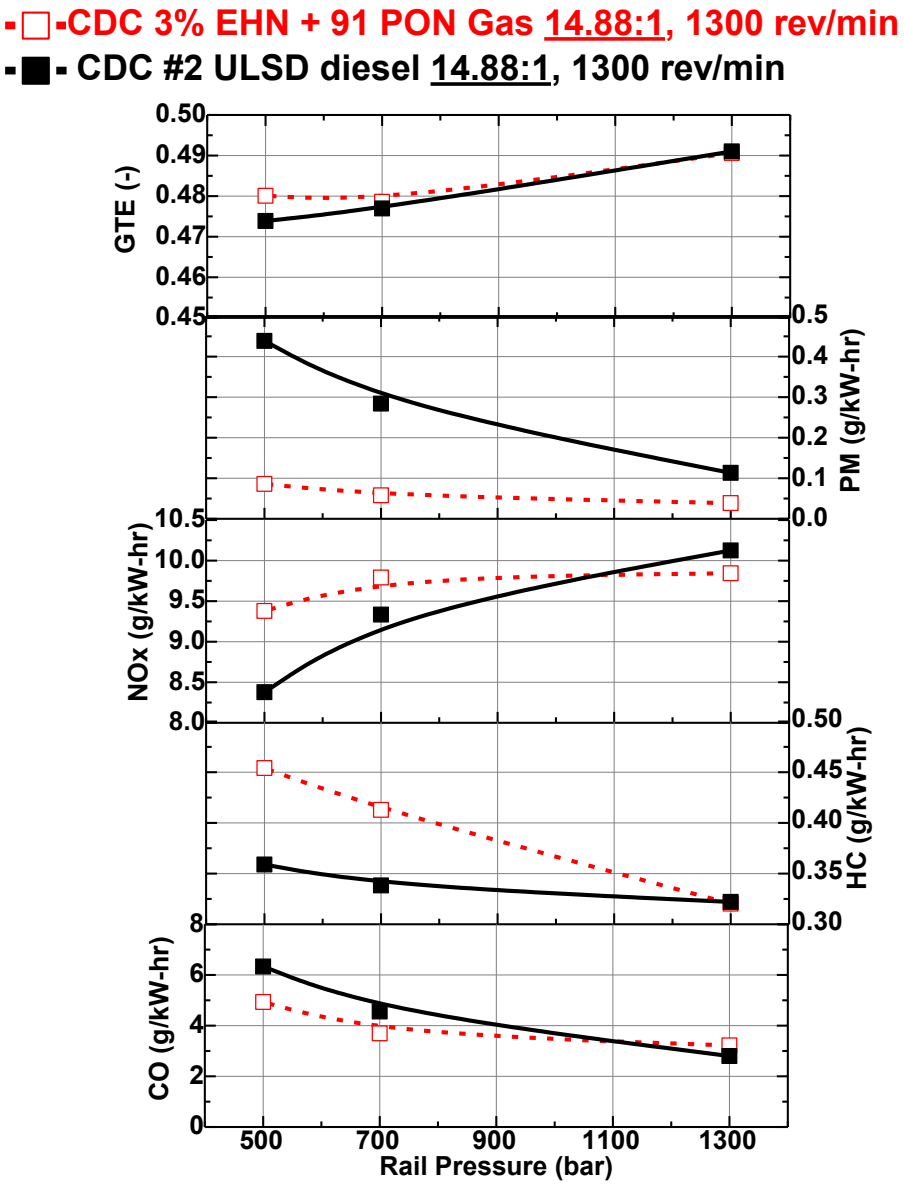

Figure 51 Key emissions and performance metrics of ULSD and 3% EHN in 91 PON gasoline as a function of rail pressure.

The emissions and performance trends also suggest a lower cetane number of EHN gasoline through higher HC and CO and lower PM, particularly at low injection pressures. The added mixing time with a lower cetane number fuel has

been shown by Hanson et al. [11] to increase the emissions of HC and CO and decrease PM. Regardless of the fuel reactivity, in the mixing controlled combustion process, there is little difference in gross thermal efficiency of ULSD and EHN. A small deviation (≤0.5% GTE) was only seen at the lower injection pressures.

Lastly, the NO_X emissions of the sweep were interesting. At the lower injection pressures, the NO_X of EHN doped gasoline was higher than that of ULSD with similar emissions at higher injection pressures. These suggest that injection pressure, and thus spray breakup effects, may contribute to a different process in the conversion of fuel-borne NO_X in EHN than ULSD.

Based on the present mixing controlled combustion study, and previous work by Hanson et al. [11], it is concluded that 3% EHN in 91 PON gasoline's reactivity behaves in-between that of gasoline and ULSD. Similar results were shown by Rothamer and Murphy [139], where kerosene-like fuels were compared to ULSD. Their results demonstrate that the lower cetane number of fuels between that of gasoline and ULSD were shown to increase ignition delay.

5.2.3 RCCI with 3% EHN Gasoline

The above mixing controlled combustion section demonstrated that 3% EHN in 91 PON gasoline has a slightly lower reactivity, but higher volatility than ULSD. In RCCI combustion, fuel-air mixing time is significantly increased compared to conventional mixing controlled processes. However, the reactivity (cetane or octane number) of the fuel and the fuel volatility (See Appendix B) are important

factors in RCCI combustion, as seen in Figure 52 with the corresponding operating conditions in Appendix A. The results show that a higher fraction of reactive fuel is required and the heat release is shorter with the use of EHN-doped gasoline.

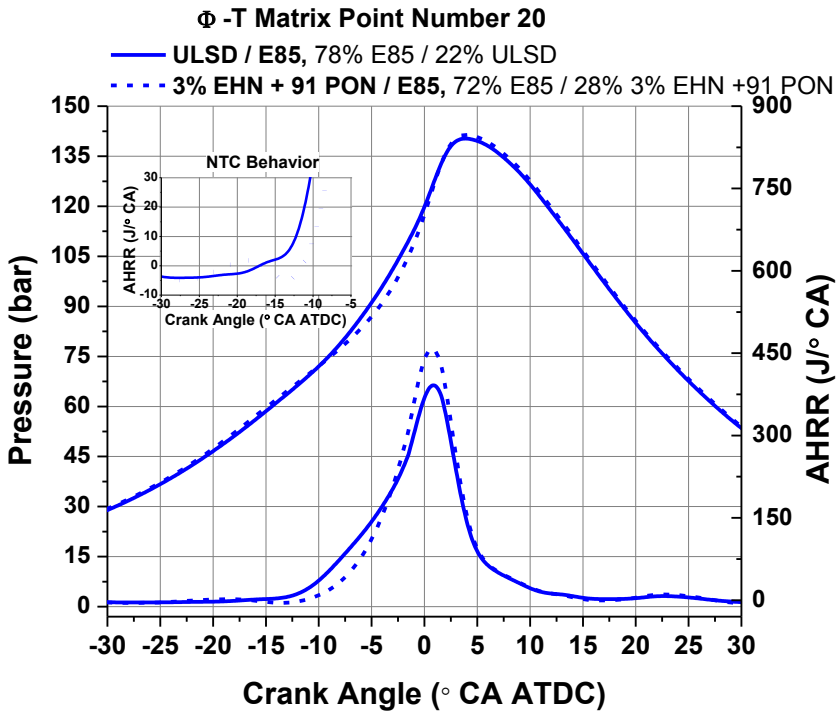

Figure 52 RCCI heat release at matched conditions in Φ-T space (matrix point #20) with 3% EHN gasoline and ULSD DI and E85 PFI fueling. Operation with EHN gasoline demonstrates reduced reactivity stratification as the onset of HTHR is more abrupt, and the peak heat release rate is higher.

The shorter AHRR in Figure 52 also suggests that reactivity (cetane number) of EHN doped gasoline is less than that of ULSD. This is in agreement with the previous section's mixing controlled results. Interestingly, in Figure 52, NTC behavior was not observed with ULSD/E85, but with EHN gasoline/E85 it was. As suggested by Splitter et al. [39] and later by Hanson et al. [136], the NTC of cetane improved gasoline occurs earlier in the combustion process and is smaller than that of ULSD. However, in the present work, the use of E85 is

observed to suppress NTC in ULSD operation more than EHN doped gasoline. Based on the previous literature by Hashimoto [56, and 57] and Splitter et al. [55], as reviewed in Chapter 2, the early chemistry reactions of EHN doped gasoline exhibit reduced interaction with ethanol than ULSD. The specific reason for this is unknown, but is likely to be from the lower activation energy of EHN [116] causing increased $\dot{R}+O_2$ rates at lower pressures and temperatures. This agrees with the findings of Mehl et al. [52] where at higher pressures and temperatures a fuel may exhibit ITHR if it does not exhibit NTC.

The combination of these observations demonstrates that the effective reactivity of EHN doped gasoline results in shorter heat release than ULSD at the tested conditions. However, as shown in Figure 53, as temperature increases these discrepancies are reduced, as the combustion event becomes more HCCI-like (abrupt).

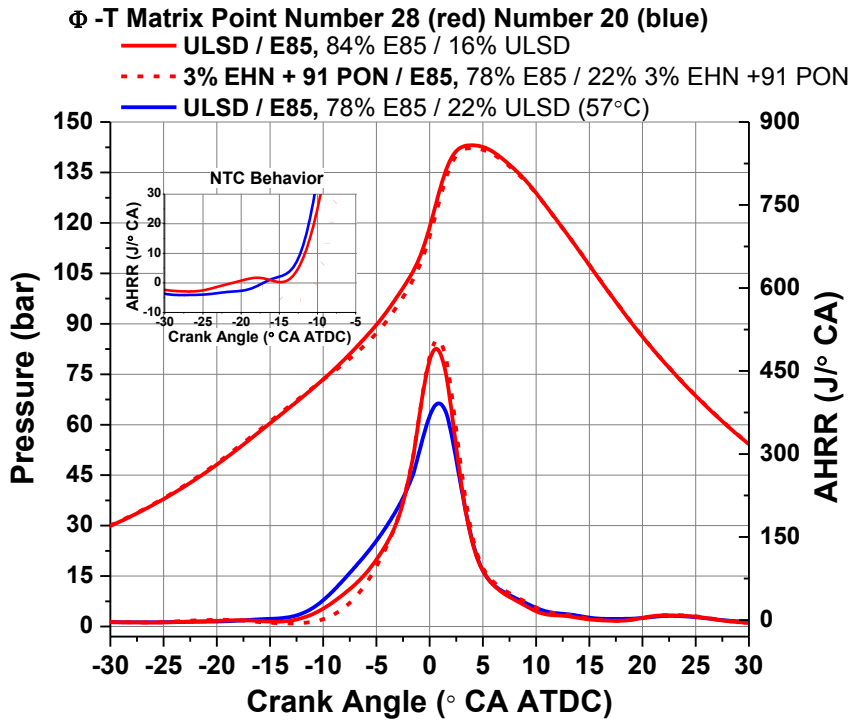

Figure 53 Pressure and Heat release behavior at matched Φ-T conditions (matrix point #28) for ULSD/E85 (red) and EHN Gas/E85 (dashed red). Also plotted for reference is the AHRR of matched fueling ratios for EHN gas/E85 (dashed red) and ULSD/E85 (blue, matrix point #20). The results demonstrate that at matched Φ-T conditions of fuel delivery ratios. EHN gasoline displays a reduced reactivity gradient as compared to ULSD/E85, with matched fueling ratios exhibiting a larger difference.

Also plotted in blue in Figure 53 is the heat release of the same reactivity split of ULSD/E85 and EHN doped gasoline/E85 RCCI operation.

5.2.4 Operable Limits of E85 Fuels

In sections 5.2.2 and 5.2.3, EHN mixed with gasoline was shown to exhibit reduced reactivity as compared to ULSD. This reduces the maximum achievable reactivity gradient of RCCI and thus, affects the operable area. Figure 54 demonstrates the Φ-T operable window of EHN/E85 relative to USLD/E85. The tests are operated at the conditions in Table 16 with the specific operating parameters shown in Appendix A. In both tests, constraints of 97% combustion

efficiency and 12 bar/°CA were set as the upper and lower limits of acceptable operation, since operation outside these bounds demonstrated deteriorated efficiency and performance.

In all subsequent Φ-T figures, the combustion efficiency limits are shown by a black line, and the PPRR limit is shown by a blue line. Additionally, the matrix points are color coded to represent the constraint status of the condition, where the color coding is shown in Table 23.

Table 23 Φ-T matrix constraint satisfaction color key

Condition			
	Both Constraints satisfied	**One Constraint satisfied**	**No Constraints satisfied**

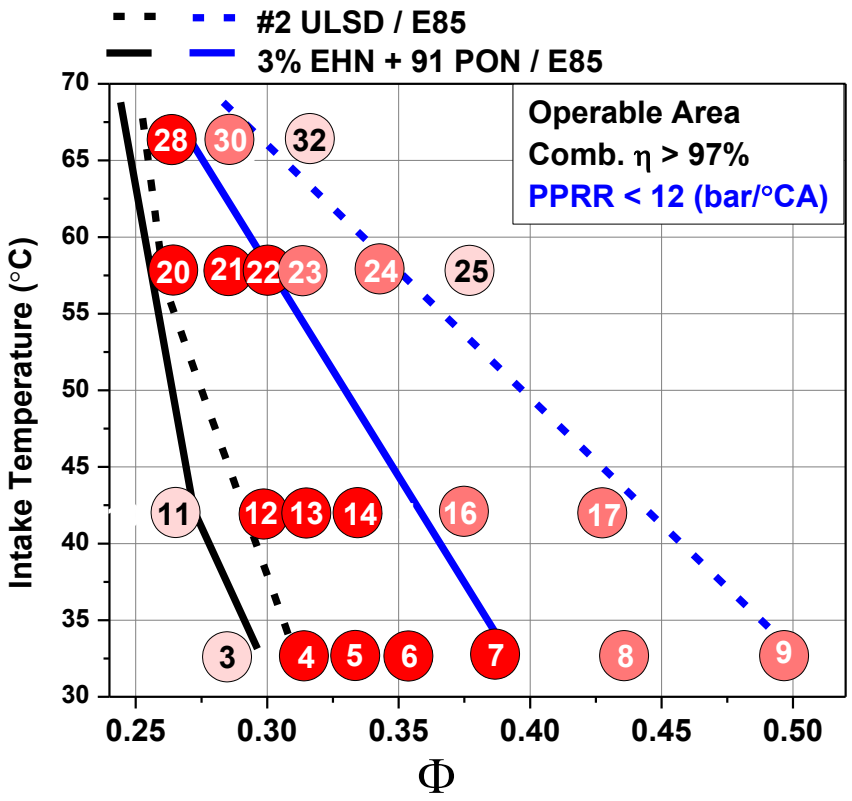

Figure 54 Operable space of Φ-T matrix with the tested E85 based fuels. Note that the larger reactivity gradient of ULSD/E85 offers a larger operable window than the reduced reactivity gradient of EHN gasoline/E85.

In Figure 54 EHN gas/E85 and ULSD/E85 are plotted, thus the conditional color code represents conditions satisfied by both fuels (i.e., dark red signifies that both ULSD and EHN gasoline satisfied the condition). In general, as temperature is increased, the charge must be diluted more in order to remain within the constraint limits.

5.2.5 Comparisons of Constant Φ, Temperature, and PPRR in Φ-T Space

In this section the effects of pressure and temperature are examined to better understand the relation between the combustion process and the engine cycle that contributes to higher efficiency.

For brevity, only comparison with the EHN gasoline results is presented. However, similar trends were observed with both fueling strategies, see Appendix A (data) and Appendix B (Impingement). Chapter 2 showed that intake temperature and pressure variations provide means of controlling the heat release timing in HCCI. In RCCI the added ability to trim the fuel properties to maintain constant combustion phasing enables comparisons of performance at a fixed combustion phasing, but with several different intake pressure and temperature combinations. In this section the pressure and temperature effect were independently varied, and then simultaneously varied in their combination to maintain a constant pressure rise rate. The results indicate conditions of loss minimization and resulting high efficiency-operation.

5.2.5.1 Constant Φ Sweeping Intake Temperature

To isolate the effects of temperature, a constant equivalence ratio was selected, and the intake temperature was varied at fixed combustion phasing and load. To maintain constant phasing as required, the ratios of the low and high reactivity fuels were adjusted. The operation implemented is represented by the dashed light green line in Figure 55. The corresponding AHRR events (right), and the engine operating conditions are summarized in Table 16 with specific operating conditions and performance given in Appendix A Table A. 2.

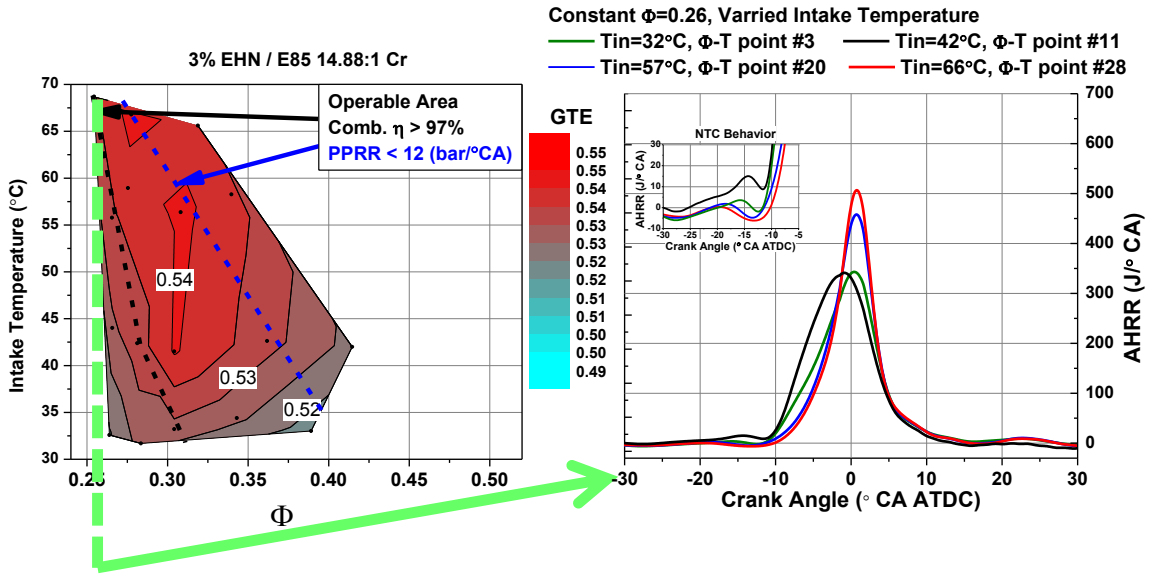

Figure 55 AFR_c based GTE contours and associated AHRR for fixed Φ, varied T operation.

The AHRR trends of Figure 55 demonstrate that as intake temperature increases, the combustion event becomes more abrupt. As the fuel mixture becomes more homogeneous with higher intake temperature operation, the smoothing present in the early stages of the heat release is reduced. However, the end of combustion appears to be unaffected.

The corresponding efficiency and HX losses (see Equation 40) are presented in Table 24. (Note: these data use the emissions mass measurements to determine the energy flow. Minor differences exist with the emission based measurement, but with EHN these were found to be minimal see Appendix B - Impingement and Chapter 4 section 4.8.2).

Table 24 key losses and parameters of constant Φ varied T operation

Φ-T Condition	**3**	**11**	**20**	**28**
T intake (°C)	32	42	57	66
Φ (-)	.263	.268	.268	.263
E85 (% energy)	55.8	65.5	75.0	78.1
Comb. Eff. (-) (fraction of fuel energy)	.945	.953	.967	**.972**
HX (-)(fraction of fuel energy)	**.087**	.099	.100	.121
GTE (-) (fraction of fuel energy)	.519	.529	.534	**.535**
NTE (-) (fraction of fuel energy)	.480	.492	**.494**	.493
BTE (-) (fraction of fuel energy)	.407	.427	**.428**	.426

From the table it is observed that heat losses increase with increasing intake temperature, as does combustion efficiency. As described in Chapter 4 Equation 40 and 28, the HX losses and exhaust losses (EXH) were lumped to more clearly determine the effects of incomplete combustion on GTE. The results of combustion and HX+ EXH losses are plotted in Figure 56. Also plotted in the figure are trends from richer, Φ=0.31, with varied intake temperature operation.

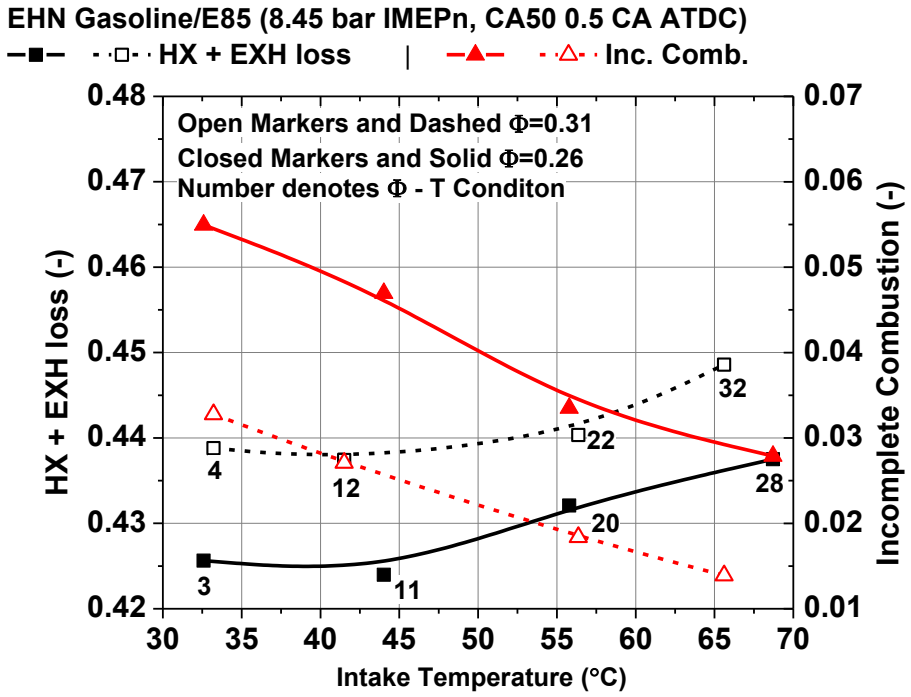

Figure 56 Losses associated with sweeping intake temperature at constant Φ, the operating conditions are in Table 16 with the Φ-T matrix data in marked for reference in Appendix A. The dashed lines with open markers denote richer operation at Φ=0.31 demonstrating a tradeoff in reduced combustion efficiency for increased HX+EXH losses

It is clear from Figure 56 that as intake temperature increases, incomplete combustion decreases with associated, but less drastic, increases in HX + EXH. The trends are observed to be Φ independent, but with faster (see Figure 55) and richer combustion having higher HX+EHX and lower incomplete combustion. The incomplete combustion at Φ=0.26 and Φ=0.31 conditions are observed to be predominantly from higher CO emissions, as shown in Figure 57.

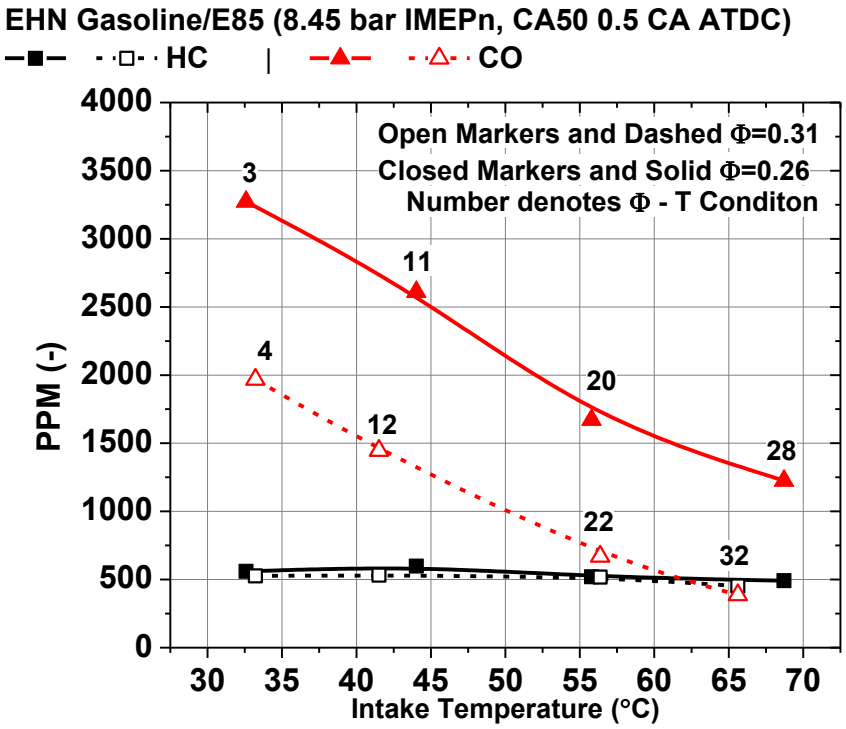

Figure 57 Incomplete combustion species at constant Φ conditions, the operating conditions are in Table 16 with the Φ-T matrix data in marked for reference in Appendix A, Table A. 2. Note that CO is the dominant emission for all but the highest temperatures, with richer operation exhibiting lower CO.

The combined results of constant Φ, varied intake temperature operation show that GTE is primarily dominated by combustion efficiency, as HX+EXH losses are less affected. Overall incomplete combustion sensitivity was only observed in the CO emissions. These results support conclusion that crevice effects likely dominate HC emissions, and that local mixing and equivalence ratios are dominate CO emissions. The richer Φ conditions (e.g., maximum GTE in Figure 55) showed reduced incomplete combustion compared to HX + EXH losses.

5.2.5.2 Constant Temperature Sweeping Φ

This section investigates fixed intake temperature operation with changing Φ (i.e., changing boost), for the conditions in the Φ-T matrix of Figure 44 and Table 16. For the comparison, two intermediate temperature conditions were selected, viz., 57°C and 42°C. Figure 58 and Table 25 depict the results of the higher of the two (57°C), where the dashed green line represents the swept operable space.

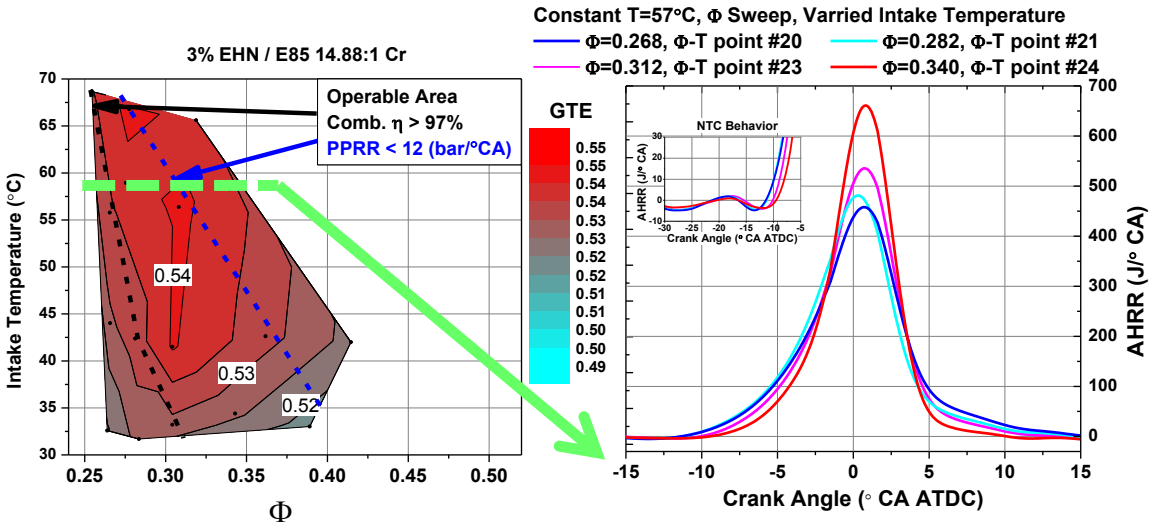

Figure 58 AFR_c based GTE contours and associated AHRR for constant T varied Φ operation. The operating conditions are in Table 16 with the tested operating point data provided as in Appendix A, Table A. 2.

Figure 58 illustrates that intake pressure affects the heat release shape, similar to the intake temperature trends in Figure 55. However, the end of combustion is seen to change with varied Φ. As shown in Table 25, the required adjustments to the fueling ratios were reduced; unlike those of the constant intake temperature runs (see Table 24). In the present approach, (fixed IMEPn (6.45 bar) and overall turbocharger efficiency (65%)) the choice of fueling ratios

is influenced by the amount of trapped hot residuals. For example, the exhaust backpressure ratio, and thus trapped residual, increase as the charge is leaned. The opposite effect occurs as the charge is enriched the backpressure ratio must be reduced (see Appendix A, Table A. 2). In 2-stroke engine RCCI experiments Labaza [140] demonstrated that the presence of hot residuals changes AHRR behavior and requires changes to the fueling ratios.

Table 25 Losses and parameters of constant T varied Φ operation

Φ-T Condition	20	21	23	24
T intake (°C)	57	57	57	57
Φ (-)	.263	.268	.268	.263
P Intake (bar)	2.13	1.97	1.74	1.63
P Exhaust (bar)	2.44	2.18	1.88	1.79
E85 (% fuel energy)	74.9	72.4	69.5	72.1
Comb. Eff. (-)	.966	.973	.982	**.986**
HX (-) (fraction fuel energy)	.124	.122	.128	.149
GTE (-) (fraction fuel energy)	.528	**.541**	**.541**	.538
NTE (-) (fraction fuel energy)	.499	.511	**.514**	.507
BTE (-) (fraction fuel energy)	.426	.446	**.449**	.441

Figure 58 shows that with increased boost pressure there is an observed spreading of the heat release trace. This result proves interesting because the neat ethanol results by Sjöeberg and Dec reviewed in Chapter 2 demonstrated that there was little to no pressure dependence of ethanol. Thus, in E85 RCCI, it is likely that the more reactive fuel portion may accelerate the kinetics and spread out the heat release event (similar to the results of Dec and Yang [21] with gasoline at high boost pressure).

It was shown previously in Figure 48 that the late heat release shape reflects incomplete combustion. In contrast, the results in Figure 55t showed that at constant Φ and varied intake temperature, the tailing edge remains nearly constant regardless of fueling. Based on this and he present analysis, it is likely that the tailing portion of the heat release trace reflects more changes in combustion efficiency, through both local or global effects, while the early portion of the main heat release trace is dominated more by a local fuel and ignition effects.

In terms of efficiency, the heat release behavior appears to be coupled to Φ (trapped mass), as displayed in Figure 59 .

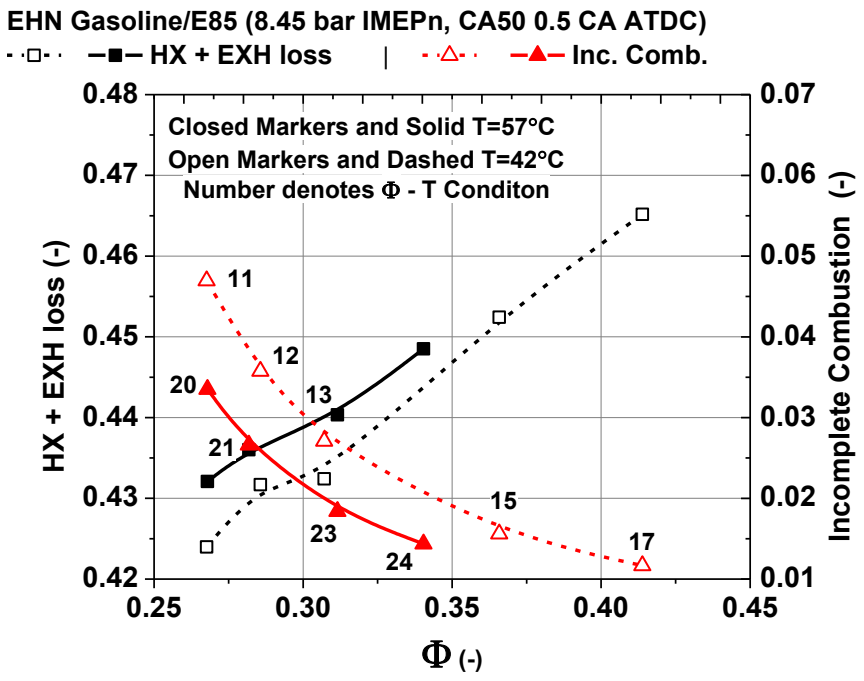

Figure 59 Losses associated with sweeping Φ (boost) at constant temperature, the operating conditions are in Table 16 with the Φ-T matrix data in marked for reference in Appendix A, Table A. 2. The dashed lines with open markers denote cooler operation at T_{in}=42°C. The results demonstrate a tradeoff in combustion efficiency and increased HX+EXH losses.

The combined results of Figure 58 and Figure 59, show that the longer AHRR with leaner operation lowers HX + EXH losses, but increases incomplete combustion. The trends of these losses seem to exhibit a one-to-one tradeoff, meaning that the range of the losses is similar over the sweep of Φ.

Similar to constant Φ varied intake temperature operation, incomplete combustion is increased with leaner operation. The associated sources of incomplete combustion are plotted in Figure 60 where the major contributing species was found to be CO.

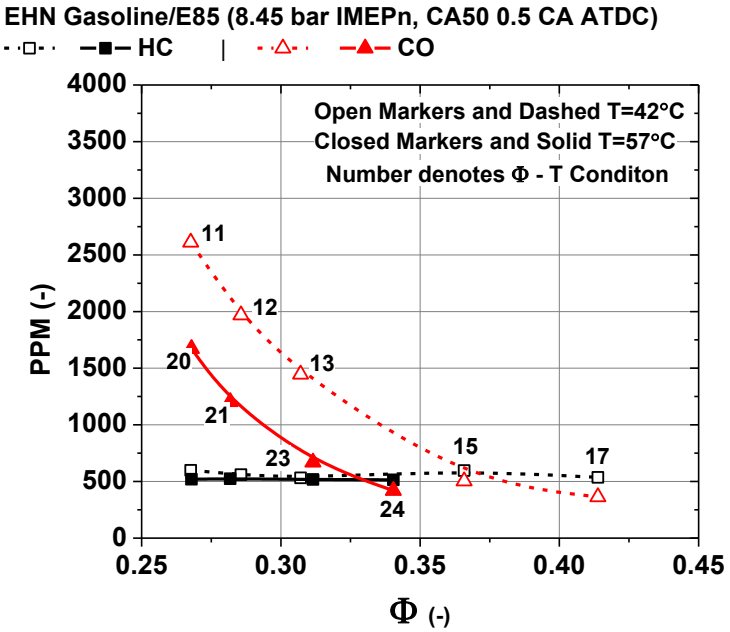

Figure 60 Incomplete combustion species at constant temperature varied Φ conditions, the operating conditions are in Table 16 with the Φ-T matrix data in marked for reference in Appendix A, Table A. 2. Note that CO is the dominant emission for all but the highest Φ, with hotter operation exhibiting lower CO.

The results of Figure 60 show a tradeoff in HX + EXH and combustion efficiency as Φ (analogous to boost) is swept. That is, the highest intake pressures offer the lowest heat transfer and exhaust losses, but at the expense of combustion efficiency. However, only after appreciable combustion efficiency losses are had

at very lean conditions, is gross efficiency negatively affected. This relation enables a window for efficiency optimization.

5.2.5.3 Constant PPRR by Simultaneously Sweeping Φ and Temperature

The present section investigates whether a similar combustion process can be maintained across a range of temperature and pressure conditions. Figure 61 proves that this is possible by balancing intake temperature and pressure changes. The operating conditions are summarized in Table 26.

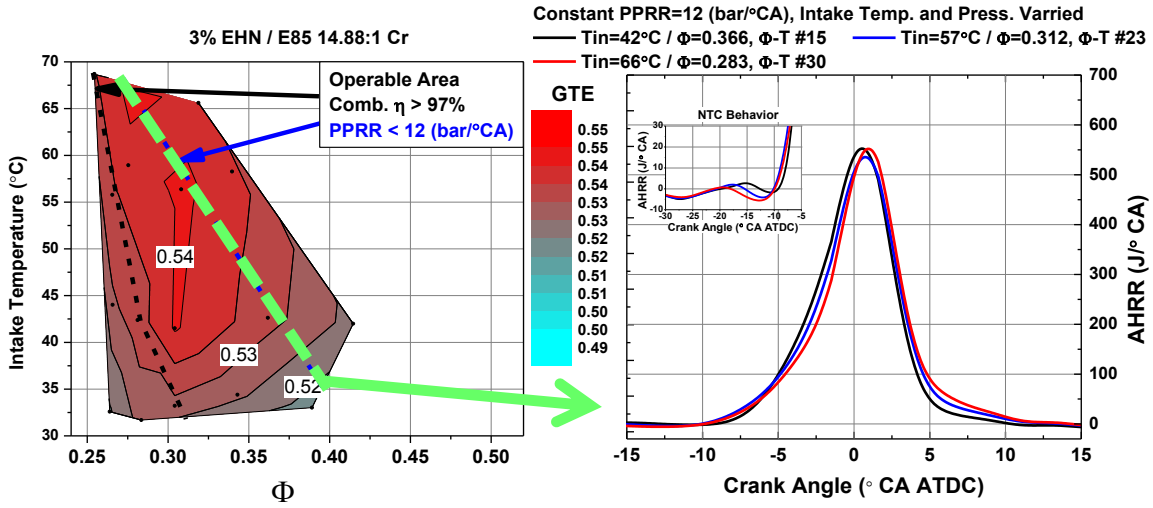

Figure 61 AFR_c based GTE contours and associated AHRR for constant PPRR with simultaneously varied Φ and T operation, with the Φ-T matrix data in marked for reference in Appendix A, Table A. 2.

This combustion strategy provides high efficiency and demonstrates a pathway for maintaining high efficiency across a range of operating conditions. The above conditions provide, a constant heat release rate, as is often assumed to be possible in simulations, such as those by Lavoie et al. [58].

As indicated in Table 26 and Figure 62, at constant PPRR operation conditions, combustion efficiency is almost constant, better isolating the effects of

the trapped mass. Figure 61 shows that leaner conditions tend to have the highest gross efficiencies. This approach demonstrates the dependency of the heat release on operating conditions, because conditions must be balanced as to maintain similar combustion. Note in Figure 61, that the combustion events are not identical, although they perform similarly. They exhibit slightly different leading and tailing heat release behaviors, as exhibited in the independent temperature and pressure sweeps (seen in Figure 55 and Figure 58).

Table 26 Losses and parameters of constant PPRR operation through simultaneous variation of Φ and T, the Φ-T matrix data in marked for reference in Appendix A, Table A. 2.

Φ-T condition	**15**	**23**	**30**
T intake (°C)	**42**	**57**	**66**
P intake (bar)	**1.47**	**1.74**	**1.96**
Φ (-)	**.366**	**.312**	**.283**
E85 (% fuel energy)	59.5	69.5	76.7
Comb. Eff. (-)	.984	.982	.981
HX (-) (fraction fuel energy)	.163	.128	**.124**
GTE (-) (fraction fuel energy)	.532	.541	**.542**
NTE (-) (fraction fuel energy)	.507	**.514**	.507
BTE (-) (fraction fuel energy)	.445	**.449**	.440

Table 26 illustrates that the combustion efficiency is nearly constant but the HX trend is not. These results were plotted as a function of equivalence ratio with the previous constant intake temperature and varied Φ results. The two trends are plotted in Figure 62, where the fixed PPRR results are solid markers

and lines and while fixed temperature results are open markers and dashed lines.

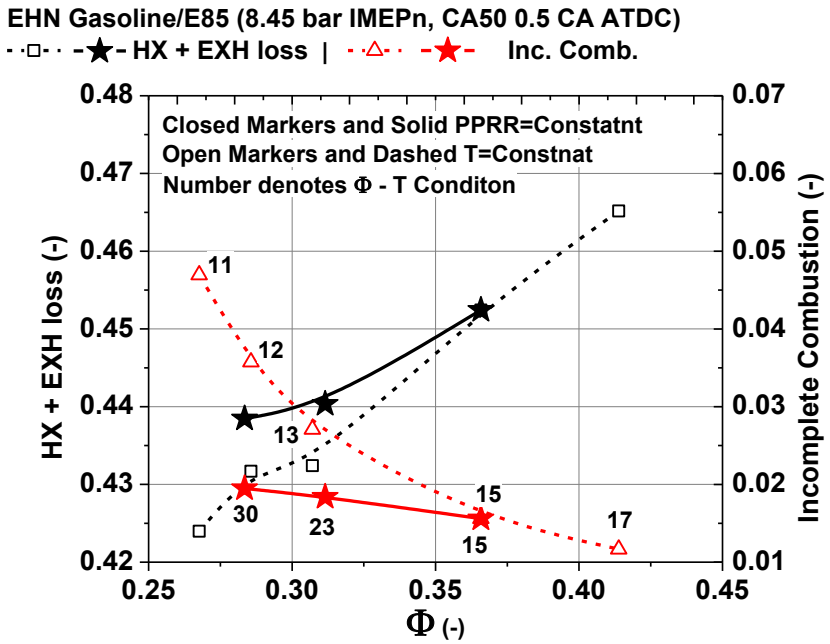

Figure 62 Losses associated with sweeping Φ (boost) at constant PPRR. The dashed lines with open markers denote constant temperature operation at T_{in}=57°C. The constant PPRR results (closed markers solid lines) demonstrate a nearly constant combustion efficiency with increased HX+EXH losses as Φ is swept. This demonstrates that losses can be optimized through modulation of initial conditions. Φ-T matrix data in marked for reference to Appendix A, Table A. 2.

The results indicate that incomplete combustion has a strong dependence on the details of the combustion event, and potentially weaker pressure and temperature dependencies. Additionally, the figure shows that the associated HX + EXH losses are dilution dependent. Leaner operation offers reduced losses, even with similar combustion efficiency. This demonstrates that through proper choice of initial conditions, simultaneously low combustion and HX+EXH losses can be realized, thus maximizing GTE.

The reason for the high combustion efficiency are seen in the emissions trends of CO and HC in Figure 63. It is again observed that for a given engine geometry, operating load, phasing, and fuel selection, HC emissions are dominated by geometry effects and less by the thermodynamic conditions. However, CO emissions are highly dependent on thermodynamic effects, where the intake pressure and temperature combinations required for constant PPRR can be used to offset mixing differences in charge preparation. This offers a pathway to reduce CO emissions with simultaneous low heat losses.

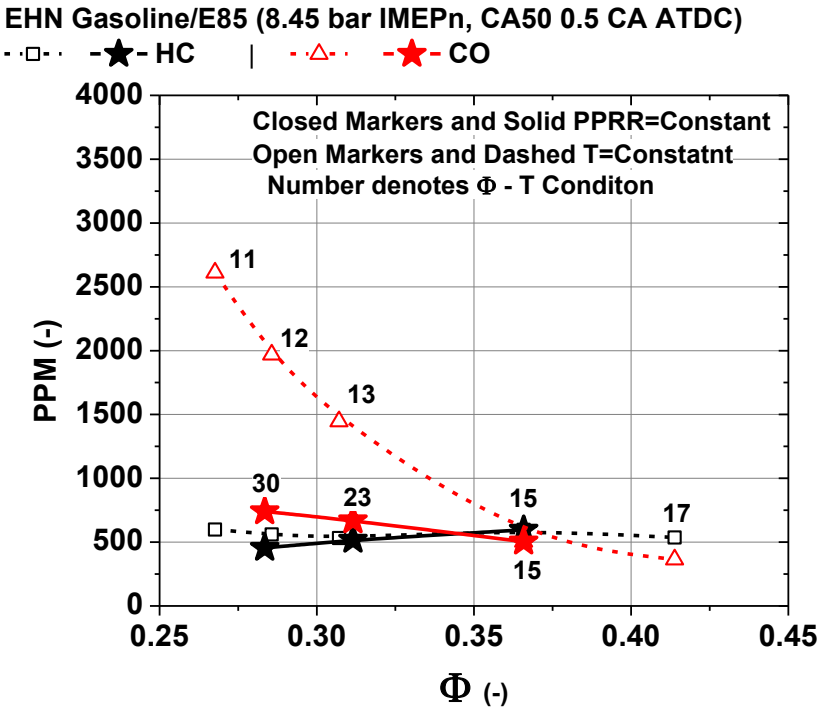

Figure 63 CO and HC emissions at constant temperature, varied Φ conditions (dashed) and at constant PPRR condition (solid). At the constant combustion process condition (PPRR), combustion efficiency is constant, suggesting that initial conditions can be used to control engine incomplete combustion species (primarily CO) in RCCI. Φ-T matrix data in marked for reference to Appendix A, Table A. 2.

5.2.6 Fuel Composition Effects on Reactivity

The previous sections demonstrated that by using combinations of fuel reactivity, intake temperature, and Φ (intake pressure), it is possible to manipulate and control RCCI heat release. However, to match the combustion phasing and load, each of these effects needed to be balanced. It was also observed that reducing the direct injected fuel's reactivity resulted in a more abrupt combustion event, which had a direct influence on the number of Φ-T conditions that are operable within the present prescribed ≥97% combustion efficiency and ≤12 bar/°CA constraints. The present section also explores the effects of a reduced reactivity gradient, and investigates the effects of increased port fuel reactivity by using 91 PON gasoline in place of E85.

For these tests the engine was operated with poi the Φ-T matrix points shown in Figure 44 using the hardware and conditions described in Table 16, where 0% EGR is used at 8.45 bar IMEPn and CA 50 of 0.5°CA ATDC. The constraints of ≥97% combustion efficiency and ≤12 bar/°CA were again imposed as operable limits. Figure 64 illustrates the Φ-T matrix conditions that were operable.

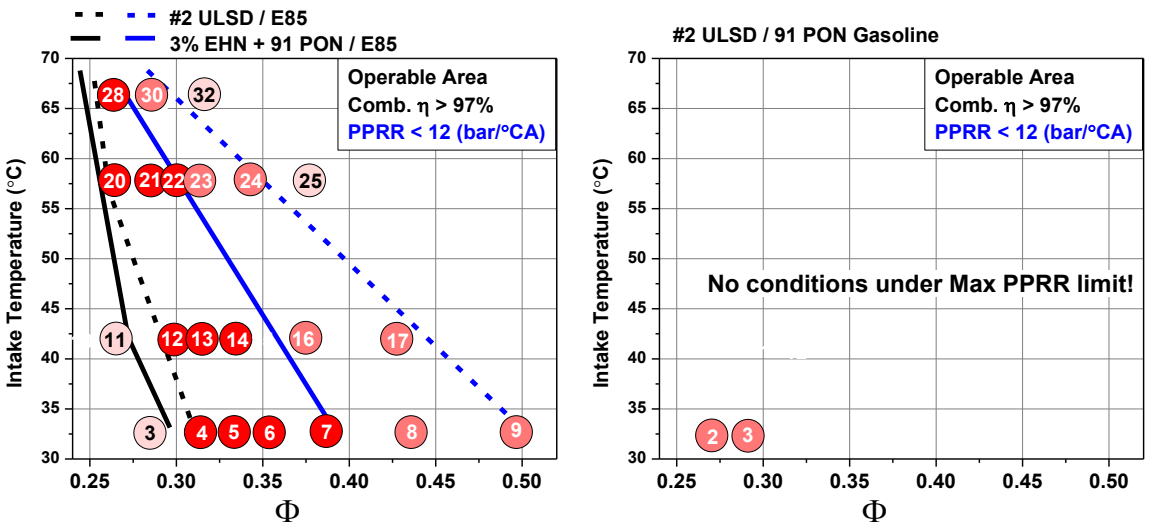

Figure 64 Operable space of Φ-T matrix with the tested E85 based fuels (left), 91 PON gasoline (right). With gasoline base fuel (port) no conditions satisfied the constraints.

Figure 64 shows that, when gasoline is used in place of E85 as the low-reactivity fuel, only two operating conditions were possible. Neither condition met the ≤12 bar/°CA PPRR constraints. The results clearly demonstrate that 91 PON gasoline behaves much differently than E85. This is extremely interesting as the PON of ethanol is ~99.15, as stated by Eyidogan et al. [141]. Thus, in the present study, the PON of the E85 used[§§§] is roughly 97, and the PON difference between the tested E85 and gasoline is relatively small (91 vs. 97). Based on the PON number, the observed large difference in the operable window of Figure 64 would not have been suspected. To explore the reasons for this, the effect of boost pressure was examined.

A fuel's PON (also referred to as anti-knock index (AKI)) is determined by the research and motor octane tests. These tests were originally designed to

[§§§] E85 used in the preset work is 85% ethanol blended with 91 PON gasoline by volume

characterize gasoline reactivity, for use in SI combustion, and are conducted at non-boosted conditions. For conventional SI combustion, this is an appropriate test. However, as shown in the literature review of Chapter 2, pressure has an effect on fuel reactivity. For instance, Dec and Yang [21], showed in highly boosted HCCI that gasoline becomes more reactive (at intake pressures greater than ~2 bar). Likewise, it was shown by Sjöberg and Dec [51] that, at the same conditions, ethanol's reactivity showed no pressure dependency.

As in the cited studies, the pressure dependency of gasoline was also observed in present research with RCCI. Figure 65, shows AHRR of gasoline/ULSD operation at the operating conditions listed in Table 27. The operating conditions are nearly identical to those of Mehl et al. [52], as discussed in Chapter 2, in which the increased reactivity of gasoline was computationally explored. The conditions in Table 27 and the combustion behavior in Figure 65 show that as the intake pressure is increased, the amount of reactive fuel required for constant phasing operation is reduced, resulting in 0% needed at 1.89 bar (with HCCI operation). For reference the conditions in Table 27 are similar to the conditions in the ΦT matrix, but the load was reduced 0.5 bar IMEPn to reduce knocking tendency and expand the operable range. The results can be seen in Appendix A, Table A. 8.

Table 27 Engine operating parameters for gasoline reactivity sensitivity

Intake Pressure (bar)	**1.89**	**1.56**
Load (IMEPn)	7.92	8.06
CA50 (°CA ATDC)	4.9	4.4
Speed (rev/min)	1300	1300
Piston Bowl Shape	Bathtub	Bathtub
Cr (-)	14.88:1	14.88:1
DI Timing (°CA ATDC)		60/35
DI Dwell Bias (%SOI1, % SOI2)		~60/40
PFI Timing (°CA ATDC)	-320	-320
EGR (%)	0	0
Intake Temperature (°C)	32	32
Overall Turbocharger η (%)	71	71
Low Reactivity Fuel, PFI	91 PON gasoline	91 PON gasoline
High Reactivity Fuel, DI		ULSD
PFI Fuel Fraction (-) (by energy)	1.0	.896
DI Fuel Fraction (-) (by energy)		.104
PPRR (bar/°CA)	12.9	7.6

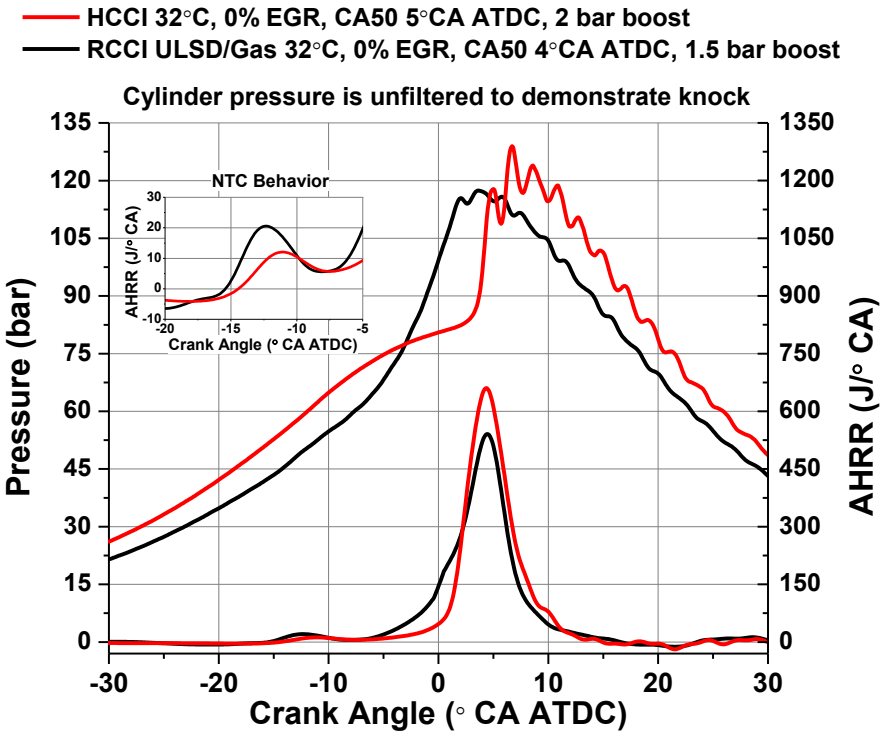

Figure 65 RCCI and HCCI operation at matched phasing. As intake pressure is increased from 1.5 to 2 bar absolute, RCCI operation was not possible as 91 PON gasoline exhibited HCCI.

The results shown in Figure 65 illustrate that gasoline's reactivity is not constant. This is important from an engine efficiency perspective, as the previous experimental results demonstrated that increased intake pressure (increased dilution) is effective at increasing engine efficiency. Therefore, if efficiency is to be maximized, fuel reactivity sensitivity becomes increasingly important.

5.2.7 Gas Composition Effects on Reactivity

To enable a wider range of operation with reactive fuels, the gas composition can be changed, viz. via the use of EGR. EGR addition has been demonstrated by many researchers as an effective strategy for ULSD LTC, where use of heavy EGR is commonly used to increase ignition delay of reactive fuels. Additionally, EGR effects RCCI heat release event. For example, Figure 66 demonstrates that at air dilute conditions, adding EGR offers additional charge dilution, spreading the heat release. The operating conditions of the points are shown in Table 28, with the operating conditions in Table 16.

Table 28 Engine operating parameters for EGR dilution effects

Φ-T Matrix Condition	**2**	**3**	**12**	**13**
EGR	0	0	45	45
Intake Temperature (°C)	32	32	42	42
Intake Pressure (bar)	1.89	1.72	2.04	1.94
Exhaust Pressure (bar)	1.98	1.82	2.35	2.24
Overall Turbocharger η (%)	74	72	63	61
Low Reactivity Fuel (PFI)	91 PON Gasoline	91 PON Gasoline	91 PON Gasoline	91 PON Gasoline
High Reactivity Fuel (DI)	ULSD	ULSD	ULSD	ULSD
PFI Fuel Fraction (-) (by energy)	.957	.925	.89	.88
DI Fuel Fraction (-) (by energy)	.043	.075	.11	.12

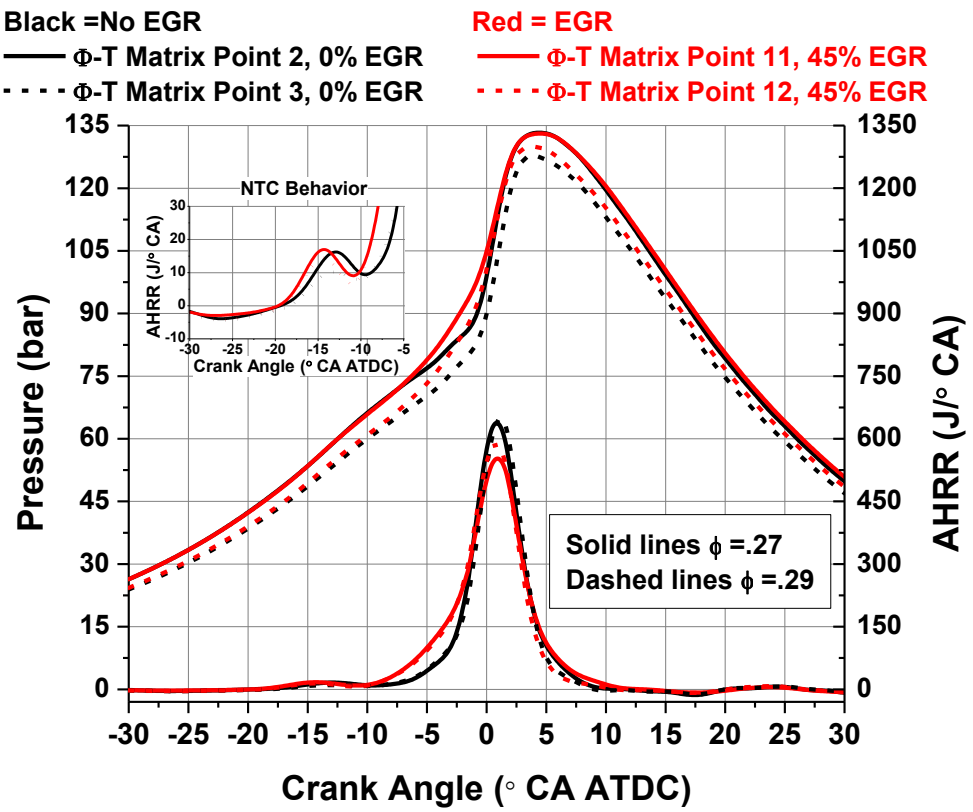

Figure 66 Matched Φ′ operation with and without EGR at lean conditions. Note that with EGR (red) the intake temperaurre is higher and the heat relase rate is longer, while operation without EGR (black) is shorter even when operated at cooler temperatures.

These trends demonstrate the benefit of EGR dilution vs. air dilution. EGR changes the molecular composition of the reactants. Specifically, EGR decreases the number density of O_2. In place of O_2, combustion products containing oxygen, such as CO, CO_2, and H_2O are introduced. As explained in Chapter 2, these products have both a thermodynamic and reactivity effect on the engine cycle and combustion process.

By considering the relative gas compositions, it is seen that there are fewer fuel-O_2 molecular collisions when 45% EGR is used due to the presence of CO_2 and H_2O. This has a direct impact on the reactivity enhancing pathways of gasoline described by Mehl et al. [52] in Chapter 2 that showed that $\dot{R}+O_2$

pathways are critical for enhancing gasoline kinetics at high pressure. Thus, when the concentration of O_2 is reduced with EGR, reactivity suppression occurs.

The result of adding 45% EGR to the conditions in Figure 66 and Table 28 were that with EGR, additional reactive fuel (ULSD) was required to maintain the same combustion phasing. This was needed in addition to employing increased intake temperature, which is independently an effective method of increasing the fuel's reactivity. Thus, it is concluded that EGR is a very effective method to suppress fuel reactivity, and that using EGR offers the potential to improve the heat release control of pressure sensitive fuels at lean conditions.

5.2.8 Gas Composition Effects on Φ-T Matrix Results

To explore the reactivity suppression behavior of EGR in RCCI, operation with 45% EGR was conducted with the conditions of the Φ-T matrix. The only difference in operation was the inclusion of EGR, and all other Φ-T parameters were the same as those stated in Table 16, in Figure 44 and with the color coding of Table 23. Figure 67 demonstrates the Φ-T operable area with 45% EGR.

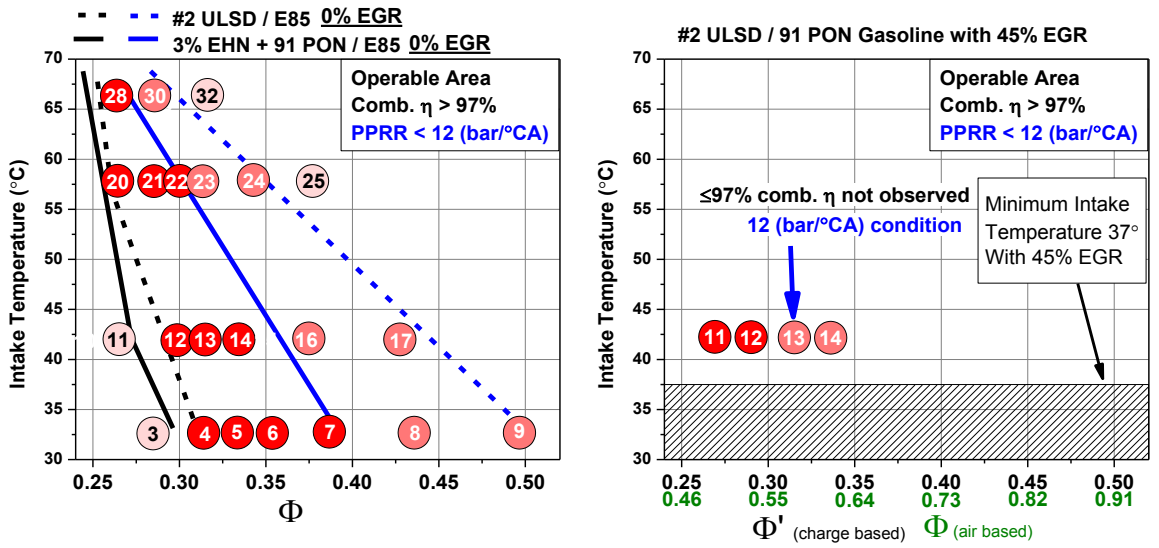

Figure 67 Operable areas of E85 based fuels with 0% EGR (right) and gasoline based fueling with EGR (right). (With 0% EGR gasoline HCCI is encountered, prohibiting RCCI at the tested conditions). When 45% EGR is introduced the operable area expands enabling RCCI operation at select points within the Φ-T space.

The results show that with 45% EGR, the operable of the Φ-T space is increased when fueled with ULSD/Gasoline. As noted in Figure 67, the minimum intake temperature with 45% EGR was 37°C. The reason for the increased temperature with 45% EGR was to prevent condensation of exhaust water in the EGR cooler. The operating conditions used for the test are shown in Table 29.

Table 29 Φ-T operating parameters with 45% EGR

Φ-T Points	11-14
EGR (%)	45
Intake Temperature (°C)	42
Intake Pressure (bar)	See Appendix A
Exhaust Pressure (bar)	See Appendix A
Overall Turbocharger η (%)	~65
Low Reactivity Fuel (PFI)	91 PON gasoline
High Reactivity Fuel (DI)	ULSD
PFI Fuel Fraction (-) (by energy)	See Appendix A
DI Fuel Fraction (-) (by energy)	See Appendix A

Although the results demonstrate that the operable window with EGR is increased, the potential effects of EGR on performance also need to be addressed. The losses of operation with and without EGR are plotted in Figure 68.

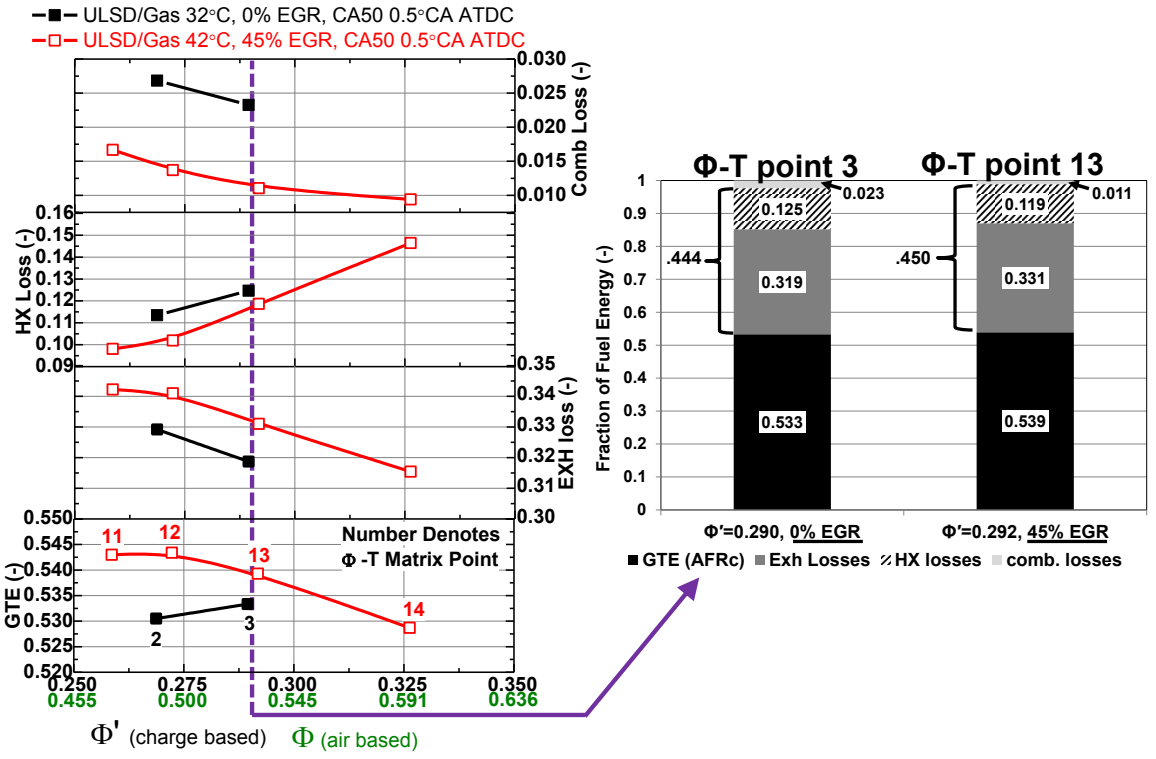

Figure 68 Φ-T matrix points and operation with 91 PON gasoline with and without EGR

From Figure 68 it is seen with EGR the GTE is increased. The major contributor to this is a result of reduced incomplete combustion with EGR, as HX + EXH losses are essentially equal for the compared cases. It is unclear if the reduction of incomplete combustion is from EGR or intake temperature effects. However, in Figure 56 it was shown that for a given Φ, increased intake temperature reduced incomplete combustion.

To determine the effect of EGR on combustion efficiency, engine operation with and without EGR was conducted at a fixed load, intake pressure, combustion phasing, and speed. Intake temperature was swept from 32 to 66°C where operation with and without EGR was required to maintain phasing. The operating conditions are presented in Table 30, and pressure and AHRR traces are seen in Figure 72 (detailed in Appendix A, Table A. 8). Figure 69 shows the corresponding energy budgets.

Table 30 Intake temperature sweep (0% EGR load is slightly low, as higher load operation was not possible without excessive knock).

Condition	**HCCI**	**RCCI**	**RCCI**	**HCCI**
Φ-T Matrix point	**2**	**12**	**21**	**30**
Intake Temperature (°C)	**32**	**42**	**57**	**66**
EGR	0	45	45	45
Intake Pressure (bar)	1.88	1.94	1.91	1.98
Load (IMEPn)	8.35	9.12	9.04	9.08
CA50 (°CA ATDC)	5.2	4.9	5.0	5.8
Speed (rev/min)	1300	1300	1300	1300
Piston Bowl Shape	Bathtub	Bathtub	Bathtub	Bathtub
Cr (-)	14.88:1	14.88:1	14.88:1	14.88:1
DI Timing (°CA ATDC)		-60/-35	-60/-35	
DI Dwell Bias (%SOI1, % SOI2)		~60/40	~60/40	
PFI Timing (°CA ATDC)	-320	-320	-320	-320
Φ′ (-) (charge based)	.266	.284	.300	.295
Exhaust Pressure (bar)	2.10	2.13	2.09	2.26
Overall Turbocharger η (%)	74	65	64	62
Low Reactivity Fuel (PFI)	Gasoline	Gasoline	Gasoline	Gasoline
High Reactivity Fuel (DI)	ULSD	ULSD	ULSD	ULSD
PFI Fuel Fraction (-) (by energy)	1.0	.925	.89	1.0
DI Fuel Fraction (-) (by energy)		.075	.11	
PPRR (bar/°CA)	12.5	7.7	9.4	11.4

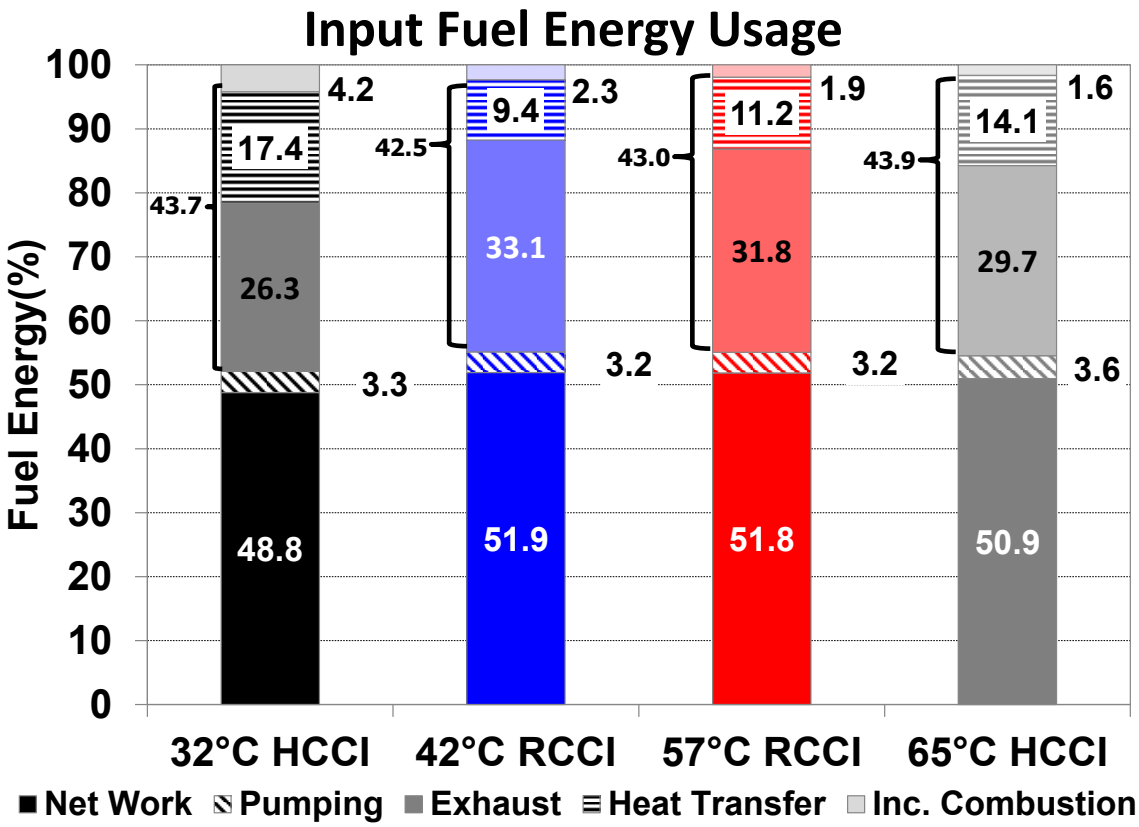

Figure 69 Energy budget of HCCI with and without EGR, and RCCI with EGR at matched conditions. It is seen that operation with 45% EGR reduces incomplete combustion by approximately half. Additionally, RCCI exhibits reduced HX and HX+Exh losses as compared to HCCI operation.

The results expose that operation with EGR offers higher engine efficiency. Based on the γ relations shown by Lavoie et al. [58] in Figure 11, the present higher GTE with EGR are unanticipated. However, the current results demonstrate that combustion product recycling with EGR affects the magnitude of incomplete combustion.

The concentrations of the emissions from the above cases, are plotted in Figure 70.

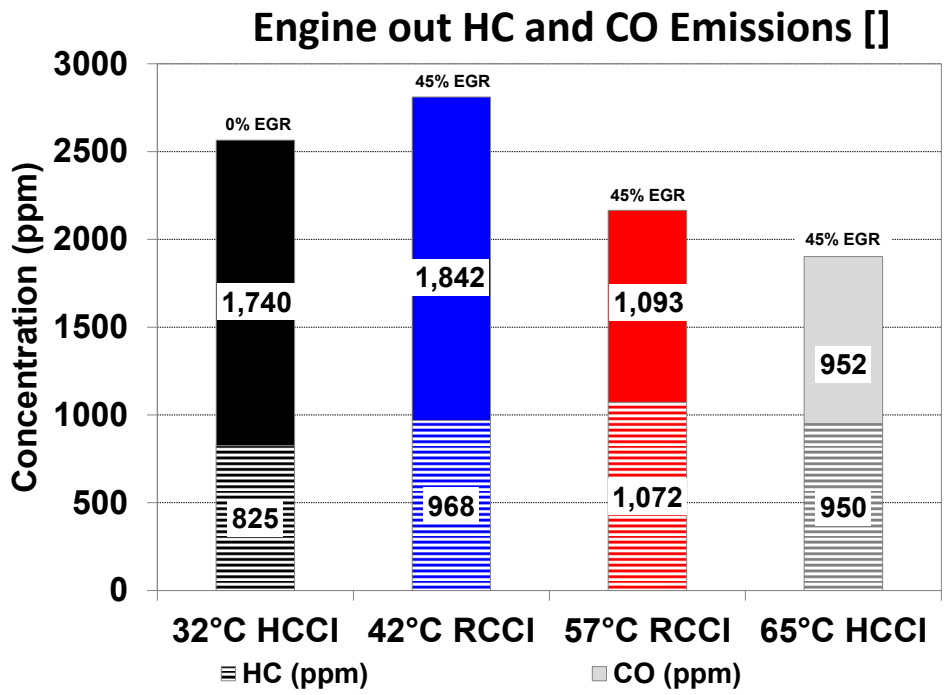

Figure 70 Incomplete combustion species emissions concentrations of RCCI bounded by HCCI

The results show that with EGR, the emissions are not radically changed. In fact, it is seen that the emission reduction trends more with increased temperature than with EGR. These results are supported by the findings shown previously in Figure 60, where increased temperature was found to reduce emissions at fixed Φ. The results prove that EGR does not inherently reduce emissions through improvements to combustion, or by a second opportunity to burn recycled combustion products. Therefore, a different effect must be present.

When EGR is used, the system-out (tailpipe) mass flow rate is reduced because the incoming fresh air is replaced with EGR. Thus, with EGR the mass flow of emissions are reduced. This relation is critical for reducing incomplete combustion, as shown in Equations (35, and 39) in Chapter 4. The mass of HC and CO emissions dictate the loss in fuel energy, not their concentrations. This

concept is illustrated in Figure 71, where incomplete combustion is plotted with the relative loss contributions of CO and HC are noted.

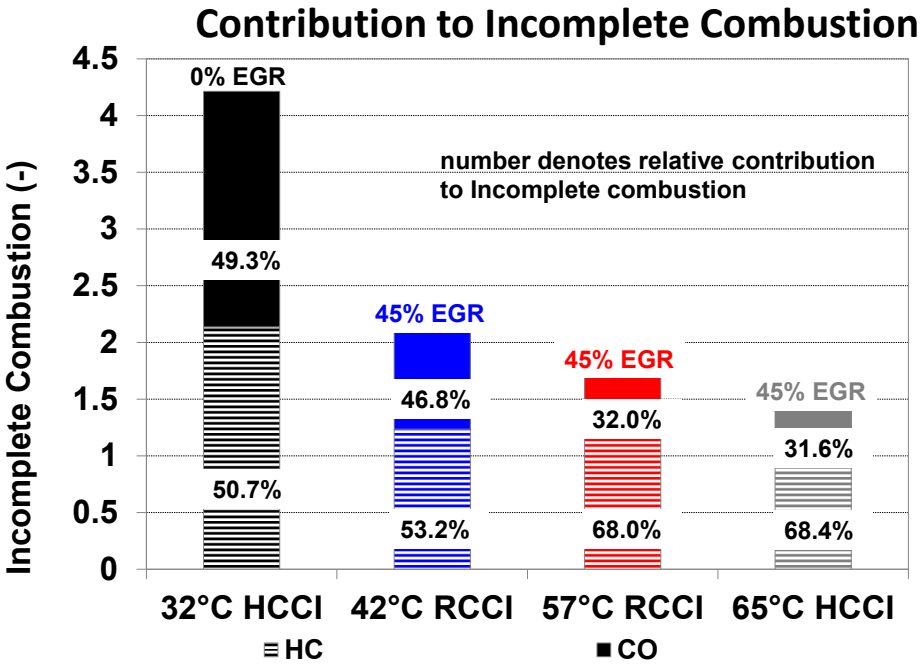

Figure 71 Incomplete combustion by emission type of RCCI bounded by HCCI

The results establish that the use of EGR reduces incomplete combustion, and that increased intake temperature furthers these reductions. Although the use of EGR reduces the maximum GTE potential from γ ratio effects, the results show this loss is offset by larger reductions in incomplete combustion (in Chapter 6 the γ effect of air vs. EGR will be seen to be ~0.5% in GTE). Therefore, the results of Figure 71 show that with 45% EGR a ~50% reduction in incomplete combustion can be achieved. This demonstrates a pathway for achieving the 60% GTE goal, as outlined in the initial computational studies of Chapter 3.

5.3 Charge Preparation Effects

The present section investigates charge stratification effects as a means of increasing premixed combustion's operable window. The literature review of Chapter 2 discussed that inhomogeneity in a premixed charge results in heat release smoothing. This increases combustion stability and the knock free, low noise operable range. For example, previous work by Sjöberg and Dec [44], and later at higher engine loads by Yang et al. [45], has demonstrated that Φ stratification can reduce engine knock, enabling higher loads and engine efficiencies. Likewise Kokjohn and Reitz [47] demonstrated that the simultaneous introduction of reactivity + Φ stratification can further the heat release control beyond Φ stratification alone.

The effects of reactivity + Φ stratification can be observed in Figure 72, which depicts the pressure and AHRR traces of operation for Figure 69 to Figure 71, and the operating conditions in Table 30.

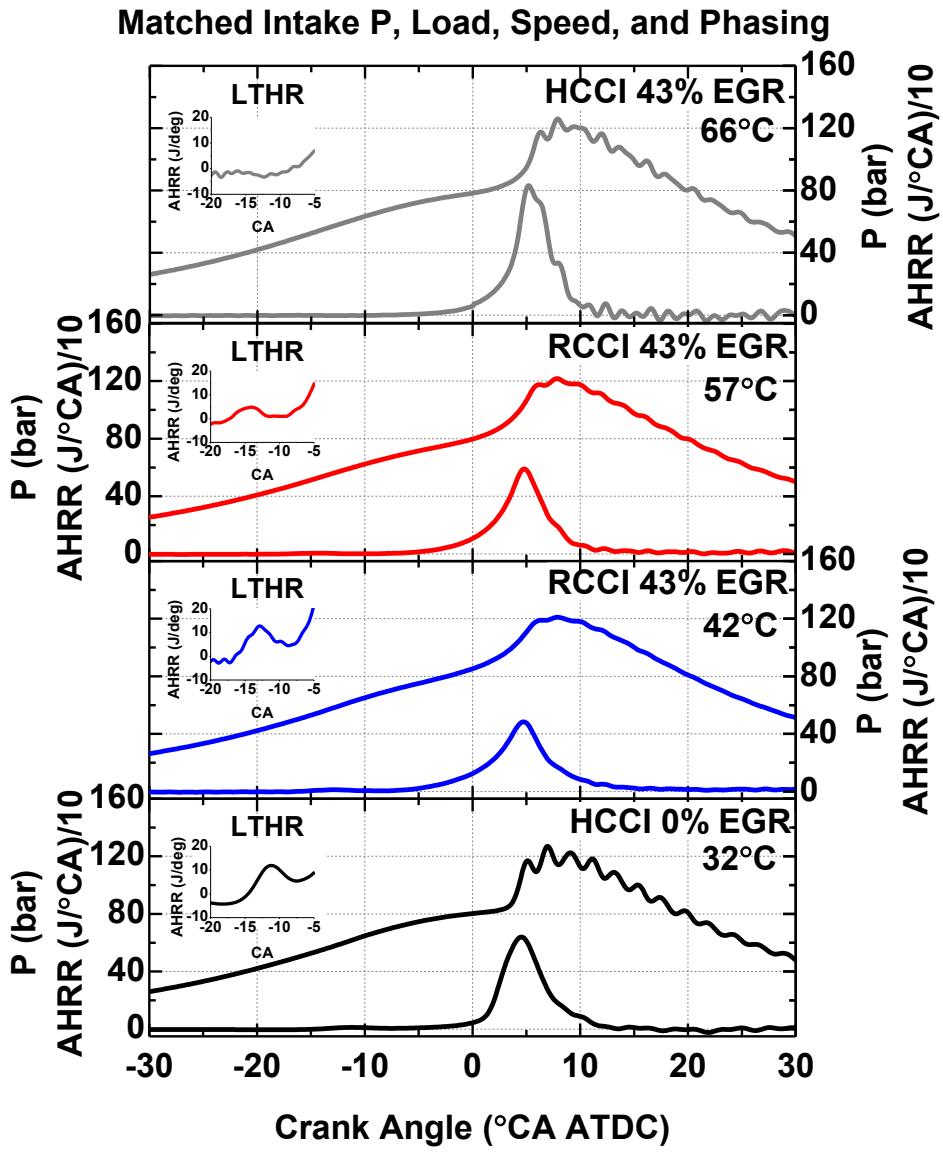

Figure 72 Matched phasing, intake pressure, speed, and load operation of RCCI and HCCI. Pressure traces are unfiltered to display knocking intensity.

The trends demonstrate that regardless of EGR, when the charge is not stratified (i.e., HCCI) the pressure rise rate at matched phasing results in large pressure oscillations. It was shown in section 2.8 of Chapter 2 that the pressure oscillation amplitude (knocking intensity) leads to increased convective losses through boundary layer thinning. To maximize engine efficiency this source of heat

transfer loss needs to be mitigated, and the introduction of Φ + reactivity stratification is a pathway.

To investigate the effect of charge gradients on combustion and heat transfer, various injection timings were tested. The injection timings spanned combustion strategies ranging from HCCI to diesel pilot-like operation. The tests were conducted at the conditions shown in Table 31 with the injection strategies of Table 32. Detailed run data is presented in Appendix A, Table A. 9.

Table 31 Operating parameters for charge preparation tests

Load (IMEPn)	7.44±0.04
CA50 (°CA ATDC)	5.0±0.5
Φ′ (-)	0.242±0.002
Speed (rev/min)	1300
Piston Bowl Shape	Bathtub
Cr (-)	14.88:1
EGR (%)	45
Intake Temperature (°C) (air+EGR)	57 (66 HCCI only)
EGR Cooler out Temperature (°C)	75
Intake Pressure (bar)	2.02 (2.08 HCCI only)
Exhaust Pressure (bar)	2.28 (2.35 HCCI only)
Overall Turbocharger η (%)	65±1
Low Reactivity Fuel (PFI)	91 PON gasoline
High Reactivity Fuel (DI)	ULSD

Table 32 Injection strategies for charge preparation tests

Condition	HCCI	RCCI 320	RCCI 320/35	RCCI 60	RCCI 60/35	RCCI 35
DI 1 timing (°CA ATDC)		-320	-320	-60	-60	-35
DI 2 timing (°CA ATDC)			-35		-35	
PFI Timing (°CA ATDC)	-320	-320	-320	-320	-320	-320
PFI Fuel (%) (% total energy)	100	95.9	96.2	96.6	95.0	97.6
DI Fuel (%) (% total energy)	-	4.1	3.8	3.4	5.0	2.4
DI injection 1 (%) (% DI energy)	-	100	~70	100	~67	100
DI injection 2 (%) (% DI energy)	----	-	~30	-	~33	-

The performance of the sweep is shown in Figure 73, where key efficiency and operational parameters are indicated. The trends demonstrate that operation

with intermediate DI timings (-320/-35, -60, and -60/-35 °CA ATDC) offered highest GTE. Interestingly, the -60, and -60/-35 °CA ATDC conditions also exhibited the highest incomplete combustion. Fully premixed and very stratified (diesel pilot in Figure 73) operation exhibits lower efficiency.

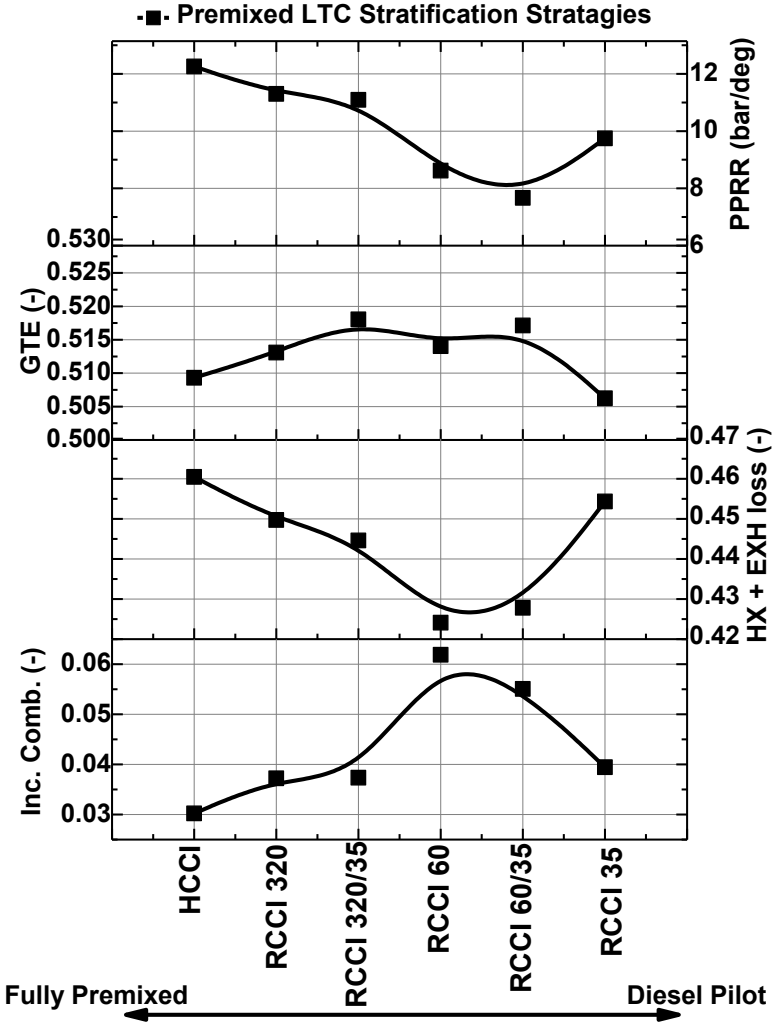

Figure 73 Losses and performance of different charge preparation strategies. The results demonstrate the HX + EXH losses are the most dominant if efficiency is to be maximized. These losses were generally observed to trend proportional to PPRR and inverse effects with incomplete combustion.

Similar trends in Figure 59 at constant temperature and varied Φ, showed that low HX+EHX losses coincided with increased incomplete combustion.

However, in the present study, Φ and T are fixed at 0.242 and 57°C, respectively (except for HCCI with 66°C). Therefore the present results demonstrate that other factors can affect heat transfer and incomplete combustion.

With fixed Φ and intake temperature, the results of Figure 73 demonstrate that the highest efficiencies are obtained with the lowest HX+ EXH losses, but with the highest incomplete combustion. This trend was not observed in the Φ-T matrix tests. Interestingly, the present results show that the highest efficiencies coincide with the lowest PPRR. In the previous Φ-T matrix analysis it was found that incomplete combustion and PPRR were related, and a constant PPRR resulted in constant incomplete combustion. Thus, both studies illustrate that PPRR can be a good indicator of losses. In the present fixed Φ-T, varied charge preparation study higher PPRR operation is found to lower incomplete combustion, but to also lower efficiency.

The reasons for this are indicated in Figure 75, which depicts unfiltered pressure traces and from Figure 74, which shows the breakdown of individual losses for HX and EXH.

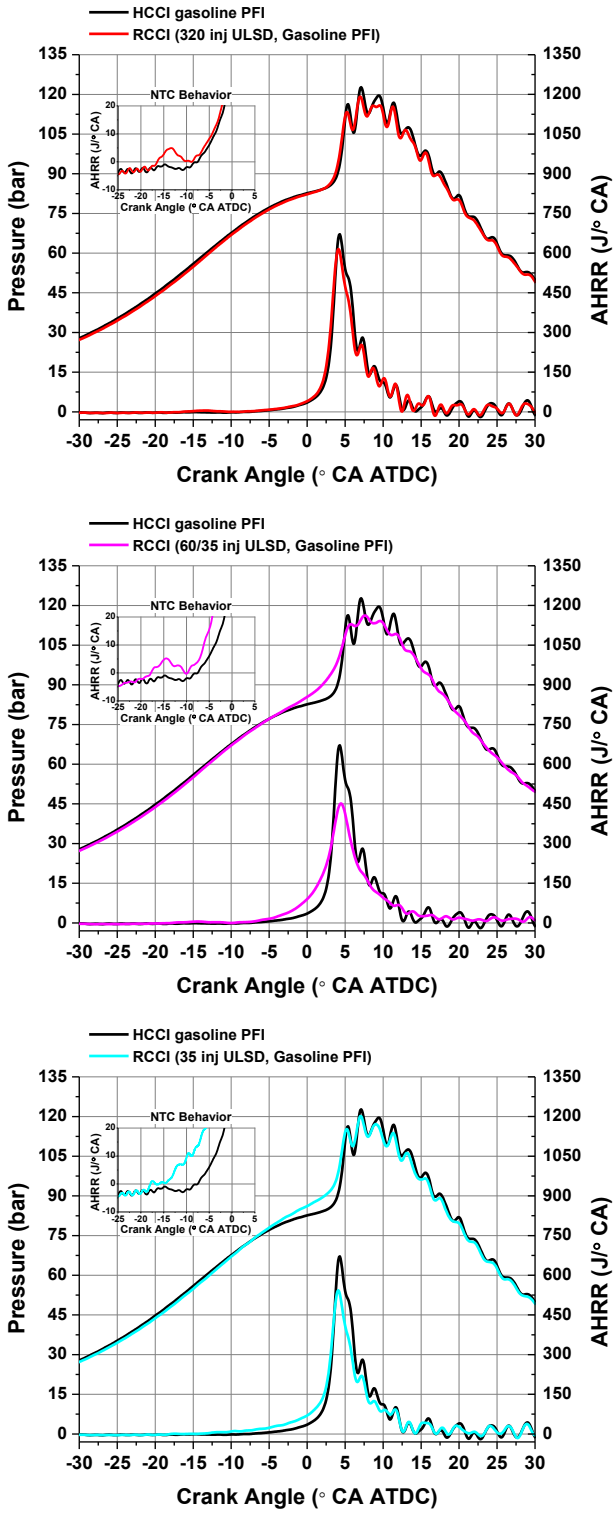

Figure 74 Unfiltered Cylinder Pressure and AHRR for select charge preparation strategies. Note that only the intermediate (highest gross efficiency) strategies exhibit low pressure oscillatory behavior. As fuel is introduced early into the cycle (red and traces in top sub-figure), the charge is over stratified and the entire charge knocks. This condition is effectively lower octane fuel HCCI. Likewise, as fuel is introduced late into the cycle (as in the cyan traces in bottom sub-figure) the charge is over stratified and end gas knock is encountered.

From the pressure traces in Figure 74 it is obvious that the under (SOI 320) or over (SOI 35) stratified cases, result in high pressure oscillations, commonly referred to as knock. In the present results it is ambiguous to decree that the observed oscillations are only from knock, as Tess [118] has shown that the test engine exhibits pressure oscillatory behavior from geometry resonance effects alone in CDC operation. However, the trends of Figure 73 and Figure 75 show that increased PPRR coincides with increased heat losses, and in Figure 74, these conditions also display higher pressure oscillation amplitude. These relations suggest that knock is present for cases with overly homogeneous or stratified conditions, which increases heat losses, but the degree of knock is difficult to quantify.

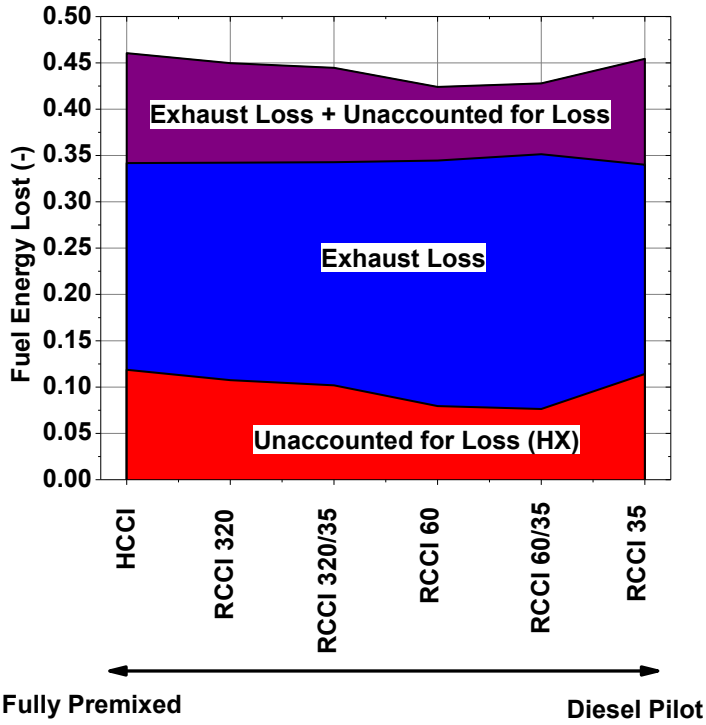

Figure 75 Exhaust and unaccounted for (HX) losses as functions of charge preparation strategy (see Chapter 4 for discussion of the unaccounted for losses). The exhaust losses (EXH) were observed to be relatively constant, while HX losses were observed to be dependent on charge preparation, with the lowest losses observed at intermediate RCCI injection timings with single or double injections.

From Figure 75 it is seen that at the fixed Φ-T condition, exhaust (EXH) losses are constant and only HX losses vary with PPRR. This PPRR HX relation is investigated in Figure 76, which depicts a linear relation between unaccounted for losses (HX) and PPRR. Note that a wide range of Φ and intake temperature and EGR conditions are plotted (see Table A. 1 to Table A. 13in Appendix A). Conditions of 18.7:1 Cr are those operated in the oil cooling matrix, to be described in Table 36 of the following section, and detailed in Appendix A Table A. 10 to Table A. 13 for all operated conditions.

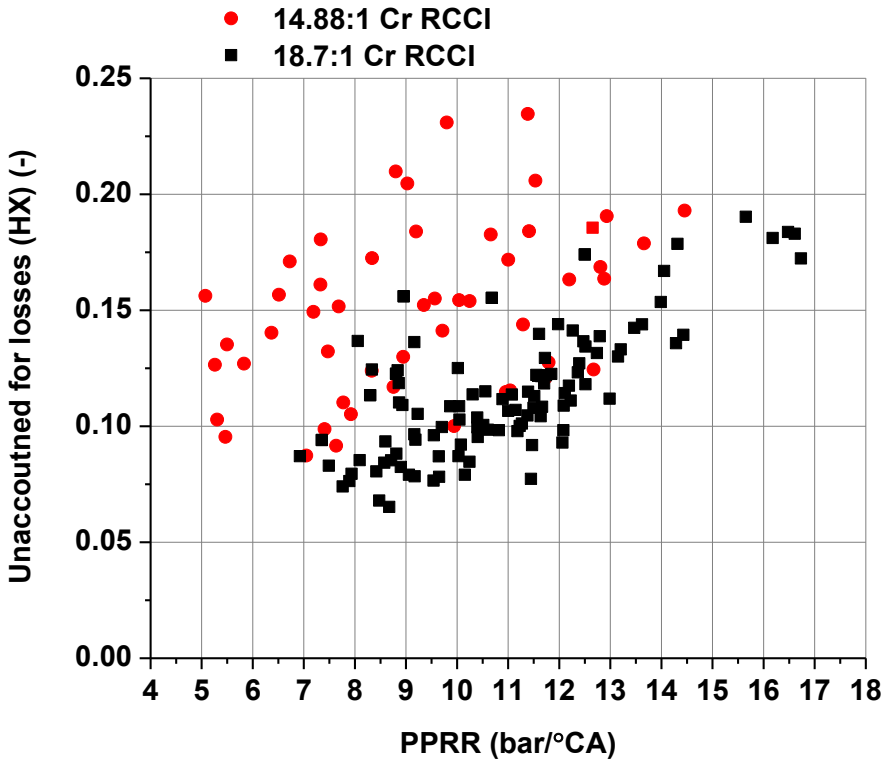

Figure 76 Unaccounted for losses (HX) plotted as a function of PPRR. The trends suggest that a proportional relation between PPRR and HX, with higher values of PPRR increasing HX.

The linear trends of Figure 76 suggest that PPRR linearly tracks with heat transfer. Similarly, cited research in Chapter 2, Figure 24 from [103] indicated that knocking intensity tracked linearly with heat transfer. These findings suggest that for premixed auto ignition strategies, PPRR trends may be a useful metric to predict HX trends. Although PPRR is less quantitative than knocking intensity, the calculation of PPRR only requires the derivative of cylinder pressure. Thus, PPRR could be a computationally fast and simple metric to use in control strategies focused on increasing engine efficiency.

The PPRR distribution of cases from Table 30 (RCCI and by HCCI) are shown in Figure 77, where a statistical approach has been used through box plots. This type of analysis partitions the cumulative probability distribution (CDF) into quarters, where the box represents the interquartile range. This visually depicts the area where a 50% probability outcome was observed.

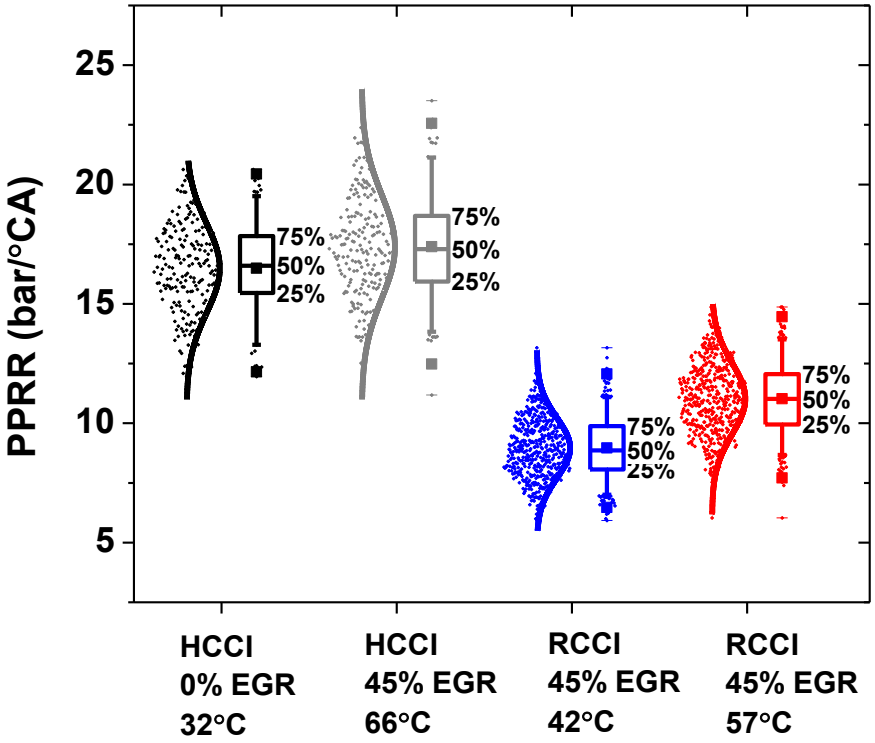

Figure 77 Box plot statistical analysis of PPRR in HCCI and RCCI operation at matched load, intake density, and phasing.

The statistical analysis indicates that the interquartile and outlier range is somewhat tighter for RCCI than for HCCI, demonstrating more repeatable operation. This also demonstrates that PPRR seems to be a stronger function of the degree of full premixing. In turn, this suggests that when the combustion event is free of fuel reactivity gradients, the variability in ignition timing is larger. This has a direct effect on engine efficiency, as the variability in PPRR shows that the combustion process of HCCI is less stable.

Additionally, Figure 72 showed that the low temperature 0% EGR HCCI condition exhibited NTC behavior with gasoline, which has been suggested by Sjöberg and Dec [142] to enable lower combustion variability, and to enable later phasing. In the present, relatively advanced, 5°CA ATDC phasing, a slight

variability advantage is observed with lower intake temperature 0% EGR HCCI compared to higher intake temperature 45% EGR HCCI, as the data is clustered closer to the mean of the normal distribution and the 95% confidence range (whiskers) is tighter. The box analysis demonstrates that with HCCI 50% of the data fell within a ~2.5 bar/°CA range of the median, where RCCI was within ~2 bar/°CA range of the median.

Lastly, if PPRR is to be used as a metric for indicating heat transfer losses, the distribution trend of PPRR should be known. By using a P test, it can be determined if the distributions are Normal or Gaussian. The relation for a P test is seen in Equations 43 and 44.

$$Q_1 = (\sigma * Z_1) + X \tag{43}$$

$$Q_3 = (\sigma * Z_3) + X \tag{44}$$

Where Z_1 is +0.67 and Z_3 -0.67, sigma is the standard deviation and X is the mean. If the above determination of Q are close to the CDF calculated values, then the distribution is Normal, otherwise the distribution is Gaussian. The analysis for the presented data is presented in Table 33 below, where it was found that both HCCI and RCCI PPRR are normally distributed.

Table 33 RCCI and HCCI cumulative distribution function (CDF) statistics, 9 bar IMEPg operation CA50 5°CA ATDC, where all units are in bar/°CA.

	Mean	**σ**	**Q_1**	**Q_3**	**IQR**	**Normal**
HCCI 0% EGR 32°C	16.5	1.9	15.5	17.8	2.4	Yes
HCCI 45% EGR 66°C	17.4	2.2	15.9	18.7	2.8	Yes
RCCI 45% EGR 42°C	9.0	1.3	8.1	9.9	1.8	Yes
RCCI 45% EGR 57°C	11.0	1.5	9.9	12.1	2.1	Yes

This type of analysis is useful as PPRR is often a concern for production applications and control strategies, as well as indicating losses. This analysis shows that RCCI and HCCI have similar PPRR behavior, but different magnitudes and spreads.

5.4 High Compression Ratio, and Efficiency Experiments

The simulation results of Chapter 3 suggested that 60% GTE may be possible with RCCI. The results suggested that the compression ratio would need to be raised (18.7:1), and simultaneous 50% reductions in heat transfer and incomplete combustion were required. The findings from the Φ-T matrix and charge preparation sections demonstrated that combustion efficiency and Φ (intake pressure) could be optimized for simultaneous reductions. Also, Chapter 2 section 2.7.3 discussed that modulation of piston oil jet cooling is a potential method to reduce incomplete combustion and increase efficiency. These findings are combined in the next section to explore high Cr and efficiency RCCI.

5.4.1 RCCI Piston Temperatures

Recent fast response in-cylinder temperature and heat flux measurements by Hendricks [111] have demonstrated that the heat flux and corresponding piston surface temperatures of RCCI combustion are reduced compared to equivalent CDC operation. For instance, the cycle averaged in-cylinder temperatures were up to 60°C cooler with RCCI vs. CDC at a matched 9 bar IMEPg, Φ=.34. Figure

78 exhibits the findings where the term degrees of cooling vs. conventional diesel is defined as.

$$℃\ of\ Cooling\ vs. Conventional\ Diesel\ \equiv\ (℃\ CDC) - (℃\ RCCI) \qquad (45)$$

These steady-state average temperatures are also presented in Splitter et al. [143], with the operating conditions summarized in Table 34(see Hendricks [111] for detailed experimental instrumentation and results). As can be seen in Figure 78, the largest piston surface temperature difference occurs at the piston bowl lip (thick black line).

Table 34 Operating parameters for piston temperature tests [111]

Combustion Mode	**CDC**	**RCCI**
Data Point in [111]	**24**	**26**
Load (IMEPn)	9.08	9.18
CA50 (°CA ATDC)	4.6	4.0
Φ (-)	0.376	0.337
Speed (rev/min)	1300	1300
Piston Bowl Shape	Open Crater (instrumented)	Open Crater (instrumented)
Cr (-)	16.1:1	16.1:1
EGR (%)	0	0
Intake Temperature (°C)	32	32
Intake Pressure (bar)	1.80	1.73
Exhaust Pressure (bar)	1.94	1.90
Low Reactivity Fuel (PFI)	91 PON gasoline	
High Reactivity Fuel (DI)	ULSD	ULSD
DI 1 timing (°CA ATDC)	-11	-59
DI 2 timing (°CA ATDC)		-36
PFI Timing (°CA ATDC)		-320
PFI Fuel (%) (% total energy)		85
DI Fuel (%) (% total energy)	100	15
DI injection 1 (%) (% DI energy)	100	60
DI injection 2 (%) (% DI energy)		40

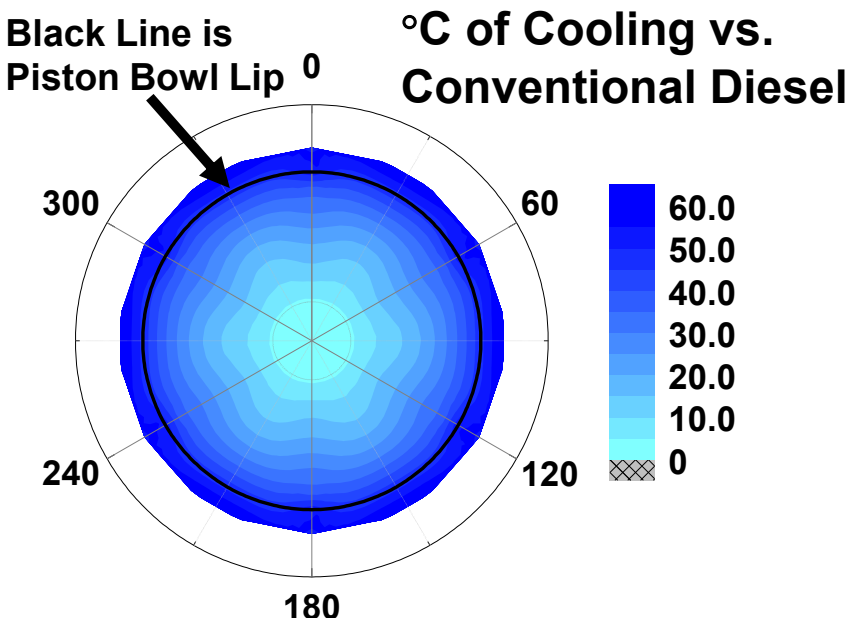

Figure 78 Steady state average piston surface temperature reduction for ULSD/E85 RCCI relative to matched CDC ~0.34 Φ operation at ~9 bar IMEPg 1300 (rev/min).

Additionally, Hendricks [111] measured piston oil gallery surface temperatures. Fast response thermocouples were installed in the inlet and outlet of the oil gallery, which recorded piston surface temperatures inside the gallery. Diagrams and specifications of the instrumentation can be found in Hendricks [111]. Assuming that the mass flowrate, and phase of the oil are constant between RCCI and CDC operation, an estimate of the relative heat transferred in the oil gallery can be made. Figure 79 displays the trends in the difference in oil gallery inlet and outlet temperatures. The corresponding operating conditions are seen in Table 35, for conditions detailed in Hendricks [111].

Table 35 Operating parameters for oil gallery temperature comparison tests

Data Point (See [111])	Combustion	Φ′	Speed	Load
48	CDC	0.40	1300	4.9
24	CDC	0.40	1300	9.1
50	CDC	0.40	1300	12.5
58	CDC	0.40	1750	5.4
59	CDC	0.40	1750	8.6
60	CDC	0.40	1750	12.5
54	CDC	0.60	1300	5.8
53	CDC	0.60	1300	8.5
52	CDC	0.60	1300	12.4
51	CDC	0.60	1300	15.5
65	CDC	0.60	1750	4.9
64	CDC	0.60	1750	7.4
62	CDC	0.60	1750	12.5
63	CDC	0.60	1750	15.1
84	RCCI	0.35	1300	5.2
25	RCCI	0.38	1300	9.2
31	RCCI	0.41	1300	12.7
92	RCCI	0.35	1700	8.5
98	RCCI	0.44	1700	12.5
100	RCCI	0.5	1700	15.0

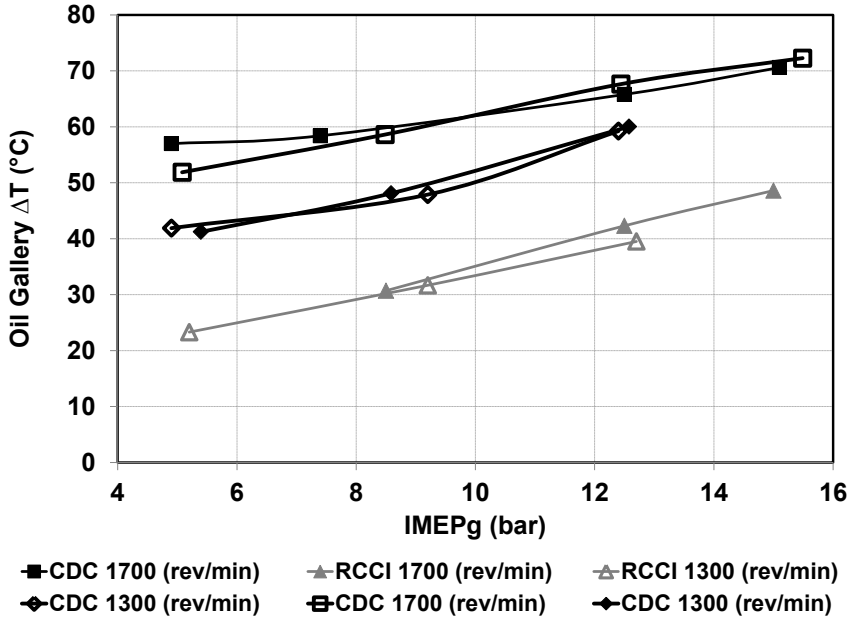

Figure 79 Steady state piston oil gallery surface temperatures vs. load for CDC and RCCI. The trends show that engine speed effects are minimal, while charge dilution and combustion processes with RCCI exhibit almost a 3-fold-reduction in ΔT at low loads compared to 0.6 Φ CDC operation, and a 2-fold-reduction compared to matched Φ CDC (Φ=0.4).

From the figure it is seen that for the given load, the rise in oil gallery temperature is much lower with RCCI than with CDC. As expected, lean CDC operation (Φ=0.4) tends to have a lower ΔT than richer (matched load) CDC operation (Φ=0.6). In light of the piston oil gallery cooling literature reviewed in Chapter 2, in RCCI and lean CDC operation, oil gallery jet cooling is likely not required. In particular, cooling in RCCI may actually magnify incomplete combustion, decreasing efficiency.

To combat these losses, experiments with and without piston oil cooling were conducted. For operation without cooling, the oil spray jet was physically welded shut. It should be noted that on the SCOTE engine there are two oil jets in the same housing. One jet is directed vertically and one is angled towards the wrist pin. The vertical jet is the oil gallery cooling jet which was welded shut. The other jet was unaltered, because it lubricates the wrist pin (Gehrke [113]).

5.4.2 High Cr RCCI with and Without Piston Oil Gallery Cooling

Higher compression ratio increases cylinder pressure. The result is that at lean mid-load conditions, cylinder pressures can be above the self-imposed SCOTE operation limit (pressure data clipped above 165 bar). Therefore in the present experiments the engine load was reduced to 6.45 bar IMEPn, with the back pressure set with an optimistic value of ~65-75% simulated overall turbocharger efficiency. This efficiency was selected based on Millam [6], where it is stated to be state-of-the-art. To reduce the possibility of fuel-liner impingement (to be

discussed in Appendix B), the engine was fueled with port fuel injection of E85, and direct injection of 3% EHN doped 91 PON gasoline. The operating conditions and injection strategy for the tests are seen in Table 36, and a graphical representation of the sweep of conditions is shown in Figure 80. The detailed results are presented in Appendix A, Table A. 10 to Table A. 13.

Table 36 Conditions of with oil galley cooling tests, (see Appendix A, Table A. 10 to Table A. 13)

Load (IMEPn)	6.45±.05
CA50 (°CA ATDC)	0.5±1.0
Speed (rev/min)	1300
Piston Bowl Shape	Pancake
Cr (-)	18.7:1
DI Timing (°CA ATDC)	-60/-35
DI Dwell Bias (%SOI1, % SOI2)	~60/40
PFI Timing (°CA ATDC)	-320
EGR (%)	0 or 40±2
Intake Temperature (°C)	22±3 (with 0% EGR) 40±3 (with 40% EGR
Intake Pressure (bar)	1.13-1.81 (varied)
Φ′ (-)	0.22-.37
Exhaust Pressure (bar)	Varied to fix turbo. η
Overall Turbocharger η (%)	65-75
Low Reactivity Fuel (PFI)	E85
High Reactivity Fuel (DI)	3% EHN + 91 PON Gasoline
PFI Fuel Fraction (-) (by energy)	See Appendix A
DI Fuel Fraction (-) (by energy)	See Appendix A

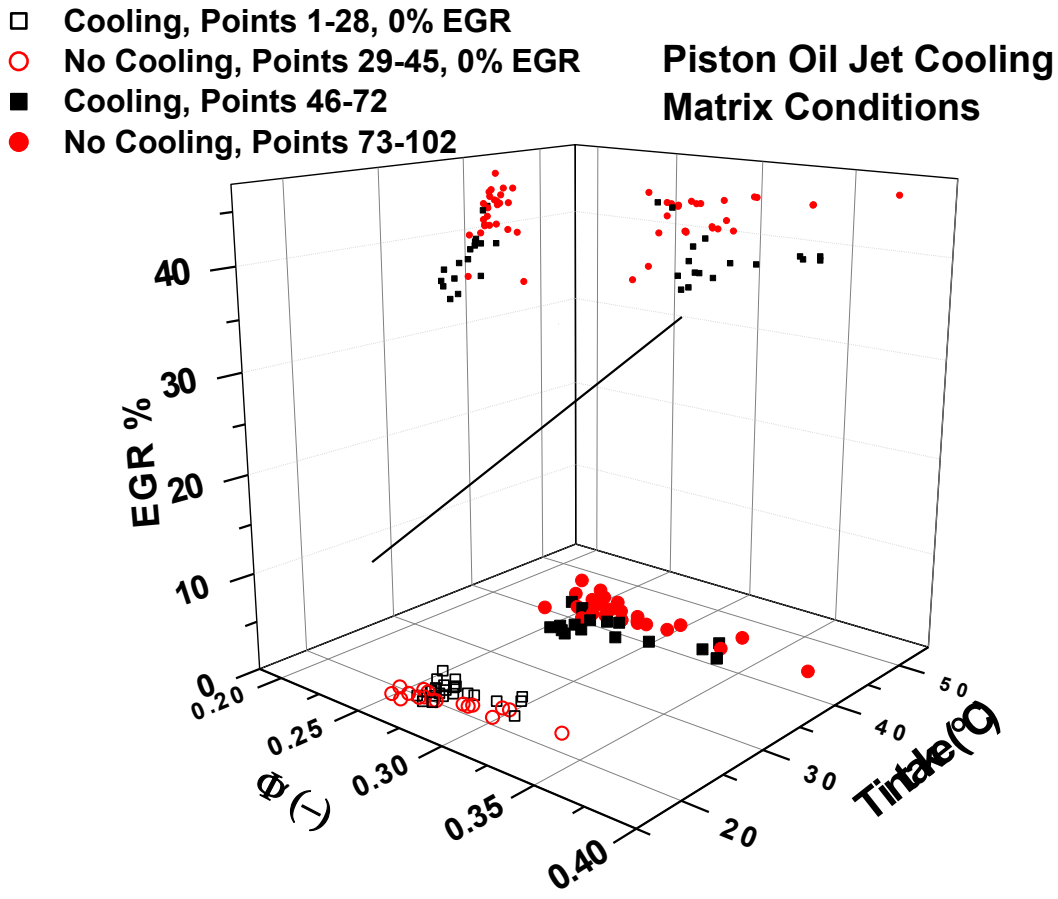

Figure 80 Conditions of with oil galley cooling tests, 102 total data points, as described in Table A. 10 to Table A. 13.

5.4.2.1 Piston Oil Gallery Cooling Emissions Analysis

As discussed in Chapter 2, eliminating piston oil gallery cooling may also reduce CO emissions. Figure 81 demonstrates the observed combustion efficiency sources and losses in RCCI. Direct comparisons can be made between the red circle and black square marker data. The respective open markers denote 22°C intake temperature 0% EGR operation, while the closed markers denote 43°C intake temperature, 40% EGR operation.

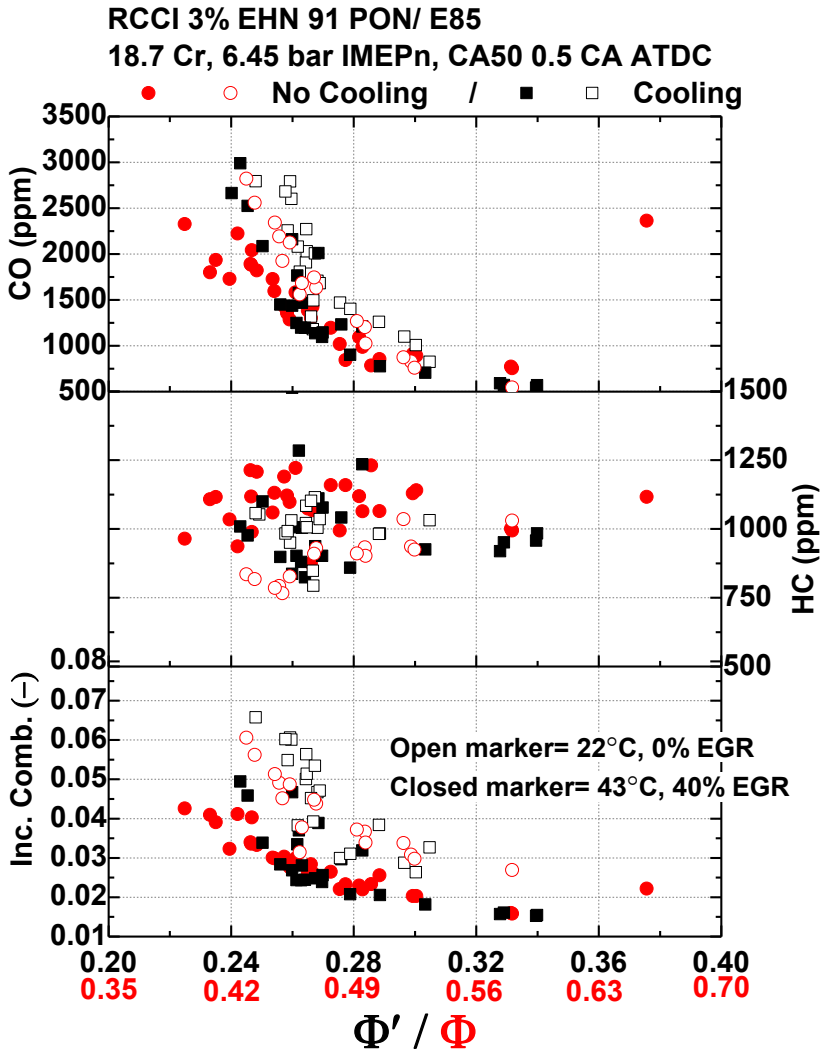

Figure 81 Incomplete combustion and emissions as function of Φ/Φ′ for operation with (black squares) and without (red circles) piston oil gallery cooling. Open or closed markers denote conditions with (closed) or without EGR (open). The results show that without piston oil cooling the lean limit is extended, and that without EGR, incomplete combustion is lower at a given Φ.

The results show that without oil cooling, the lean combustion limit is extended, through reduced CO emissions. The trends in CO are in agreement with the trends observed by Luff et al. [98], where up to a 5-10% reduction was seen in CDC without piston oil gallery cooling. With 40% EGR and 43°C intake temperature a similar trend is seen in Figure 81, but the CO emissions magnitude is lower. This trend is supported by the previous EGR and intake

temperature findings in Figure 70, where CO emissions reductions were due to intake temperature increases, and in Figure 71 where incomplete combustion was reduced with increased EGR.

Interestingly, without oil cooling, HC was found to exhibit no meaningful overall trend (±~100 PPM). This suggests that for a given combustion process, HC emission are generally from sources that are independent of EGR, intake temperature, and intake pressure (with fixed load and combustion timing, as in the figure). Based on this, the incomplete combustion decreases without piston oil gallery cooling are predominantly due to decreased CO emissions, particularly at very lean conditions.

Previous CDC piston oil galley cooling studies suggested that NO_X emissions may increase when the oil gallery cooling jet was turned off [98]. However, in the present study this was not observed. The use of overly lean charges reduces the NO_X emissions formation processes, even with fuel-borne NO_X in the DI fuel (3% EHN). Similar low NO_X results with EHN were seen in mixing controlled LTC by Ikes et al. [71], and in RCCI by Hanson et al. [136] and Kaddatz et al. [144]. In the present study, the NO_X emission trends are shown in Figure 82. It is observed that with or without EGR, the NO_X emissions without cooling were quite similar, with EGR operation tending to have lower NO_X. Of course, EGR is commonly used to reduce NO_X formation in CDC.

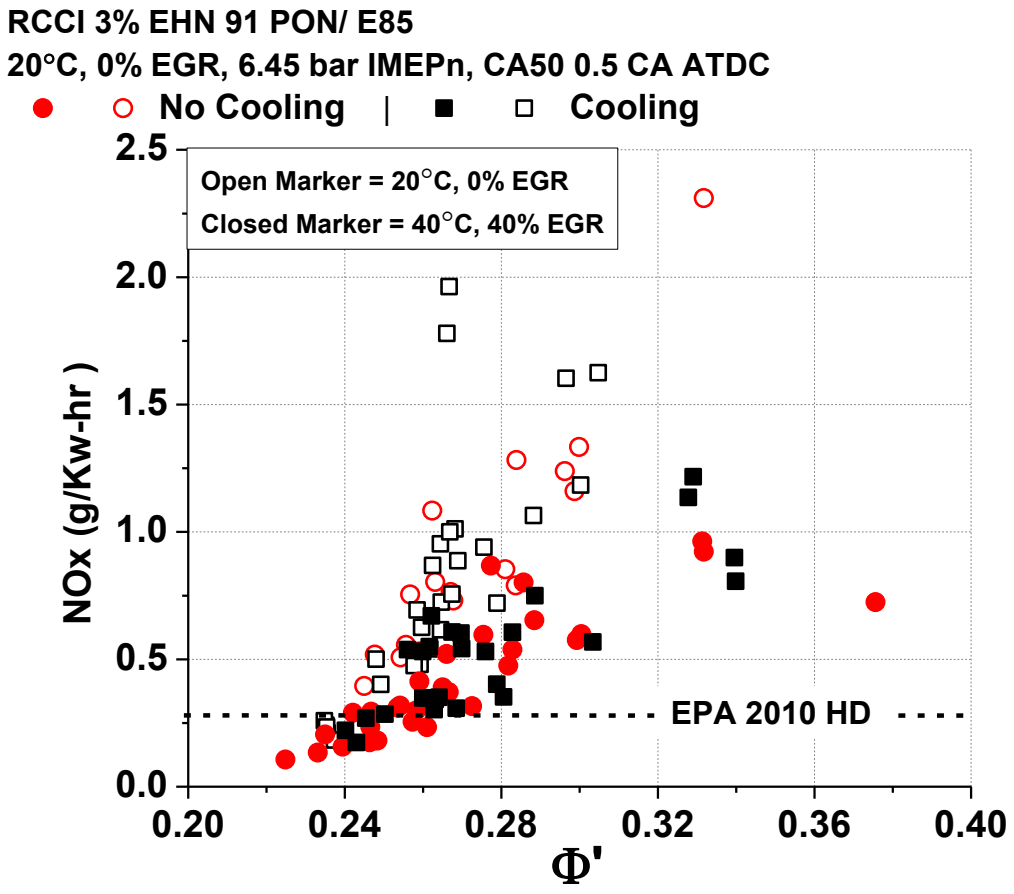

Figure 82 NO_X emissions as a function of charge dilution with or without EGR and with and without the use of the piston oil cooling jet. With lean operation and EGR, NO_X emissions with EHN/gasoline were below EPA 2010 regulations in-cylinder.

Figure 82 depicts that lean EGR operation enabled EPA 2010 NO_X limits to be met in-cylinder. Lastly, Figure 83 shows that EPA 2010 PM emissions were also met, with near zero levels recorded at all data points (AVL 415S smoke meter used, as discussed in Chapter 4).

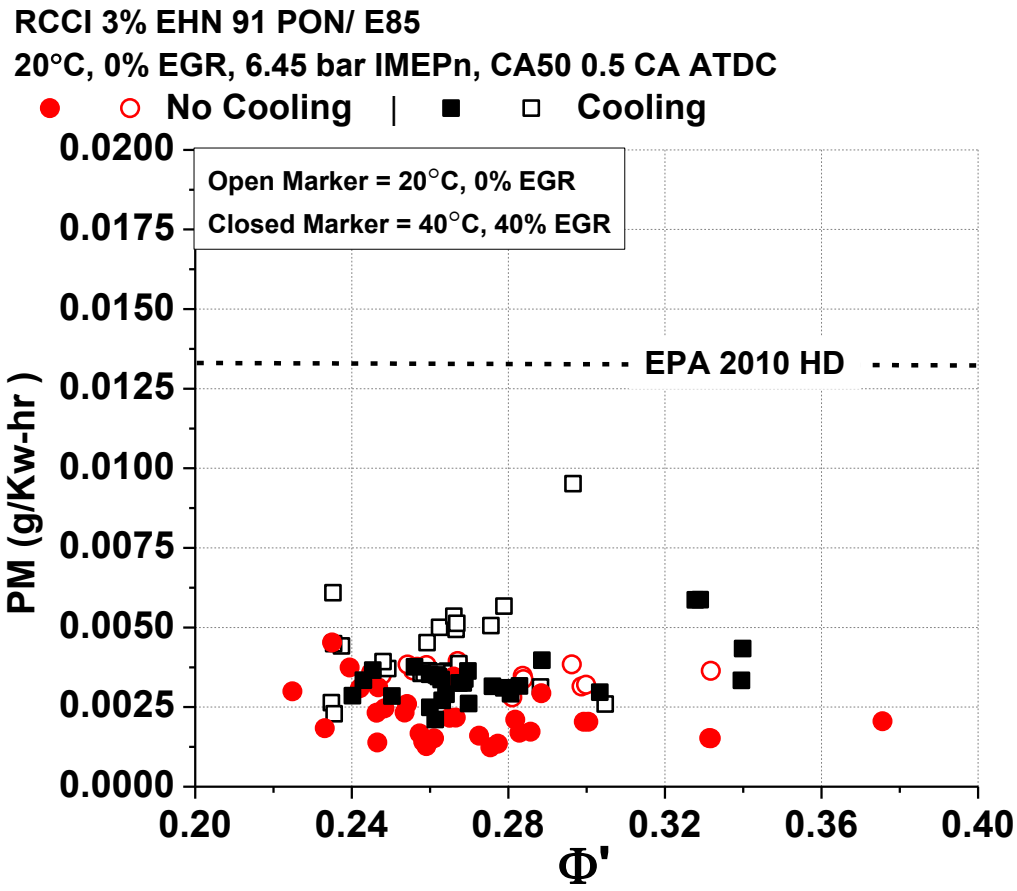

Figure 83 AVL 415S smoke emissions for EHN gasoline/gasoline RCCI. For all conditions near zero smoke was observed, suggesting that fuel-liner impingement was minimal.

The above emissions trends show that in relatively light load RCCI combustion, operating without piston oil gallery cooling has the potential to decrease incomplete combustion, with no significant change in NO_X or PM emissions. Furthermore, the low emissions advantages of RCCI are retained without oil gallery cooling. To examine some of the operational and efficiency differences select cases will be analyzed.

5.4.2.2 Piston Oil Gallery Cooling Efficiency Analysis

To investigate the effects of piston oil cooling on RCCI engine efficiency, a case with and without EGR and with and without oil gallery cooling was selected, for a total of four cases. The heat release, cylinder pressure, and bulk gas temperature profiles will be presented in the following sub section, along with key performance and operating metrics.

5.4.2.2.1 Efficiency with 0% EGR

To reduce knocking tendency, and to improve the operational window for operation without EGR, very cold intake temperatures were used. Intake temperatures of 20°C were used for a majority of the tests, with acceptable levels of combustion efficiency for most conditions. Some tests with temperatures as high as 32°C were conducted without EGR, but the fuel efficiency was not observed to substantially increase, and the operational window collapsed, similar to that observed in the Φ-T matrix tests in sections 5.2.3-5.2.5.

Representative high efficiency cases with 0% EGR and with and without piston oil cooling are presented in Figure 84, with performance in Table 37 and Table 38. Without EGR, similar fuel reactivates (fuel splits) were required at a matched phasing condition, suggesting that with the fuels used, piston oil cooling has a minimal effect on combustion phasing in high oxygen content and dilute conditions. The specific operating conditions for the cases are presented in Table 37, using the injection strategy described in Table 36, and detailed results of the conditions are in Table A. 10 and Table A. 11.

Table 37 Performance metrics of 0% EGR operation with and without oil gallery cooling

Piston Oil Cooling	NO	YES
Data point	43	10
RPM	1300	1300
IMEPg (bar)	6.70276	6.70224
IMEPn (bar)	6.21652	6.22988
BMEP_CF (bar)	5.02853	5.05009
FMEP_CF (bar)	1.18799	1.17979
CA50 (ATDC)	0.82835	1.14457
EGR %	0	0
PFI Fraction (E85)	0.78575	0.78453
DI Fraction (EHN gas)	0.21425	0.21547
Peak PRR (bar/deg)	9.64366	8.57514
P Intake (bar)	1.36532	1.36832
P Exhaust (bar)	1.53762	1.5647
T Intake (C)	20.08635	19.46011
Turbo Eff	0.68042	0.64305
Vol Eff	0.90847	0.92202
Comb Eff	0.95521	0.94861
HC (ppm)	909.9102	1006.03
NOx (ppm)	61.87919	57.28229
CO2ex (ppm)	35664.31	34785.71
CO2in (ppm)	15.12609	17.27776
CO (ppm)	1745.374	2029.475
HC (g/ikW-hr)	4.64599	5.2619
NOx (g/ikW-hr)	0.7638	0.72467
CO2ex (g/ikW-hr)	421.1737	421.0337
CO2in (g/ikW-hr)	0.17863	0.20912
CO (g/ikW-hr)	13.1183	15.63369
PM (g/ikW-hr)	0.00395	0.00358
Air Flow (kg/min)	2.33806	2.38325
AFR mass	40.40861	40.73879
AFR carbon	40.26571	40.78163
AFR Average	40.33716	40.76021
AFR Stoich	10.76684	10.77243
Phi mass	0.26645	0.26443
Phi carbon	0.26739	0.26415
Phi Lambda meter	0.26734	0.26545
Phi Average	0.26692	0.26429

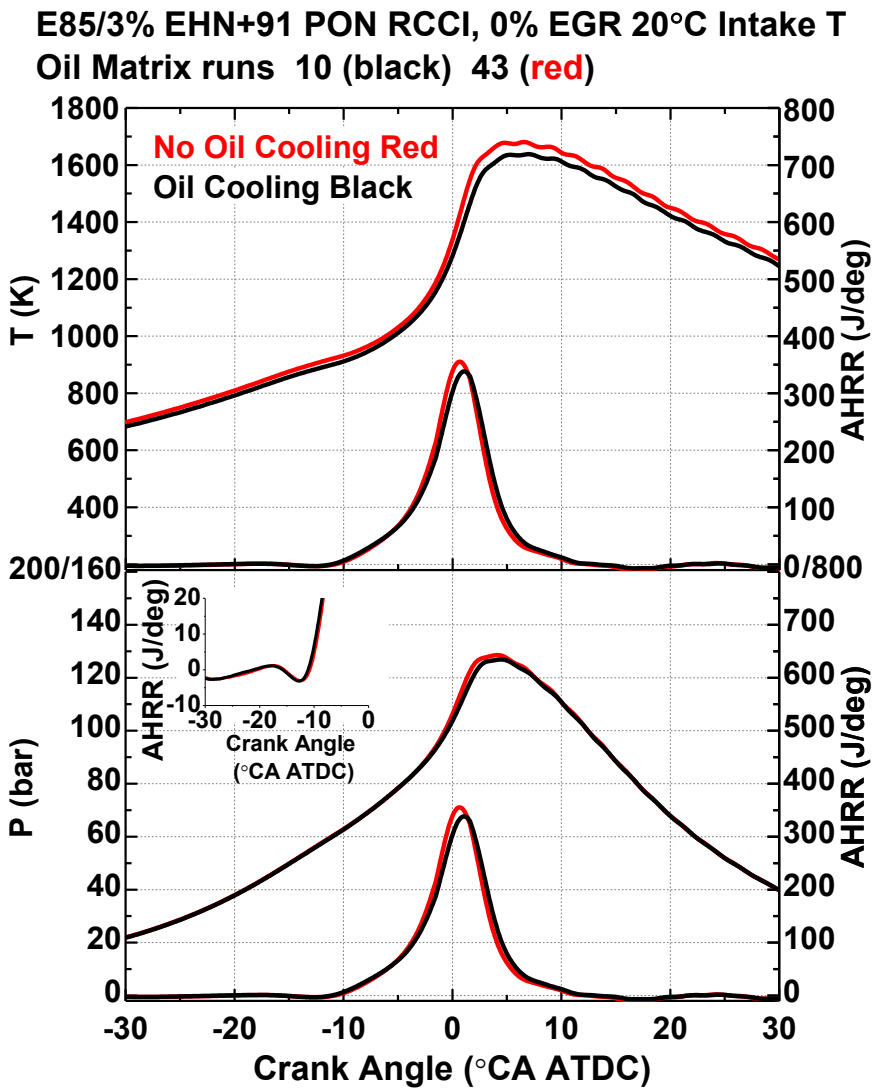

Figure 84 Cylinder pressure, temperature, and AHRR of 0% EGR RCCI with (black) and without (red) piston oil gallery cooling. Note, pressure and corresponding temperature traces are unfiltered. The IVC temperature of the cases were 314 K and 321 K for operation with and without oil cooling respectively.

The above trends suggest that at matched operating conditions (intake pressure and temperature, and fuel flow splits), there is increased bulk gas temperature when no piston cooling is present. This is likely a result of increased internal temperatures, (Figure 93 shows corresponding decreased volumetric

efficiency (VE) without cooling). Similar trends have been demonstrated by Primus [77] with thermal barrier coating CDC operation.

The results show that operation with the uncooled piston resulted in marginally shorter heat release. The performance of these cases is shown in Table 38.

Table 38 Efficiencies for operation in Figure 84

Piston Oil Cooling	NO	YES
Data point	43	10
GTE (AFR average) (%)	57.2	56.6
NTE (AFR average) (%)	53.0	52.6
BTE (AFRAverage) (%)	42.9	42.7

The data demonstrate that at operation with matched heat release, the efficiency of operation without piston oil gallery cooling is higher than with oil cooling.

5.4.2.2.2 Efficiency with 40% EGR

A similar comparison was performed with EGR operation. As discussed previously in this chapter, EGR has a dominant effect on the combustion process. The conditions compared are given in Table 39, where the cylinder pressure, temperature and AHRR traces are plotted in Figure 85. The cases were operated using the injection strategy described in Table 36, and detailed results of the conditions are in Appendix A, Table A. 12 and Table A. 13.

Table 39 Performance metrics of EGR operation with and without oil gallery cooling

Piston Oil Cooling	NO	YES
Data point	83	61
RPM	1300	1300
IMEPg (bar)	6.837014	6.77989
IMEPn (bar)	6.350036	6.28839
BMEP_CF (bar)	5.113968	5.092045
FMEP_CF (bar)	1.218711	1.220889
CA50 (ATDC)	0.452028	0.73111
EGR %	41.90999	41.69983
PFI Fraction (E85)	0.849241	0.80525
DI Fraction (EHN gas)	0.150759	0.19475
Peak PRR (bar/deg)	11.26848	10.55442
P Intake (bar)	1.57801	1.57714
P Exhaust (bar)	1.72464	1.72833
T Intake (C)	42.4612	40.672
Turbo Eff	0.721315	0.72321
Vol Eff	0.887079	0.92234
Comb Eff	0.969941	0.96613
HC (ppm)	1059.49	1099.852
NOx (ppm)	41.4307	36.28338
CO2ex (ppm)	58940.17	57702.52
CO2in (ppm)	24927.21	24288.05
CO (ppm)	1727.512	2084.966
HC (g/ikW-hr)	3.381211	3.60574
NOx (g/ikW-hr)	0.310517	0.28504
CO2ex (g/ikW-hr)	422.6377	433.6916
CO2in (g/ikW-hr)	178.7436	182.5488
CO (g/ikW-hr)	7.883875	9.97349
PM (g/ikW-hr)	0.002328	0.00285
Air Flow (kg/min)	1.421673	1.48561
AFR mass	23.91949	24.87472
AFR carbon	24.54533	25.36387
AFR Average	24.23241	25.1193
AFR Stoich	10.47478	10.67715
Phi mass	0.437918	0.42924
Phi carbon	0.426753	0.42096
Phi Lambda meter	0.444603	0.43765
Phi Average	0.432263	0.42506
PHI Charge Average	0.253519	0.25027

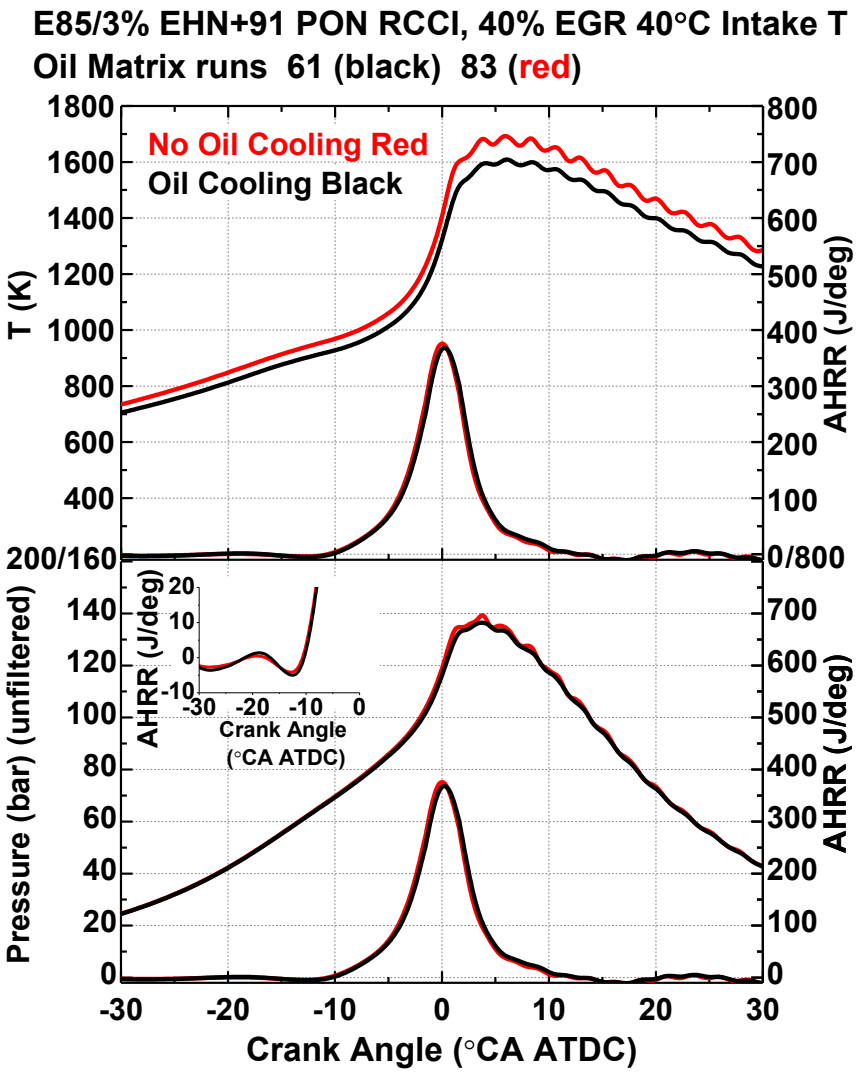

Figure 85 Cylinder pressure, temperature, and AHRR of 40% EGR RCCI operation with (black) and without (red) piston oil gallery cooling. Note, pressure and corresponding temperature traces are unfiltered. The IVC temperature of the cases were 333 and 347 K for operation with and without oil cooling, respectively.

Unlike operation without EGR, the present results required trimming of the ratio between more reactive and less reactive fuels to maintain constant combustion phasing, as seen in Table 39. These trends suggest that without piston oil cooling, there can be a marked increase of in-cylinder temperatures, as

seen Figure 85, which becomes more influential. The efficiencies of the cases in Figure 85 are given in Table 40.

Table 40 Efficiencies for operation in Figure 85

Piston Oil Cooling	NO	YES
Data point	83	61
GTE (AFR average) (%)	59.2	57.1
NTE (AFR average) (%)	55.0	53.0
BTE (AFRAverage) (%)	44.3	42.7

The trends demonstrate that at operation with matched heat release and EGR, the efficiency of operation without piston oil gallery cooling is higher than with cooling.

5.4.3 PPRR Effects with Piston Oil Gallery Cooling Modulation

To investigate the effects of temperature, a statistical analysis of the PPRR was performed similar to that presented in Figure 77. In that initial comparison, it was concluded that the higher dependency of HCCI on intake and in-cylinder temperature, led to a higher variability, and the reduced stratification of HCCI led to a higher PPRR. In the present results, Figure 86 displays the trends of RCCI operation with and without oil cooling. The data used are the cases presented in Figure 84 and Figure 85 earlier in this present sub section.

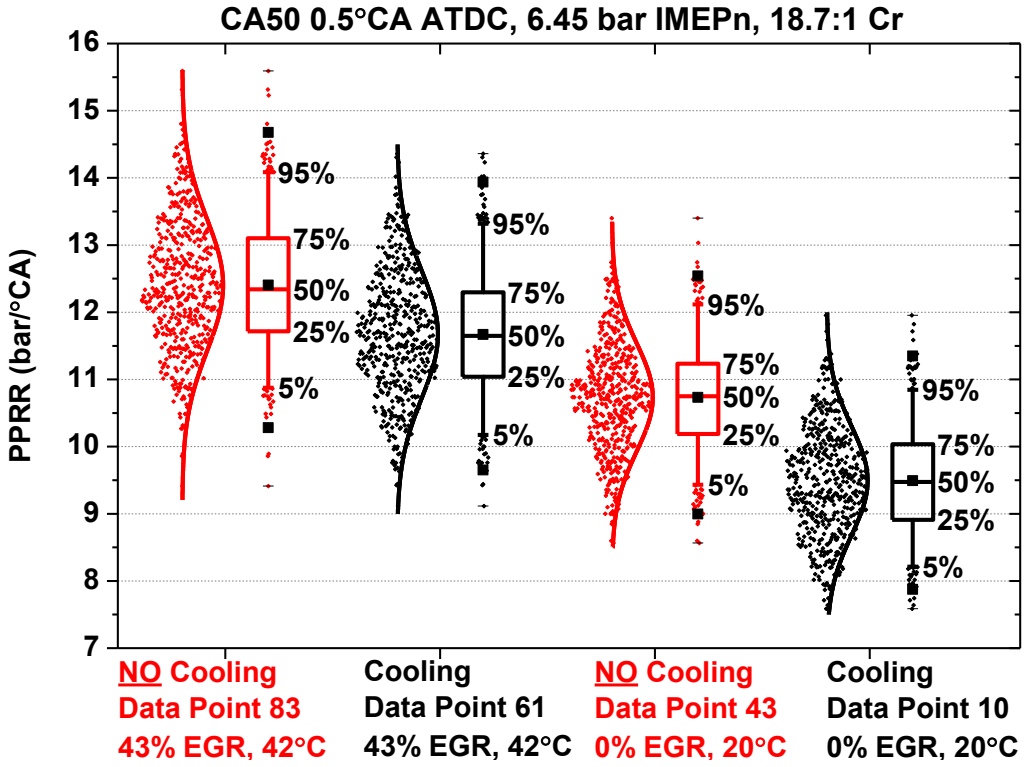

Figure 86 Box plots of PPRR for operation with EGR (left two points) and without EGR (right two points). Operation with the piston cooling jet off is in red and with the cooling jet on is in black. Conditions without piston oil gallery cooling exhibit higher PPRR values, and demonstrated similar temperature dependency to that of HCCI as previously observed.

From the figure it is seen that without piston jet oil cooling, the PPRR is higher, and the variability of the data is slightly higher (normal distribution is broader). Based on the previous analysis of HCCI and RCCI, this demonstrates that without piston oil jet cooling, the charge is more vulnerable to temperature variations. That is, the ignition process is likely to rely less on the reactive fuel and more on the bulk gas temperature. This is likely as with 0% EGR the reactive fuel portions, load and phasing are identical, but the PPRR is not. This trend was consistent across the Φ/Φ' range tested, and is demonstrated in Figure 87.

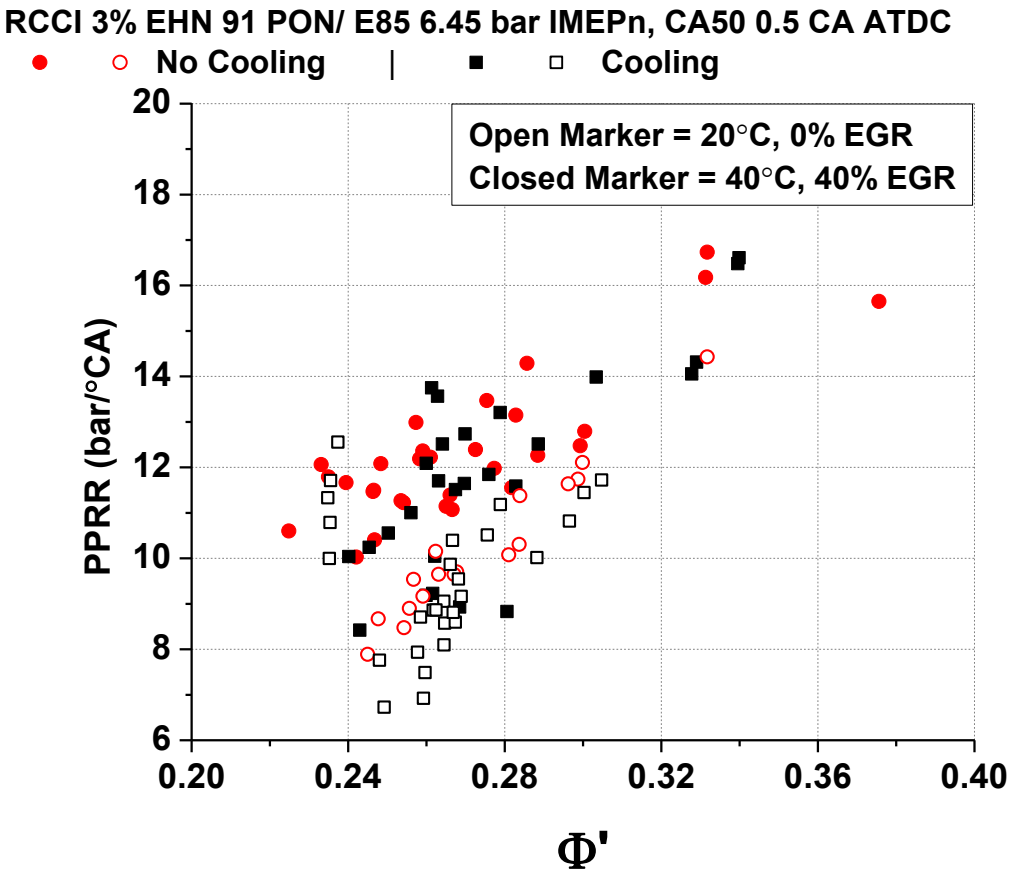

Figure 87 PPRR for tests with (red) and without (black) piston oil cooling. Open markers denote 0% EGR operation and closed markers denote 40% EGR operation. Generally operation without piston oil cooling exhibited higher PPRR for a given Φ′

In general the present findings of engine operation without piston oil cooling suggest that there are reduced incomplete combustion and less engine heat transfer loss, which are results of the increased internal surface temperatures. The following section investigates the potential interactions that this has on engine fuel efficiency.

5.4.4 Overall GTE Trends With Piston Oil Gallery Cooling Modulation

The overall trends in GTE for cases with and without oil cooling, both with and without EGR, are plotted in Figure 88. The whiskers in the figure represent the

spread in GTE calculated from the direct mass and AFR_C fuel flow rates, with the data points representing the average of the two.

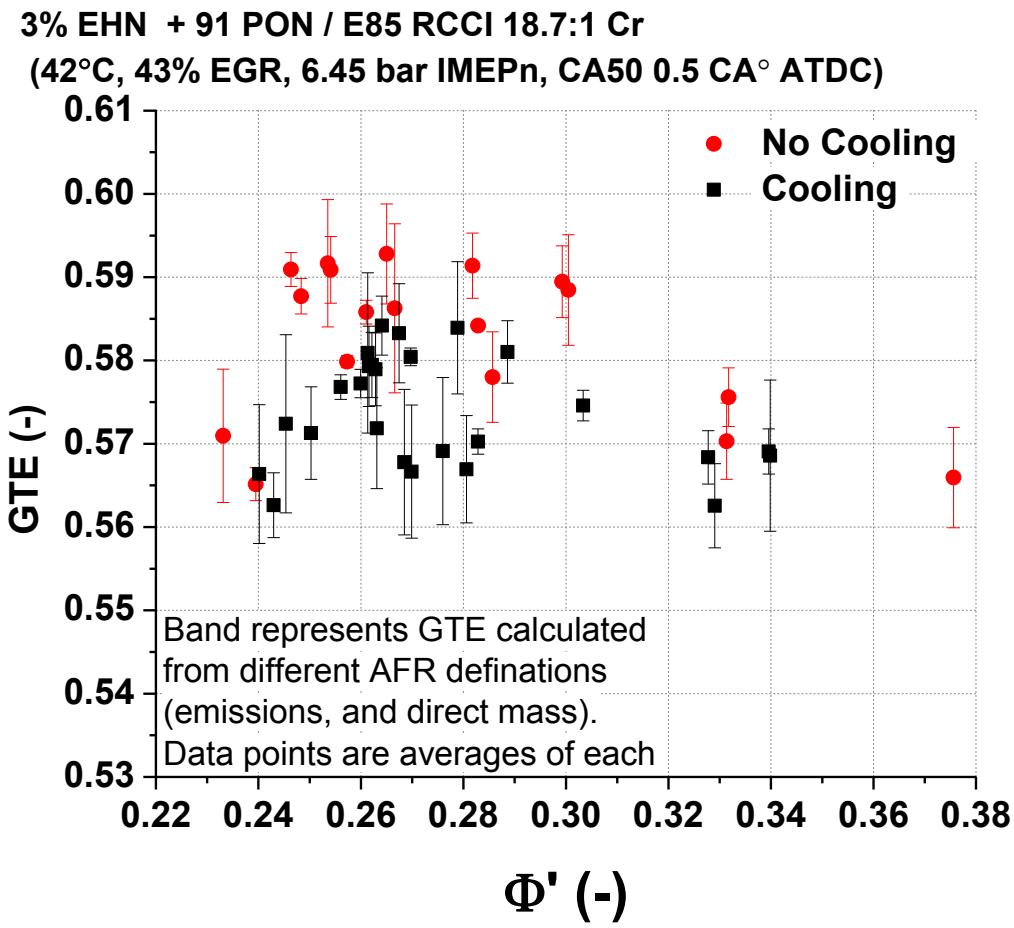

Figure 88 GTE measurements of high compression ratio RCCI with and without piston oil gallery cooling. Data points are the average GTE determined from AFC_C and direct mass (AFR_{MASS}); whiskers denote the range of GTE determined by the respective AFR approaches.

The results in Figure 88 show that RCCI is capable of achieving extremely high thermal efficiencies, approaching the 60% predicted by the GT Power simulations in Chapter 3.

5.4.4.1 Lean Limit Extension and Efficiency Effects

To examine the reasons for higher efficiency without piston oil cooling, the highest efficiency conditions with and without cooling were averaged (conditions are listed in Appendix A, Table A. 12 and Table A. 13, data points 46-53,55,64-67, 69, 70 with oil cooling and data points 83-85, 92-94 without oil cooling). The energy budget results are seen in Figure 89.

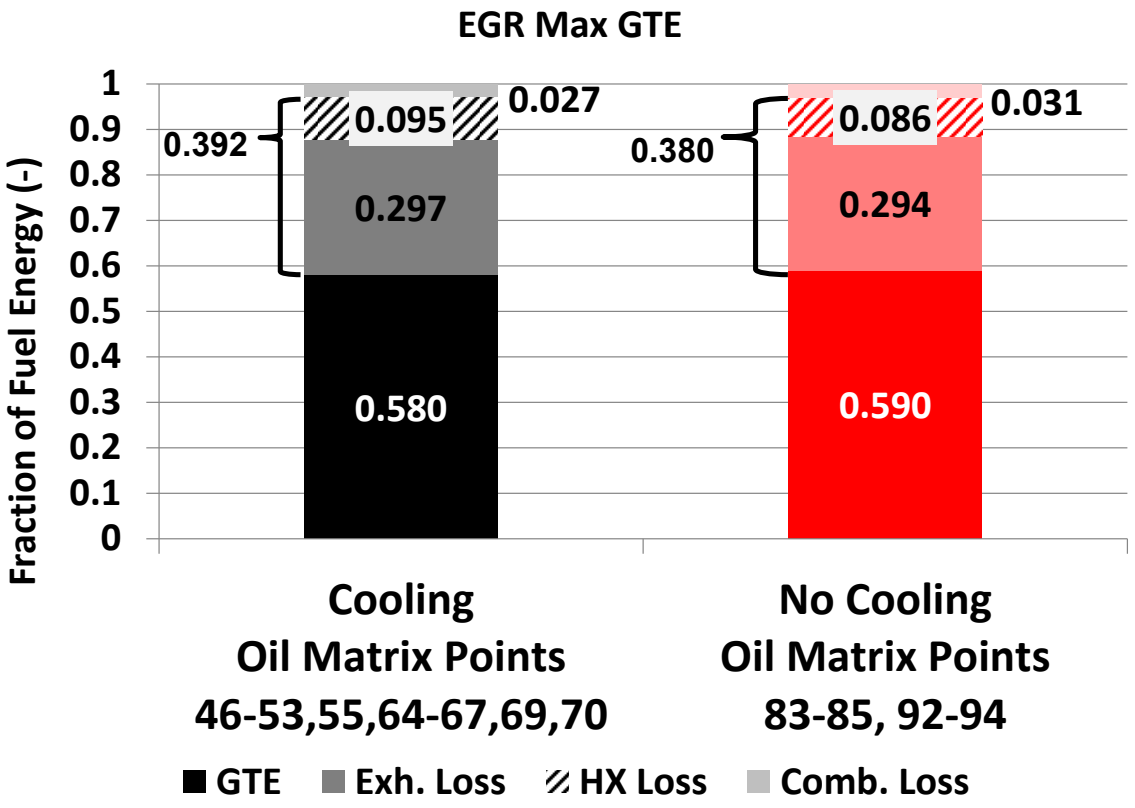

Figure 89 Energy budget with and without piston oil cooling for 40% EGR operation. The combustion efficiency for operation without oil cooling is actually worse that with cooling. However, the heat and exhaust losses are much lower, which dominate the efficiency advantage.

The results show that the gross efficiency without piston oil cooling was measurably higher. However, the reason for this is not from improved combustion efficiency. Interestingly, with EXH+ HX losses are ~1% point lower

without piston cooling. The reason for this is presented in Figure 90, which demonstrates that at the maximum efficiency point without oil cooling, the charge is leaner.

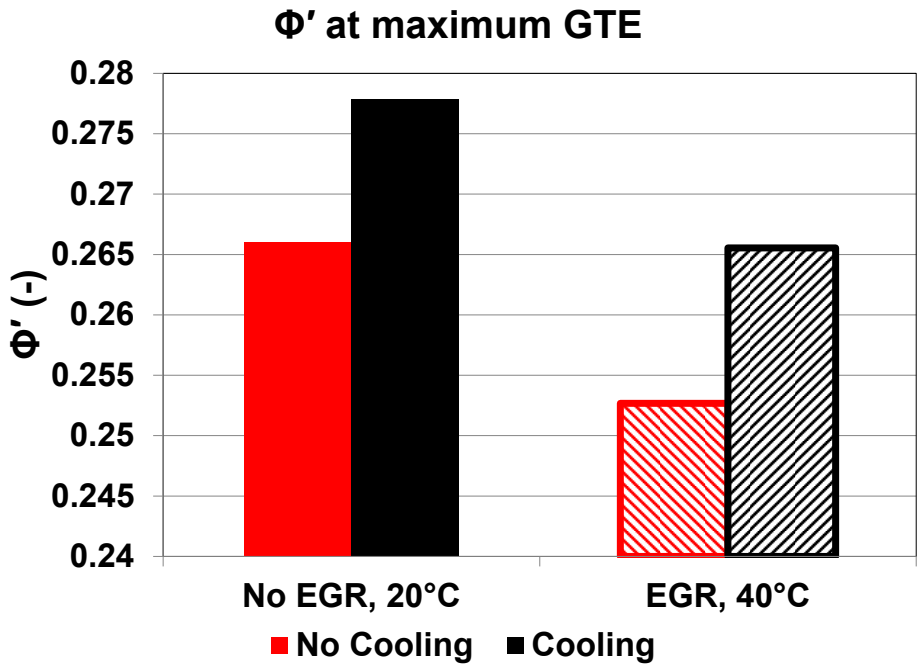

Figure 90 Φ/Φ′ of maximum efficiency operation. Without oil cooling the charge can be further leaned without GTE penalty, thereby further reducing heat losses.

The above results demonstrate that without cooling the piston, leaner operation is beneficial. To remind the reader, Figure 59 in the Φ-T matrix tests demonstrated that leaner Φ operation reduced HX+EHX losses, but at the expense of reduced combustion efficiency. The present results demonstrate that without piston oil cooling this tradeoff in losses is reduced. For example, when the engine was operated with piston oil cooling at the conditions where maximum efficiency occurred without cooling (Φ′=.253), the efficiency was reduced, and incomplete combustion rose. Figure 91 shows the result of the matched Φ′ operation (the operating conditions are listed in Appendix A, Table A. 12 and

Table A. 13, data points 53,59,61,64-66,68 with oil cooling and data points 83-85, 92-94 without oil cooling).

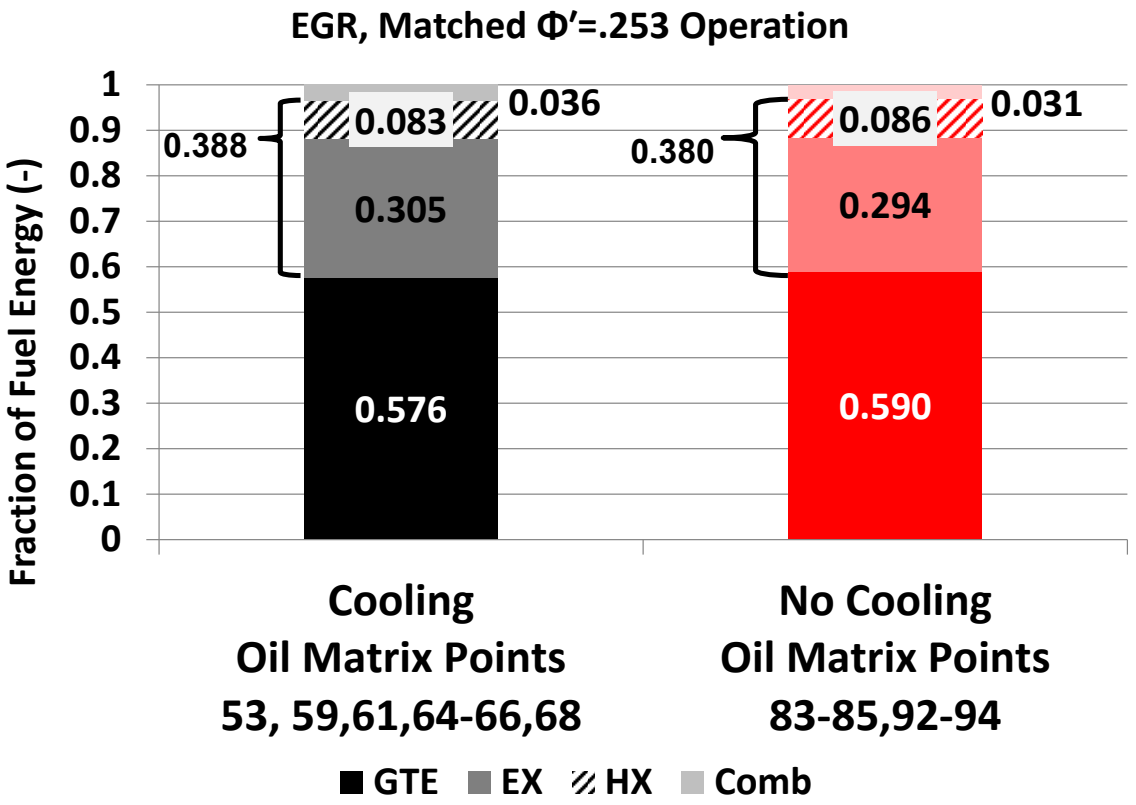

Figure 91 matched Φ′ operation with and without piston oil cooling. Without oil cooling the losses at the lean condition are reduced, increasing efficiency.

The results demonstrate that with piston oil cooling, the leaner conditions do increase incomplete combustion with cooling, but other losses are higher. The near identical HX losses for operation with and without cooling demonstrate that the lean charge is important for efficiency. However, since exhaust losses with cooling are reduced, (0.294 vs. 0.305), this is of particular interest.

At first glance, this is counterintuitive since at a given Φ, the exhaust gas temperatures without piston oil cooling tended to be ~1-5°C higher than with cooling (see Appendix A, Table A. 10 to Table A. 13,). However, it was also

observed that without oil cooling, the volumetric efficiency (VE) of the engine was reduced. The impact that this has on efficiency is subtle.

5.4.5 Volumetric Efficiency Effects of Piston Oil Gallery Cooling Modulation

To better understand the relationships and implications of VE, a more detailed investigation was performed. As seen in Table 37 and Table 39, the volumetric efficiency (VE) of the engine was reduced without piston oil cooling (~3% reduction). Based on the piston and liner temperature measurements of Luff et al. [98], it is concluded that the internal engine surface temperatures are higher without piston oil cooling. Increased internal surface temperatures would preheat the fresh incoming charge and as a result, reduce engine breathing efficiency. For example, the result for the cases shown in Figure 85 was that for a similar IVC pressure, the IVC temperature was 17°C higher for the case without oil cooling. Since the IVC pressures are the same, the result is that trapped mass (Φ) decreases correspondingly.

Based on the previous Φ-T matrix test results, a reduced trapped mass would not indicate more efficient engine operation, and it could actually imply lower engine efficiency. For example, Figure 92 demonstrates that with the 14.88:1 Cr piston fueled with 3% EHN + 91 PON gasoline/E85, the peak engine efficiency conditions coincided with the highest VE and lowest HX conditions.

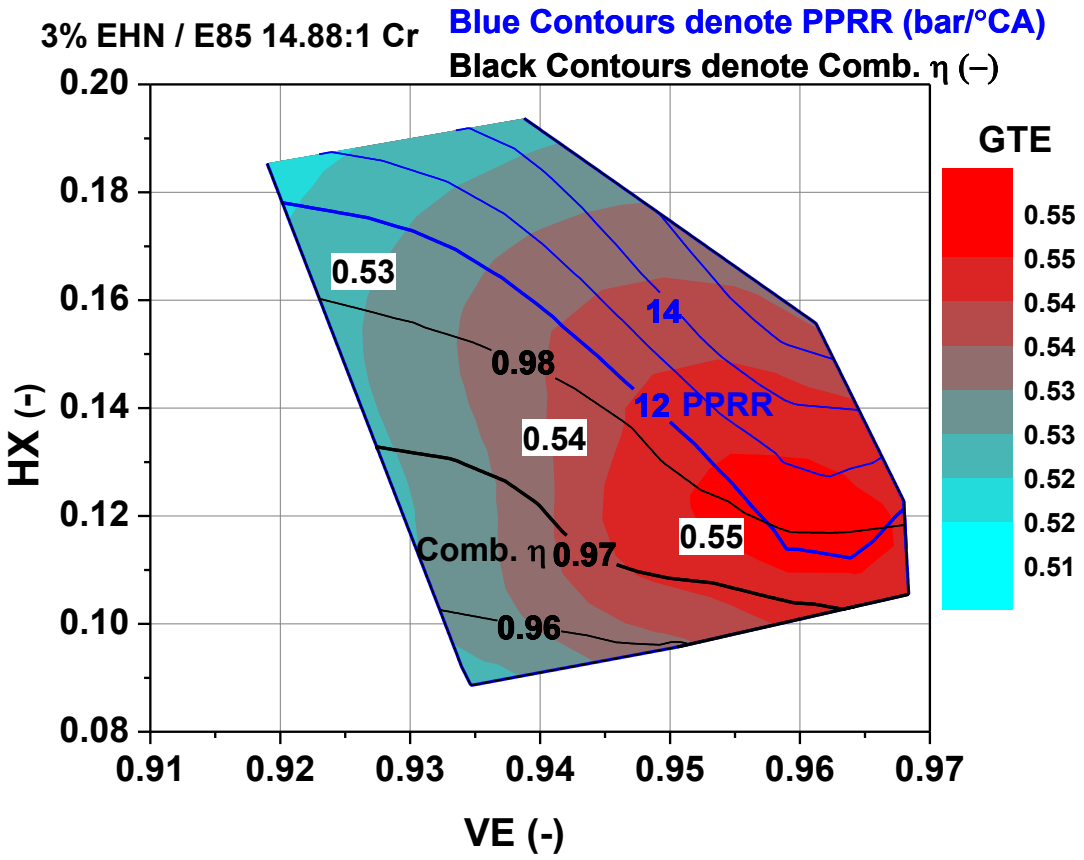

Figure 92 GTE plotted versus VE and HX for the 14.88 Cr piston data of Appendix A, Table A. 2. Contours of PPRR of 12 bar/°CA or greater are plotted in blue, and combustion efficiencies of 98% or less are plotted in black. The original Φ-T constraints of 12 bar/°CA and 97% combustion efficiency are bolded contours. The results demonstrate that good breathing and low losses are critical for high engine efficiency.

From the figure is seen that for a given VE, there is a generally a fixed GTE. Only when high levels of heat transfer (HX) are encountered (which coincide with high PPRR) or with low combustion efficiency, does this trend deviate. This relatively constant GTE as a function of VE demonstrates that breathing (i.e., trapped mass) is typically strongly correlated with efficiency. It should be noted for reference, that in Figure 92, the highest VE values simultaneously occurred with use of the highest E85 fractions (not shown), suggesting that improved charge cooling may offer increased efficiency.

However, if a reduction in trapped mass occurs from increased internal temperatures, this may indicate reduced internal heat losses, as noted in the LHR work by Primus et al. [77]. Thus, if losses are reduced, the same trapped mass is not required for a given efficiency. Figure 93 demonstrates this trend with experiments with and without piston oil cooling. The data for 14.88:1 operation is taken from the Φ-T matrix described in Figure 44, and the corresponding data can be found in Appendix A, Table A. 2.

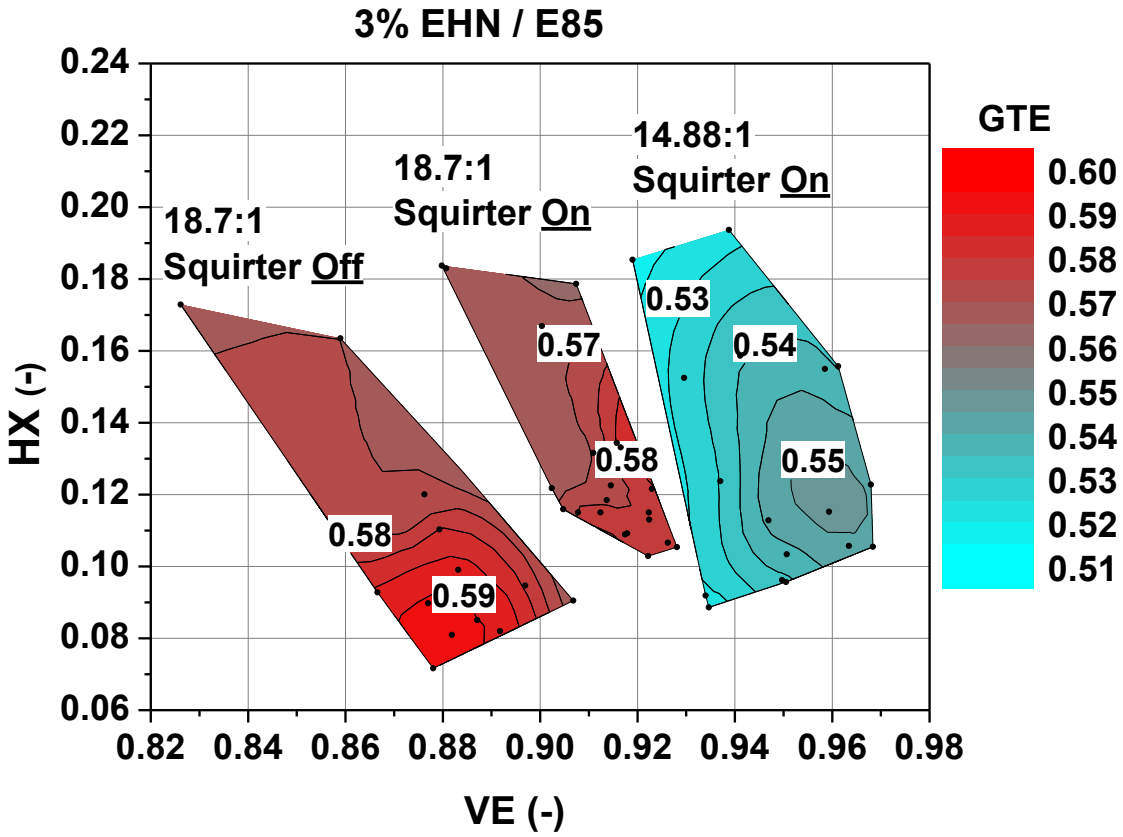

Figure 93 GTE versus HX and VE. Note that without piston oil gallery cooling, the lowest VE and HX conditions correspond to the lowest HX and associated GTE. Both 18.7 Cr conditions are with EGR operation. Note, conditions are with combustion efficiency greater than 95.5%. Data in Appendix A, Table A. 2, Table A. 12, and Table A. 13

From the figure it is seen that without piston oil cooling, the trends in efficiency are opposite; that is, the lowest HX and VE correspond to the highest

GTE. This reveals the subtle relation between volumetric efficiency and increased fuel efficiency without piston oil cooling. To determine the reasons for this trend, a similar analysis with PPRR and combustion efficiency limits is presented in Figure 94.

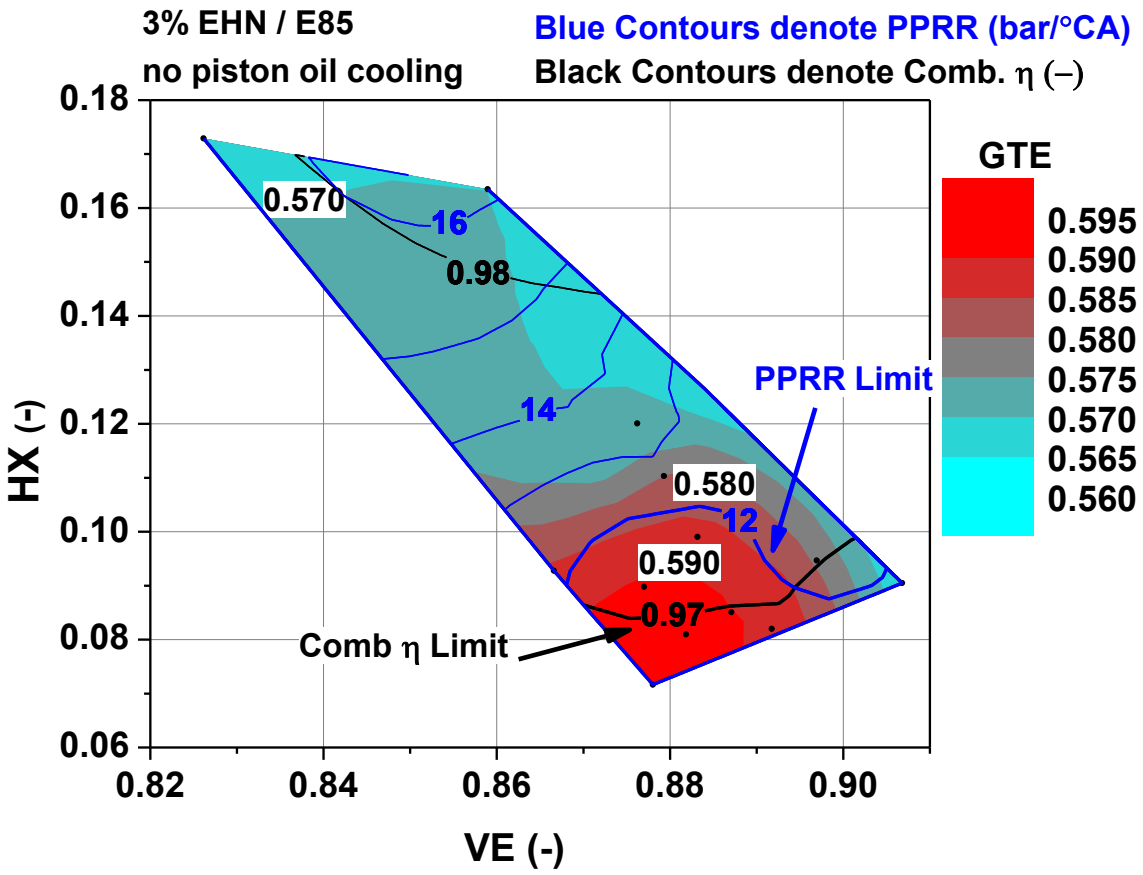

Figure 94 GTE results with 40% EGR and 18.7 Cr plotted in VE and HX space. Contour lines of PPRR of 12 bar/°CA or greater are overlaid in blue, and combustion efficiencies of 98% or less are overlaid in black. The original Φ-T constraints of 12 bar/°CA and 97% combustion efficiency are bolded contours. The results demonstrate that without piston oil cooling mediocre engine breathing exists, but that heat losses and high efficiency are simultaneously achieved. Data in Appendix A Table A. 13

Unlike the trends of Figure 92 with piston oil cooling, the contours of GTE without piston oil cooling are seen to be strongly affected by PPRR, and less by combustion efficiency. Thus, PPRR is of greater concern without oil gallery

cooling (note that PPRR was previously shown to indicate larger heat losses, HX). At the highest GTE the PPRR is minimal. This indicates that there likely is to be reduced internal engine heat transfer, which combined with lower airflow rates (reduced VE), offers the opportunity for simultaneous HX and Exhaust loss reductions, thus increasing gross thermal efficiency.

An interesting finding of the presented analysis is that unlike operation with piston oil cooling (Figure 92), the PPRR trends of Figure 94 are different. That is, PPRR lines without piston oil cooling are roughly horizontal. In operation with piston oil cooling, the horizontal PPRR lines coincided with the upper bound on GTE (likely due to knock, as previously discussed). A similar effect is likely to exist in the present analysis because the PPRR lines only generally coincide with GTE. These results suggest that without oil cooling, the operable high efficiency area is small, since knock limits high efficiency operation more than incomplete combustion.

As mentioned the VE trends of operation without piston gallery oil cooling are somewhat different. Typically reduced engine VE suggests that pumping losses will be high, as engine air exchange is more laborious. Increased pumping is encountered at lean conditions and with reduced VE. However, Figure 95 demonstrates the required overall turbocharger efficiency for cases with and without piston oil gallery cooling is indistinguishable. This is a result of the combination of VE and exhaust temperatures, as without oil gallery cooling, the reduced exhaust losses do not result in increased pumping work, as the mass flow rate of fresh charge is correspondingly reduced.

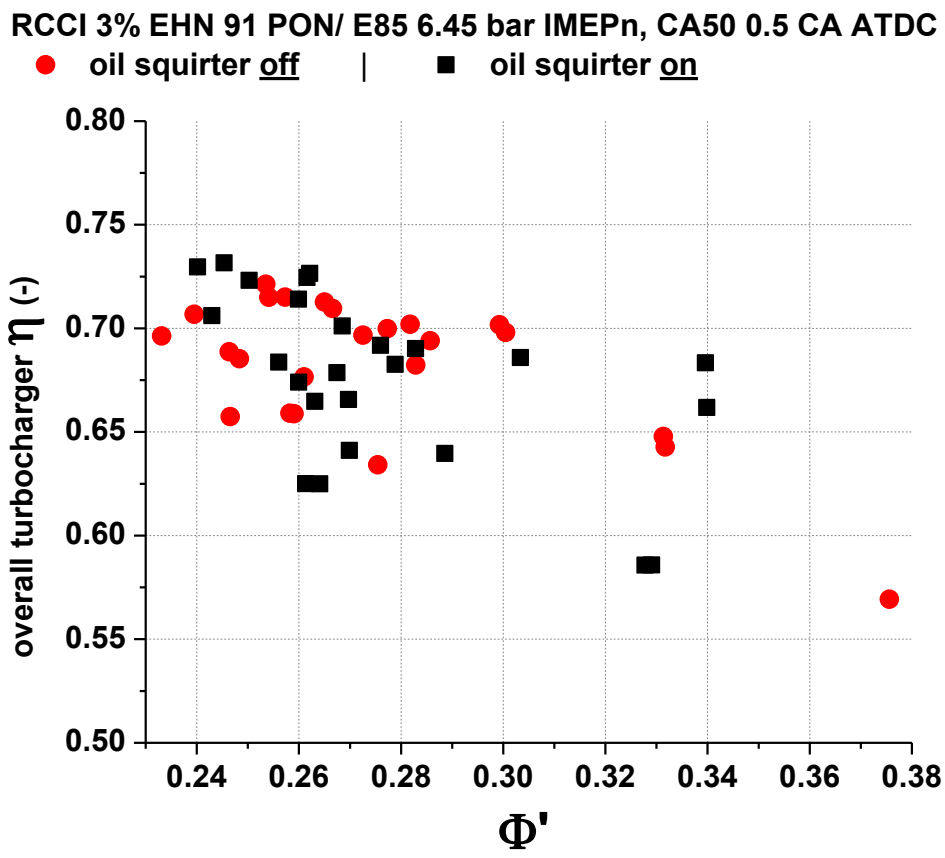

Figure 95 Simulated required overall turbocharger efficiency for the tested conditions. The simulated conditions are optimistic. Data in Appendix A Table A. 13

5.4.6 Minimization of Losses for Maximum Efficiency

Based on the trends in the combustion and HX loss results of this chapter, it is of merit to identify an optimum combination so as to provide a condition of maximum efficiency. Figure 96 plots the trends in HX and combustion efficiency with common Y axis scale.

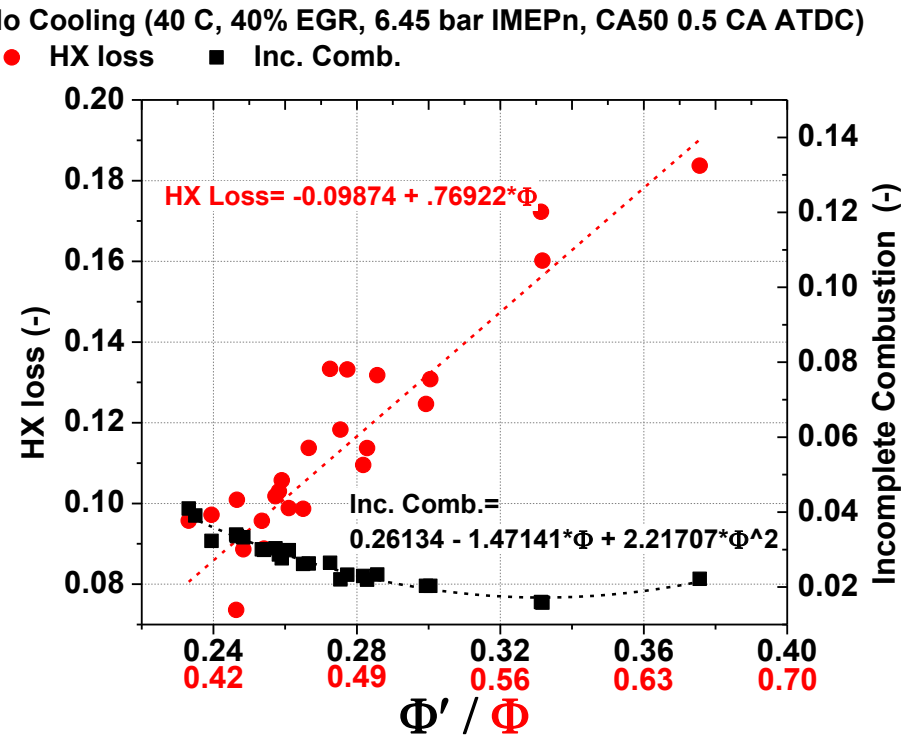

Figure 96 Combustion and heat transfer losses as function of Φ without piston oil cooling and with 40% EGR. Note that as the charge approaches the richer air based Φ, incomplete combustion increase, suggesting overly rich areas. Data in Appendix A Table A. 13

From the figure it is seen that heat transfer has a much more coupled relationship with trapped mass (indicated by the equivalence ratios) than combustion efficiency. The results in the figure are with 43% EGR and no piston oil cooling, and the operating conditions are indicated in Appendix A Table A. 13.

Using a quadratic search minimization approach, the combined loss of HX and incomplete combustion yields an optimal Φ of 0.158. However, this is below the lean limit of auto ignition, as discussed in Chapter 2. If the HX linear fit is set to an intercept of zero, the linear fit has a R^2 value of 0.98, and the Φ′ of minimal losses increases to 0.237, which is much more representative of the measured values in the range of ~0.255. Thus, it is concluded that the best

tradeoff in combustion efficiency and heat transfer occurs with trapped mass (i.e., Φ), in the vicinity of the lean limit.

Based on the experimental results of this chapter, it is useful to revisit the GT Power simulation for both support of the experimental findings, and also to determine the efficiency cycle limits. This is done in the next chapter.

CHAPTER 6 Discussion, Maximum Cycle Efficiency Limits

In Chapter 3, GT Power was used to investigate conditions for improving engine efficiency. The preliminary study varied compression ratio, intake pressure, heat transfer, and combustion efficiency. The results suggested that a higher compression ratio, in combination with reduced heat transfer and increased combustion efficiency could enable gross indicated thermal efficiencies reaching close to 60%. Using these simulation results as a pathway, the experiments verified whether the simulation's suggested operating conditions were of merit. The measurements suggested that the GT Power model was a useful predictive tool, as measurements near the 60% target were achieved. Therefore it is of interest to revisit the GT Power to compare the measured results with simulation predictions, and to use the simulation tool to explore the pragmatic maximum efficiency possible with RCCI.

Simulations were conducted using the experimental inputs of Table 41 for the initial conditions. Although not shown in the table, the experimental AHRR of cases 61 and 63 (see Figure 85) was also input into the simulations.

Table 41 Inputs for GT Power simulations of high efficiency operation

Oil Matrix Point	**Piston Oil Cooling**	**T IVC (K)**	**P IVC (bar)**	**P Int. (bar)**	**T Int. (K)**	**P Exh. (bar)**	**T Exh. (K)**	**Fuel Energy [****] (MJ/kg)**	**Fuel Mass[††††] (mg/cyc)**
61	**YES**	333	1.69	1.58	316	1.73	515	31.96	91.0
83	**NO**	347	1.69	1.58	316	1.72	517	30.06	90.3

[****] Average of AFR_{mass} and AFR_C based fuel energy used in simulation
[††††] Average of AFR_{mass} and AFR_C based fuel mass used in simulation

Based on the experimental results of Luff et al. [98] (see Figure 22 and Figure 23) in simulations without piston oil cooling, the modeled piston surface temperature was increased by 50°C and the liner temperature was increased by 5°C (550 vs. 500, and 405 vs. 400 K, respectively).

Using these inputs two series of simulations were performed. The first investigated the effects of operation with and without oil cooling. The second set of simulations assumed adiabatic operation with 100% combustion efficiency. It should be noted that the latter set represents the maximum cycle efficiency, and not the maximum theoretical efficiency of combustion, as that is defined from the thermodynamics of the combustion process alone, not the thermodynamics of the engine cycle.

6.1 Simulation Results and Model Validation with Experiments

In Chapter 3 it was suggested that the simulation convection coefficient (GT Power WoschniHuber correlation selected in simulation) needed to be tuned to 0.4 to match experimental results with the 14.88:1 Cr piston. It was also suggested if the convective coefficient was reduced to 0.2 from 0.4, 60% gross efficiency may be achievable. The previous chapter investigated the potential that eliminating the piston oil cooling may have on achieving reduced heat loss.

As stated in Chapter 4, compared to the 14.88:1 Cr piston, the 18.7:1 piston has a 1.2% reduction in TDC surface area, and was hand buffed to reduce surface area from machining roughness. The combination of these effects may reduce heat losses through the piston. The simulation results are presented in

Table 42. The data shows that when the convective coefficient was 0.4 (matched 14.88:1 Cr piston with oil cooling on), the expansion pressure with the higher compression ratio 18.7:1 Cr piston with the oil cooling off, was under predicted. The results in Table 42 show that the expansion pressure was under predicted by ~0.5 bar at the given condition. However when the convection coefficient was reduced to 0.2, the measured performance and cylinder pressure were matched with very good agreement, as shown in Figure 97.

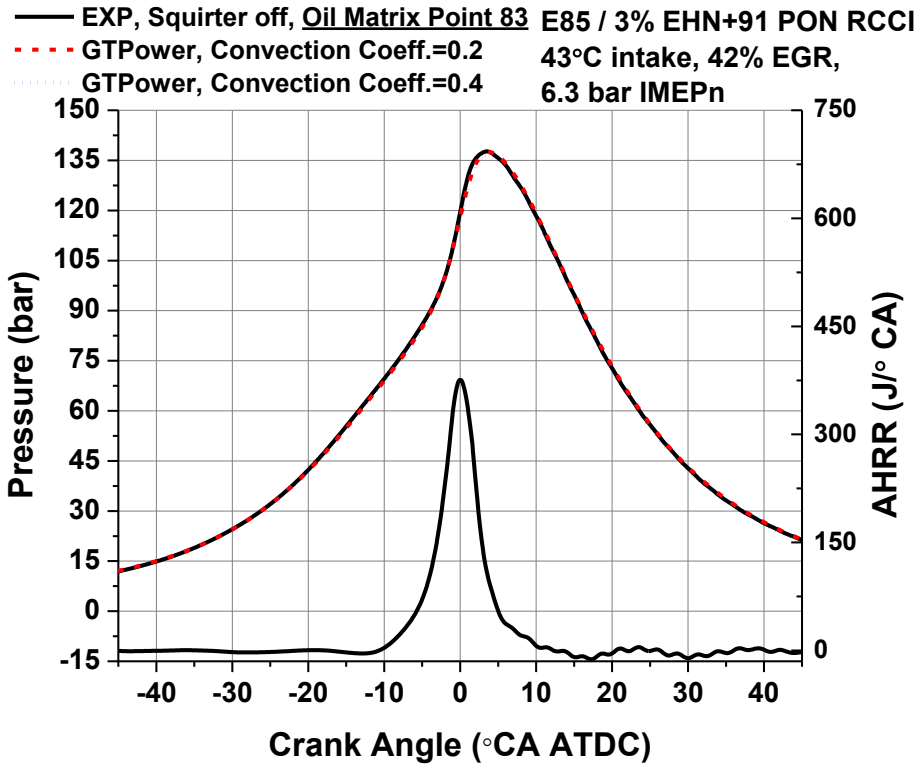

Figure 97 GT Power convection coefficient tuning for 18.7:1 Cr RCCI. With piston oil gallery cooling, the model convection coefficient needed to be reduced to 0.2

Table 42 Operating and efficiency parameters from the experiment without piston oil cooling and GT Power with various convection coefficients.

	GTE	IMEPg	NTE	IMEPn	BTE	BMEP
	(%)	(bar)	(%)	(bar)	(%)	(bar)
EXP (pt. 83)	59.1	6.82	55.0	6.27	43.7	5.11
GT Power HX =0.2	58.8	6.79	54.9	6.25	45.0	5.14
GT Power HX =0.4	56.7	6.47	52.8	6.02	43.0	4.91

Based on these findings it is seen that for the case without oil cooling, heat loss was reduced as compared to previous results. However, it is unclear whether the effect is due to the reduced piston surface area, or to the increase in surface temperature, or a combination of both. To investigate this, operation with oil cooling was also modeled. The results in Figure 98 and Table 43 demonstrate that with piston oil cooling, there are additional in-cylinder heat losses. These simulation results support the findings of the previous chapter, where operation without piston oil cooling yielded higher efficiency, and reduced heat loss.

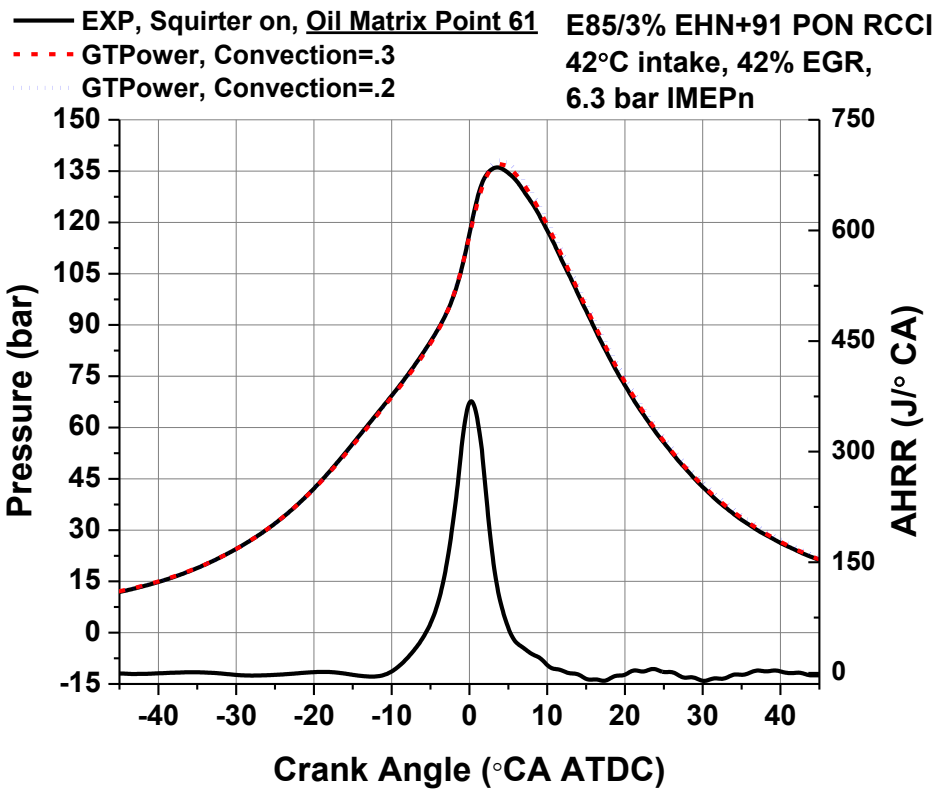

Figure 98 Comparison of convection coefficients for operation with piston oil cooling, and 18.7:1 Cr. The results suggest that the reduced surface area and smooth surface finish of the high compression ratio piston may in-and-of-itself reduce heat transfer somewhat as compared to the 14.88:1 bathtub profile, which required a convection coefficient of 0.4.

Table 43 Operating and efficiency parameters from the experiment with piston oil cooling and GT Power with various convection coefficients.

	GTE (%)	IMEPg (bar)	NTE (%)	IMEPn (bar)	BTE (%)	BMEP (bar)
EXP (pt. 61)	57.2	6.78	53.0	6.29	42.2	5.06
GT Power HX =0.3	57.1	6.75	53.2	6.29	43.7	5.17
GT Power HX =0.2	58.1	6.87	54.3	6.42	44.8	5.3

The presented results provide a baseline for setting model constants for operation with the high compression ratio piston with and without piston oil cooling.

6.2 Simulation with Adiabatic and 100% Combustion Efficiency Operation

The simulation was used to determine the maximum possible cycle efficiency. For the maximum cycle efficiency simulations, 100% combustion efficiency was assumed and the heat transfer coefficient was set to zero, simulating adiabatic operation. Both the cases with and without oil cooling were modeled, but only to demonstrate the difference in performance relative to the measured condition. Results for operation with the cooling jet off are shown in Figure 99 and Table 44, where results with cooling on are shown in Figure 100 and Table 45. It should be noted that since all losses that contribute to gross efficiency were set to zero (except for exhaust losses), the predicted gross efficiency should be the same. However, the trapped mass and intake pressure of the two modeled cases, are slightly different from one another, resulting in slightly different gross efficiency (0.1% GTE). For each condition, the measured results are presented in black and the simulation results are presented in magenta.

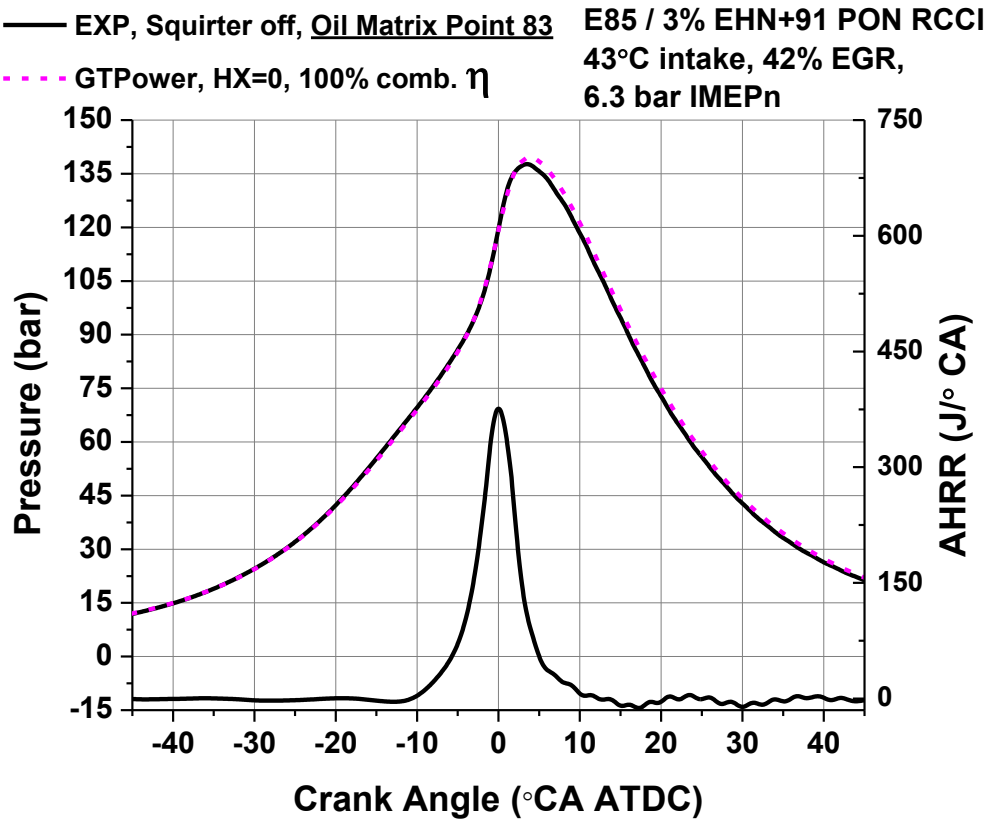

Figure 99 Experimental operation without piston oil gallery cooling (black) and GT Power simulation of matched initial condition operation with 100% combustion efficiency and adiabatic operation (dashed magenta). The results demonstrate that very lean RCCI operation without piston oil cooling is nearly adiabatic

Table 44 Operating and efficiency parameters from the experiment without piston oil cooling and GT Power with adiabatic 100% combustion efficiency operation assumed.

	GTE (%)	IMEPg (bar)	NTE (%)	IMEPn (bar)	BTE (%)	BMEP (bar)
EXP (pt. 83)	59.1	6.82	55.0	6.27	43.7	5.11
GT Power HX =0 100% comb. η	62.4	7.12	58.5	6.85	48.6	5.55

Based on the values in Table 46, when RCCI was operated without oil cooling, the measurements yielded ~95% of the maximum cycle gross efficiency predicted by GT Power (adiabatic, and 100% combustion efficiency). However, the measured (correlated) brake efficiency is predicted to be only 90% of the

simulated maximum predicted by GT Power (FMEP is equal for both due to equal peak pressure (PP) and FMEP correlation). Thus, the discrepancy is not from a difference in friction, but results from the fact that under adiabatic operation the expansion pressure increases disproportionally more than peak pressures, enabling additional brake work to be extracted. This also suggests that to achieve adiabatic operation the liner material and temperature may play an important role. The simulations suggest that from cylinder pressure alone, reduced engine heat loss improves brake efficiency more than gross efficiency. Similar findings were presented by Takahashi et al. [145], where it was shown through CFD and single cylinder experiments that piston liner temperature and material are important factors in determining engine heat loss, and for increasing engine efficiency.

Although the simulations suggest that brake efficiency increases with adiabatic operation, it should be noted that the possibility of additional brake efficiency benefits with LHR are ambiguous. In the measurements there were increased exhaust temperatures, which would be expected to reduce PMEP. However, as demonstrated in Figure 93 of Chapter 5, when the engine rejects less heat, the VE typically decreases, reducing airflow. Thus, even with higher exhaust temperatures there is uncertainty in predicting exhaust losses, as there is the potential that with LHR they may actually decrease. These counterintuitive relations result in brake efficiency estimates being somewhat suspect when using a cycle simulation tool such as GT Power. However, regardless of the relative

estimated improvement, the experiments showed an improvement in all metrics of efficiency with the piston oil cooling jet off, as seen in Figure 99 and Table 44.

When comparing the maximum cycle efficiency results to operation with oil cooling, a larger difference in performance was observed. This supports the previous conclusion that there is reduced heat transfer without piston oil cooling. When operated adiabatically, there is notably higher expansion pressure, and thus performance. Figure 100 and Table 45 demonstrate the observed trends.

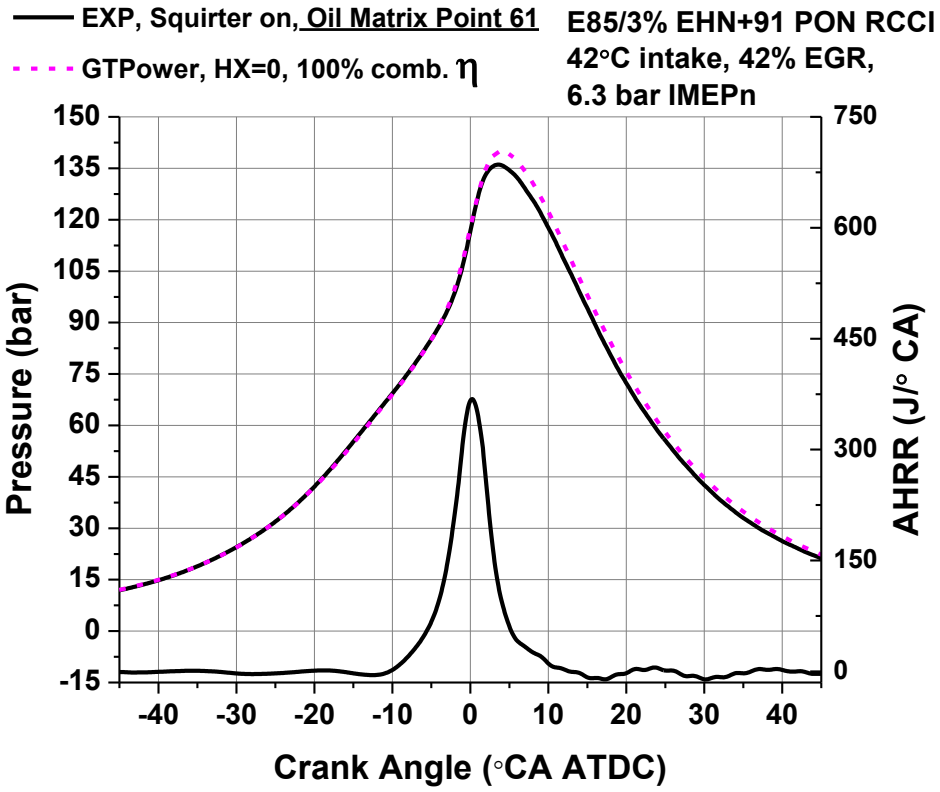

Figure 100 Experimental operation with piston oil gallery cooling (black) and GT Power simulation of matched initial condition operation with 100% combustion efficiency and adiabatic operation (dashed magenta). The results demonstrate that very lean RCCI operation with piston oil cooling is not quite as close to adiabatic as operation without piston oil gallery cooling. This is seen by the increased difference in expansion pressure of the above case.

Table 45 Key operating and efficiency parameters from the experiment with piston oil cooling and GT Power with adiabatic 100% combustion efficiency operation assumed.

	GTE (%)	IMEPg (bar)	NTE (%)	IMEPn (bar)	BTE (%)	BMEP (bar)
EXP (pt. 61)	57.2	6.78	53.0	6.29	42.2	5.06
GT Power HX =0 100% comb. η	62.3	7.37	58.5	6.92	49.0	5.79

Using a similar relative analysis to that of operation with piston oil jet cooling, RCCI with piston oil cooling achieved 92% of cycle maximum predicted by GT Power. Therefore, it is concluded that at a relatively low load, RCCI operation without piston oil cooling offers a potential additional 2% improvement in efficiency (or ~3% relative to the cycle maximum).

The present modeled cases were simulated with 43% EGR. The experiments demonstrated that operation with EGR reduced incomplete combustion by ~50% (increased combustion efficiency). Based on the simulation guidance in Chapter 3, a simultaneous 50% reduction in heat transfer and incomplete combustion was required to achieve 60% GTE. However, in those simulations it was assumed that air would be the only diluent. To reduce the onset of knock (i.e., pressure oscillations) and increase combustion efficiency, EGR was used. This not only affects the combustion event, but also the cycle thermodynamics. Specifically EGR reduces the ratio of specific heats (γ). Thus, it is of merit to investigate the thermodynamic penalty of operating with EGR, as a means to verify if the decrease in incomplete combustion with EGR offsets the expansion pressure penalty of its usage.

6.3 Cylinder Gas Composition Effects on Efficiency

If it can be assumed that EGR is not required to increase combustion efficiency and prevent knocking, the ratio of specific heats (γ_u/γ_b) would be more favorable for increasing efficiency. As mentioned in Chapter 2, comprehensive computational study of this was performed by Lavoie et al. [58]. Again, the assumption that EGR is not required is only valid if the same heat release behavior can be achieved with it. This may require changes to temperature, fuel properties/chemistry, or other operational conditions, as demonstrated in Chapter 5. However, under the assumption that these conditions could be achieved, the following results were predicted by GT Power to demonstrate the calculated improvement in efficiency as compared to experimental results (using EGR).

Predictions without piston oil cooling were made, as they achieved the highest measured and simulated efficiencies. The GT Power results of matched operation, but without EGR are presented the Figure 101 and Table 46.

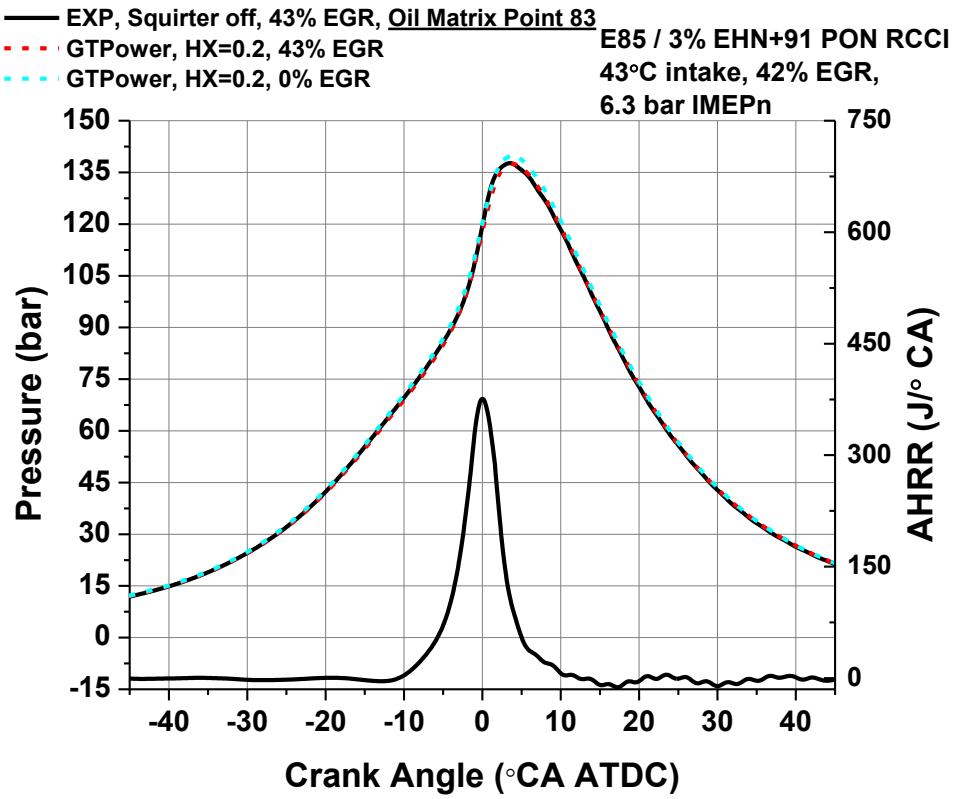

Figure 101 Experimental operation without piston oil gallery cooling (black) and GT Power simulation of matched initial conditions, combustion efficiency, and expansion pressure (red), and GT Power simulations with 0% EGR assumed with matched conditions (cyan). The results demonstrate that if 0% EGR could be used with matched AHRR and combustion efficiency, greater expansion work and thus efficiency could be realized.

Table 46 Operating and efficiency parameters from the experiment and GT Power simulations. GT Power simulations with air demonstrates higher efficiency potential than with EGR (assuming that matched combustion efficiency and AHRR are possible)

	GTE	IMEPg	NTE	IMEPn	BTE	BMEP
	(%)	(bar)	(%)	(bar)	(%)	(bar)
EXP (pt. 83)	59.1	6.82	55.0	6.27	43.7	5.11
GT Power HX =0.2	58.8	6.79	54.9	6.25	45.0	5.14
GT Power HX =0.2 0% EGR	59.3	6.76	55.3	6.31	45.5	5.18

These results assume that similar heat losses exist to those of the experimental cases with EGR. However, operation without EGR may change the heat transfer of the engine, as the specific heat of EGR gases is higher than air.

In practice this tends to reduce in-cylinder temperatures, potentially reducing heat transfer. In the table it is seen that using EGR reduces the theoretical efficiency by ~0.5%. Therefore, if the combustion efficiency is not increased by at least 1% point (assuming 50% GTE) or the heat transfer is not reduced to impact GTE by 0.5%, there is no efficiency-based reason to use EGR. In the experiments the combustion efficiency without EGR was ~95-96%, and with EGR it was ~97-98%, which indicates that even though EGR reduces the thermodynamic efficiency limit of the cycle, it offers greater combustion efficiency benefits, netting higher cycle efficiency.

In the limit of adiabatic 100% combustion efficiency operation, the combustion product (i.e., unburned fuel) recycling benefits of EGR are not realized. Thus, only the thermodynamic benefits of the more favorable gamma ratio of air are observed. In this configuration the cycle pressure and performance are seen in Figure 102 and Table 47.

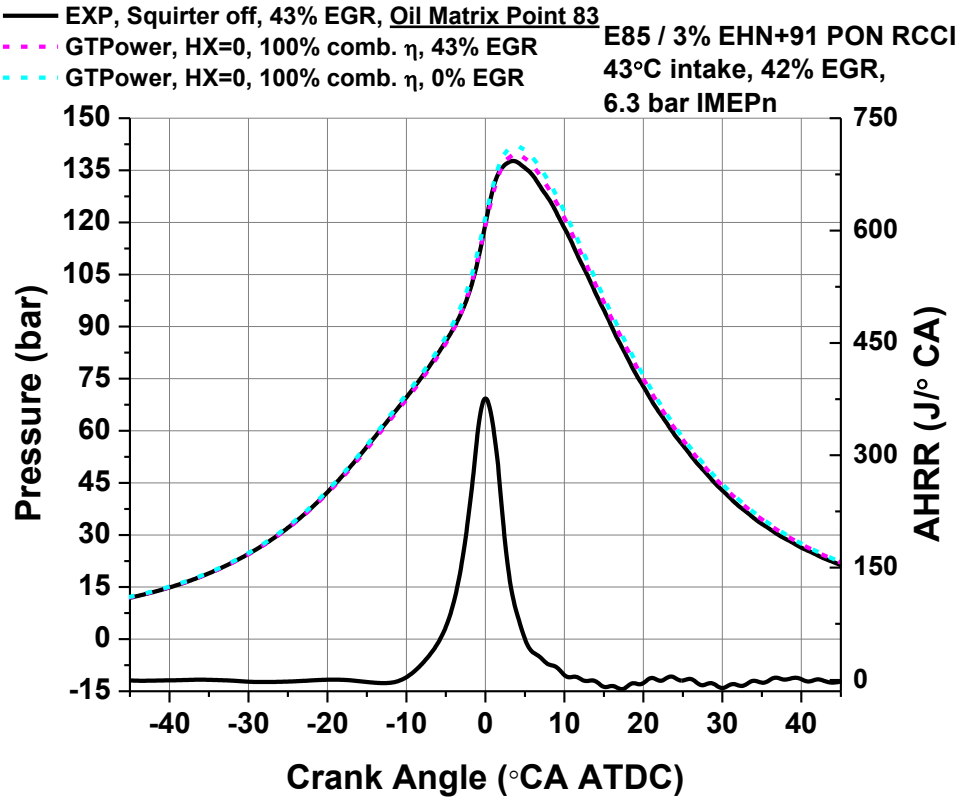

Figure 102 Experimental operation without piston oil gallery cooling (black) and GT Power simulation of matched initial conditions, but with 100% combustion efficiency and adiabatic operation (magenta), and GT Power simulations with 0% EGR and assumed adiabatic 100% combustion efficiency operation (cyan). The results demonstrate that if 0% EGR and no losses even greater expansion work and thus efficiency could be realized.

Table 47 Operating and efficiency parameters from the experiment and adiabatic 100% combustion efficiency GT Power simulations. GT Power simulations with air demonstrates higher efficiency potential than with EGR.

	GTE	IMEPg	NTE	IMEPn	BTE	BMEP
	(%)	(bar)	(%)	(bar)	(%)	(bar)
EXP (pt. 83)	59.1	6.82	55.0	6.27	43.7	5.11
GT Power HX =0 100% comb. η	62.4	7.12	58.5	6.67	48.6	5.55
GT Power HX =0 100% comb. η 0% EGR	63.1	7.19	59.1	6.75	49.2	5.61

6.4 Combustion Duration Effects on Efficiency

The effects of combustion duration can be examined by assuming instantaneous TDC combustion (0.1°CA combustion duration). When operated with air this is the assumption made in Otto cycle (air standard) analysis. This combustion profile was simulated in GT Power using the same initial conditions as for the previous simulations of oil Matrix point 83 (i.e., no piston oil cooling, 43% EGR, 42°C intake pressure), except 0% EGR was used for the Otto cycle operation. The results are shown in Figure 103, where the Otto cycle results are indicated in orange.

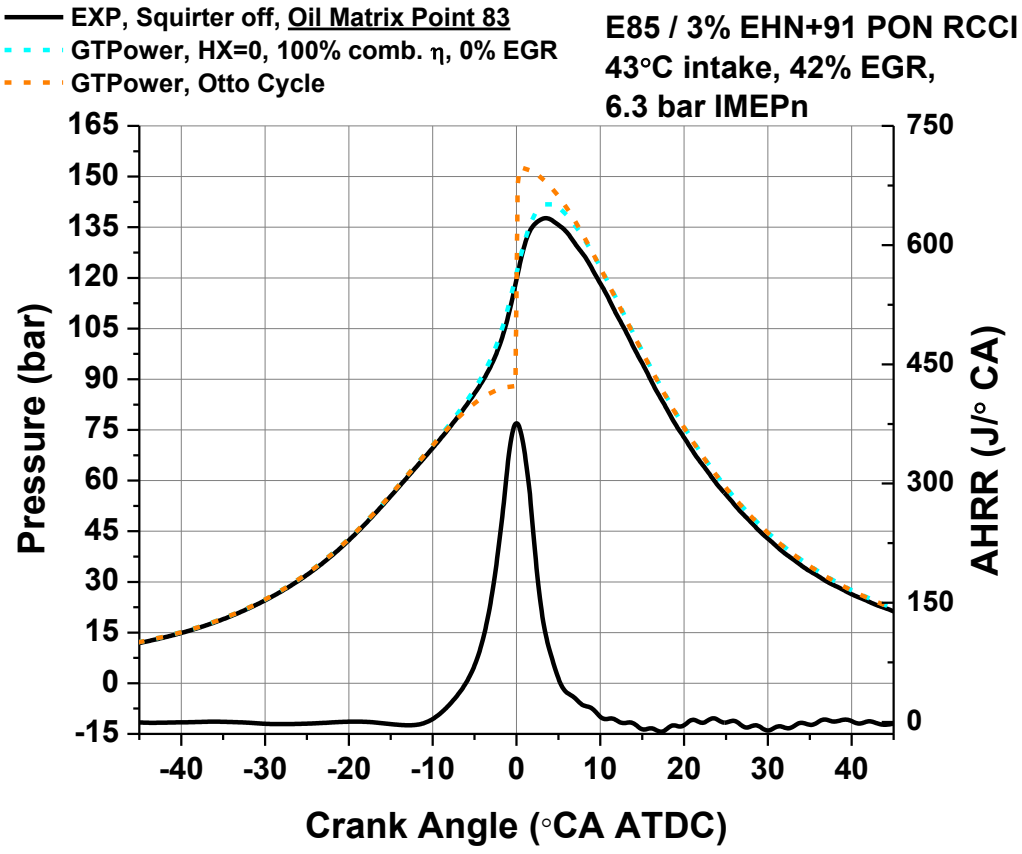

Figure 103 Experimental operation without piston oil gallery cooling (black), GT Power simulations with 0% EGR and assumed adiabatic 100% combustion efficiency operation (cyan), and GT Power simulation of the Otto cycle (air standard) (orange). The results demonstrate that if 0% EGR and no losses even greater expansion work and thus efficiency could be realized.

Table 48 Operating and efficiency parameters from the experiment, adiabatic 100% combustion efficiency GT Power simulations with air, and GT Power Otto cycle (air standard) simulation.

	GTE (%)	IMEPg (bar)	NTE (%)	IMEPn (bar)	BTE (%)	BMEP (bar)
EXP (pt. 83)	59.1	6.82	55.0	6.27	43.7	5.11
GT Power HX =0 100% comb. η 0% EGR	63.1	7.19	59.1	6.75	49.2	5.61
GT Power Otto Cycle	63.2	7.21	59.3	6.77	49.0	5.58

From these results it is seen that in the limit of adiabatic, 100% combustion efficiency operation, using fresh air raises the maximum theoretical cycle efficiency by ~0.7% absolute percentage points (~1% relative), and an additional 0.1% if the Otto cycle is assumed. These results suggest that the maximum gross efficiency potential is approximately 63%. The present RCCI experiments using EGR described in Chapter 5have demonstrated that engine operation can be realized within 94% of this limit (59.1% GTE).

Overall the GT Power predictions and measurements of efficiencies and MEP are in good agreement. The trends suggest that extremely high gross efficiencies are possible with RCCI, and that with the piston oil cooling jet off, there is reduced engine heat transfer and higher efficiency. In Chapter 3 GT Power was used as a predictive tool for determining a pathway to 60% GTE. The results of the present and previous Chapters confirm that RCCI is an extremely efficient combustion process, whereby with proper geometry and conditions, near maximum theoretical efficiency can be achieved.

6.4 Turbocharger Effects on Efficiencies

Throughout this experimental and simulation campaign the assumption of 65-75% overall turbocharger efficiency was used, based on the findings of Millam [6]. However, other researchers such as Chadwell et al. [16], have suggested that in LTC these turbocharger efficiencies may not be currently practical. The present section explores the affect that turbocharger efficiency has on efficiencies.

In GT Power five cases were simulated. The cases are based on oil matrix point 83 as a base condition (case # 1, Table 49), but all assume 0% EGR. The initial conditions of intake and exhaust surge tank pressure were altered to alter the turbocharger efficiency as calculated from equation 8. Additionally, the maximum cycle efficiency case with air and adiabatic 100% combustion efficiency assumed was added (as shown in Table 47 and Figure 102, Case #5 in Table 49).

Table 49 to GT Power overall turbocharger efficiency simulation input modifications to Table 41 to oil matrix data point 83

CASE#	**1**	**2**	**3**	**4**	**5**
Turbo eff. (%)	73	**57**	**100**	**94**	73
Combustion efficiency (%)	98	98	98	98	**100**
Convection coeff. (-)	0.2	0.2	.2	0.2	**0**
Back pressure (bar)	1.72	**1.92**	**1.52**	1.72	1.72
Intake pressure (bar)	1.58	1.58	1.58	**1.78**	1.58
EGR %	0	0	0	0	0
AHRR (J/°CA)	Exp. Oil pt. 83	Exp. Oil pt. 83	Exp. Oil pt. 83	Exp. Oil pt. 83	Exp. Oil pt. 83

Based on these conditions the GTE and NTE were determined. The simulation results of GTE are shown in Figure 104.

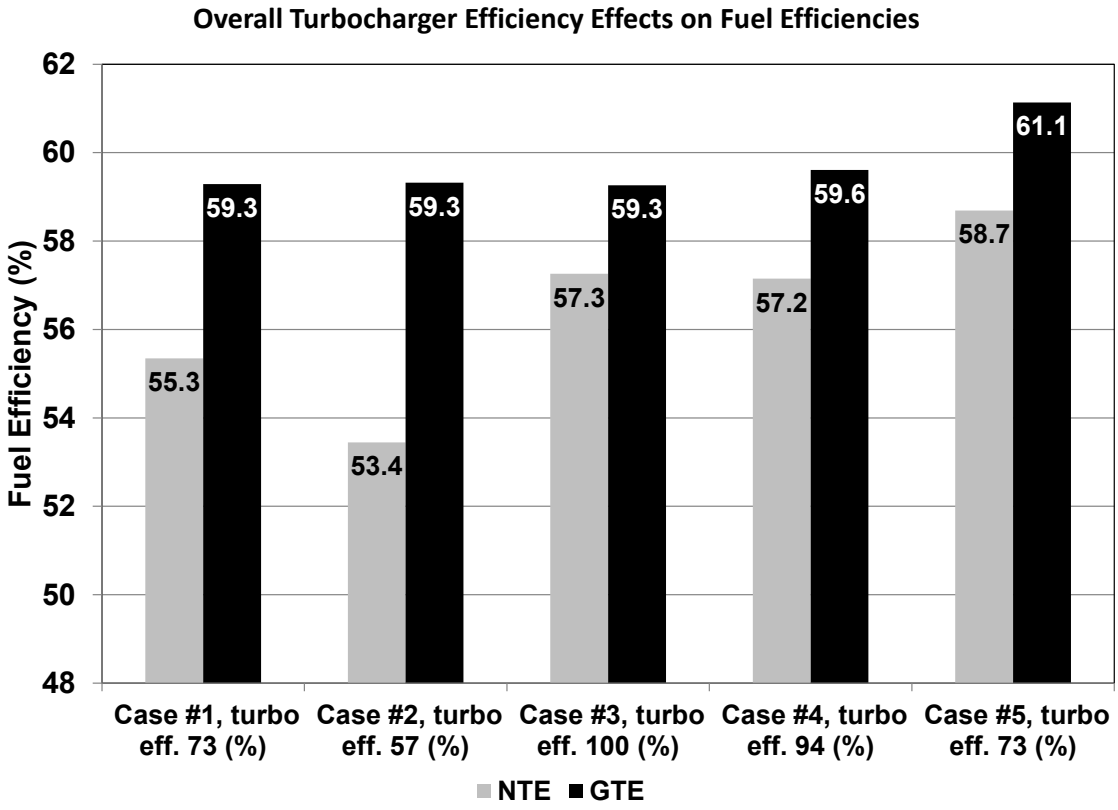

Figure 104 GTE and NTE for cases 1-5 of Table 49

The results show that only NTE is affected by overall turbo charger efficiency, and that GTE is affected by intake pressure (Φ) (case 4) or reductions in losses (HX and combustion eff., case 5). Also, the NTE remains approximately equal in cases 3 and 4 while the GTE does not (case 3 and 4 both assume ~100% overall turbocharger efficiency, case 4 has increased intake pressure). Based on these findings, if higher or lower turbocharger efficiency is assumed to set exhaust

backpressure conditions (as explained in Chapter 4), there is no difference to GTE, but the NTE follows overall turbocharger efficiency.

CHAPTER 7 Conclusions and Suggestions for Future Research

7.1 Study Findings and Conclusions

This research has focused on improving the understanding of sources of engine inefficiency. Experimental measurements coupled with zero-dimensional engine cycle simulations were used. RCCI was used since it offers very high efficiency potential. Initially, cycle simulations were used to explore engine cycle conditions that may increase engine efficiency. The goal was to demonstrate 60% GTE in a typical HD on-road platform engine. The simulations were initially tuned to match existing experimental data. Then the code was used to explore conditions that may offer increased efficiency. The results suggested that to achieve the goal of 60% GTE, lean operation with a high compression ratio was required. Simultaneously, 50% reductions in incomplete combustion and heat transfer were also required.

Based on the simulation results an experimental campaign was conducted to determine the possibility of simultaneously reducing incomplete combustion and heat transfer. The study found that HC emissions were a function of piston crevice and squish geometry, and CO emissions were sensitive to local equivalence ratio. Moreover, CO losses were observed to increase at the lean conditions suggested for high efficiency operation by the simulations. It was found that an optimized injection strategy and intake temperature together with fuel reactivity trimming could be used to reduce CO related efficiency losses.

To determine if simultaneous heat transfer loss reductions were possible, a matrix of conditions with varied Φ (.26-.5) and intake temperatures (32 -66°C) was formulated and tested. The conditions used fixed engine load and speed (1300 rev/min, 8.45 bar IMEPn, CA 50 of 0.5°CA ATDC). It was found that the trapped mass had a dominant effect on heat transfer and incomplete combustion, where for simultaneous reductions, constant PPRR operation through intake pressure and temperature modulation was required. It was found that by maintaining lean conditions with sufficient fully premixed fuel, simultaneous reductions in heat transfer and incomplete combustion could be achieved.

It was found that the use of EGR increases the operable window of RCCI, and was found to offer improved combustion efficiency. Operation with high PPRR was observed to increase heat transfer and incomplete combustion. It was observed that details of the charge preparation strategy were critical for reducing heat transfer losses. Fully premixed HCCI operation was found to be knock limited, reducing efficiency. Through proper charge preparation, RCCI was found to generally offer more advanced high efficiency, knock free, combustion phasing simultaneously and at higher loads.

The combined effects were adopted with an 18.7:1 compression ratio minimized surface are piston design in the experimental tests, as suggested by the initial computational study. Experiments with and without piston oil gallery cooling was conducted, and it was found that the use of piston oil gallery cooling hinders RCCI efficiency. Without cooling, the lean limit could be extended, and the indicated efficiency generally increased at all tested conditions. Gross

efficiencies in excess of 59% were measured, with corresponding near zero levels of NO_X and PM. Finally, the experimental results were simulated in the zero-dimensional code, and were found to represent efficiencies as high as 95% of the theoretical cycle limit that would be reached with adiabatic, 100% combustion efficiency operation (air standard Otto cycle). The results show that with optimized combustion management and thermodynamic conditions, 60% gross engine efficiencies are possible with RCCI, approaching that of “perfect” practical operation.

7.2 Suggestions for Future Research

The present results show that fuel properties, the combustion process, and combustion chamber geometry are critical for achieving high efficiency. Piston oil gallery cooling is not required in RCCI at the high efficiency operation point of the present study. Investigations of modulated piston oil galley cooling on a multi-cylinder engine would thus be of interest. The results in Chapter 6 demonstrates that RCCI without piston oil cooling is nearly adiabatic, therefore additional efficiency gains must be had through incomplete combustion reductions.

HC emissions were found to be relatively constant, and further understanding of HC emissions sources would be beneficial. For instance, piston-to-wall clearances and reduced cylinder head crevices should be investigated. These were found to be sources of increased HC emissions, which hinder the attainment of the maximum possible efficiency. Additionally, speciation of engine-out HC emissions with and without piston oil cooling may lead to

further understanding of HC sources in RCCI, potentially offering pathways for further reductions.

Furthering the understanding of heat transfer process in RCCI would also help determine pathways for further reducing heat transfer losses. Operation with the instrumented piston used in [111] would be of merit. Additionally the optical cylinder head described in [115], may provide additional heat flux measurement locations. For these tests measurements with and without piston oil gallery cooling would be of interest. Likewise with this instrumentation, gasoline PCCI and HCCI would be useful for comparing losses relative to RCCI.

Cetane improvers were found to be advantageous to increase the injection timing window (see Appendix B), and to some extent to improve combustion efficiency. Similar effects may exist with the case of gaseous and other high volatility fuels (either direct injected or port injected). These fuels may expand the high efficiency and high load window of RCCI significantly, offering low losses.

The results from the present study should be continued across a wide range of loads and speeds, where an improved understanding of RCCI efficiency, and potentially more important, control parameters may exist. Furthering this work in those areas will be of merit for the technology and engine efficiency knowledge as a whole.

References

1. Stone, Richard, “Introduction to Internal Combustion Engines” Third Edition, SAE, 1999

2. De Nevers, Noel, “Air Pollution Control Engineering”, McGraw Hill, 2000

3. Kim J., “Reduction in NO_x and CO Emissions in Stoichiometric Diesel Combustion Using a Three-Way Catalyst” J. Eng. Gas Turbines Power Volume 132, Issue 7, 072803

4. Bunker B., “U.S. HDV GHG and Fuel Efficiency Final Rule” 17 annual Directions in Engine-Efficiency and Emissions Research (DEER) conference presentation, presented October 4, 2011, available at http://www1.eere.energy.gov/vehiclesandfuels/resources/proceedings/2011_deer_presentations.html, 2011.

5. Theis, J. R., Ura,J . A., Li, J. J., Surnilla, G. G., Roth, J. M., and Goralski Jr., C. T. “NOx Release Characteristics of Lean NOx Traps During Rich Purges”, SAE Transactions, 2003, vol. 12, no4, pp. 758-775, 2003.

6. Milliam D., “DOE Final Report DE-FC05-00OR22806 Heavy Truck Engine Program Final Report for Caterpillar/DOE Heavy Truck Clean Diesel Cooperative Research Program, DOE contract No. DE-FC05-00OR22806”, Published March 31, 2007, 2007.

7. Johnson T.V., “Diesel Emissions in Review”, SAE International Journal of Engines June 2011 vol. 4 no. 1 143-157, 2011.

8. Johnson, T.V., “Diesel Emission Control in Review” SAE Technical paper 2006-01-003, 2006.

9. Kamimoto T., Yokota H., Kobayashi H., “Effect of high pressure injection on soot formation processes in a rapid compression machine to simulate diesel flames”, SAE Paper 871610, 1987.

10. Kalghatgi, G.T., Risberg, P. and Ångström, H.-E., “Partially Pre-Mixed Auto Ignition of Gasoline to Attain Low Smoke and Low NO_x at High Load in a Compression Ignition Engine and Comparison with a Diesel Fuel”, SAE paper 2007-01-0006, 2007.

11. Hanson, R.M., Splitter, D.A., Reitz, R.D., “Operating a Heavy-Duty Direct-Injection Compression-Ignition Engine with Gasoline for Low Emissions”, SAE paper 2009-01-1442, 2009.

12. Turns, S.R., “An introduction to combustion: Concepts and Applications”, New York, McGraw-Hill inc., 1995.

13. Kamimoto T. and Bae M., "High combustion temperature for the reduction of particulate in diesel engines", SAE Technical Paper 880423, 1988.

14. Sun Y., "Diesel combustion optimization and emissions reduction using adaptive injection strategies (AIS) with improved numerical models", PhD Thesis, University of Wisconsin-Madison, 2007.

15. Hardy, W., “An Experimental Investigation of Advanced Diesel Combustion Strategies for Emissions Reductions in a Heavy-Duty Diesel Engine at High Speed and Medium Load”, M.S. Thesis, University of Wisconsin – Madison, 2005.

16. Chadwell C., Alger T., and Roberts C., “Boosting Simulation of High Efficiency Alternative Combustion Mode Engines”, SAE International Journal of Engines June 2011 vol. 4 no. 1 375-393, 2011

17. Onishi S, Jo S.H., Shoda K., Jo P.D., Kato S.: ”Active Thermo-Atmosphere Combustion (ATAC) – A New Combustion Process for Internal Combustion Engines”, SAE Technical Paper 790501, 1979

18. Najt P.M., Foster D.E., “Compression-ignited homogeneous charge combustion” SAE Technical Paper 830264, 1983

19. Thring, R.H., “Homogeneous Charge Compression Ignition (HCCI) Engines”, SAE Technical Paper 892068, 1989.

20. M. Christensen, A. Hultqvist and B. Johansson, "Demonstrating the multi-fuel capability of a homogeneous charge compression ignition engine with variable compression ratio", SAE Technical Paper 1999-01-3679, 1999.

21. Dec J., Yang Y., “Boosted HCCI for High Power without Engine Knock and with Ultra-Low NOx Emissions - using Conventional Gasoline”, SAE International Journal of Engines August 2010 vol. 3 no. 1 750-767, 2010.

22. Yun H., Wermuth N., Najt P., “High Load HCCI Operation Using Different Valving Strategies in a Naturally-Aspirated Gasoline HCCI Engine”, SAE International Journal of Engines June 2011 vol. 4 no. 1 1190-1201, 2011.

23. Shibata G., Oyama K., Urushihara T., and Nakano T., “Correlation of Low Temperature Heat Release With Fuel Composition and HCCI Engine Combustion”, SAE 2005-01-0138, 2005.

24. Shibata G., and Urushihara T., “Realization of Dual Phase High Temperature Heat Release Combustion of Base Gasoline Blends from Oil Refineries and a Study of HCCI Combustion Processes”, SAE International Journal of Engines October 2009 vol. 2 no. 1 145-163, 2009.

25. Bessonette P.W., Schleyer C.H., Duffy K.P., Hardy W.L., and Liechty M.P., "Effects of fuel property changes on heavy-duty HCCI combustion", SAE Technical Paper 2007-01-0191, 2007.

26. Dec J.E., Hwang W., Sjöberg M., “Potential of thermal stratification and combustion retard for reducing pressure-rise rates in HCCI engines, based on multi-zone modeling and experiments” SAE Technical paper, 2006-01-1518, 2006

27. Sjöberg M., Dec J.E., Cernansky N.P., “Potential of Thermal Stratification and Combustion Retard for Reducing Pressure-Rise Rates in HCCI Engines, Based on Multi-Zone Modeling and Experiments”, SAE 2005-01-0113, 2005.

28. Herold R.E., Krasselt J.M., Foster D.E., Ghandhi J.B., Reuss D.L., Najt P.M., “Investigations into the Effects of Thermal and Compositional Stratification on HCCI Combustion - Part II: Optical Engine Results”, SAE Technical Paper 2009-01-1106, 2009.

29. Kalghatgi G.T., “Auto-Ignition Quality of Practical Fuels and Implications for Fuel Requirements of Future SI and HCCI Engines”, SAE 2005-01-0239, 2005.

30. Kalghatgi G.T., Risberg P., and Ångström H., “Advantages of Fuels with High Resistance to Auto-ignition in Late-injection, Low-Temperature, Compression Ignition Combustion” SAE 2006-01-3385, 2006.

31. Inagaki K., Fuyuto T., Nishikawa K., Nakakita K. and Sakata I., "Dual-fuel PCI combustion controlled by in-cylinder stratification of ignitability", SAE Technical Paper 2006-01-0028, 2006.

32. Kokjohn S.L., Hanson R.M., Splitter D.A., and Reitz R.D., "Experiments and Modeling of Dual-Fuel HCCI and PCCI Combustion Using In-Cylinder Fuel Blending", SAE Technical Paper 2009-01-2647", 2009.

33. Hanson R.M., Splitter D.A., Kokjohn S.L., and Reitz R.D., "An Experimental Investigation of Fuel Reactivity Controlled PCCI Combustion in a Heavy-Duty Engine", SAE Technical Paper 2010-01-0864, 2010.

34. Hanson, R.M., “Experimental Investigation of Fuel Effects on Low Temperature Combustion in a Heavy Duty Compression-Ignition Engine”, M.S. Thesis, University of Wisconsin – Madison, 2009.

35. Kokjohn, S.L., Musculus; M., Splitter, D.A., Reitz R.D., “Investigation of Fuel Reactivity Stratification for Controlling PCI Heat-Release Rates Using High-Speed Chemiluminescence Imaging and Fuel Tracer Fluorescence," SAE Int. J. Engines 5(2):248-269, 2012, doi:10.4271/2012-01-0375.

36. Splitter D.A, Kokjohn S.L., Rein K.D., Hanson R.D., Sanders S.T., Reitz R.D., “An Optical Investigation of Ignition Process in Fuel Reactivity Controlled PCCI Combustion”, SAE International Journal of Engines August 2010 vol. 3 no. 1 142-162, 2010.

37. Splitter D.A, Wissink M.L., Hendricks T.L, Ghandhi J.B., and Reitz R.D., “Comparison of RCCI, HCCI, and CDC Operation from Low to Full Load”, THIESEL 2012 Conference on Thermo- and Fluid Dynamic Processes in Direct Injection Engines, 2012.

38. Splitter D.A., Hanson R.M., Kokjohn S.L., Wissink M.L., and Reitz R.D., “Injection Effects in Low Load RCCI Dual-Fuel Combustion” SAE Technical paper 2011-24-0047, 2011.

39. Splitter, D.A., Hanson, R.M., and Reitz, R.D., “High Efficiency, Low Emissions RCCI Combustion by Use of a Fuel Additive”, SAE International Journal of Fuels and Lubricants December 2010 vol. 3 no. 2 742-756, 2010.

40. Eng J.A., Leppard, W.R., and Sloane, T.M., “The Effect of Di-Tertiary Butyl Peroxide (DTBP) Addition to Gasoline on HCCI Combustion” SAE 2003- 01-3170, 2003.

41. Vandersickel A., Hartmann M., Vogel K., Wright Y.M., Fikri M., Starke R., Schulz C., Boulouchos K., “The autoignition of practical fuels at HCCI conditions: High-pressure shock tube experiments and phenomenological modeling”, Fuel 93 (2012) 492–501, 2012

42. Herzler J., Jerig L., and Roth P., “Shock tube study of the ignition of lean n-heptane/air mixtures at intermediate temperatures and high pressures”, Proceedings of the Combustion Institute, Volume 30, Issue 1, January 2005, Pages 1147-1153, ISSN 1540-7489, 10.1016/j.proci.2004.07.008.

43. Ciezki HK, Adomeit G. Shock-tube investigation of self-ignition of n-heptane air mixtures under engine relevant conditions. Combust Flame 1993;93:421–33

44. Sjöberg, M. and Dec, J., "Smoothing HCCI Heat-Release Rates Using Partion Fuel Stratification with Two-Stage Ignition Feuls," SAE Technical Paper 2006-01-0629, 2006, doi:10.4271/2006-01-0629.

45. Yang, Y., Dec, J., Dronniou, N., Sjöberg, M., "Partial Fuel Stratification to Control HCCI Heat Release Rates: Fuel Composition and Other Factors Affecting Pre-Ignition Reactions of Two-Stage Ignition Feuls,"*SAE Int. J. Engines* 4(1):1903-1920, 2011, doi:10.4271/2011-01-1359.

46. Dec, J.E., Yang, Y., Dronniou, N., “Boosted HCCI - Controlling Pressure-Rise Rates for Performance Improvements using Partial Fuel Stratification with Conventional Gasoline”, SAE International Journal of Engines June 2011 volume 1, pages 1169-1189, 2011

47. Kokjohn, S.L., Reitz, R.D., "Characterization of Dual-Fuel PCCI Combustion in a Light-Duty Engine," presented at 2010 International Multidimensional Engine Modeling User's Group Meeting, https://imem.cray.com/2010/Meeting-2010/7_Kokjohn%20and%20Reitz.pdf, USA, 2010

48. Fikri M., Herzler J., Starke R., Schulz C., Roth P., Kalghatgi G.T., “Autoignition of gasoline surrogates mixturesat intermediate temperatures and high pressures”, Combustion and Flame 152 (2008) 276–281,2008

49. Herzler J., Fikri M., Hitzbleck K., Starkea R., Schulza C., Roth P., Kalghatgi G.T., “Shock-tube study of the autoignition of *n*-heptane/toluene/air mixtures at intermediate temperatures and high pressures” , Combustion and Flame 149 (2007) 25–31, 2007

50. Westbrook C.K., Pitz W.J., Herbinet O., Curran H.J., Silke E.J., A comprehensive detailed chemical kinetic reaction mechanism for combustion of n-alkane hydrocarbons from n-octane to n-hexadecane, Combustion and Flame, Volume 156, Issue 1, January 2009, Pages 181-199, ISSN 0010-2180, 10.1016/j.combustflame.2008.07.014.

51. Sjöberg, M. and Dec, J., "Ethanol Autoignition Characteristics and HCCI Performance for Wide Ranges of Engine Speed, Load and Boost," SAE Int. J. Engines 3(1):84-106, 2010, doi:10.4271/2010-01-0338

52. Mehl, M., Pitz, W., Sarathy, M., Yang, Y. et al., "Detailed Kinetic Modeling of Conventional Gasoline at Highly Boosted Conditions and the Associated Intermediate Temperature Heat Release," SAE Technical Paper 2012-01-1109, 2012, doi:10.4271/2012-01-1109

53. Yates, A., Swarts, A., and Viljoen, C., "Correlating Auto-Ignition Delays And Knock-Limited Spark-Advance Data For Different Types Of Fuel," SAE Technical Paper 2005-01-2083, 2005, doi:10.4271/2005-01-2083.

54. Curran H.J., Dunphy M.P., Simmie J.M., Westbrook C.P, Pitz W.J., “Shock tube ignition of ethanol, isobutene and MTBE: Experiments and modeling”,

Symposium (International) on Combustion Volume 24, Issue 1, 1992, Pages 769–776 Twenty-Fourth Symposium on Combustion, 1992

55. Splitter D.A., Hanson R.M., Kokjohn S.L., and Reitz R.D., “Improving Engine Performance by Optimizing Fuel Reactivity with a Dual Fuel PCCI Strategy”, THIESEL 2010 Conference on Thermo- and Fluid Dynamic Processes in Diesel Engines, 2010

56. Hashimoto, K., "Effect of Ethanol on the HCCI Combustion," SAE Technical Paper 2007-01-2038, 2007, doi:10.4271/2007-01-2038.

57. Hashimoto, K., "Inhibition Effect of Ethanol on Homogeneous Charge Compression Ignition of Heptane," SAE Technical Paper 2008 -01-2504 , 2008, doi:10.4271/2008-01-2504.

58. Lavoie G.A., E. Ortiz-Soto, Babajimopoulos A., Martz J.B., Assanis D.N., “Thermodynamic sweet spot under highly dilute and boosted gasoline engine conditions”, Draft submitted to International Journal of Engine Research, March 2012.

59. Szybist J.P., Youngquist A., Wagner R.M., Moore W., Foster M., and Confer K., “Investigation of Knock limited Compression Ratio of Ethanol Gasoline Blends”, SAE Technical Paper 2010-01-0619, 2010.

60. Foster D.E., “Low Temperature Combustion- A Thermodynamic Pathway to High Efficiency Engines”, National Petroleum Council Fuels Study, prepared March 2012.

61. Sjöberg, M., Dec, J., and Hwang, W., "Thermodynamic and Chemical Effects of EGR and Its Constituents on HCCI Autoignition," SAE Technical Paper 2007 -01-0207, 2007, doi:10.4271/2007-01-0207.

62. Gauthier B.M., Davidson D.F., Hanson R.K., “Shock tube determination of ignition delay times in full-blend and surrogate fuel mixtures”, Combustion and Flame 139 (2004) 300–311, 2004

63. Machrafi H., Cavadias S., “Three-stage autoignition of gasoline in an HCCI engine: An experimental and chemical kinetic modeling Investigation”, Combustion and Flame 155 (2008) 557–570, 2008

64. Heywood, J. B., “Internal Combustion Engine Fundamentals,” McGraw-Hill Inc., 1988

65. Shibata G., Urushihara T., “Auto-Ignition Characteristics of Hydrocarbons and Development of HCCI Fuel Index”, SAE 2007-01-0220, 2007.

66. Kalghatgi G.T., “Auto-Ignition Quality of Practical Fuels and Implications for Fuel Requirements of Future SI and HCCI Engines”, SAE 2005-01-0239, 2005.

67. Higgens B, Siebers D., Mueller C, and Aradil A., “Effects of an Ignition-Enhancing, Diesel-Fuel Additive on Diesel-Spray Evaporation, Mixing, Ignition, and Combustion”, Twenty-Seventh Symposium (International) on Combustion/The Combustion Institute, 1998/pp. 1873–1880.

68. Thompson, A.A., Lambert, S.W., Mulqueen, S.C., “Prediction and precision of cetane number improver response Equations”, SAE 972901, 1997.

69. “Guidance on Quantifying NO_x Benefits for Cetane Improvement Programs for Use in SIPs and Transportation Conformity” EPA420-B-04-005, June 2004.

70. Hartmann M., Tian K., Hofrath C., Fikri M., Schubert A., Schießl R., Starke R., Atakan B., Schulz C., Maas U., Kleine Jäger F., Kühling K., “Experiments and modeling of ignition delay times, flame structure and intermediate species of EHN-doped stoichiometric n-heptane/air combustion”, Proceedings of the Combustion Institute, Volume 32, Issue 1, 2009, Pages 197-204, ISSN 1540-7489, 10.1016/j.proci.2008.06.068.

71. Ickes A.M., Bohac S.V., and Assanis D.N., “Effect of 2-Ethylhexyl Nitrate Cetane Improver on NOx Emissions from Premixed Low-Temperature Diesel Combustion”, Energy Fuels 2009, 23, 4943–4948 : DOI:10.1021/ef900408e

72. Caton J.A, “On the destruction of availability (exergy) due to combustion processes -with specific application to internal-combustion engines”, Energy, Volume 25, Issue 11, November 2000, Pages 1097-1117, 2000.

73. Caton J.A. “A Review of Investigations Using the Second Law of Thermodynamics to Study Internal- Combustion Engines” SAE Transactions 2000, vol. 109, no. 3, pp. 1252-1266, 2000.

74. Rakopoulos C.D., and Giakoumis E.G., “Second-law analyses applied to internal combustion engines operation” Progress in Energy and Combustion Science volume 32, pages 2-47, 2006.

75. Edo, T., and Foster, D.E., VI International Symposium on Alcohol Fuels Technology, Ottawa Canada, 1984

76. Edwards D., “Defining Engine Efficiency Limits”, 17 annual Directions in Engine-Efficiency and Emissions Research (DEER) conference presentation, presented October 5, 2011, available at http://www1.eere.energy.gov/vehiclesandfuels/pdfs/deer_2011/wednesday/presentations/deer11_edwards.pdf, accessed Nov 15, 2011.

77. Primus R.J., Hoag K.L., Flynn P.F., Brands M.C., “An appraisal of advanced engine concepts using second law analysis techniques”, SAE Technical Paper 841287, 1984.

78. Montgomery D, “An Otto Rankine Combined Cycle for High Efficiency. Distributed Power Generation” ERC Symposium presentation, presented June 10, 2009, accessed Oct 29, 2011 http://www.erc.wisc.edu/documents/symp09-Montgomery.pdf.

79. Edwards D.K., Wagner R., and Briggs T., “Investigating potential light-duty efficiency improvements through simulation of turbo-compounding and waste-heat recovery systems”, SAE Technical Paper 2010-01-2209, 2010.

80. Warnatz J., Maas U., Dibble R.W., "Combustion Physical and Chemical Fundamentals, Modeling and Simulation, Experiments, Pollution Formation", 4th edition, Springer Berlin Heidelber, New York, 2006

81. Teh K.Y., Miller S.L., and Edwards C.F. “Thermodynamic requirements for maximum internal combustion engine cycle efficiency. Part 1: Optimal combustion strategy”, International Journal of Engine Research 2008 Volume 9, pages 449-469, 2008.

82. Miller S.L., Svrcek M.N., The K.Y. and Edwards C.F., “Assessing the feasibility of increasing engine efficiency through extreme compression”, International journal of Engine Research 2011 Issue 12, Pages 293-307, 2011

83. Blarigan P.V., Paradiso N., and Goldsborough S., “Homogeneous Charge Compression Ignition with a Free Piston: A New Approach to Ideal Otto Cycle Performance”, SAE Technical paper 982484, 1998.

84. Blarigan P.V., “Free Piston Engine” 2011 DOE Vehicle Technologies Program Annual Merit Review May 10, 2011, accessed Oct 29, 2011, http://www1.eere.energy.gov/vehiclesandfuels/pdfs/merit_review_2011/adv_combustion/ace008_vanblarigan_2011_o.pdf.

85. Burke, R. and Brace, C., "The Effects of Engine Thermal Conditions on Performance, Emissions and Fuel Consumption," SAE Technical Paper 2010-01-0802, 2010, doi:10.4271/2010-01-0802.

86. Carlson, N. Thermal barrier coating on high temperature industrial gas turbine engines. NASA CR-135147, National Aeronautics and Space Administration and Energy Research and Development Administration, Ohio, USA, 1977.

87. Hoag K.L, Brands M.C., and Bryzik W., "Cummins/TACOM Adiabatic Engine Program," SAE 850356, Society of Automotive Engineers, 1985.

88. Yonushonis T.M., "Thick Thermal Barrier Coatings for Diesel Components," NASA CR-187111, National Aeronautics and Space Administration, Aug 1991.

89. Clarke D.R., and Levi, C.G, “Materials Design For The Next Generation Thermal Barrier Coatings”, Annual Review of Materials Research Vol. 33: 383-417, 2003.

90. Yonushonis T.M., “Overview of thermal barrier coatings in diesel engines” Journal of Thermal Spray Technology, 1997, 6(1), 50-56, 1997

91. U.S. Army Tank Automotive Command (TACOM) undercontracts DAAE07-84-C-R082and DAAE07-9l-C-R005 Z. Metall. In press.

92. Ramaswamy P., Seetharamu S., Verma K.B., Raman N., and Rao K.J., “Thermomechanical fatigue characterization of zirconia (8%Y2O3-ZrO2) and mullite thermal barrier coatings on diesel engine components: Effect of coatings on engine performance”, Proceedings of the Institution of Mechanical Engineers, Part C: Journal of Mechanical Engineering Science May 1, 2000 vol. 214 no. 5 729-742, 2000.

93. Hultqvist, A., Christensen, M., and Johansson, B., “The Application of Ceramic and Catalytic Coatings to Reduce the Unburned Hydrocarbon Emissions from a Homogeneous Charge Compression Ignition Engine”, SAE 2000-01-1833, 2000

94. Güralp O., Hoffman M., Assanis D., Filipi Z., Kuo T.W., Najt P., and Rask R., “Characterizing the Effect of Combustion Chamber Deposits on a Gasoline HCCI Engine”, SAE Technical paper 2006-01-3277, 2006

95. Güralp O., Hoffman M., Assanis D., Filipi Z., Kuo T.W., Najt P., and Rask R., “Thermal Characterization of Combustion Chamber Deposits on the HCCI Engine Piston and Cylinder Head Using Instantaneous Temperature Measurements“ SAE Technical Paper, 2009-01-06688, 2009.

96. Hopwood, A.B., Chynoweth, S., Kalghatgi, G.T., “A Technique to Measure Thermal Diffusivity and Thickness of Combustion Chamber Deposits In-Situ”, SAE Paper 982590, 1998.

97. Kajiwara, H., Fujioka, Y., and Negishi, H., "Prediction of Temperatures on Pistons with Cooling Gallery in Diesel Engines using CFD Tool," SAE Technical Paper 2003-01-0986, 2003, doi:10.4271/2003-01-0986.

98. Luff, D., Law, T., Shayler, P. and Pegg, I., “The Effect of Piston Cooling Jets on Diesel Engine Piston Temperatures, Emissions and Fuel Consumption,” SAE Int. J. Engines 5(3):2012, doi:10.4271/2012-01-1212.

99. Lyforde-Pike, E. J. and Heywood, J. B., “Thermal boundary layer thickness in the cylinder of a spark-ignition engine”, Int. J. Heat Mass Transfer 27, 1873-1878, 1984

100. Dec, J.E., Hwang, W., “Characterizing the Development of Thermal Stratification in an HCCI Engine Using Planar-Imaging Thermometry”, SAE International Journal of Engines October 2009 vol. 2 no. 1 421-438, 2009.

101. Lu, J.-H., Ezekoye, D., Iiyama, A., Greif, R. and Sawyer, R. F., “Effect of Knock on Time-Resolved Engine Heat Transfer”, SAE paper 890158, 1989.

102. Syrimis, M., Shigahara, K. and Assanis, D., “Correlation between knock intensity and heat transfer under light and heavy knocking conditions in a spark ignition engine”, SAE paper 960495, 1996.

103. Grandin, B., Denbratt, I., Bood, J., Brackmann, C. et al., "The Effect of Knock on the Heat Transfer in an SI Engine: Thermal Boundary Layer Investigation using CARS Temperature Measurements and Heat Flux Measurements," SAE Technical Paper 2000-01-2831 2000, doi:10.4271/2000-01-2831.

104. Grandin, B. and Denbratt, I., "The Effect of Knock on Heat Transfer in SI Engines," SAE Technical Paper 2002-01-0238 , 2002, doi:10.4271/2002-01-0238.

105. Patterson, M. and Hampson, G., "Heat Release Design Method for HCCI in Diesel Engines with Simulation," SAE Technical Paper 2008-28-0006, 2008, doi:10.4271/2008-28-0006.

106. Herold R.E., Wahl M.H., Regner G., Lemke J.U., and Foster D.E., “Thermodynamic Benefits of Opposed-Piston Two-Stroke Engines” SAE Technical Paper 2011-01-2216, 2011.

107. Caton J.A., “The thermodynamic characteristics of high efficiency, internal-combustion engines”, Energy Conversion and Management Volume 58, June 2012, Pages 84–93, 2012

108. Mamalis, S., Nair, V., Andruskiewicz, P., Assanis, D. et al., "Comparison of Different Boosting Strategies for Homogeneous Charge Compression Ignition Engines - A Modeling Study," *SAE Int. J. Engines*3(1):296-308, 2010, doi:10.4271/2010-01-0571.

109. George, S., Morris, G., Dixon, J., Pearce, D. et al., "Optimal Boost Control for an Electrical Supercharging Application," SAE Technical Paper 2004-01-0523, 2004, doi:10.4271/2004-01-0523.

110. Kokjohn, S.L., Hanson, R.M., Splitter, D.A., and Reitz, R.D., “Fuel reactivity controlled compression ignition (RCCI): a pathway to controlled high-efficiency clean combustion”, International Journal of Engine Research June 2011 vol. 12 no. 3209-226, 2011.

111. Hendricks T.L., “Instantaneous Heat Flux Measurements in Internal Combustion Engines”, PhD. Thesis, University of Wisconsin – Madison, 2011.

112. Splitter D.A., Kokjohn S.L., Wissink M.L., and Reitz R.D. “Effect of Compression Ratio and Piston Geometry on RCCI Load Limits and Efficiency” SAE Technical Paper 2012-01-0383, 2012, doi:10.4271/2012-01-0383.

113. Gehrke C. Caterpillar Engine Research, Private Communication, April 2011.

114. Wissink, M.L., Lim, J.H., Splitter, D.A.,, Hanson, R.M., and Reitz, R.D., Investigation of injection strategies to improve high efficiency RCCI combustion with diesel and gasoline direct injection, Paper ICEF2012-92107, Proceedings of ASME Internal Combustion Engine Division Fall Technical Conference, Vancouver, BC, Canada, September 23, 2012 - September 26, 2012

115. Splitter D.A. “Experimental Investigation of Fuel Reactivity Controlled Combustion in a Heavy-Duty Internal Combustion Engine”, M.S. Thesis, University of Wisconsin-Madison 2010.

116. Oxley J.C., Smith J.L., Rogers E., Ye W., Aradi A.A, and Henly T.J., “Heat-Release Behavior of Fuel Combustion Additives”, Energy & Fuels 2001, 15, 1194-1199, 2001.

117. DelVescovo D., Private Communication, University of Wisconsin, Madison 2012.

118. Tess M., “Diesel Engine Size Scaling at Medium Load Without EGR” M.S. Thesis, University of Wisconsin 2010

119. Kar, K. Cheng, W.K., “Speciated Engine-Out Organic Gas Emissions from a PFI-SI Engine Operating on Ethanol/Gasoline Mixtures”, SAE International Journal of Fuels and Lubricants March 2010 vol. 2 no. 2 91-101, 2009.

120. Sung K., Private Communication, University of Wisconsin, Madison 2011

121.Eng J.A., "Characterization of pressure waves in HCCI combustion", SAE Technical Paper 2002-01-2859, 2002

122.Wissink M.L. Private Communication, University of Wisconsin, Madison 2011.

123.Gamma Technologies GTPower Suite 4 user's manual, accessed May 1, 2012.

124.Hanson, R., Curran, S., Wagner, R., Kokjohn, S. et al., "Piston Bowl Optimization for RCCI Combustion in a Light-Duty Multi-Cylinder Engine," SAE Int. J. Engines 5(2):286-299, 2012, doi:10.4271/2012-01-0380.

125.Donaldson G.., Private Communication, University of Wisconsin, Madison 2010

126.F-chart Software Engineerign Equaiton Solver (EES) 4 user's manual, accessed Sept 14, 2010.

127.ETAS Lambda Meter LA4 User's Guide, accessed Sept 14, 2010

128.Buglass, J., Morgan, T., and Graupner, J., "Interactions Between Exhaust Gas Composition and Oxygen Sensor Performance," SAE Technical Paper 982646, 1998, doi:10.4271/982646.

129.Regitz, S. and Collings, N., "Study of Cycle-By-Cycle Air-to-Fuel Ratio Determined from the Exhaust Gas Composition and a Novel Fast Response Device Based on a Wide Band Lambda Sensor," SAE Technical Paper 2008-012439, 2008, doi:10.4271/2008-01-2439.

130.Alkidas A.C., "Combustion-chamber crevices: the major source of engine-out hydrocarbon emissions under fully warmed conditions", Progress in Energy and Combustion Science 25 (1999) 253–273, 1999.

131.Salazar, V.M., and Ghandhi, J.B., "Ring Pack Crevice Effects on the Hydrocarbon Emissions from an Air-Cooled Utility Engine", SAE International Journal of Engines April 2009 vol. 1no. 1 1319-1331

132.Vera, H., and Ghandhi, J.B., "Investigation of Post-Flame Oxidation of Unburned Hydrocarbons in Small Engines", SAE International Journal of Engines June 2011 vol. 4no. 1 67-81, 2011.

133.Prikhodko V.Y., Curran S.J., Barone T.L., Lewis S.A., Storey J.M., Cho K., Wagner R.M., and Parks J.E., "Emission Characteristics of a Diesel Engine Operating with In-Cylinder Gasoline and Diesel Fuel Blending", SAE

International Journal of Fuels and Lubricants December 2010 vol. 3 no. 2 946-955, 2010.

134. Splitter, D., Hanson, R., Kokjohn, S., and Reitz, R., "Reactivity Controlled Compression Ignition (RCCI) Heavy-Duty Engine Operation at Mid-and High-Loads with Conventional and Alternative Fuels," SAE Technical Paper 2011-01-0363, 2011, doi:10.4271/2011-01-0363.

135. Curran, S., Prikhodko, V., Cho, K., Sluder, C. et al., "In-Cylinder Fuel Blending of Gasoline/Diesel for Improved Efficiency and Lowest Possible Emissions on a Multi-Cylinder Light-Duty Diesel Engine," SAE Technical Paper 2010-01-2206, 2010, doi:10.4271/2010-01-2206.

136. Hanson, R.M., Kokjohn, S.L., Splitter D.A., and Reitz, R.D., “Fuel Effects on Reactivity Controlled Compression Ignition (RCCI) Combustion at Low Load”, SAE International Journal of Engines June 2011 vol. 4no. 1 394-411, 2011.

137. Ekoto I.W., Colban W.F. Miles P.C., Park S.W., Foster D.E., Reitz R.D., Aronsson U., and Andersson Ö., “UHC and CO Emissions Sources from a Light-Duty Diesel Engine Undergoing Dilution-Controlled Low-Temperature Combustion”, SAE International Journal of Engines March 2010 vol. 2no. 2 411-430, 2009.

138. Bacha J.D, and Lesnini D.G., “Diesel Fuel Thermal Stability at 300°F”, 6th international conference on Stability and Handling of liquid fuels October 13-17, 1997

139. Rothamer D.A., Murphy L, “Systematic study of ignition delay for jet fuels and diesel fuel in a heavy-duty diesel engine”, Proceedings of the Combustion Institute, Available online 4 August 2012, ISSN 1540-7489, 10.1016/j.proci.2012.06.085.

140. Labaza M.L., “Demonstration of Reactivity Controlled Compression Ignition (RCCI) Combustion in a Two-Stroke Cycle Engine” M.S. Thesis, University of Wisconsin – Madison, 2012

141. Eyidogan M., Ozsezen A.N., Canakci M., Turkcan A., “Impact of alcohol–gasoline fuel blends on the performance and combustion characteristics of an SI engine”, Fuel, Volume 89, Issue 10, October 2010, Pages 2713-2720, ISSN 0016-2361, 10.1016/j.fuel.2010.01.032.

142. Sjöberg, M. and Dec, J., "EGR and Intake Boost for Managing HCCI Low-Temperature Heat Release over Wide Ranges of Engine Speed," SAE Technical Paper 2007-01-0051, 2007, doi:10.4271/2007-01-0051

143.Splitter D.A. “Effect of Compression Ratio and Piston Geometry on RCCI Load Limit”, 17 annual Directions in Engine-Efficiency and Emissions Research (DEER) conference presentation, presented October 5, 2011, available at http://www1.eere.energy.gov/vehiclesandfuels/pdfs/deer_2011/wednesday/presentations/deer11_splitter.pdf, accessed Nov 15, 2011

144.Kaddatz, J., Andrie, M., Reitz, R., and Kokjohn, S., "Light-Duty Reactivity Controlled Compression Ignition Combustion Using a Cetane Improver," SAE Technical Paper 2012-01-1110, 2012, doi:10.4271/2012-01-1110.

145.Takahashi, D., Nakata, K., and Yoshihara, Y., "Engine Thermal Control for Improving the Engine Thermal Efficiency and Anti-Knocking Quality," SAE Technical Paper 2012-01-0377, 2012, doi:10.4271/2012-01-0377.

146.Benajes J., García-Oliver J.M., Ricardo Novella R., Kolodziej C., “Increased particle emissions from early fuel injection timing Diesel low-temperature combustion”, Fuel 94 (2012) 184–190, 2012

Appendix A, Data

Φ-T Matrix Conditions

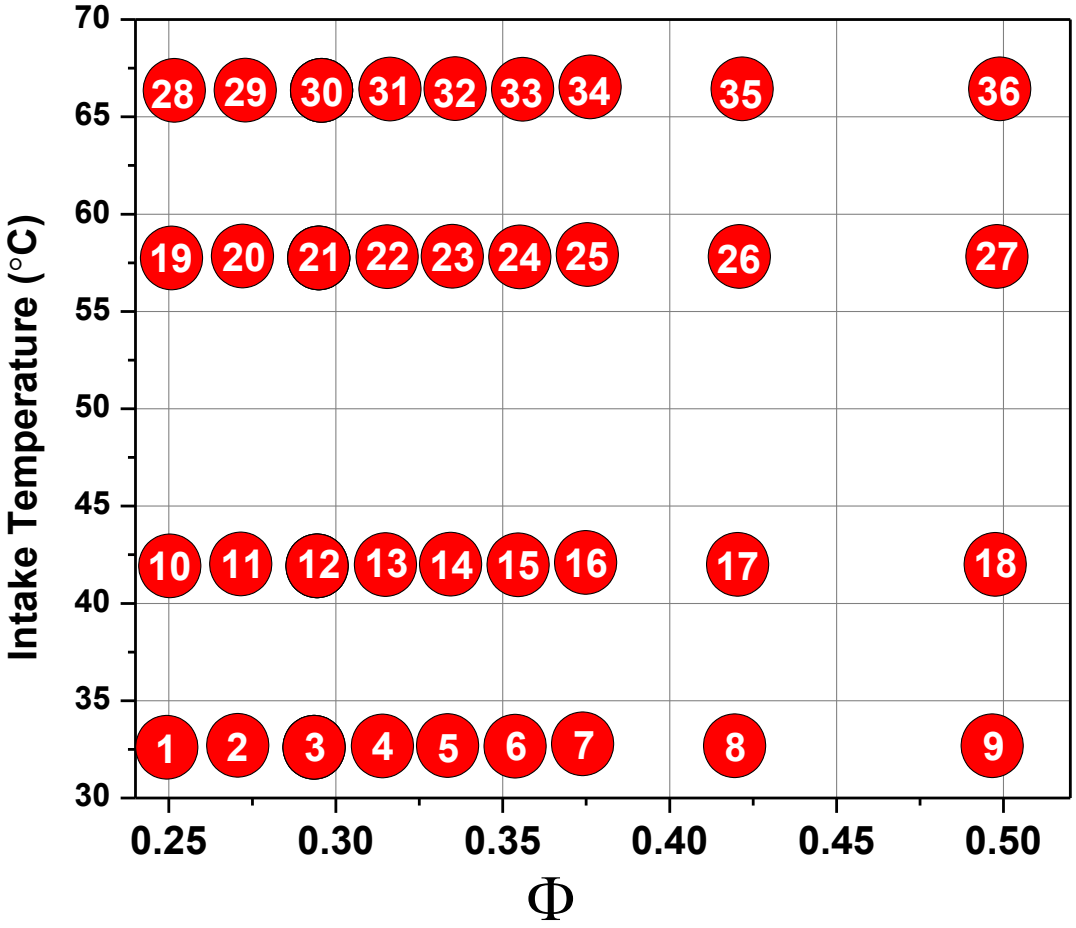

Figure A. 1 Φ-T test matrix conditions

Table A. 1 ULSD / DI E85 PFI, Φ-T Matrix result

MATRIX POINT	1	2	3	4	5	6	7	8	9
RPM	No Data	No Data	1300	1300	1300	No Data	1300	1300	1300
IMEPg (bar)	----------	----------	9.07932	8.95696	8.97432	----------	8.91841	8.82676	8.88272
IMEPn (bar)	----------	----------	8.50293	8.433	8.46719	----------	8.48247	8.46311	8.51267
BMEP_CF (bar)	----------	----------	7.30319	7.27541	7.32582	----------	7.38008	7.37325	7.43831
FMEP_CF (bar)	----------	----------	1.19974	1.15759	1.14136	----------	1.10239	1.08986	1.07436
CA50 (ATDC)	----------	----------	-0.37221	0.01941	0.18943	----------	0.68337	0.20834	0.58446
COV of IMEPg	----------	----------	2.49917	2.52835	2.61086	----------	2.05248	2.08657	1.81682
COV of PPRR	----------	----------	5.88297	6.9565	7.59538	----------	10.42	7.57542	6.86163
EGR %	----------	----------	0	0	0	----------	0	0	0
Fuel 1	----------	----------	E85	E85	E85	----------	E85	E85	E85
Fuel 2	----------	----------	ULSD	ULSD	ULSD	----------	ULSD	ULSD	ULSD
Fuel1 Flow (g/s)	----------	----------	0.97924	0.92694	0.93117	----------	0.92483	0.91914	0.95897
Fuel2 Flow (g/s)	----------	----------	0.41702	0.4205	0.42519	----------	0.43585	0.45212	0.45057
Fuel1 Fraction	----------	----------	0.70133	0.68793	0.68652	----------	0.67969	0.67029	0.68034
Fuel2 Fraction	----------	----------	0.29867	0.31207	0.31348	----------	0.32031	0.32971	0.31966
Fuel Energy (J/cyc)	----------	----------	4300.653	4172.229	4202.158	----------	4226.842	4275.37	4377.52
Fuel H/C	----------	----------	2.37219	2.35714	2.35557	----------	2.34798	2.33761	2.3487
Fuel O/C	----------	----------	0.23882	0.23283	0.2322	----------	0.22918	0.22505	0.22947
Fuel MW/C	----------	----------	18.22223	18.11121	18.09963	----------	18.0436	17.9672	18.049
RI (MW/m^2)	----------	----------	0.95457	1.03143	1.17546	----------	1.96714	3.76197	6.38909
Peak HRR (J/deg)	----------	----------	295.7225	335.7979	363.4613	----------	455.7228	547.736	672.065
Peak PRR (bar/deg)	----------	----------	5.30263	5.26049	5.49763	----------	6.72501	9.02675	11.3857
PP (bar)	----------	----------	130.8801	122.4507	119.2042	----------	111.4099	108.903	105.804
LPP (ATDC)	----------	----------	4.7	5.3	5.4	----------	4.8	4.6	3.9
P Intake (bar)	----------	----------	1.91701	1.71273	1.6153	----------	1.39817	1.25331	1.14312
P Exhaust (bar)	----------	----------	2.1389	1.8997	1.79325	----------	1.54614	1.35915	1.26438
T Intake (C)	----------	----------	31.93778	35.20813	32.97776	----------	33.47857	34.9145	32.5
T Exhaust Tank (C)	----------	----------	292.6016	305.6414	318.4606	----------	346.1578	361.71	378.932
Gross Therm Eff	----------	----------	0.51531	0.52401	0.52128	----------	0.51501	0.50393	0.49529
Net Therm Eff	----------	----------	0.48259	0.49336	0.49182	----------	0.48984	0.48317	0.47466
Brake Therm Eff (CF)	----------	----------	0.4145	0.42563	0.42553	----------	0.42618	0.42095	0.41475
Turbo Eff	----------	----------	0.6608	0.6408	0.62258	----------	0.60525	0.71592	0.77903
Vol Eff	----------	----------	0.93856	0.94241	0.93693	----------	0.93096	0.93162	0.9126
comb loss	----------	----------	0.05097	0.03465	0.02943	----------	0.01841	0.0166	0.01518
Comb Eff	----------	----------	0.94903	0.96535	0.97057	----------	0.98159	0.9834	0.98482
Exhaust Loss	----------	----------	0.33097	0.31431	0.31084	----------	0.29046	0.26796	0.24962
Pumping Loss	----------	----------	0.03271	0.03065	0.02946	----------	0.02517	0.02076	0.02063
Heat Transfer Loss	----------	----------	0.10276	0.12703	0.13844	----------	0.17612	0.2115	0.2399
HC (ppm)	----------	----------	540.2619	667.4575	723.9909	----------	702.442	762.083	763.679
NOx (ppm)	----------	----------	85.94303	161.7597	239.2862	----------	591.3412	1027.26	1272.71
CO2ex (ppm)	----------	----------	37512.6	42723.53	45644.14	----------	54539.46	61864.1	71178.5
CO2in (ppm)	----------	----------	293.5982	326.4499	338.1618	----------	348.9748	346.799	342.468
CO (ppm)	----------	----------	3380.276	1941.985	1471.45	----------	705.001	619.687	730.756
PM (mg/m^3)	----------	----------	6.3	10.43	11.32	----------	15.14	18.39	23.23
HC (g/kg-fuel)	----------	----------	13.03146	14.71229	15.12122	----------	12.54536	12.039	10.4992
NOx (g/kg-fuel)	----------	----------	5.23306	9.05602	12.70163	----------	26.92437	41.5475	44.5941
CO2ex (g/kg-fuel)	----------	----------	2185.325	2288.378	2318.038	----------	2375.81	2393.86	2386.12
CO2in (g/kg-fuel)	----------	----------	17.10378	17.48546	17.17355	----------	15.2018	13.4196	11.4806
CO (g/kg-fuel)	----------	----------	125.3293	66.20156	47.5601	----------	19.54575	15.2614	15.5911
PM (g/kg-fuel)	----------	----------	0.12627	0.21285	0.22995	----------	0.30217	0.35962	0.42577
HC (g/ikW-hr)	----------	----------	2.72837	3.01317	3.11141	----------	2.60583	2.54626	2.26821
NOx (g/ikW-hr)	----------	----------	1.09564	1.85473	2.61355	----------	5.59254	8.78736	9.63398
CO2ex (g/ikW-hr)	----------	----------	457.5371	468.6745	476.9702	----------	493.4865	506.305	515.489
CO2in (g/ikW-hr)	----------	----------	3.58098	3.58114	3.53371	----------	3.15761	2.83826	2.48023
CO (g/ikW-hr)	----------	----------	26.23995	13.55851	9.78619	----------	4.0599	3.22781	3.36826
PM (g/ikW-hr)	----------	----------	0.02644	0.04359	0.04732	----------	0.06277	0.07606	0.09198
Air Flow (kg/min)	----------	----------	3.25981	2.89337	2.73268	----------	2.34642	2.09498	1.8866
AFR mass	----------	----------	38.91096	35.78851	33.57849	----------	28.7408	25.463	22.3074
AFR carbon	----------	----------	38.88574	35.88031	34.07785	----------	29.37118	26.1778	22.7739
AFR Average	----------	----------	38.89835	35.83441	33.82817	----------	29.05599	25.8204	22.5406
AFR Stoich	----------	----------	11.1518	11.21432	11.22089	----------	11.25277	11.2966	11.2497
Phi mass	----------	----------	0.2866	0.31335	0.33417	----------	0.39153	0.44365	0.5043
Phi carbon	----------	----------	0.28678	0.31255	0.32927	----------	0.38312	0.43153	0.49397
GTE emisisons based	----------	----------	0.51497	0.52535	0.52903	----------	0.52631	0.51808	0.50565
EXH emissions based	----------	----------	0.33118	0.31351	0.30629	----------	0.28423	0.26065	0.24451
HX emisisons based	----------	----------	0.10288	0.12649	0.13525	----------	0.17106	0.20467	0.23466

Table A. 1 ULSD / DI E85 PFI, Φ-T Matrix result Continued

MATRIX POINT	10	11	12	13	14	15	16	17	18
RPM	No Data	1300	1300	1300	1300	No Data	1300	1300	No Data
IMEPg (bar)	----------	8.99191	9.05039	8.96044	8.98705	----------	8.86241	8.87115	----------
IMEPn (bar)	----------	8.47373	8.48654	8.45887	8.48326	----------	8.40355	8.43063	----------
BMEP_CF (bar)	----------	7.25128	7.28946	7.28778	7.32584	----------	7.27798	7.31874	----------
FMEP_CF (bar)	----------	1.22245	1.19708	1.17109	1.15742	----------	1.12557	1.11189	----------
CA50 (ATDC)	----------	-0.21092	-0.40774	-0.53844	-0.3941	----------	-0.20805	-0.29837	----------
COV of IMEPg	----------	2.44759	2.61388	2.42461	2.19384	----------	2.18176	2.10741	----------
COV of PPRR	----------	6.96445	7.02243	8.39015	8.15837	----------	8.04166	6.75773	----------
EGR %	----------	0	0	0	0	----------	0	0	----------
Fuel 1	----------	E85	E85	E85	E85	----------	E85	E85	----------
Fuel 2	----------	ULSD	ULSD	ULSD	ULSD	----------	ULSD	ULSD	----------
Fuel1 Flow (g/s)	----------	1.03989	1.01889	0.96882	0.96488	----------	0.94712	0.98762	----------
Fuel2 Flow (g/s)	----------	0.35725	0.38086	0.39038	0.39429	----------	0.4075	0.40265	----------
Fuel1 Fraction	----------	0.7443	0.72791	0.71278	0.7099	----------	0.69918	0.71038	----------
Fuel2 Fraction	----------	0.2557	0.27209	0.28722	0.2901	----------	0.30082	0.28962	----------
Fuel Energy (J/cyc)	----------	4230.321	4266.131	4167.522	4172.201	----------	4175.899	4266.85	----------
Fuel H/C	----------	2.42171	2.40258	2.3852	2.38191	----------	2.36976	2.38246	----------
Fuel O/C	----------	0.25853	0.25092	0.244	0.24269	----------	0.23785	0.24291	----------
Fuel MW/C	----------	18.58757	18.44648	18.31821	18.29397	----------	18.20432	18.29801	----------
RI (MW/m^2)	----------	0.97547	1.17977	1.49701	1.98795	----------	2.90679	5.94226	----------
Peak HRR (J/deg)	----------	337.7104	359.323	392.0239	432.9101	----------	491.0013	620.8356	----------
Peak PRR (bar/deg)	----------	5.46436	5.82832	6.36848	7.18919	----------	8.33652	11.53434	----------
PP (bar)	----------	135.4214	130.3479	125.1497	122.416	----------	116.0467	113.3109	----------
LPP (ATDC)	----------	5.2	4.1	4.3	4.5	----------	4.2	3.7	----------
P Intake (bar)	----------	2.03425	1.86842	1.71626	1.62303	----------	1.44372	1.30741	----------
P Exhaust (bar)	----------	2.17736	2.0715	1.87971	1.80481	----------	1.61021	1.46014	----------
T Intake (C)	----------	45.37921	41.58685	44.25308	43.00448	----------	42.94123	43.44683	----------
T Exhaust Tank (C)	----------	294.4131	298.0965	308.1232	320.3456	----------	342.4922	362.4265	----------
Gross Therm Eff	----------	0.51883	0.51782	0.5248	0.52577	----------	0.51802	0.50748	----------
Net Therm Eff	----------	0.48893	0.48556	0.49543	0.4963	----------	0.4912	0.48228	----------
Brake Therm Eff (CF)	----------	0.4184	0.41707	0.42684	0.42858	----------	0.42541	0.41867	----------
Turbo Eff	----------	0.71372	0.66161	0.6573	0.61937	----------	0.5888	0.57581	----------
Vol Eff	----------	0.95779	0.94419	0.9532	0.94496	----------	0.94593	0.93028	----------
comb loss	----------	0.04984	0.03785	0.02774	0.02108	----------	0.0169	0.01558	----------
Comb Eff	----------	0.95016	0.96215	0.97226	0.97892	----------	0.9831	0.98442	----------
Exhaust Loss	----------	0.33473	0.31287	0.30306	0.29922	----------	0.28736	0.26616	----------
Pumping Loss	----------	0.0299	0.03226	0.02938	0.02947	----------	0.02682	0.0252	----------
Heat Transfer Loss	----------	0.0966	0.13146	0.14439	0.15393	----------	0.17772	0.21078	----------
HC (ppm)	----------	624.1037	700.5067	671.3141	615.8786	----------	627.1509	715.0727	----------
NOx (ppm)	----------	11.93016	76.93106	151.7358	234.6863	----------	480.6314	954.3469	----------
CO2ex (ppm)	----------	35436.93	39691.45	43339.05	46695.76	----------	52955.85	61353.68	----------
CO2in (ppm)	----------	350.919	365.0264	361.3132	355.2974	----------	358.4794	359.5833	----------
CO (ppm)	----------	2835.613	1944.184	1259.561	861.3362	----------	621.9946	562.6781	----------
PM (mg/m^3)	----------	4.91	8.72	11.32	11.53	----------	17.07	18	----------
HC (g/kg-fuel)	----------	16.0337	16.53294	14.81762	12.77557	----------	11.56154	11.40759	----------
NOx (g/kg-fuel)	----------	0.75851	4.52776	8.41038	12.24117	----------	22.38923	38.27402	----------
CO2ex (g/kg-fuel)	----------	2155.569	2234.975	2298.267	2330.268	----------	2360.122	2354.138	----------
CO2in (g/kg-fuel)	----------	21.34581	20.55417	19.16041	17.73048	----------	15.97661	13.7972	----------
CO (g/kg-fuel)	----------	109.7778	69.67464	42.51107	27.35665	----------	17.64286	13.74084	----------
PM (g/kg-fuel)	----------	0.1011	0.17096	0.22803	0.22914	----------	0.33779	0.33791	----------
HC (g/ikW-hr)	----------	3.39169	3.48119	3.06005	2.63047	----------	2.40588	2.43393	----------
NOx (g/ikW-hr)	----------	0.16045	0.95337	1.73686	2.52044	----------	4.65906	8.16618	----------
CO2ex (g/ikW-hr)	----------	455.979	470.5989	474.6247	479.7989	----------	491.1265	502.2808	----------
CO2in (g/ikW-hr)	----------	4.51539	4.32791	3.9569	3.65068	----------	3.32463	2.94378	----------
CO (g/ikW-hr)	----------	23.22188	14.67077	8.77914	5.6327	----------	3.67137	2.93176	----------
PM (g/ikW-hr)	----------	0.02139	0.036	0.04709	0.04718	----------	0.07029	0.0721	----------
Air Flow (kg/min)	----------	3.38108	3.09824	2.84894	2.68144	----------	2.38814	2.12347	----------
AFR mass	----------	40.33336	36.89037	34.93399	32.88074	----------	29.38274	25.45635	----------
AFR carbon	----------	40.58116	37.66748	35.55687	33.52658	----------	30.03418	25.95736	----------
AFR Average	----------	40.45726	37.27892	35.24543	33.20366	----------	29.70846	25.70686	----------
AFR Stoich	----------	10.95133	11.0278	11.09836	11.1118	----------	11.16183	11.10956	----------
Phi mass	----------	0.27152	0.29893	0.3177	0.33794	----------	0.37988	0.43642	----------
Phi carbon	----------	0.26986	0.29277	0.31213	0.33143	----------	0.37164	0.42799	----------
GTE emisisons based	----------	0.52202	0.52873	0.53416	0.5361	----------	0.52951	0.51747	----------
EXH emissions based	----------	0.33269	0.30642	0.29775	0.29346	----------	0.28112	0.26102	----------
HX emisisons based	----------	0.09546	0.12701	0.14034	0.14936	----------	0.17247	0.20593	----------

Table A. 1 ULSD / DI E85 PFI, Φ-T Matrix result Continued

MATRIX POINT	19	20	21	22	23	24	25	26	27
RPM	No Data	1301	1300	1300	1300	1300	1300	No Data	No Data
IMEPg (bar)	----------	9.11463	9.09898	9.03123	9.0631	8.98681	9.01711	----------	----------
IMEPn (bar)	----------	8.5032	8.51509	8.48483	8.55883	8.51018	8.5402	----------	----------
BMEP_CF (bar)	----------	7.25313	7.28391	7.27897	7.37004	7.3401	7.3777	----------	----------
FMEP_CF (bar)	----------	1.25006	1.23117	1.20586	1.1888	1.17009	1.1625	----------	----------
CA50 (ATDC)	----------	-0.36413	-0.52053	-0.14958	0.26889	0.12055	-0.10614	----------	----------
COV of IMEPg	----------	2.83228	2.51581	2.47127	2.32615	2.34018	2.3626	----------	----------
COV of PPRR	----------	7.53669	7.23992	7.6578	7.06439	6.66485	6.32832	----------	----------
EGR %	----------	0	0	0	0	0	0	----------	----------
Fuel 1	----------	E85	E85	E85	E85	E85	E85	----------	----------
Fuel 2	----------	ULSD	ULSD	ULSD	ULSD	ULSD	ULSD	----------	----------
Fuel1 Flow (g/s)	----------	1.10574	1.09544	1.07839	1.08556	1.07231	1.08569	----------	----------
Fuel2 Flow (g/s)	----------	0.30726	0.31027	0.31101	0.31415	0.32662	0.32671	----------	----------
Fuel1 Fraction	----------	0.78255	0.77928	0.77615	0.77556	0.76652	0.76868	----------	----------
Fuel2 Fraction	----------	0.21745	0.22072	0.22385	0.22444	0.23348	0.23132	----------	----------
Fuel Energy (J/cyc)	----------	4209.354876	4196.428	4153.058	4184.869	4197.921	4234.629	----------	----------
Fuel H/C	----------	2.46749	2.46351	2.45971	2.459	2.4481	2.4507	----------	----------
Fuel O/C	----------	0.27676	0.27517	0.27366	0.27338	0.26904	0.27007	----------	----------
Fuel MW/C	----------	18.92532	18.89594	18.86798	18.86272	18.78228	18.80146	----------	----------
RI (MW/m^2)	----------	2.00017	2.66666	3.31969	3.84421	4.65471	6.67747	----------	----------
Peak HRR (J/deg)	----------	429.05761	466.5444	510.1599	552.4918	587.529	660.3221	----------	----------
Peak PRR (bar/deg)	----------	7.92208	8.94559	9.71346	10.24463	11.00208	12.93057	----------	----------
PP (bar)	----------	140.90232	137.1667	132.103	128.6915	124.9494	123.4315	----------	----------
LPP (ATDC)	----------	4.4	4	4.1	4.4	4.1	3.3	----------	----------
P Intake (bar)	----------	2.10772	1.97561	1.85547	1.75896	1.64187	1.53913	----------	----------
P Exhaust (bar)	----------	2.32931	2.19256	2.04957	1.9272	1.80017	1.7112	----------	----------
T Intake (C)	----------	56.78599	58.74725	58.79083	58.34914	57.67965	60.80741	----------	----------
T Exhaust Tank (C)	----------	301.32076	305.4481	312.6128	319.3552	328.8953	341.4519	----------	----------
Gross Therm Eff	----------	0.52853	0.52924	0.53079	0.52862	0.52254	0.51975	----------	----------
Net Therm Eff	----------	0.49308	0.49528	0.49868	0.49921	0.49482	0.49227	----------	----------
Brake Therm Eff (CF)	----------	0.42059	0.42367	0.42781	0.42987	0.42679	0.42526	----------	----------
Turbo Eff	----------	0.67492	0.65715	0.64652	0.64367	0.62934	0.59371	----------	----------
Vol Eff	----------	0.95765	0.96039	0.95604	0.9561	0.95294	0.95367	----------	----------
comb loss	----------	0.03434	0.02582	0.02118	0.01919	0.01661	0.01537	----------	----------
Comb Eff	----------	0.96566	0.97418	0.97882	0.98081	0.98339	0.98463	----------	----------
Exhaust Loss	----------	0.33146	0.31355	0.3046	0.29492	0.2846	0.27139	----------	----------
Pumping Loss	----------	0.03546	0.03396	0.03211	0.02941	0.02771	0.02749	----------	----------
Heat Transfer Loss	----------	0.10567	0.13138	0.14343	0.15727	0.17625	0.19349	----------	----------
HC (ppm)	----------	499.36907	566.0583	575.5627	592.1664	572.4085	607.0674	----------	----------
NOx (ppm)	----------	9.0637	25.95257	62.36704	113.5645	200.7649	360.5273	----------	----------
CO2ex (ppm)	----------	36507.47577	39672.13	42363.81	45018.01	48555.39	53282.5	----------	----------
CO2in (ppm)	----------	346.58657	346.021	342.0215	343.172	352.5576	355.0367	----------	----------
CO (ppm)	----------	1801.91613	1083.876	756.8233	638.9142	546.6	494.8877	----------	----------
PM (mg/m^3)	----------	4.3	4	7.24	9.97	11.43	13.98	----------	----------
HC (g/kg-fuel)	----------	12.85979	13.68941	13.1628	12.79472	11.51528	11.15435	----------	----------
NOx (g/kg-fuel)	----------	0.56733	1.52789	3.47731	5.98388	9.89158	16.20734	----------	----------
CO2ex (g/kg-fuel)	----------	2186.26286	2234.558	2259.836	2269.449	2288.806	2291.668	----------	----------
CO2in (g/kg-fuel)	----------	20.75546	19.48985	18.24464	17.29999	16.61887	15.27005	----------	----------
CO (g/kg-fuel)	----------	68.67788	38.85506	25.69437	20.49927	16.39845	13.54676	----------	----------
PM (g/kg-fuel)	----------	0.08466	0.07762	0.14081	0.19251	0.21862	0.25947	----------	----------
HC (g/ikW-hr)	----------	2.71205	2.87927	2.75692	2.69022	2.4404	2.37864	----------	----------
NOx (g/ikW-hr)	----------	0.11965	0.32136	0.72832	1.25817	2.09629	3.45618	----------	----------
CO2ex (g/ikW-hr)	----------	461.06881	469.9911	473.3183	477.174	485.0591	488.6936	----------	----------
CO2in (g/ikW-hr)	----------	4.37719	4.09927	3.8213	3.63749	3.52198	3.25631	----------	----------
CO (g/ikW-hr)	----------	14.48372	8.17232	5.38164	4.31017	3.47527	2.88882	----------	----------
PM (g/ikW-hr)	----------	0.01785	0.01633	0.02949	0.04048	0.04633	0.05533	----------	----------
Air Flow (kg/min)	----------	3.38419	3.15989	2.95394	2.80417	2.61413	2.42947	----------	----------
AFR mass	----------	39.91738	37.46491	35.43413	33.38988	31.1444	28.66841	----------	----------
AFR carbon	----------	40.01801	37.71736	35.77581	33.85476	31.71118	28.99814	----------	----------
AFR Average	----------	39.9677	37.59114	35.60497	33.62232	31.42779	28.83327	----------	----------
AFR Stoich	----------	10.77288	10.78815	10.80273	10.80547	10.84767	10.83757	----------	----------
Phi mass	----------	0.26988	0.28795	0.30487	0.32362	0.3483	0.37803	----------	----------
Phi carbon	----------	0.2692	0.28603	0.30196	0.31917	0.34208	0.37373	----------	----------
GTE emisisons based	----------	0.52986	0.53281	0.53591	0.53598	0.53205	0.52573	----------	----------
EXH emissions based	----------	0.33063	0.31145	0.30169	0.29087	0.27951	0.2683	----------	----------
HX emisisons based	----------	0.10517	0.12991	0.14122	0.15396	0.17183	0.1906	----------	----------

Table A. 1 ULSD / DI E85 PFI, Φ-T Matrix result Continued

MATRIX POINT	28	29	30	31	32	33	34	35	36
RPM	1300	No Data	1300	No Data	1300	No Data	No Data	No Data	No Data
IMEPg (bar)	9.05162	----------	8.88993	----------	8.86775	----------	----------	----------	----------
IMEPn (bar)	8.31316	----------	8.32079	----------	8.36997	----------	----------	----------	----------
BMEP_CF (bar)	7.04726	----------	7.09725	----------	7.16728	----------	----------	----------	----------
FMEP_CF (bar)	1.2659	----------	1.22354	----------	1.20269	----------	----------	----------	----------
CA50 (ATDC)	0.02934	----------	-0.03391	----------	-0.17405	----------	----------	----------	----------
COV of IMEPg	2.65838	----------	2.66023	----------	2.53923	----------	----------	----------	----------
COV of PPRR	7.06756	----------	6.63064	----------	7.42473	----------	----------	----------	----------
EGR %	0	----------	0	----------	0	----------	----------	----------	----------
Fuel 1	E85	----------	E85	----------	E85	----------	----------	----------	----------
Fuel 2	ULSD	----------	ULSD	----------	ULSD	----------	----------	----------	----------
Fuel1 Flow (g/s)	1.2027	----------	1.13809	----------	1.12501	----------	----------	----------	----------
Fuel2 Flow (g/s)	0.22659	----------	0.25714	----------	0.27424	----------	----------	----------	----------
Fuel1 Fraction	0.84147	----------	0.8157	----------	0.80401	----------	----------	----------	----------
Fuel2 Fraction	0.15853	----------	0.1843	----------	0.19599	----------	----------	----------	----------
Fuel Energy (J/cyc)	4158.722	----------	4103.337	----------	4135.057	----------	----------	----------	----------
Fuel H/C	2.54135	----------	2.50853	----------	2.49391	----------	----------	----------	----------
Fuel O/C	0.30616	----------	0.2931	----------	0.28727	----------	----------	----------	----------
Fuel MW/C	19.47025	----------	19.22814	----------	19.12023	----------	----------	----------	----------
RI (MW/m^2)	3.76747	----------	4.34824	----------	5.92115	----------	----------	----------	----------
Peak HRR (J/deg)	525.9464	----------	550.2196	----------	612.352	----------	----------	----------	----------
Peak PRR (bar/deg)	10.95577	----------	11.29089	----------	12.80572	----------	----------	----------	----------
PP (bar)	144.1125	----------	135.6403	----------	131.4707	----------	----------	----------	----------
LPP (ATDC)	3.9	----------	3.9	----------	3.6	----------	----------	----------	----------
P Intake (bar)	2.19433	----------	1.95479	----------	1.7905	----------	----------	----------	----------
P Exhaust (bar)	2.55024	----------	2.17135	----------	1.95454	----------	----------	----------	----------
T Intake (C)	67.73309	----------	68.81071	----------	66.35868	----------	----------	----------	----------
T Exhaust Tank (C)	305.5052	----------	310.8425	----------	317.3747	----------	----------	----------	----------
Gross Therm Eff	0.53126	----------	0.52882	----------	0.52345	----------	----------	----------	----------
Net Therm Eff	0.48792	----------	0.49496	----------	0.49407	----------	----------	----------	----------
Brake Therm Eff (CF)	0.41362	----------	0.42218	----------	0.42307	----------	----------	----------	----------
Turbo Eff	0.63508	----------	0.64868	----------	0.6514	----------	----------	----------	----------
Vol Eff	0.95216	----------	0.96624	----------	0.95874	----------	----------	----------	----------
comb loss	0.02509	----------	0.02133	----------	0.018	----------	----------	----------	----------
Comb Eff	0.97491	----------	0.97867	----------	0.982	----------	----------	----------	----------
Exhaust Loss	0.32796	----------	0.30489	----------	0.28686	----------	----------	----------	----------
Pumping Loss	0.04334	----------	0.03386	----------	0.02938	----------	----------	----------	----------
Heat Transfer Loss	0.11569	----------	0.14497	----------	0.17168	----------	----------	----------	----------
HC (ppm)	449.8093	----------	564.0904	----------	590.0403	----------	----------	----------	----------
NOx (ppm)	6.38201	----------	42.43572	----------	154.3227	----------	----------	----------	----------
CO2ex (ppm)	36522.46	----------	40552.4	----------	44725.23	----------	----------	----------	----------
CO2in (ppm)	349.7316	----------	354.0809	----------	354.7483	----------	----------	----------	----------
CO (ppm)	1097.755	----------	711.967	----------	509.5875	----------	----------	----------	----------
PM (mg/m^3)	2.05	----------	4.9	----------	7.76	----------	----------	----------	----------
HC (g/kg-fuel)	11.80874	----------	13.47648	----------	12.86669	----------	----------	----------	----------
NOx (g/kg-fuel)	0.39584	----------	2.42538	----------	8.09617	----------	----------	----------	----------
CO2ex (g/kg-fuel)	2167.281	----------	2217.473	----------	2244.896	----------	----------	----------	----------
CO2in (g/kg-fuel)	20.75344	----------	19.36173	----------	17.8059	----------	----------	----------	----------
CO (g/kg-fuel)	41.45932	----------	24.77784	----------	16.27886	----------	----------	----------	----------
PM (g/kg-fuel)	0.03774	----------	0.09405	----------	0.14752	----------	----------	----------	----------
HC (g/ikW-hr)	2.5386	----------	2.87951	----------	2.76403	----------	----------	----------	----------
NOx (g/ikW-hr)	0.0851	----------	0.51823	----------	1.73923	----------	----------	----------	----------
CO2ex (g/ikW-hr)	465.9134	----------	473.8057	----------	482.2502	----------	----------	----------	----------
CO2in (g/ikW-hr)	4.46149	----------	4.13701	----------	3.82508	----------	----------	----------	----------
CO (g/ikW-hr)	8.91276	----------	5.29426	----------	3.49704	----------	----------	----------	----------
PM (g/ikW-hr)	0.00811	----------	0.0201	----------	0.03169	----------	----------	----------	----------
Air Flow (kg/min)	3.38793	----------	3.05307	----------	2.79483	----------	----------	----------	----------
AFR mass	39.50589	----------	36.4704	----------	33.2897	----------	----------	----------	----------
AFR carbon	39.68697	----------	36.64715	----------	33.70949	----------	----------	----------	----------
AFR Average	39.59643	----------	36.55877	----------	33.4996	----------	----------	----------	----------
AFR Stoich	10.49802	----------	10.61822	----------	10.67277	----------	----------	----------	----------
Phi mass	0.26573	----------	0.29115	----------	0.3206	----------	----------	----------	----------
Phi carbon	0.26452	----------	0.28974	----------	0.31661	----------	----------	----------	----------
GTE emisisons based	0.5337	----------	0.53138	----------	0.53005	----------	----------	----------	----------
EXH emissions based	0.32646	----------	0.30341	----------	0.28329	----------	----------	----------	----------
HX emisisons based	0.11475	----------	0.14387	----------	0.16866	----------	----------	----------	----------

Table A. 2 3% EHN+ 91 PON Gasoline DI / E85 PFI, Φ-T Matrix results

MATRIX POINT	1	2	3	4	5	6	7	8	9
RPM	No Data	1300	1300	1300	1300	No Data	1299	No Data	No Data
IMEPg (bar)	----------	8.73785	8.62388	8.57746	8.57458	----------	8.49453	----------	----------
IMEPn (bar)	----------	8.07942	8.06735	8.09194	8.07421	----------	8.0602	----------	----------
BMEP_CF (bar)	----------	6.84822	6.87167	6.92279	6.93154	----------	6.94367	----------	----------
FMEP_CF (bar)	----------	1.2312	1.19568	1.16915	1.14267	----------	1.11653	----------	----------
CA50 (ATDC)	----------	-1.30752	-1.37675	-1.32879	-1.20223	----------	-1.26776	----------	----------
COV of IMEPg	----------	2.79235	2.81248	2.51646	2.36522	----------	2.16285	----------	----------
COV of PPRR	----------	7.82696	8.37683	8.45879	8.52304	----------	8.86811	----------	----------
EGR %	----------	0	0	0	0	----------	0	----------	----------
Fuel 1	----------	E85	E85	E85	E85	----------	E85	----------	----------
Fuel 2	----------	3% EHN + 91 PON	3% EHN + 91 PON	3% EHN + 91 PON	3% EHN + 91 PON	----------	3% EHN + 91 PON	----------	----------
Fuel1 Flow (g/s)	----------	0.70681	0.63401	0.6125	0.60315	----------	0.58906	----------	----------
Fuel2 Flow (g/s)	----------	0.55916	0.57844	0.58425	0.59051	----------	0.61045	----------	----------
Fuel1 Fraction	----------	0.55832	0.52292	0.5118	0.50529	----------	0.49108	----------	----------
Fuel2 Fraction	----------	0.44168	0.47708	0.4882	0.49471	----------	0.50892	----------	----------
Fuel Energy (J/cyc)	----------	4118.016	3996.037	3960.424	3959.622	----------	4002.797	----------	----------
Fuel H/C	----------	2.28698	2.25618	2.2467	2.24118	----------	2.22923	----------	----------
Fuel O/C	----------	0.18553	0.17201	0.16785	0.16543	----------	0.16019	----------	----------
Fuel MW/C	----------	17.28371	17.03646	16.9603	16.91598	----------	16.82009	----------	----------
RI (MW/m^2)	----------	1.59429	2.02028	2.55649	4.02161	----------	6.90077	----------	----------
Peak HRR (J/deg)	----------	339.8474	378.4643	422.2018	510.5894	----------	611.3687	----------	----------
Peak PRR (bar/deg)	----------	7.04832	7.63339	8.32863	10.04078	----------	12.65441	----------	----------
PP (bar)	----------	137.171	130.0674	124.761	119.4668	----------	114.2794	----------	----------
LPP (ATDC)	----------	3.6	4	4.3	3	----------	2.7	----------	----------
P Intake (bar)	----------	2.01014	1.81277	1.67805	1.5056	----------	1.35122	----------	----------
P Exhaust (bar)	----------	2.31227	2.03022	1.83759	1.69917	----------	1.4973	----------	----------
T Intake (C)	----------	32.58861	31.69122	33.2146	34.4044	----------	33.01648	----------	----------
T Exhaust Tank (C)	----------	276.5205	295.309	295.6989	316.1174	----------	336.0081	----------	----------
Gross Therm Eff	----------	0.51792	0.52677	0.52864	0.52857	----------	0.51799	----------	----------
Net Therm Eff	----------	0.47889	0.49277	0.49872	0.49773	----------	0.4915	----------	----------
Brake Therm Eff (CF)	----------	0.40592	0.41974	0.42666	0.42729	----------	0.42342	----------	----------
Turbo Eff	----------	0.65358	0.64154	0.66039	0.58816	----------	0.60822	----------	----------
Vol Eff	----------	0.93468	0.93399	0.93703	0.92959	----------	0.91899	----------	----------
comb loss	----------	0.05495	0.04186	0.03277	0.02115	----------	0.01291	----------	----------
Comb Eff	----------	0.94505	0.95814	0.96723	0.97885	----------	0.98709	----------	----------
Exhaust Loss	----------	0.3373	0.3392	0.31504	0.29977	----------	0.28401	----------	----------
Pumping Loss	----------	0.03903	0.03399	0.02992	0.03084	----------	0.02649	----------	----------
Heat Transfer Loss	----------	0.08983	0.09217	0.12354	0.15051	----------	0.1851	----------	----------
HC (ppm)	----------	559.9034	510.3994	526.6123	518.2523	----------	440.5374	----------	----------
NOx (ppm)	----------	99.80999	201.9615	331.6896	574.0427	----------	924.7046	----------	----------
CO2ex (ppm)	----------	33995.65	37767.74	41489.88	48338.71	----------	55690.74	----------	----------
CO2in (ppm)	----------	25.15086	25.76535	32.41338	29.95421	----------	25.56916	----------	----------
CO (ppm)	----------	3272.619	2582.54	1968.112	1160.621	----------	628.0854	----------	----------
PM (mg/m^3)	----------	0.68	0.55	0.49	0.62	----------	0.72	----------	----------
HC (g/kg-fuel)	----------	14.79231	12.48434	11.96582	10.35552	----------	7.75774	----------	----------
NOx (g/kg-fuel)	----------	7.01807	13.33836	20.44126	31.19146	----------	44.53329	----------	----------
CO2ex (g/kg-fuel)	----------	2286.971	2386.428	2446.31	2512.928	----------	2566.01	----------	----------
CO2in (g/kg-fuel)	----------	1.69196	1.62803	1.91115	1.55719	----------	1.17813	----------	----------
CO (g/kg-fuel)	----------	140.1182	103.8571	73.85514	38.40053	----------	18.41856	----------	----------
PM (g/kg-fuel)	----------	0.01442	0.01244	0.01109	0.01358	----------	0.01561	----------	----------
HC (g/ikW-hr)	----------	2.91775	2.38959	2.27291	1.96261	----------	1.49255	----------	----------
NOx (g/ikW-hr)	----------	1.3843	2.55305	3.88283	5.91151	----------	8.56798	----------	----------
CO2ex (g/ikW-hr)	----------	451.1004	456.7788	464.6776	476.2582	----------	493.6875	----------	----------
CO2in (g/ikW-hr)	----------	0.33374	0.31162	0.36302	0.29512	----------	0.22667	----------	----------
CO (g/ikW-hr)	----------	27.63803	19.87897	14.02882	7.27779	----------	3.54364	----------	----------
PM (g/ikW-hr)	----------	0.00285	0.00238	0.00211	0.00257	----------	0.003	----------	----------
Air Flow (kg/min)	----------	3.39678	3.07001	2.83691	2.5154	----------	2.24012	----------	----------
AFR mass	----------	44.71928	42.20102	39.50857	35.12169	----------	31.12552	----------	----------
AFR carbon	----------	44.84827	42.22705	39.49209	34.95563	----------	31.10437	----------	----------
AFR Average	----------	44.78377	42.21403	39.50033	35.03866	----------	31.11494	----------	----------
AFR Stoich	----------	11.79998	11.9636	12.01496	12.04506	----------	12.11074	----------	----------
Phi mass	----------	0.26387	0.28349	0.30411	0.34295	----------	0.38909	----------	----------
Phi carbon	----------	0.26311	0.28332	0.30424	0.34458	----------	0.38936	----------	----------
GTE emisisons based	----------	0.51941	0.52709	0.52842	0.52607	----------	0.51764	----------	----------
EXH emissions based	----------	0.33827	0.33941	0.31491	0.29836	----------	0.28381	----------	----------
HX emisisons based	----------	0.08737	0.09163	0.1239	0.15442	----------	0.18564	----------	----------

Table A. 2 3% EHN+ 91 PON Gasoline DI / E85 PFI, Φ-T Matrix results Continued

MATRIX POINT	10	11	12	13	14	15	16	17	18
RPM	No Data	1300	1300	1300	No Data	1300	No Data	1300	No Data
IMEPg (bar)	----------	9.07579	8.90239	8.94839	----------	8.8494	----------	8.82351	----------
IMEPn (bar)	----------	8.45257	8.39799	8.45727	----------	8.4408	----------	8.46516	----------
BMEP_CF (bar)	----------	7.3297	7.3102	7.38553	----------	7.40144	----------	7.44686	----------
FMEP_CF (bar)	----------	1.12287	1.08779	1.07175	----------	1.03937	----------	1.01831	----------
CA50 (ATDC)	----------	0.67149	0.86037	0.78424	----------	0.63861	----------	1.20143	----------
COV of IMEPg	----------	2.83633	2.63665	2.80398	----------	2.38375	----------	2.25513	----------
COV of PPRR	----------	8.08402	8.53818	8.61818	----------	8.30426	----------	6.89981	----------
EGR %	----------	0	0	0	----------	0	----------	0	----------
Fuel 1	----------	E85	E85	E85	----------	E85	----------	E85	----------
Fuel 2	----------	3% EHN + 91 PON	3% EHN + 91 PON	3% EHN + 91 PON	----------	3% EHN + 91 PON	----------	3% EHN + 91 PON	----------
Fuel1 Flow (g/s)	----------	0.86767	0.81563	0.79345	----------	0.74523	----------	0.77295	----------
Fuel2 Flow (g/s)	----------	0.45782	0.45783	0.46985	----------	0.50656	----------	0.51507	----------
Fuel1 Fraction	----------	0.6546	0.64048	0.62808	----------	0.59533	----------	0.60011	----------
Fuel2 Fraction	----------	0.3454	0.35952	0.37192	----------	0.40467	----------	0.39989	----------
Fuel Energy (J/cyc)	----------	4156.755	4015.4	4002.387	----------	4015.665	----------	4124.416	----------
Fuel H/C	----------	2.37545	2.36202	2.35036	----------	2.32015	----------	2.32451	----------
Fuel O/C	----------	0.22435	0.21846	0.21334	----------	0.20008	----------	0.20199	----------
Fuel MW/C	----------	17.99402	17.88621	17.79257	----------	17.55002	----------	17.58501	----------
RI (MW/m^2)	----------	1.715	2.04737	2.7442	----------	5.96373	----------	9.04281	----------
Peak HRR (J/deg)	----------	395.3345	441.204	503.4695	----------	703.2485	----------	863.934	----------
Peak PRR (bar/deg)	----------	7.4045	7.77275	8.75597	----------	12.19742	----------	14.45493	----------
PP (bar)	----------	138.7297	129.9591	125.9486	----------	117.8537	----------	112.588	----------
LPP (ATDC)	----------	4.2	4.3	4.2	----------	3.6	----------	3.8	----------
P Intake (bar)	----------	2.05188	1.86373	1.71964	----------	1.46561	----------	1.31398	----------
P Exhaust (bar)	----------	2.30678	2.02692	1.88133	----------	1.59389	----------	1.41065	----------
T Intake (C)	----------	44.0193	42.38169	41.51037	----------	42.62242	----------	42	----------
T Exhaust Tank (C)	----------	282.1602	293.871	306.956	----------	332.5097	----------	350.9449	----------
Gross Therm Eff	----------	0.53294	0.54116	0.54572	----------	0.5379	----------	0.52218	----------
Net Therm Eff	----------	0.49634	0.5105	0.51577	----------	0.51306	----------	0.50098	----------
Brake Therm Eff (CF)	----------	0.4304	0.44437	0.45041	----------	0.44989	----------	0.44071	----------
Turbo Eff	----------	0.66914	0.67347	0.6447	----------	0.63882	----------	0.70913	----------
Vol Eff	----------	0.95053	0.95066	0.94691	----------	0.9411	----------	0.93877	----------
comb loss	----------	0.04695	0.03574	0.02708	----------	0.0156	----------	0.01167	----------
Comb Eff	----------	0.95305	0.96426	0.97292	----------	0.9844	----------	0.98833	----------
Exhaust Loss	----------	0.32754	0.32662	0.3185	----------	0.29243	----------	0.27171	----------
Pumping Loss	----------	0.0366	0.03066	0.02995	----------	0.02484	----------	0.02121	----------
Heat Transfer Loss	----------	0.09257	0.09648	0.1087	----------	0.15407	----------	0.19443	----------
HC (ppm)	----------	598.1026	559.9313	531.7344	----------	596.0463	----------	536.0981	----------
NOx (ppm)	----------	80.10744	149.1001	230.6506	----------	635.484	----------	921.1812	----------
CO2ex (ppm)	----------	35237.57	38615.33	42361.07	----------	52026.38	----------	59420.7	----------
CO2in (ppm)	----------	61.89977	64.86068	64.40341	----------	64.02218	----------	69.46601	----------
CO (ppm)	----------	2610.806	1968.916	1445.419	----------	503.2164	----------	363.3652	----------
PM (mg/m^3)	----------	0.78	83.03	83.03	----------	0.78	----------	0.78	----------
HC (g/kg-fuel)	----------	15.54626	13.60035	11.98541	----------	11.21193	----------	8.88208	----------
NOx (g/kg-fuel)	----------	5.32296	9.31392	13.44101	----------	31.33179	----------	39.92368	----------
CO2ex (g/kg-fuel)	----------	2240.162	2307.852	2361.771	----------	2454.131	----------	2463.865	----------
CO2in (g/kg-fuel)	----------	3.93516	3.87641	3.59071	----------	3.01998	----------	2.88039	----------
CO (g/kg-fuel)	----------	105.6355	74.89229	51.28926	----------	15.10743	----------	9.58924	----------
PM (g/kg-fuel)	----------	0.016	1.80532	1.80216	----------	0.01672	----------	0.01614	----------
HC (g/ikW-hr)	----------	3.0911	2.64864	2.30361	----------	2.1592	----------	1.76518	----------
NOx (g/ikW-hr)	----------	1.05838	1.81387	2.58338	----------	6.03389	----------	7.93425	----------
CO2ex (g/ikW-hr)	----------	445.4175	449.45	453.9356	----------	472.6174	----------	489.6575	----------
CO2in (g/ikW-hr)	----------	0.78244	0.75492	0.69014	----------	0.58159	----------	0.57244	----------
CO (g/ikW-hr)	----------	21.00379	14.58513	9.85787	----------	2.90939	----------	1.90572	----------
PM (g/ikW-hr)	----------	0.00318	0.00352	0.00346	----------	0.00322	----------	0.00321	----------
Air Flow (kg/min)	----------	3.39904	3.10379	2.86044	----------	2.41438	----------	2.16351	----------
AFR mass	----------	42.73936	40.62156	37.73777	----------	32.14573	----------	27.9954	----------
AFR carbon	----------	42.42954	39.97651	37.37737	----------	31.7906	----------	28.0472	----------
AFR Average	----------	42.58445	40.29903	37.55757	----------	31.96816	----------	28.0213	----------
AFR Stoich	----------	11.35493	11.4202	11.47754	----------	11.62889	----------	11.60681	----------
Phi mass	----------	0.26568	0.28114	0.30414	----------	0.36176	----------	0.4146	----------
Phi carbon	----------	0.26762	0.28567	0.30707	----------	0.3658	----------	0.41383	----------
GTE emisisons based	----------	0.52907	0.53256	0.54051	----------	0.53196	----------	0.52315	----------
EXH emissions based	----------	0.32517	0.32144	0.31545	----------	0.2892	----------	0.27221	----------
HX emisisons based	----------	0.09881	0.11026	0.11696	----------	0.16324	----------	0.19296	----------

Table A. 2 3% EHN+ 91 PON Gasoline DI / E85 PFI, Φ-T Matrix results Continued

MATRIX POINT	19	20	21	22	23	24	25	26	27
RPM	No Data	1300	1300	No Data	1300	1300	No Data	No Data	No Data
IMEPg (bar)	----------	9.17804	9.09923	----------	9.00434	9.02424	----------	----------	----------
IMEPn (bar)	----------	8.49236	8.55262	----------	8.5509	8.55171	----------	----------	----------
BMEP_CF (bar)	----------	7.35877	7.43704	----------	7.47158	7.48028	----------	----------	----------
FMEP_CF (bar)	----------	1.13359	1.11558	----------	1.07932	1.07142	----------	----------	----------
CA50 (ATDC)	----------	0.9566	0.52148	----------	0.85945	0.87585	----------	----------	----------
COV of IMEPg	----------	2.72345	2.61231	----------	2.59774	2.37418	----------	----------	----------
COV of PPRR	----------	8.23083	8.38875	----------	7.84334	7.03354	----------	----------	----------
EGR %	----------	0	0	----------	0	0	----------	----------	----------
Fuel 1	----------	E85	E85	----------	E85	E85	----------	----------	----------
Fuel 2	----------	3% EHN + 91 PON	3% EHN + 91 PON	----------	3% EHN + 91 PON	3% EHN + 91 PON	----------	----------	----------
Fuel1 Flow (g/s)	----------	1.03054	0.95887	----------	0.9044	0.96642	----------	----------	----------
Fuel2 Flow (g/s)	----------	0.34469	0.36495	----------	0.39662	0.37298	----------	----------	----------
Fuel1 Fraction	----------	0.74936	0.72432	----------	0.69515	0.72153	----------	----------	----------
Fuel2 Fraction	----------	0.25064	0.27568	----------	0.30485	0.27847	----------	----------	----------
Fuel Energy (J/cyc)	----------	4154.609	4039.481	----------	4015.998	4091.558	----------	----------	----------
Fuel H/C	----------	2.46992	2.44419	----------	2.41492	2.44136	----------	----------	----------
Fuel O/C	----------	0.2658	0.25451	----------	0.24167	0.25327	----------	----------	----------
Fuel MW/C	----------	18.75244	18.54593	----------	18.31089	18.5232	----------	----------	----------
RI (MW/m^2)	----------	3.06546	3.96113	----------	4.96357	8.67254	----------	----------	----------
Peak HRR (J/deg)	----------	560.7262	598.4598	----------	672.7167	875.0476	----------	----------	----------
Peak PRR (bar/deg)	----------	9.94042	11.03982	----------	11.79314	15.25535	----------	----------	----------
PP (bar)	----------	141.4098	136.9075	----------	127.841	125.8673	----------	----------	----------
LPP (ATDC)	----------	4	3.6	----------	3.8	3.5	----------	----------	----------
P Intake (bar)	----------	2.12608	1.97396	----------	1.74244	1.63496	----------	----------	----------
P Exhaust (bar)	----------	2.43952	2.17908	----------	1.87653	1.78979	----------	----------	----------
T Intake (C)	----------	55.78621	58.93984	----------	56.36321	58.27376	----------	----------	----------
T Exhaust Tank (C)	----------	298.9235	309.4958	----------	322.7981	330.6903	----------	----------	----------
Gross Therm Eff	----------	0.53922	0.54982	----------	0.54727	0.53835	----------	----------	----------
Net Therm Eff	----------	0.49893	0.5168	----------	0.51971	0.51016	----------	----------	----------
Brake Therm Eff (CF)	----------	0.43233	0.44939	----------	0.45411	0.44625	----------	----------	----------
Turbo Eff	----------	0.64196	0.65328	----------	0.6585	0.62525	----------	----------	----------
Vol Eff	----------	0.94972	0.96837	----------	0.96798	0.9585	----------	----------	----------
comb loss	----------	0.03351	0.02661	----------	0.01838	0.01435	----------	----------	----------
Comb Eff	----------	0.96649	0.97339	----------	0.98162	0.98565	----------	----------	----------
Exhaust Loss	----------	0.33498	0.32804	----------	0.31628	0.29326	----------	----------	----------
Pumping Loss	----------	0.04028	0.03303	----------	0.02756	0.02819	----------	----------	----------
Heat Transfer Loss	----------	0.09229	0.09552	----------	0.11807	0.15403	----------	----------	----------
HC (ppm)	----------	519.3875	524.5654	----------	517.9732	513.9909	----------	----------	----------
NOx (ppm)	----------	52.75187	89.99245	----------	197.7704	279.0559	----------	----------	----------
CO2ex (ppm)	----------	36276.77	38827.68	----------	43799.08	48313.83	----------	----------	----------
CO2in (ppm)	----------	69.51122	63.69508	----------	61.85831	88.68946	----------	----------	----------
CO (ppm)	----------	1671.579	1203.563	----------	669.6506	418.8469	----------	----------	----------
PM (mg/m^3)	----------	0.81	0.77	----------	0.8	0.85	----------	----------	----------
HC (g/kg-fuel)	----------	13.49355	12.92635	----------	11.50686	10.43062	----------	----------	----------
NOx (g/kg-fuel)	----------	3.36181	5.50037	----------	11.0372	14.06332	----------	----------	----------
CO2ex (g/kg-fuel)	----------	2211.857	2270.495	----------	2338.602	2329.494	----------	----------	----------
CO2in (g/kg-fuel)	----------	4.23822	3.72465	----------	3.30285	4.27624	----------	----------	----------
CO (g/kg-fuel)	----------	64.866	44.79295	----------	22.75628	12.85308	----------	----------	----------
PM (g/kg-fuel)	----------	0.01584	0.01616	----------	0.01716	0.01709	----------	----------	----------
HC (g/ikW-hr)	----------	2.75264	2.56032	----------	2.26352	2.10768	----------	----------	----------
NOx (g/ikW-hr)	----------	0.6858	1.08946	----------	2.17114	2.84172	----------	----------	----------
CO2ex (g/ikW-hr)	----------	451.2112	449.7165	----------	460.0282	470.7122	----------	----------	----------
CO2in (g/ikW-hr)	----------	0.86458	0.73774	----------	0.64971	0.86408	----------	----------	----------
CO (g/ikW-hr)	----------	13.23244	8.87213	----------	4.47641	2.59717	----------	----------	----------
PM (g/ikW-hr)	----------	0.00323	0.0032	----------	0.00338	0.00345	----------	----------	----------
Air Flow (kg/min)	----------	3.39305	3.18165	----------	2.82931	2.61365	----------	----------	----------
AFR mass	----------	41.12076	40.0565	----------	36.24475	32.52268	----------	----------	----------
AFR carbon	----------	40.75287	39.1485	----------	35.84717	32.44843	----------	----------	----------
AFR Average	----------	40.93682	39.6025	----------	36.04596	32.48555	----------	----------	----------
AFR Stoich	----------	10.91695	11.03266	----------	11.16752	11.04555	----------	----------	----------
Phi mass	----------	0.26549	0.27543	----------	0.30811	0.33963	----------	----------	----------
Phi carbon	----------	0.26788	0.28182	----------	0.31153	0.3404	----------	----------	----------
GTE emisisons based	----------	0.53439	0.53736	----------	0.54127	0.53712	----------	----------	----------
EXH emissions based	----------	0.33198	0.32061	----------	0.31281	0.29259	----------	----------	----------
HX emisisons based	----------	0.10011	0.11542	----------	0.12754	0.15593	----------	----------	----------

Table A. 2 3% EHN+ 91 PON Gasoline DI / E85 PFI, Φ-T Matrix results Continued

MATRIX POINT	28	29	30	31	32	33	34	35	36
RPM	1300	No Data	1300	No Data	1300	No Data	No Data	No Data	No Data
IMEPg (bar)	9.05191		8.88367		8.87867				
IMEPn (bar)	8.35541		8.30793		8.37465				
BMEP_CF (bar)	7.21818		7.20527		7.28686				
FMEP_CF (bar)	1.13723		1.10266		1.08779				
CA50 (ATDC)	0.99495		1.06373		1.10453				
COV of IMEPg	3.06765		2.69829		2.49414				
COV of PPRR	7.75942		7.06707		6.6513				
EGR %	0		0		0				
Fuel 1	E85		E85		E85				
Fuel 2	3% EHN + 91 PON		3% EHN + 91 PON		3% EHN + 91 PON				
Fuel1 Flow (g/s)	1.04599		1.00089		1.04385				
Fuel2 Flow (g/s)	0.29263		0.30444		0.32139				
Fuel1 Fraction	0.78139		0.76677		0.76459				
Fuel2 Fraction	0.21861		0.23323		0.23541				
Fuel Energy (J/cyc)	3991.951		3915.815		4099.16				
Fuel H/C	2.50368		2.48815		2.48585				
Fuel O/C	0.28061		0.2738		0.27279				
Fuel MW/C	19.02354		18.89883		18.8804				
RI (MW/m^2)	4.2528		5.40612		8.74084				
Peak HRR (J/deg)	648.9314		714.8812		889.3776				
Peak PRR (bar/deg)	11.72592		12.6721		15.67733				
PP (bar)	142.319		133.677		129.9593				
LPP (ATDC)	3.9		3.8		3.6				
P Intake (bar)	2.18216		1.96082		1.77669				
P Exhaust (bar)	2.52052		2.21896		1.93592				
T Intake (C)	68.71044		66.78848		65.60883				
T Exhaust Tank (C)	295.9251		309.4806		322.2648				
Gross Therm Eff	0.55348		0.55375		0.52869				
Net Therm Eff	0.51089		0.51786		0.49867				
Brake Therm Eff (CF)	0.44135		0.44913		0.4339				
Turbo Eff	0.64811		0.63177		0.64678				
Vol Eff	0.96345		0.95937		0.96124				
comb loss	0.02788		0.01949		0.01391				
Comb Eff	0.97212		0.98051		0.98609				
Exhaust Loss	0.32796		0.32077		0.29484				
Pumping Loss	0.04259		0.03589		0.03001				
Heat Transfer Loss	0.09068		0.10599		0.16257				
HC (ppm)	490.9812		454.5452		451.7027				
NOx (ppm)	50.26766		112.8694		239.2705				
CO2ex (ppm)	36099.72		39598.97		44416.72				
CO2in (ppm)	216.6113		192.4383		148.8185				
CO (ppm)	1225.227		739.903		386.2836				
PM (mg/m^3)	0.83		0.72		0.74				
HC (g/kg-fuel)	12.97571		11.13644		9.97582				
NOx (g/kg-fuel)	3.21234		6.73083		12.87455				
CO2ex (g/kg-fuel)	2207.14		2259.278		2286.561				
CO2in (g/kg-fuel)	13.24364		10.97936		7.66113				
CO (g/kg-fuel)	47.67651		26.86718		12.65623				
PM (g/kg-fuel)	0.01624		0.01455		0.01459				
HC (g/ikW-hr)	2.61243		2.22776		2.08836				
NOx (g/ikW-hr)	0.64675		1.34645		2.69518				
CO2ex (g/ikW-hr)	444.3692		451.9508		478.6733				
CO2in (g/ikW-hr)	2.66638		2.19634		1.6038				
CO (g/ikW-hr)	9.59883		5.37457		2.64948				
PM (g/ikW-hr)	0.00327		0.00291		0.00305				
Air Flow (kg/min)	3.39934		3.05882		2.78663				
AFR mass	42.32377		39.05565		34.01884				
AFR carbon	40.88101		38.23108		34.58637				
AFR Average	41.60239		38.64336		34.3026				
AFR Stoich	10.76886		10.83646		10.84653				
Phi mass	0.25444		0.27746		0.31884				
Phi carbon	0.26342		0.28345		0.31361				
GTE emisisons based	0.53461		0.54206		0.53751				
EXH emissions based	0.31678		0.314		0.29976				
HX emisisons based	0.12073		0.12445		0.14883				

Table A. 3 ULSD DI / 91 PON Gasoline PFI, Φ-T Matrix results

MATRIX POINT	1	2	3	4-36
RPM	No Data	1300	1300	No Data
IMEPg (bar)	----------	8.73054	8.61335	----------
IMEPn (bar)	----------	8.26908	8.18147	----------
BMEP_CF (bar)	----------	7.05785	6.99712	----------
FMEP_CF (bar)	----------	1.21122	1.18435	----------
CA50 (ATDC)	----------	1.33982	1.33038	----------
COV of IMEPg	----------	2.43011	2.44317	----------
COV of PPRR	----------	9.42429	10.98825	----------
EGR %	----------	0	0	----------
Fuel 1	----------	91 Gasolin	91 Gasolin	----------
Fuel 2	----------	#2 ULSD	#2 ULSD	----------
Fuel1 Flow (g/s)	----------	0.9481	0.90209	----------
Fuel2 Flow (g/s)	----------	0.04313	0.07322	----------
Fuel1 Fraction	----------	0.95649	0.92492	----------
Fuel2 Fraction	----------	0.04351	0.07508	----------
Fuel Energy (J/cyc)	----------	4039.328	3969.906	----------
Fuel H/C	----------	1.87518	1.87168	----------
Fuel O/C	----------	0	0	----------
Fuel MW/C	----------	13.90018	13.89665	----------
RI (MW/m^2)	----------	6.37589	6.94482	----------
Peak HRR (J/deg)	----------	562.2101	587.7669	----------
Peak PRR (bar/deg)	----------	13.89766	14.06114	----------
PP (bar)	----------	133.1767	127.8026	----------
LPP (ATDC)	----------	4.4	3.9	----------
P Intake (bar)	----------	1.88629	1.72346	----------
P Exhaust (bar)	----------	1.97755	1.81532	----------
T Intake (C)	----------	32.82975	32.85337	----------
T Exhaust Tank (C)	----------	280.1699	291.1393	----------
Gross Therm Eff	----------	0.52757	0.52959	----------
Net Therm Eff	----------	0.49968	0.50303	----------
Brake Therm Eff (CF)	----------	0.42649	0.43021	----------
Turbo Eff	----------	0.73946	0.7217	----------
Vol Eff	----------	0.94119	0.93912	----------
comb loss	----------	0.02684	0.02326	----------
Comb Eff	----------	0.97316	0.97674	----------
Exhaust Loss	----------	0.32919	0.31873	----------
Pumping Loss	----------	0.02789	0.02655	----------
Heat Transfer Loss	----------	0.11641	0.12842	----------
HC (ppm)	----------	645.541	664.7964	----------
NOx (ppm)	----------	1.11737	1.57491	----------
CO2ex (ppm)	----------	37517.35	40799.53	----------
CO2in (ppm)	----------	93.68719	78.5957	----------
CO (ppm)	----------	873.6132	685.2076	----------
PM (mg/m^3)	----------	2.58	1.71	----------
HC (g/kg-fuel)	----------	16.52713	15.76276	----------
NOx (g/kg-fuel)	----------	0.09467	0.12361	----------
CO2ex (g/kg-fuel)	----------	3041.142	3063.655	----------
CO2in (g/kg-fuel)	----------	7.59425	5.90179	----------
CO (g/kg-fuel)	----------	45.06979	32.74678	----------
PM (g/kg-fuel)	----------	0.07387	0.04891	----------
HC (g/ikW-hr)	----------	2.55461	2.42997	----------
NOx (g/ikW-hr)	----------	0.01463	0.01906	----------
CO2ex (g/ikW-hr)	----------	470.0709	472.2897	----------
CO2in (g/ikW-hr)	----------	1.17385	0.90981	----------
CO (g/ikW-hr)	----------	6.96646	5.04821	----------
PM (g/ikW-hr)	----------	0.01142	0.00754	----------
Air Flow (kg/min)	----------	3.20716	2.92364	----------
AFR mass	----------	53.9258	49.9606	----------
AFR carbon	----------	54.22683	50.31366	----------
AFR Average	----------	54.07631	50.13713	----------
AFR Stoich	----------	14.57122	14.56625	----------
Phi mass	----------	0.27021	0.29155	----------
Phi carbon	----------	0.26871	0.28951	----------
GTE emisisons based	----------	0.53051	0.53333	----------
EXH emissions based	----------	0.33102	0.32098	----------
HX emisisons based	----------	0.11163	0.12243	----------

Table A. 4 ULSD DI / 91 PON Gasoline PFI, Φ-T Matrix results with EGR

MATRIX POINT	1-10	11	12	13	14	15-36
RPM	No Data	1300	1300	1299	1284	No Data
IMEPg (bar)	----------	9.18241	9.17149	9.06685	9.06868	----------
IMEPn (bar)	----------	8.48898	8.50544	8.46104	8.48638	----------
BMEP_CF (bar)	----------	7.26372	7.29462	7.2657	7.31778	----------
FMEP_CF (bar)	----------	1.22525	1.21083	1.19534	1.1686	----------
CA50 (ATDC)	----------	0.93111	0.94961	0.70463	0.94273	----------
COV of IMEPg	----------	2.65377	2.37565	2.28039	2.36953	----------
COV of PPRR	----------	9.57501	9.361	9.37549	9.9074	----------
EGR %	----------	46.3477	46.91931	44.8692	45.76129	----------
Fuel 1	----------	91 Gasolin	91 Gasolin	91 Gasolin	91 Gasolin	----------
Fuel 2	----------	#2 ULSD	#2 ULSD	#2 ULSD	#2 ULSD	----------
Fuel1 Flow (g/s)	----------	0.92089	0.90492	0.90026	0.88048	----------
Fuel2 Flow (g/s)	----------	0.11648	0.12854	0.13208	0.15508	----------
Fuel1 Fraction	----------	0.88771	0.87562	0.87206	0.85025	----------
Fuel2 Fraction	----------	0.11229	0.12438	0.12794	0.14975	----------
Fuel Energy (J/cyc)	----------	4216.737	4199.004	4197.114	4255.985	----------
Fuel H/C	----------	1.86756	1.86622	1.86583	1.86341	----------
Fuel O/C	----------	0	0	0	0	----------
Fuel MW/C	----------	13.8925	13.89115	13.89075	13.88832	----------
RI (MW/m^2)	----------	2.96528	3.21064	4.28919	5.25069	----------
Peak HRR (J/deg)	----------	491.0346	514.7466	562.7447	605.0768	----------
Peak PRR (bar/deg)	----------	10.64066	10.88277	12.27952	13.40799	----------
PP (bar)	----------	135.9822	133.0977	130.043	125.3305	----------
LPP (ATDC)	----------	4.7	4.5	3.8	3.4	----------
P Intake (bar)	----------	2.03671	1.9445	1.81277	1.65399	----------
P Exhaust (bar)	----------	2.34665	2.24114	2.05876	1.89448	----------
T Intake (C)	----------	42.63204	41.34018	43.31703	43.21094	----------
T Exhaust Tank (C)	----------	292.9761	303.4812	316.954	333.0511	----------
Gross Therm Eff	----------	0.53153	0.53314	0.52729	0.5201	----------
Net Therm Eff	----------	0.49139	0.49442	0.49206	0.48671	----------
Brake Therm Eff (CF)	----------	0.42046	0.42403	0.42254	0.41969	----------
Turbo Eff	----------	0.62526	0.60541	0.59531	0.55636	----------
Vol Eff	----------	0.96216	0.95181	0.95501	0.95518	----------
comb loss	----------	0.01667	0.01371	0.01104	0.00939	----------
Comb Eff	----------	0.98333	0.98629	0.98896	0.99061	----------
Exhaust Loss	----------	0.34221	0.34098	0.33101	0.31545	----------
Pumping Loss	----------	0.04014	0.03872	0.03523	0.0334	----------
Heat Transfer Loss	----------	0.10959	0.11218	0.13065	0.15506	----------
HC (ppm)	----------	639.2466	637.7532	579.1356	598.8562	----------
NOx (ppm)	----------	2.80479	3.90367	6.90114	16.59061	----------
CO2ex (ppm)	----------	69298.17	74379.55	77234.57	88512.17	----------
CO2in (ppm)	----------	32326.28	35104.32	34868.44	40714.76	----------
CO (ppm)	----------	1183.245	870.8345	621.119	525.2111	----------
PM (mg/m^3)	----------	2.96	2.96	2.87	3.33	----------
HC (g/kg-fuel)	----------	8.98293	8.39893	7.37971	6.67727	----------
NOx (g/kg-fuel)	----------	0.13051	0.17024	0.29121	0.6127	----------
CO2ex (g/kg-fuel)	----------	3084.908	3103.402	3118.146	3127.383	----------
CO2in (g/kg-fuel)	----------	1439.051	1464.688	1407.723	1438.566	----------
CO (g/kg-fuel)	----------	33.52409	23.12501	15.95957	11.81065	----------
PM (g/kg-fuel)	----------	0.04232	0.04191	0.04255	0.04742	----------
HC (g/ikW-hr)	----------	1.38163	1.28848	1.14482	1.05101	----------
NOx (g/ikW-hr)	----------	0.02007	0.02612	0.04518	0.09644	----------
CO2ex (g/ikW-hr)	----------	474.4768	476.0913	483.7187	492.2515	----------
CO2in (g/ikW-hr)	----------	221.3344	224.697	218.3804	226.431	----------
CO (g/ikW-hr)	----------	5.1562	3.5476	2.47581	1.859	----------
PM (g/ikW-hr)	----------	0.00651	0.00643	0.0066	0.00746	----------
Air Flow (kg/min)	----------	1.84038	1.72671	1.66576	1.47875	----------
AFR mass	----------	29.56805	27.84649	26.89286	23.79949	----------
AFR carbon	----------	30.20609	28.38195	27.50434	24.19314	----------
AFR Average	----------	29.88707	28.11422	27.1986	23.99631	----------
AFR Stoich	----------	14.56038	14.55847	14.55791	14.55447	----------
Phi mass	----------	0.49244	0.52281	0.54133	0.61155	----------
Phi carbon	----------	0.48203	0.51295	0.52929	0.60159	----------
GTE emisisons based	----------	0.543	0.54339	0.53928	0.52871	----------
EXH emissions based	----------	0.34221	0.34098	0.33101	0.31545	----------
HX emisisons based	----------	0.09812	0.10193	0.11866	0.14646	----------
charge based PHI	----------	0.2642	0.27751	0.29844	0.33169	----------
Emission charge based PHI	----------	0.258615	0.272276	0.291802	0.326288	----------

Table A. 5 ULSD DI / 91 PON Gasoline PFI, Φ-T Matrix with EGR and CA50 5.0°CA ATDC

MATRIX POINT	1-10	11	12	13	14	15	16	17
RPM	No Data	1300	1300	1300	1300	1300	1300	1300
IMEPg (bar)	----------	9.08233	9.11862	9.01961	8.98913	8.92697	8.92628	8.86596
IMEPn (bar)	----------	8.50239	8.56034	8.48645	8.50505	8.45794	8.48033	8.44809
BMEP_CF (bar)	----------	7.11887	7.17563	7.12656	7.16015	7.1277	7.16648	7.1655
FMEP_CF (bar)	----------	1.38352	1.38471	1.35989	1.3449	1.33023	1.31385	1.28259
CA50 (ATDC)	----------	5.79267	4.93053	5.46094	5.30466	5.33798	5.07469	5.65552
COV of IMEPg	----------	3.87902	3.17837	2.96611	2.34403	2.26878	2.01075	1.49729
COV of PPRR	----------	16.03646	14.02674	16.52178	14.79833	14.6107	11.71084	12.49877
EGR %	----------	46.4601	46.49533	46.53764	44.47459	44.70067	43.55034	43.75067
Fuel 1	----------	91 Gasoline	91 Gasoline	91 Gasoline	91 Gasoline	91 Gasoline	91 Gasoline	91 Gasoline
Fuel 2	----------	#2 ULSD	#2 ULSD	#2 ULSD	#2 ULSD	#2 ULSD	#2 ULSD	#2 ULSD
Fuel1 Flow (g/s)	----------	0.96913	0.93307	0.89973	0.873	0.84582	0.80032	0.70458
Fuel2 Flow (g/s)	----------	0.06607	0.10227	0.12519	0.14557	0.18247	0.26796	0.38928
Fuel1 Fraction	----------	0.93618	0.90122	0.87786	0.85708	0.82255	0.74916	0.64412
Fuel2 Fraction	----------	0.06382	0.09878	0.12214	0.14292	0.17745	0.25084	0.35588
Fuel Energy (J/cyc)	----------	4215.37478	4210.59377	4164.61128	4135.67056	4169.80678	4320.31153	4406.61633
Fuel H/C	----------	1.87293	1.86906	1.86647	1.86417	1.86035	1.85224	1.84065
Fuel O/C	----------	0	0	0	0	0	0	0
Fuel MW/C	----------	13.89791	13.89401	13.8914	13.88908	13.88523	13.87706	13.86538
RI (MW/m^2)	----------	1.65951	1.78585	1.36837	1.85518	1.96069	2.0938	1.69852
Peak HRR (J/deg)	----------	456.14793	461.16324	438.78066	480.82965	488.7358	497.93752	476.14856
Peak PRR (bar/deg)	----------	7.47177	7.68127	6.51313	7.32507	7.33226	7.28098	6.21221
PP (bar)	----------	120.11619	120.41276	114.20864	110.46015	106.79433	102.69781	94.88363
LPP (ATDC)	----------	8.2	7.5	8.3	8.3	8.4	8.2	9.2
P Intake (bar)	----------	2.04826	1.94382	1.82808	1.66844	1.56864	1.44097	1.31567
P Exhaust (bar)	----------	2.24021	2.13304	2.00682	1.82628	1.70827	1.58456	1.41994
T Intake (C)	----------	44.34341	43.68765	43.08856	43.46857	42.57288	44.7407	45.03513
T Exhaust Tank (C)	----------	296.7745	303.70562	304.69365	326.83741	342.85955	365.54498	396.89837
Gross Therm Eff	----------	0.5259	0.5286	0.52864	0.53054	0.52256	0.50431	0.4911
Net Therm Eff	----------	0.49232	0.49624	0.49739	0.50197	0.4951	0.47912	0.46795
Brake Therm Eff (CF)	----------	0.41221	0.41597	0.41769	0.42259	0.41723	0.40489	0.3969
Turbo Eff	----------	0.66797	0.64956	0.6402	0.61767	0.60879	0.57513	0.62353
Vol Eff	----------	0.90893	0.9018	0.89749	0.89379	0.87786	0.85352	0.83038
comb loss	----------	0.03252	0.02322	0.02135	0.01658	0.01361	0.01133	0.03026
Comb Eff	----------	0.96748	0.97678	0.97865	0.98342	0.98639	0.98867	0.96974
Exhaust Loss	----------	0.32627	0.3173	0.3026	0.29942	0.2912	0.2663	0.25394
Pumping Loss	----------	0.03358	0.03236	0.03125	0.02857	0.02746	0.0252	0.02315
Heat Transfer Loss	----------	0.11271	0.12842	--	0.10959	0.11218	0.13065	0.15506
HC (ppm)	----------	1072.79842	968.45903	959.02903	1027.45349	942.93709	979.02416	1142.28358
NOx (ppm)	----------	1.01472	1.47031	1.58273	2.75982	6.11022	23.47032	13.94901
CO2ex (ppm)	----------	69706.93627	75510.75857	80005.08623	86153.13966	94462.89612	111219.0187	127438.6995
CO2in (ppm)	----------	32593.64631	35316.57634	37439.91346	38531.69788	42440.1071	48655.28094	55973.53388
CO (ppm)	----------	2869.91491	1842.30598	1746.5703	939.97945	793.07131	646.65499	6294.68496
PM (mg/m^3)	----------	1.65	1.77	1.45	1.48	1.11	0.63	1.11
HC (g/kg-fuel)	----------	14.55212	12.35426	11.58484	11.64867	9.79348	8.66809	8.46055
NOx (g/kg-fuel)	----------	0.04556	0.0621	0.06331	0.10363	0.21024	0.68883	0.34276
CO2ex (g/kg-fuel)	----------	2994.23535	3051.18213	3061.83211	3095.01605	3109.66653	3122.93358	2996.02621
CO2in (g/kg-fuel)	----------	1400.04787	1427.04574	1432.84302	1384.23537	1397.10496	1366.19809	1315.91248
CO (g/kg-fuel)	----------	78.45863	47.37866	42.54138	21.49176	16.616	11.55628	94.18463
PM (g/kg-fuel)	----------	0.02318	0.02453	0.01985	0.02123	0.01558	0.00837	0.01427
HC (g/ikW-hr)	----------	2.25812	1.90972	1.7922	1.79699	1.53582	1.41232	1.42111
NOx (g/ikW-hr)	----------	0.00707	0.0096	0.00979	0.01599	0.03297	0.11223	0.05757
CO2ex (g/ikW-hr)	----------	464.62906	471.65042	473.67209	477.45461	487.66058	508.82969	503.23979
CO2in (g/ikW-hr)	----------	217.25177	220.59212	221.66393	213.53995	219.0952	222.59908	221.03262
CO (g/ikW-hr)	----------	12.17478	7.32377	6.58124	3.31544	2.60574	1.8829	15.82011
PM (g/ikW-hr)	----------	0.0036	0.00379	0.00307	0.00327	0.00244	0.00136	0.0024
Air Flow (kg/min)	----------	1.73535	1.63626	1.53316	1.44554	1.33319	1.20721	1.06755
AFR mass	----------	27.93909	26.33988	24.93147	23.65305	21.60868	18.83414	16.26584
AFR carbon	----------	29.10624	27.47339	26.07411	24.55463	22.58673	19.40656	16.29198
AFR Average	----------	28.52266	26.90664	25.50279	24.10384	22.0977	19.12035	16.27891
AFR Stoich	----------	14.56802	14.56251	14.55882	14.55554	14.5501	14.53852	14.52195
Phi mass	----------	0.52142	0.55287	0.58395	0.61538	0.67335	0.77192	0.89279
Phi carbon	----------	0.50051	0.53006	0.55836	0.59278	0.64419	0.74916	0.89136
GTE emisisons based	----------	0.54787	0.55135	0.55287	0.55076	0.54621	0.51964	0.49188
EXH emissions based	----------	0.32627	0.3173	0.3026	0.29942	0.2912	0.2663	0.25394
HX emisisons based	----------	0.09334	0.10813	0.12319	0.13324	0.14898	0.20272	0.22391
charge based PHI	----------	0.27917	0.29581	0.3122	0.34169	0.37236	0.43575	0.50219
Emission charge based PHI	----------	0.26797	0.28361	0.29851	0.32914	0.35623	0.4229	0.50138

Table A. 5 ULSD DI / 91 PON Gasoline PFI, Φ-T Matrix with EGR and CA50 5.0°CA ATDC

MATRIX POINT	18-20	21	22	23	24	25	26
RPM	No Data	1300	1300	1300	1300	1300	1300
IMEPg (bar)	----------	9.046	9.03557	8.93267	8.90204	8.90906	8.86662
IMEPn (bar)	----------	8.46932	8.48404	8.45568	8.44225	8.46666	8.46855
BMEP_CF (bar)	----------	7.08075	7.09994	7.08481	7.10148	7.14637	7.16923
FMEP_CF (bar)	----------	1.38858	1.3841	1.37087	1.34077	1.32029	1.29933
CA50 (ATDC)	----------	6.14332	4.95211	4.85077	5.10342	5.21931	5.74388
COV of IMEPg	----------	2.71455	2.45661	2.3475	2.28372	2.03789	1.91245
COV of PPRR	----------	13.75162	13.50413	12.33701	13.08991	10.73081	9.77488
EGR %	----------	45.6842	45.81741	43.44573	44.76487	45.17392	42.22931
Fuel 1	----------	91 Gasoline	91 Gasoline	91 Gasoline	91 Gasoline	91 Gasoline	91 Gasoline
Fuel 2	----------	#2 ULSD	#2 ULSD	#2 ULSD	#2 ULSD	#2 ULSD	#2 ULSD
Fuel1 Flow (g/s)	----------	1.00579	0.95579	0.95906	0.90228	0.84296	0.83223
Fuel2 Flow (g/s)	----------	0.03141	0.06811	0.07742	0.11944	0.1972	0.22966
Fuel1 Fraction	----------	0.96971	0.93348	0.9253	0.8831	0.81041	0.78372
Fuel2 Fraction	----------	0.03029	0.06652	0.0747	0.1169	0.18959	0.21628
Fuel Energy (J/cyc)	----------	4228.7329	4169.00124	4218.92289	4152.41955	4216.07847	4299.96458
Fuel H/C	----------	1.87664	1.87263	1.87172	1.86705	1.85901	1.85606
Fuel O/C	----------	0	0	0	0	0	0
Fuel MW/C	----------	13.90166	13.89761	13.8967	13.89199	13.88388	13.88091
RI (MW/m^2)	----------	2.765	2.73515	3.77018	3.06431	3.04956	4.12943
Peak HRR (J/deg)	----------	541.8862	536.70971	589.48105	560.3854	562.83631	615.77575
Peak PRR (bar/deg)	----------	9.56469	9.35101	10.65855	9.19827	8.79932	9.79913
PP (bar)	----------	121.37943	120.26001	116.95359	109.4272	104.308	99.06732
LPP (ATDC)	----------	9	7.7	7.4	7.9	8.2	8.5
P Intake (bar)	----------	2.0699	1.91233	1.76587	1.61569	1.47657	1.34306
P Exhaust (bar)	----------	2.25874	2.08763	1.88862	1.73562	1.6079	1.44701
T Intake (C)	----------	56.91239	55.51413	58.54632	57.45883	57.76921	58.15655
T Exhaust Tank (C)	----------	303.175	318.80698	330.41269	346.80946	365.63507	395.34577
Gross Therm Eff	----------	0.52215	0.52902	0.5168	0.52328	0.51578	0.50331
Net Therm Eff	----------	0.48886	0.49672	0.48921	0.49625	0.49017	0.48072
Brake Therm Eff (CF)	----------	0.40871	0.41569	0.40989	0.41744	0.41373	0.40696
Turbo Eff	----------	0.66894	0.64235	0.50544	0.62789	0.59287	0.62128
Vol Eff	----------	0.90226	0.89194	0.89282	0.87223	0.84571	0.84458
comb loss	----------	0.02274	0.01924	0.01643	0.01405	0.0123	0.01169
Comb Eff	----------	0.97726	0.98076	0.98357	0.98595	0.9877	0.98831
Exhaust Loss	----------	0.30729	0.30525	0.28534	0.27641	0.25624	0.24941
Pumping Loss	----------	0.03329	0.03229	0.0276	0.02703	0.02561	0.0226
Heat Transfer Loss	----------	0.13316	0.1341	0.12273	0.12606	0.12154	0.10995
HC (ppm)	----------	1000.78712	1072.22155	1075.24547	1064.78734	1135.47277	952.23683
NOx (ppm)	----------	1.08022	1.56709	2.39614	5.52363	15.58559	20.36042
CO2ex (ppm)	----------	73017.5425	79687.54876	83544.91188	96569.34629	115385.5746	124958.9405
CO2in (ppm)	----------	33568.22352	36720.99825	36516.13106	43443.4544	52336.90751	52993.44492
CO (ppm)	----------	1562.14793	1092.93571	711.49139	687.1768	662.13421	1148.95673
PM (mg/m^3)	----------	0.75	1.55	1.55	1.59	1.1	1.4
HC (g/kg-fuel)	----------	13.22921	13.08652	12.58833	10.81907	9.67964	7.48784
NOx (g/kg-fuel)	----------	0.04725	0.06331	0.09286	0.18584	0.4402	0.53056
CO2ex (g/kg-fuel)	----------	3055.6555	3079.93498	3097.56338	3108.51778	3117.98704	3115.39051
CO2in (g/kg-fuel)	----------	1404.77101	1419.27175	1353.8949	1398.42254	1414.26517	1321.19618
CO (g/kg-fuel)	----------	41.60649	26.88484	16.78926	14.07811	11.38756	18.231
PM (g/kg-fuel)	----------	0.01035	0.02148	0.02211	0.02185	0.0141	0.01873
HC (g/ikW-hr)	----------	2.06508	2.01895	1.98858	1.69055	1.53859	1.22089
NOx (g/ikW-hr)	----------	0.00738	0.00977	0.01467	0.02904	0.06997	0.08651
CO2ex (g/ikW-hr)	----------	476.9872	475.16279	489.3226	485.72573	495.60648	507.96259
CO2in (g/ikW-hr)	----------	219.28447	218.96083	213.875	218.51244	224.79856	215.42026
CO (g/ikW-hr)	----------	6.49476	4.14771	2.6522	2.19979	1.81006	2.97255
PM (g/ikW-hr)	----------	0.00162	0.00331	0.00349	0.00341	0.00224	0.00305
Air Flow (kg/min)	----------	1.69878	1.5543	1.48585	1.30142	1.14359	1.09331
AFR mass	----------	27.29745	25.3001	23.89265	21.2292	18.32395	17.15973
AFR carbon	----------	28.42959	26.34122	25.3191	22.10885	18.71059	17.33159
AFR Average	----------	27.86352	25.82066	24.60587	21.66902	18.51727	17.24566
AFR Stoich	----------	14.57331	14.56759	14.5663	14.55965	14.54818	14.54397
Phi mass	----------	0.53387	0.57579	0.60966	0.68583	0.79394	0.84756
Phi carbon	----------	0.51261	0.55303	0.57531	0.65854	0.77754	0.83916
GTE emisisons based	----------	0.5438	0.55079	0.54766	0.54496	0.52667	0.50835
EXH emissions based	----------	0.30729	0.30525	0.28534	0.27641	0.25624	0.24941
HX emisisons based	----------	0.12616	0.12472	0.15057	0.16458	0.20479	0.23055
charge based PHI	----------	0.28998	0.31198	0.34479	0.37882	0.43529	0.48964
Emission charge based PHI	----------	0.27843	0.29965	0.32536	0.36375	0.42629	0.48479

Table A. 5 ULSD DI / 91 PON Gasoline PFI, Φ-T Matrix with EGR and CA50 5.0°CA ATDC

MATRIX POINT	27-29	30	31	32-36
RPM	No Data	1300	1300	No Data
IMEPg (bar)	----------	9.07788	9.07476	----------
IMEPn (bar)	----------	8.45028	8.4393	----------
BMEP_CF (bar)	----------	7.06004	7.02162	----------
FMEP_CF (bar)	----------	1.39025	1.41768	----------
CA50 (ATDC)	----------	5.84399	5.17665	----------
COV of IMEPg	----------	2.29989	2.39734	----------
COV of PPRR	----------	13.27315	12.43766	----------
EGR %	----------	48.46197	48.05745	----------
Fuel 1	----------	91 Gasoline	91 Gasoline	----------
Fuel 2	----------	#2 ULSD	#2 ULSD	----------
Fuel1 Flow (g/s)	----------	1.02514	1.04275	----------
Fuel2 Flow (g/s)	----------	0.01891	0.017	----------
Fuel1 Fraction	----------	0.98189	0.98396	----------
Fuel2 Fraction	----------	0.01811	0.01604	----------
Fuel Energy (J/cyc)	----------	4258.54769	4322.90082	----------
Fuel H/C	----------	1.87799	1.87822	----------
Fuel O/C	----------	0	0	----------
Fuel MW/C	----------	13.90302	13.90325	----------
RI (MW/m^2)	----------	3.95735	5.27356	----------
Peak HRR (J/deg)	----------	624.2197	679.41475	----------
Peak PRR (bar/deg)	----------	11.40872	13.65689	----------
PP (bar)	----------	121.79708	128.65597	----------
LPP (ATDC)	----------	8.3	7.5	----------
P Intake (bar)	----------	1.98247	2.08999	----------
P Exhaust (bar)	----------	2.25992	2.3542	----------
T Intake (C)	----------	64.97058	65.07371	----------
T Exhaust Tank (C)	----------	306.744	304.64276	----------
Gross Therm Eff	----------	0.52032	0.5124	----------
Net Therm Eff	----------	0.48435	0.47651	----------
Brake Therm Eff (CF)	----------	0.40466	0.39647	----------
Turbo Eff	----------	0.61199	0.63378	----------
Vol Eff	----------	0.91108	0.93575	----------
comb loss	----------	0.01636	0.01694	----------
Comb Eff	----------	0.98364	0.98306	----------
Exhaust Loss	----------	0.28352	0.29963	----------
Pumping Loss	----------	0.03597	0.03588	----------
Heat Transfer Loss	----------	0.13308	0.13617	----------
HC (ppm)	----------	950.35734	948.72442	----------
NOx (ppm)	----------	2.23483	2.39418	----------
CO2ex (ppm)	----------	82890.5907	79125.17169	----------
CO2in (ppm)	----------	40370.37766	38227.07945	----------
CO (ppm)	----------	951.81516	922.73433	----------
PM (mg/m^3)	----------	1.4	1.35	----------
HC (g/kg-fuel)	----------	11.19818	11.70289	----------
NOx (g/kg-fuel)	----------	0.08713	0.09771	----------
CO2ex (g/kg-fuel)	----------	3091.77527	3089.60382	----------
CO2in (g/kg-fuel)	----------	1505.79377	1492.65434	----------
CO (g/kg-fuel)	----------	22.59524	22.93119	----------
PM (g/kg-fuel)	----------	0.01729	0.01736	----------
HC (g/ikW-hr)	----------	1.7534	1.86061	----------
NOx (g/ikW-hr)	----------	0.01364	0.01554	----------
CO2ex (g/ikW-hr)	----------	484.10618	491.20796	----------
CO2in (g/ikW-hr)	----------	235.77524	237.31317	----------
CO (g/ikW-hr)	----------	3.53793	3.64577	----------
PM (g/ikW-hr)	----------	0.00271	0.00276	----------
Air Flow (kg/min)	----------	1.52176	1.66018	----------
AFR mass	----------	24.29251	26.10963	----------
AFR carbon	----------	25.46592	26.61441	----------
AFR Average	----------	24.87921	26.36202	----------
AFR Stoich	----------	14.57523	14.57556	----------
Phi mass	----------	0.59999	0.55824	----------
Phi carbon	----------	0.57234	0.54766	----------
GTE emisisons based	----------	0.54545	0.5223	----------
EXH emissions based	----------	0.28352	0.29963	----------
HX emisisons based	----------	0.15467	0.16112	----------
charge based PHI	----------	0.30922	0.28997	----------
Emission charge based PHI	----------	0.29497	0.28447	----------

Table A. 6 ULSD and 3% EHN + 91 PON Gasoline Mixing Controlled Combustion

Inj. P	**1300**	**700**	**500**	**1300**	**700**	**500**
RPM	1300	1300	1300	1300	1300	1300
IMEPg (bar)	8.87939	8.82944	8.87482	8.87996	8.88586	8.867
IMEPn (bar)	8.47501	8.42348	8.46173	8.45378	8.45714	8.45533
BMEP_CF (bar)	7.43566	7.39124	7.43783	7.43064	7.44551	7.45291
FMEP_CF (bar)	1.03935	1.03224	1.02389	1.02314	1.01162	1.00242
CA50 (ATDC)	2.31133	2.54449	3.05834	2.7567	3.46457	4.288
COV of IMEPg	0.99568	1.32755	1.929	0.79511	1.18472	1.47529
COV of PPRR	10.75931	4.29364	3.99861	4.79475	8.55643	6.01026
EGR %	0	0	0	0	0	0
Fuel 1	E85	E85	E85	E85	E85	E85
Fuel 2	3% EHN + 91 PON	3% EHN + 91 PON	3% EHN + 91 PON	#2 ULSD	#2 ULSD	#2 ULSD
Fuel1 Flow (g/s)	0	0	0	0	0	0
Fuel2 Flow (g/s)	1.12391	1.14569	1.14799	1.12229	1.15622	1.16124
Fuel1 Fraction	0	0	0	0	0	0
Fuel2 Fraction	1	1	1	1	1	1
Fuel Energy (J/cyc)	4417.487	4503.11	4512.134	4414.114	4547.569	4567.314
Fuel H/C	1.886	1.886	1.886	1.7723	1.7723	1.7723
Fuel O/C	0.00958	0.00958	0.00958	0	0	0
Fuel MW/C	14.0644	14.0644	14.0644	13.79648	13.79648	13.79648
RI (MW/m^2)	2.91935	5.17987	5.07479	1.3259	1.92202	1.75253
Peak HRR (J/deg)	331.6786	444.9927	437.4472	304.5028	261.1199	222.6186
Peak PRR (bar/deg)	8.90003	11.81044	11.60664	5.9135	7.06031	6.70314
PP (bar)	117.8493	116.0714	113.9847	113.7976	110.9171	108.6166
LPP (ATDC)	4.3	4.3	4.6	4.6	5	5.2
P Intake (bar)	1.72041	1.72046	1.72186	1.72123	1.72085	1.7178
P Exhaust (bar)	1.82678	1.82517	1.83772	1.83251	1.82218	1.81822
T Intake (C)	32.36011	32.78827	32.81643	33.79413	32.14167	31.65391
T Exhaust Tank (C)	332.412	339.2883	342.6341	335.8889	360.1843	362.5116
Gross Therm Eff	0.49063	0.47859	0.48009	0.49104	0.47694	0.47387
Net Therm Eff	0.46829	0.45659	0.45774	0.46747	0.45393	0.45187
Brake Therm Eff (CF)	0.41086	0.40064	0.40236	0.41089	0.39963	0.3983
Turbo Eff	0.65624	0.65144	0.64041	0.65706	0.64039	0.64016
Vol Eff	0.92758	0.93336	0.93248	0.92185	0.91891	0.92826
comb loss	0.00629	0.00729	0.00922	0.00573	0.00801	0.01043
Comb Eff	0.99371	0.99271	0.99078	0.99427	0.99199	0.98957
Exhaust Loss	0.32819	0.33045	0.33326	0.32735	0.3454	0.35027
Pumping Loss	0.02234	0.022	0.02235	0.02357	0.02301	0.022
Heat Transfer Loss	0.17489	0.18367	0.17742	0.17589	0.16965	0.16543
HC (ppm)	90.38545	113.2184	124.8256	96.76361	101.0995	105.5051
NOx (ppm)	849.3192	821.0768	788.3012	912.5613	836.7212	738.7256
CO2ex (ppm)	48076.42	47824.78	47603.95	51195.18	52164.93	51393.72
CO2in (ppm)	56.58943	55.00301	54.34651	80.95034	88.71388	90.71971
CO (ppm)	455.8578	508.4161	681.1545	414.9307	670.7926	917.0299
PM (mg/m^3)	8.6	12.53	18.68	25.3	60.6	92.04
HC (g/kg-fuel)	1.85876	2.33673	2.57821	1.87123	1.90964	2.01265
NOx (g/kg-fuel)	57.12576	55.4259	53.25296	58.83914	52.69554	46.98579
CO2ex (g/kg-fuel)	3093.761	3088.698	3076.721	3158.107	3143.151	3127.426
CO2in (g/kg-fuel)	3.64158	3.55229	3.5125	4.99363	5.34538	5.5205
CO (g/kg-fuel)	18.67006	20.89794	28.01899	16.29053	25.72389	35.51585
PM (g/kg-fuel)	0.22532	0.32747	0.48762	0.65939	1.6032	2.46111
HC (g/ikW-hr)	0.32031	0.4128	0.45404	0.32197	0.33829	0.35885
NOx (g/ikW-hr)	9.8441	9.79138	9.37816	10.12407	9.33491	8.37735
CO2ex (g/ikW-hr)	533.1269	545.6404	541.8287	543.3949	556.8027	557.6058
CO2in (g/ikW-hr)	0.62753	0.62754	0.61857	0.85922	0.94692	0.98428
CO (g/ikW-hr)	3.21729	3.69177	4.93431	2.803	4.55693	6.33231
PM (g/ikW-hr)	0.03883	0.05785	0.08587	0.11346	0.284	0.4388
Air Flow (kg/min)	2.88726	2.90127	2.90065	2.8574	2.86306	2.89169
AFR mass	42.81566	42.20542	42.11193	42.43409	41.2705	41.50293
AFR carbon	43.29172	43.44063	43.46256	41.51126	40.55617	40.93781
AFR Average	43.05369	42.82302	42.78724	41.97268	40.91333	41.22037
AFR Stoich	14.38064	14.38064	14.38064	14.42368	14.42368	14.42368
Phi mass	0.33587	0.34073	0.34149	0.33991	0.34949	0.34753
Phi carbon	0.33218	0.33104	0.33087	0.34746	0.35565	0.35233
GTE emisisons based	0.496085	0.483911	0.485428	0.4965	0.482243	0.479139
EXH emissions based	0.331839	0.334124	0.336965	0.33099	0.34924	0.354165
HX emisisons based	0.165786	0.174674	0.168387	0.16678	0.160507	0.156267

Table A. 7 Gasoline RCCI boost sweep

P Intake (bar)	**1.56188**	**1.88827**
RPM	1300	1300
IMEPg (bar)	8.18074	8.4843
IMEPn (bar)	8.03928	7.91892
BMEP_CF (bar)	6.90702	6.52875
FMEP_CF (bar)	1.13226	1.39017
CA50 (ATDC)	0.35487	4.95565
COV of IMEPg	2.26546	2.93685
COV of PPRR	10.43883	10.86481
EGR %	0	0
Fuel 1	91 Gasoline	91 Gasoline
Fuel 2	#2 ULSD	#2 ULSD
Fuel1 Flow (g/s)	0.78818	0.98896
Fuel2 Flow (g/s)	0.19097	0.00756
Fuel1 Fraction	0.80497	0.99241
Fuel2 Fraction	0.19503	0.00759
Fuel Energy (J/cyc)	3893.93691	4066.2382
Fuel H/C	1.85247	1.87916
Fuel O/C	0	0
Fuel MW/C	13.87729	13.90419
RI (MW/m^2)	2.74186	5.94339
Peak HRR (J/deg)	386.99996	591.1897
Peak PRR (bar/deg)	8.59381	12.8874
PP (bar)	117.38471	121.77908
LPP (ATDC)	3.8	7.2
P Intake (bar)	1.56188	1.88827
P Exhaust (bar)	1.45396	2.09571
T Intake (C)	32.4317	33.31331
T Exhaust Tank (C)	279.96214	250.37682
Gross Therm Eff	0.51426	0.50929
Net Therm Eff	0.5054	0.47536
Brake Therm Eff (CF)	0.43929	0.39191
Turbo Eff	0.71104	0.71098
Vol Eff	0.92712	0.92712
comb loss	0.03292	0.03827
Comb Eff	0.96708	0.96173
Exhaust Loss	0.30552	0.28293
Pumping Loss	0.00887	0.03394
Heat Transfer Loss	0.14876	0.16951
HC (ppm)	1020.76829	768.29376
NOx (ppm)	26.87652	0.50928
CO2ex (ppm)	41626.28037	36419.90236
CO2in (ppm)	65.3836	7.50361
CO (ppm)	873.22819	1554.46315
PM (mg/m^3)	8.8	1.41
HC (g/kg-fuel)	23.43359	19.81696
NOx (g/kg-fuel)	2.04521	0.04346
CO2ex (g/kg-fuel)	3030.58158	2973.405
CO2in (g/kg-fuel)	4.76022	0.61261
CO (g/kg-fuel)	40.46205	80.77137
PM (g/kg-fuel)	0.27635	0.03598
HC (g/ikW-hr)	3.81848	3.16885
NOx (g/ikW-hr)	0.33326	0.00695
CO2ex (g/ikW-hr)	493.83018	475.46598
CO2in (g/ikW-hr)	0.77567	0.09796
CO (g/ikW-hr)	6.59325	12.91585
PM (g/ikW-hr)	0.04503	0.00575
Air Flow (kg/min)	2.86757	3.15756
AFR mass	48.81055	52.80979
AFR carbon	48.76671	54.55721
AFR Average	48.78863	53.6835
AFR Stoich	14.53885	14.57689
Phi mass	0.29786	0.27603
Phi carbon	0.29813	0.26719
GTE emisisons based	0.5138	0.52615
EXH emissions based	0.30525	0.29229
HX emisisons based	0.14803	0.14329

Table A. 8 Gasoline HCCI and Gasoline/ULSD RCCI at Matched Conditions

Condition	32°C HCCI	42°C RCCI	57°C RCCI	66°C HCCI
RPM	1300	1300	1300	1300
IMEPg (bar)	8.34748	9.11862	9.03557	9.07788
IMEPn (bar)	7.7925	8.56034	8.48404	8.45028
BMEP_CF (bar)	6.41029	7.17563	7.09994	7.06004
FMEP_CF (bar)	1.38221	1.38471	1.3841	1.39025
CA50 (ATDC)	5.17722	4.93053	4.95211	5.84399
COV of IMEPg	3.0018	3.17837	2.45661	2.29989
COV of PPRR	11.31647	14.02674	13.50413	13.27315
EGR %	0	46.49533	45.81741	48.46197
Fuel 1	91 Gasoline	91 Gasoline	91 Gasoline	91 Gasoline
Fuel 2	#2 ULSD	#2 ULSD	#2 ULSD	#2 ULSD
Fuel1 Flow (g/s)	0.99244	0.93307	0.95579	1.02514
Fuel2 Flow (g/s)		0.10227	0.06811	
Fuel1 Fraction	1	0.90122	0.93348	1
Fuel2 Fraction	0	0.09878	0.06652	0
Fuel Energy (J/cyc)	4062.903	4210.59377	4169.00124	4258.54769
Fuel H/C	1.88	1.86906	1.87263	1.88
Fuel O/C	0	0	0	0
Fuel MW/C	13.905	13.89401	13.89761	13.905
RI (MW/m^2)	5.70223	1.78585	2.73515	3.95735
Peak HRR (J/deg)	571.26365	461.16324	536.70971	624.2197
Peak PRR (bar/deg)	12.53824	7.68127	9.35101	11.40872
PP (bar)	119.78782	120.41276	120.26001	121.79708
LPP (ATDC)	7.2	7.5	7.7	8.3
P Intake (bar)	1.8846	1.94382	1.91233	1.98247
P Exhaust (bar)	2.0963	2.13304	2.08763	2.25992
T Intake (C)	34.42543	43.68765	55.51413	64.97058
T Exhaust Tank (C)	228.50299	303.70562	318.80698	306.744
Gross Therm Eff	0.50149	0.5286	0.52902	0.52032
Net Therm Eff	0.46815	0.49624	0.49672	0.48435
Brake Therm Eff (CF)	0.38511	0.41597	0.41569	0.40466
Turbo Eff	0.74004	0.64956	0.64235	0.61199
Vol Eff	0.93024	0.9018	0.89194	0.91108
comb loss	0.04214	0.02322	0.01924	0.01636
Comb Eff	0.95786	0.97678	0.98076	0.98364
Exhaust Loss	0.25301	0.3173	0.30525	0.28352
Pumping Loss	0.03334	0.03236	0.03229	0.03597
Heat Transfer Loss	0.20335	0.13088	0.14649	0.1798
HC (ppm)	824.95747	968.45903	1072.22155	950.35734
NOx (ppm)	0.22576	1.47031	1.56709	2.23483
CO2ex (ppm)	35984.9866	75510.75857	79687.54876	82890.5907
CO2in (ppm)	6.04752	35316.57634	36720.99825	40370.37766
CO (ppm)	1740.17696	1842.30598	1092.93571	951.81516
PM (mg/m^3)	1.13	1.77	1.55	1.4
HC (g/kg-fuel)	21.38376	12.35426	13.08652	11.19818
NOx (g/kg-fuel)	0.01936	0.0621	0.06331	0.08713
CO2ex (g/kg-fuel)	2952.3226	3051.18213	3079.93498	3091.77527
CO2in (g/kg-fuel)	0.49616	1427.04574	1419.27175	1505.79377
CO (g/kg-fuel)	90.86521	47.37866	26.88484	22.59524
PM (g/kg-fuel)	0.02759	0.02453	0.02148	0.01729
HC (g/ikW-hr)	3.47202	1.90972	2.01895	1.7534
NOx (g/ikW-hr)	0.00314	0.0096	0.00977	0.01364
CO2ex (g/ikW-hr)	479.36074	471.65042	475.16279	484.10618
CO2in (g/ikW-hr)	0.08056	220.59212	218.96083	235.77524
CO (g/ikW-hr)	14.75354	7.32377	4.14771	3.53793
PM (g/ikW-hr)	0.00448	0.00379	0.00331	0.00271
Air Flow (kg/min)	3.15057	1.63626	1.5543	1.52176
AFR mass	52.74478	26.33988	25.3001	24.29251
AFR carbon	54.80376	27.47339	26.34122	25.46592
AFR Average	53.77427	26.90664	25.82066	24.87921
AFR Stoich	14.5776	14.56251	14.56759	14.57523
Phi mass	0.27638	0.55287	0.57579	0.59999
Phi carbon	0.266	0.53006	0.55303	0.57234
GTE emisisons based	0.52107	0.55135	0.55079	0.54545
EXH emissions based	0.26289	0.33095	0.31781	0.29722
HX emisisons based	0.1739	0.09448	0.11216	0.14097
charge based PHI	0.27638	0.29581	0.31198	0.30922
Emission charge based PHI	0.266	0.28361	0.29965	0.29497

Table A. 9 Charge Preparation Strategies HCCI to Diesel Pilot

Condition	HCCI	RCCI single 320	RCCI double 320/35	RCCI single 60	RCCI double 60/35	RCCI single 35
RPM	1300	1300	1300	1300	1300	1300
IMEPg (bar)	8.08275	8.04098	8.05925	8.05665	8.11855	8.03093
IMEPn (bar)	7.4454	7.41446	7.43157	7.42024	7.48057	7.40591
BMEP_CF (bar)	6.41031	6.38715	6.40176	6.04543	6.45348	6.37491
FMEP_CF (bar)	1.03509	1.02731	1.02981	1.37481	1.0271	1.031
CA50 (ATDC)	5.4026	5.19773	4.97182	5.68687	4.95812	4.97742
COV of IMEPg	3.84625	4.24054	3.70031	4.56297	4.35119	4.25018
COV of PPRR	11.24729	10.83887	10.02083	47.83129	14.26031	12.29778
EGR %	45.7745	45.08454	45.15788	45.16936	45.18448	45.07784
Fuel 1	91 Gasoline	91 Gasoline	91 Gasoline	91 Gasoline	91 Gasoline	91 Gasoline
Fuel 2	#2 ULSD	#2 ULSD	#2 ULSD	#2 ULSD	#2 ULSD	#2 ULSD
Fuel1 Flow (g/s)	0.94626	0.89983	0.896	0.90668	0.89307	0.92678
Fuel2 Flow (g/s)	0	0.03882	0.03564	0.03177	0.04752	0.02277
Fuel1 Fraction	1	0.95864	0.96174	0.96614	0.94948	0.97602
Fuel2 Fraction	0	0.04136	0.03826	0.03386	0.05052	0.02398
Fuel Energy (J/cyc)	3784.75864	3740.14232	3712.34188	3825.63228	3584.9633	3784.36583
Fuel H/C	1.88	1.87415	1.87459	1.87625	1.87286	1.87661
Fuel O/C	0	0	0	0	0	0
Fuel MW/C	13.905	13.89915	13.89959	13.90126	13.89784	13.90162
RI (MW/m^2)	4.33034	3.75254	3.58265	2.17224	1.73028	2.75329
Peak HRR (J/deg)	517.57098	477.18397	463.54335	394.17958	378.26974	423.716
Peak PRR (bar/deg)	12.25811	11.29942	11.08968	8.62078	7.6662	9.74646
PP (bar)	122.72847	119.20333	120.44317	117.93865	116.19139	120.1652
LPP (ATDC)	7.1	7	6.9	7.2	7.6	7
P Intake (bar)	2.07796	2.01628	2.0158	2.01401	2.01285	2.0072
P Exhaust (bar)	2.35047	2.2777	2.27887	2.28242	2.28764	2.27814
T Intake (C)	61.84443	51.70988	53.72386	52.0155	49.31323	50.94992
T Exhaust Tank (C)	294.30346	280.62721	281.6475	281.8596	283.81819	281.68052
Gross Therm Eff	0.50931	0.51307	0.51805	0.51404	0.51713	0.50623
Net Therm Eff	0.46915	0.47309	0.4777	0.47343	0.47649	0.46683
Brake Therm Eff (CF)	0.398	0.40166	0.40554	0.38572	0.4052	0.39597
Turbo Eff	0.64883	0.66418	0.66184	0.65857	0.65339	0.65787
Vol Eff	0.98227	0.98842	0.99268	0.99322	0.98778	0.98889
comb loss	0.03021	0.03721	0.03736	0.06186	0.05508	0.03945
Comb Eff	0.96979	0.96279	0.96264	0.93814	0.94492	0.96055
Exhaust Loss	0.34177	0.34224	0.34277	0.34457	0.3514	0.34009
Pumping Loss	0.04016	0.03998	0.04035	0.0406	0.04064	0.0394
Heat Transfer Loss	0.1187	0.10748	0.10182	0.07953	0.07639	0.11423
HC (ppm)	866.1666	934.6748	933.19075	983.60657	920.6717	969.44529
NOx (ppm)	1.04405	0.47213	0.46333	0.66081	0.60704	0.65201
CO2ex (ppm)	61017.69742	58777.16133	59148.82558	57958.64437	57621.84725	58918.56636
CO2in (ppm)	28140.94342	26712.48709	26923.14049	26392.28982	26248.81546	26772.31562
CO (ppm)	2337.48206	3042.22018	3100.3757	6683.04505	5680	3312.9128
PM (mg/m^3)	0.69	0.32	0.75	0.96	1.44	0.6
HC (g/kg-fuel)	13.47658	14.88173	14.75739	14.97532	14.32402	15.32574
NOx (g/kg-fuel)	0.05374	0.02488	0.02425	0.03329	0.03126	0.03411
CO2ex (g/kg-fuel)	3004.87889	2963.22566	2961.65674	2793.63768	2838.58997	2948.73769
CO2in (g/kg-fuel)	1385.82953	1346.69871	1348.0758	1272.12249	1293.07941	1339.89235
CO (g/kg-fuel)	73.26241	97.61319	98.80176	205.01611	178.08427	105.52509
PM (g/kg-fuel)	0.01071	0.00511	0.01204	0.01536	0.02308	0.00947
HC (g/ikW-hr)	2.15455	2.36509	2.32252	2.37482	2.25934	2.46698
NOx (g/ikW-hr)	0.00859	0.00395	0.00382	0.00528	0.00493	0.00549
CO2ex (g/ikW-hr)	480.40015	470.93213	466.10548	443.02079	447.73352	474.65707
CO2in (g/ikW-hr)	221.55725	214.02477	212.16015	201.73579	203.95866	215.68191
CO (g/ikW-hr)	11.71271	15.51323	15.54942	32.51187	28.0894	16.98633
PM (g/ikW-hr)	0.00171	8.12E-04	0.0019	0.00244	0.00364	0.00152
Air Flow (kg/min)	1.82626	1.86216	1.85576	1.86447	1.8682	1.85924
AFR mass	32.06794	33.06426	33.19866	33.1124	33.10332	32.63393
AFR carbon	33.26069	33.99289	33.76599	32.40228	33.13623	33.74108
AFR Average	32.66431	33.52857	33.48232	32.75734	33.11978	33.1875
AFR Stoich	14.57747	14.56977	14.57039	14.57275	14.57012	14.57326
Phi mass	0.45458	0.44065	0.43888	0.4401	0.44014	0.44657
Phi carbon	0.43828	0.42861	0.43151	0.44974	0.4397	0.43191
GTE emisisons based	0.52826	0.52748	0.5269	0.50302	0.51764	0.52341
EXH emissions based	0.34177	0.34224	0.34277	0.34457	0.3514	0.34009
HX emisisons based	0.1187	0.10748	0.10182	0.07953	0.07639	0.11423
charge based PHI	0.2465	0.24198	0.24069	0.24131	0.24127	0.24526
Emission charge based	0.23766	0.23537	0.23665	0.2466	0.24103	0.23722

Oil Matrix Conditions

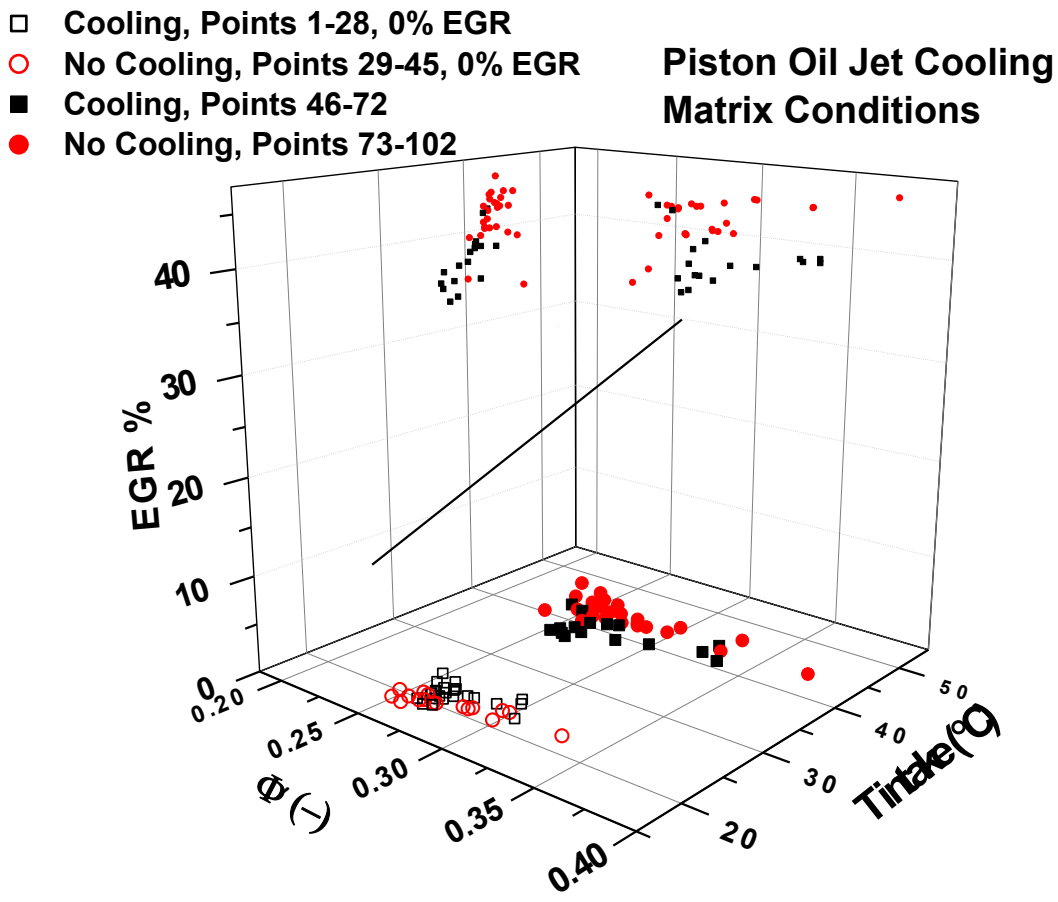

Figure A. 2 Oil Matrix Conditions

Table A. 10 0% EGR 22°C intake temperature Piston Oil Cooling On

MATRIX POINT	1	2	3	4	5	6	7	8	9
RPM	1300	1300	1300	1300	1300	1300	1300	1300	1300
IMEPg (bar)	6.75999	6.74369	6.96402	7.4639	6.67166	6.6638	6.74547	6.76276	6.74464
IMEPn (bar)	6.37564	6.35943	6.50853	7.00266	6.27825	6.26632	6.25899	6.29231	6.2757
BMEP_CF (bar)	5.2162	5.1979	5.30506	5.76576	5.11921	5.09761	5.08453	5.10039	5.07911
FMEP_CF (bar)	1.15944	1.16153	1.20347	1.2369	1.15904	1.16872	1.17446	1.19192	1.19659
CA50 (ATDC)	1.18434	0.92019	0.99159	1.58905	2.1816	1.54054	1.42939	0.30309	0.25744
COV of IMEPg	5.12189	3.46406	2.92969	2.87076	3.08941	2.91538	3.03354	2.77299	2.93249
COV of PPRR	10.79466	9.14651	8.70295	8.39937	9.09412	8.33575	8.60949	7.72334	7.91263
EGR %	0.04582	0.07734	0	0	0	0	0	0	0
Fuel 1	E85	E85	E85	E85	E85	E85	E85	E85	E85
Fuel 2	EHN + 91 Gasoline	EHN + 91 Gasoline	EHN + 91 Gasoline	EHN + 91 Gasoline	EHN + 91 Gasoline	EHN + 91 Gasoline	EHN + 91 Gasoline	EHN + 91 Gasoline	EHN + 91 Gasoline
Fuel1 Flow (g/s)	0.72225	0.71937	0.80868	0.91936	0.76333	0.74494	0.7679	0.73557	0.74487
Fuel2 Flow (g/s)	0.22678	0.23153	0.19351	0.17277	0.20849	0.21763	0.20961	0.22513	0.2324
Fuel1 Fraction	0.76104	0.75652	0.80691	0.84181	0.78546	0.77391	0.78557	0.76566	0.76219
Fuel2 Fraction	0.23896	0.24348	0.19309	0.15819	0.21454	0.22609	0.21443	0.23434	0.23781
Fuel Energy (J/cyc)	2840.6866	2851.557	2943.158	3160.303817	2879.681	2865.926	2896.373	2870.128	2923.81
Fuel H/C	2.47859	2.4739	2.52736	2.56584	2.50431	2.49208	2.50442	2.48342	2.4798
Fuel O/C	0.26945	0.26739	0.29085	0.30773	0.28073	0.27537	0.28078	0.27157	0.26998
Fuel MW/C	18.81962	18.7819	19.21112	19.52001	19.02607	18.92785	19.02698	18.85838	18.8293
RI (MW/m^2)	4.89351	4.35284	3.77967	4.06968	1.70612	1.97126	2.29902	2.81871	3.11726
Peak HRR (J/deg)	400.60904	373.8419	363.2872	401.54862	300.5468	302.5461	317.4827	310.2524	319.3633
Peak PRR (bar/deg)	11.44617	10.81773	10.51403	11.18235	6.92294	7.4888	8.09458	9.05662	9.54581
PP (bar)	122.82019	123.2379	131.6257	138.31282	122.7392	124.6751	125.8235	129.3155	130.2491
LPP (ATDC)	4.2	4.1	4.3	4.9	5.1	4.7	4.8	3.9	3.7
P Intake (bar)	1.23775	1.23906	1.36702	1.44285	1.36658	1.36745	1.36871	1.36711	1.36697
P Exhaust (bar)	1.35261	1.35841	1.52427	1.6031	1.48644	1.48706	1.57908	1.56454	1.56256
T Intake (C)	24.5084	25.16163	22.78926	22.88359	21.17546	21.31539	20.79299	21.34361	19.83872
T Exhaust Tank (C)	276.02033	261.1389	239.3876	244.82804	227.274	228.3225	232.2656	235.4207	237.3208
Gross Therm Eff	0.58086	0.57725	0.57755	0.57647	0.56551	0.56755	0.56846	0.57513	0.56306
Net Therm Eff	0.54783	0.54435	0.53978	0.54085	0.53216	0.53369	0.52746	0.53512	0.52391
Brake Therm Eff (CF)	0.4482	0.44493	0.43997	0.44532	0.43392	0.43416	0.42849	0.43376	0.42402
Turbo Eff	0.79524	0.79783	0.7064	0.70144	0.79321	0.79261	0.6289	0.64302	0.64331
Vol Eff	0.92697	0.93004	0.92849	0.93062	0.93977	0.93923	0.92804	0.92975	0.92263
comb loss	0.02634	0.02876	0.02995	0.03103	0.06061	0.0601	0.05639	0.05006	0.04672
Comb Eff	0.97366	0.97124	0.97005	0.96897	0.93939	0.9399	0.94361	0.94994	0.95328
Exhaust Loss	0.31533	0.29545	0.29192	0.29456	0.28681	0.28934	0.28977	0.29567	0.29407
Pumping Loss	0.03303	0.03289	0.03778	0.03562	0.03335	0.03385	0.041	0.04001	0.03915
Heat Transfer Loss	0.07747	0.09854	0.10058	0.09793	0.08707	0.08301	0.08538	0.07914	0.09615
HC (ppm)	677.36199	716.5102	505.6635	594.22264	950.1619	1030.953	1084.032	1020.758	1003.972
NOx (ppm)	110.12125	145.3772	79.37127	61.4412	37.06159	48.71614	48.93904	76.91151	80.6647
CO2ex (ppm)	41727.403	40786.89	37611.45	38004.156	33230.13	33537.45	34478.08	35097.04	35671.57
CO2in (ppm)	406.94165	419.2433	370.8959	380.76783	23.42208	21.76336	20.72262	23.32662	33.51329
CO (ppm)	1007.4008	1099.446	1470.303	1401.72578	2791.522	2602.099	2271.693	1909.913	1707.253
PM (mg/m^3)	0	2.05	1.13	1.31	0.96	0.77	0.77	0.8	0.78
HC (g/kg-fuel)	15.59031	16.80391	12.76544	14.84458	25.67103	27.70244	28.6159	26.81027	26.12588
NOx (g/kg-fuel)	6.19515	8.35031	4.7978	3.61706	2.42091	3.18133	3.12326	4.92746	5.1281
CO2ex (g/kg-fuel)	2245.9283	2241.406	2175.168	2140.52925	2076.729	2095.362	2105.183	2151.274	2169.645
CO2in (g/kg-fuel)	21.90315	23.03913	21.44987	21.4462	1.46377	1.35974	1.26529	1.42981	2.03837
CO (g/kg-fuel)	34.50949	38.45347	54.11793	50.24755	111.0326	103.47	88.27918	74.50759	66.08855
PM (g/kg-fuel)	0	0.04956	0.02582	0.02848	0.02281	0.0185	0.01755	0.01875	0.018
HC (g/ikW-hr)	2.97978	3.22582	2.50104	2.95713	5.09089	5.44781	5.64563	5.18514	5.15373
NOx (g/ikW-hr)	1.18408	1.603	0.94	0.72054	0.4801	0.62562	0.61619	0.95298	1.0116
CO2ex (g/ikW-hr)	429.2652	430.2791	426.1643	426.40587	411.8415	412.0626	415.3312	416.0587	427.9953
CO2in (g/ikW-hr)	4.18636	4.42278	4.20251	4.27221	0.29028	0.2674	0.24963	0.27653	0.4021
CO (g/ikW-hr)	6.59581	7.38185	10.60292	10.0096	22.01916	20.34786	17.41658	14.40985	13.03696
PM (g/ikW-hr)	0	0.00951	0.00506	0.00567	0.00452	0.00364	0.00346	0.00363	0.00355
Air Flow (kg/min)	2.12967	2.13361	2.3707	2.50715	2.41189	2.41091	2.38859	2.38574	2.37939
AFR mass	37.40071	37.39665	39.42544	38.26107	41.36359	41.7444	40.72566	41.38885	40.57881
AFR carbon	36.08458	36.82091	38.6884	37.68522	41.64616	41.64442	40.72653	40.91315	40.61753
AFR Average	36.74264	37.10878	39.05692	37.97314	41.50487	41.69441	40.7261	41.151	40.59817
AFR Stoich	10.8805	10.90129	10.66948	10.50898	10.76814	10.82129	10.76765	10.85921	10.87517
Phi mass	0.29092	0.2915	0.27062	0.27466	0.26033	0.25923	0.26439	0.26237	0.268
Phi carbon	0.30153	0.29606	0.27578	0.27886	0.25856	0.25985	0.26439	0.26542	0.26775
Phi Lambda meter	0.30879	0.30274	0.28023	0.28317	0.25889	0.25985	0.26474	0.26552	0.26881
GTE emisisons based	0.56042	0.56836	0.56676	0.5678	0.56937	0.56619	0.56847	0.56852	0.5636
EXH emissions based	0.30021	0.28543	0.28159	0.28464	0.28299	0.28392	0.28456	0.28832	0.2887
HX emisisons based	0.11061	0.11867	0.12111	0.11652	0.08856	0.08934	0.09083	0.09096	0.1019
charge based PHI	0.30027	0.29654	0.27555	0.2789	0.25926	0.25964	0.26451	0.26444	0.26818
Emission charge based PHI	0.2960865	0.293556	0.273202	0.276763495	0.259446	0.259538	0.264392	0.263896	0.267874

Table A. 10 0% EGR 22°C intake temperature Piston Oil Cooling On Continued

MATRIX POINT	10	11	12	13	14	15	16	17	18
RPM	1300	1300	1300	1300	1300	1300	1300	1300	1300
IMEPg (bar)	6.70224	6.75736	6.76646	6.65191	6.77157	6.68812	6.73254	6.75128	6.73131
IMEPn (bar)	6.22988	6.25025	6.25766	6.14096	6.26285	6.20576	6.24559	6.29101	6.27425
BMEP_CF (bar)	5.05009	5.06102	5.05193	4.94494	5.04856	5.0268	5.05916	5.12386	5.11394
FMEP_CF (bar)	1.17979	1.18923	1.20573	1.19602	1.2143	1.17895	1.18643	1.16714	1.16031
CA50 (ATDC)	1.14457	1.62532	0.68351	1.84312	1.14815	1.13825	0.82112	1.11806	0.62304
COV of IMEPg	3.036	3.25415	3.05571	3.54437	3.48376	3.18728	2.92338	2.58146	2.41636
COV of PPRR	8.53903	9.05645	8.35593	10.54672	10.10264	8.71457	8.17611	6.83852	7.20264
EGR %	0	0	0	0	0	0	0	0	0
Fuel 1	E85	E85	E85	E85	E85	E85	E85	E85	E85
Fuel 2	EHN + 91 Gasoline	EHN + 91 Gasoline	EHN + 91 Gasoline	EHN + 91 Gasoline	EHN + 91 Gasoline	EHN + 91 Gasoline	EHN + 91 Gasoline	EHN + 91 Gasoline	EHN + 91 Gasoline
Fuel1 Flow (g/s)	0.76493	0.79703	0.78165	0.82038	0.79562	0.77473	0.77143	0.7638	0.7318
Fuel2 Flow (g/s)	0.21008	0.20394	0.21393	0.18305	0.20633	0.21029	0.21464	0.23414	0.2466
Fuel1 Fraction	0.78453	0.79626	0.78512	0.81757	0.79407	0.78651	0.78233	0.76538	0.74795
Fuel2 Fraction	0.21547	0.20374	0.21488	0.18243	0.20593	0.21349	0.21767	0.23462	0.25205
Fuel Energy (J/cyc)	2890.2103	2952.733	2950.458	2933.621813	2958.274	2917.507	2925.676	2981.752	2944.367
Fuel H/C	2.50332	2.51585	2.50395	2.53899	2.51351	2.50542	2.50098	2.48312	2.46504
Fuel O/C	0.2803	0.2858	0.28057	0.29595	0.28477	0.28122	0.27927	0.27144	0.26351
Fuel MW/C	19.0181	19.11874	19.02314	19.30445	19.09991	19.03501	18.99931	18.85596	18.71085
RI (MW/m^2)	2.56274	2.13741	2.52692	1.49764	1.95304	2.58162	2.91289	3.64622	5.15018
Peak HRR (J/deg)	323.4585	317.7514	311.4281	286.74478	299.3226	325.3585	331.3193	365.0617	389.3324
Peak PRR (bar/deg)	8.57514	7.93568	8.70905	6.72859	7.76104	8.59817	9.16449	10.01455	11.72143
PP (bar)	126.89058	128.7788	132.0779	130.13507	133.7909	126.7223	128.2182	124.3608	122.9941
LPP (ATDC)	4.5	4.5	4	4.4	4.5	4.5	4.4	4.4	3.7
P Intake (bar)	1.36832	1.42846	1.42691	1.49836	1.49502	1.36677	1.36764	1.29166	1.22109
P Exhaust (bar)	1.5647	1.66213	1.65372	1.68373	1.68879	1.55967	1.56683	1.47243	1.39833
T Intake (C)	19.46011	19.87968	21.85807	23.12994	24.57087	21.12731	22.01455	23.25676	22.24529
T Exhaust Tank (C)	237.17107	235.0214	236.084	228.28044	229.9488	238.1491	240.9534	252.22	259.0818
Gross Therm Eff	0.56602	0.5586	0.55978	0.55346	0.55872	0.55955	0.56169	0.55266	0.55802
Net Therm Eff	0.52613	0.51668	0.51769	0.51095	0.51675	0.51919	0.52107	0.51498	0.52013
Brake Therm Eff (CF)	0.42649	0.41837	0.41794	0.41143	0.41656	0.42056	0.42208	0.41944	0.42394
Turbo Eff	0.64305	0.6194	0.62541	0.69985	0.68877	0.64962	0.63766	0.63293	0.61066
Vol Eff	0.92202	0.92478	0.93025	0.93498	0.94147	0.92511	0.92522	0.92375	0.91633
comb loss	0.05139	0.06023	0.05487	0.09566	0.06578	0.05343	0.04712	0.03838	0.03266
Comb Eff	0.94861	0.93977	0.94513	0.90434	0.93422	0.94657	0.95288	0.96162	0.96734
Exhaust Loss	0.29828	0.30167	0.30004	0.30368	0.30144	0.29354	0.29464	0.28389	0.27983
Pumping Loss	0.03989	0.04192	0.04209	0.04251	0.04197	0.04036	0.04063	0.03768	0.03789
Heat Transfer Loss	0.0843	0.0795	0.08531	0.04719	0.07406	0.09349	0.09655	0.12507	0.12948
HC (ppm)	1006.0302	983.2232	991.6277	1052.579	1057.328	1114.802	1035.758	982.1678	1031.696
NOx (ppm)	57.28229	36.1778	53.17323	30.48397	36.85433	59.65993	70.7621	88.50642	144.6225
CO2ex (ppm)	34785.713	33239.05	33837.28	30642.0251	31843.96	35085.94	35749.22	38522.71	41393.17
CO2in (ppm)	17.27776	19.87325	16.97162	19.18577	22.41747	23.99545	29.51037	24.41851	29.10473
CO (ppm)	2029.4749	2682.268	2257.296	5404.76417	2793.802	2006.386	1681.468	1260.937	825.4246
PM (mg/m^3)	0.78	0.78	0.78	0.78	0.84	0.84	0.74	0.69	0.58
HC (g/kg-fuel)	26.56796	26.6115	26.70719	28.33785	29.58449	29.13942	26.89314	24.06475	23.8248
NOx (g/kg-fuel)	3.65896	2.35591	3.46297	1.95562	2.48353	3.76852	4.4484	5.29029	8.21065
CO2ex (g/kg-fuel)	2125.8485	2070.894	2108.357	1880.71811	2053.059	2120.384	2150.123	2203.003	2248.351
CO2in (g/kg-fuel)	1.05589	1.23816	1.05748	1.17757	1.44531	1.45014	1.77489	1.39642	1.58088
CO (g/kg-fuel)	78.93631	106.3588	89.51566	211.12746	114.6388	77.17165	64.36459	45.89374	28.53478
PM (g/kg-fuel)	0.01805	0.01764	0.0178	0.01807	0.01951	0.01925	0.01695	0.01555	0.0131
HC (g/ikW-hr)	5.2619	5.36673	5.34976	5.81977	5.95956	5.84278	5.36245	4.84282	4.71457
NOx (g/ikW-hr)	0.72467	0.47511	0.69367	0.40163	0.50029	0.75563	0.887	1.06463	1.62476
CO2ex (g/ikW-hr)	421.03368	417.6366	422.3288	386.24503	413.5722	425.161	428.7314	443.3353	444.9144
CO2in (g/ikW-hr)	0.20912	0.2497	0.21183	0.24184	0.29115	0.29077	0.35391	0.28102	0.31283
CO (g/ikW-hr)	15.63369	21.44934	17.93104	43.35947	23.09307	15.47379	12.83421	9.23572	5.6466
PM (g/ikW-hr)	0.00358	0.00356	0.00356	0.00371	0.00393	0.00386	0.00338	0.00313	0.00259
Air Flow (kg/min)	2.38325	2.49185	2.4871	2.61363	2.61321	2.37498	2.36963	2.22506	2.09375
AFR mass	40.73879	41.4905	41.63591	43.41133	43.46899	40.18478	40.0519	37.16055	35.6662
AFR carbon	40.78163	41.52077	41.55271	40.74299	42.92959	40.33025	40.1658	38.25845	36.40009
AFR Average	40.76021	41.50563	41.59431	42.07716	43.19929	40.25751	40.10885	37.7095	36.03315
AFR Stoich	10.77243	10.7185	10.76972	10.62045	10.72854	10.76333	10.78257	10.86054	10.94069
Phi mass	0.26443	0.25834	0.25866	0.24465	0.24681	0.26785	0.26921	0.29226	0.30675
Phi carbon	0.26415	0.25815	0.25918	0.26067	0.24991	0.26688	0.26845	0.28387	0.30057
Phi Lambda meter	0.26545	0.25672	0.25758	0.24225	0.24724	0.26736	0.269	0.2886	0.30702
GTE emisisons based	0.56662	0.55901	0.55866	0.51944	0.55179	0.56157	0.56329	0.56899	0.56951
EXH emissions based	0.29278	0.29708	0.29503	0.29316	0.29493	0.28885	0.28974	0.28241	0.27628
HX emisisons based	0.09033	0.08278	0.08991	0.06723	0.08321	0.09716	0.10077	0.11877	0.12937
charge based PHI	0.26468	0.25773	0.25848	0.24919	0.24799	0.26736	0.26889	0.28825	0.30478
Emission charge based PHI	0.2642881	0.258242	0.258923	0.252658111	0.24836	0.267363	0.268833	0.288066	0.30366

Table A. 10 0% EGR 22°C intake temperature Piston Oil Cooling On Continued

MATRIX POINT	19	20	21	22	23	24	25	26	27	28
RPM	1300	1300	1300	1300	1300	1300	1300	1300	1300	1300
IMEPg (bar)	6.65795	6.6968	6.64052	6.64736	6.71924	7.09304	6.97407	7.03735	6.99022	7.04415
IMEPn (bar)	6.27465	6.21767	6.24503	6.15686	6.25542	6.52007	6.39425	6.4458	6.40756	6.46856
BMEP_CF (bar)	5.09364	5.02669	5.03172	4.93938	5.06757	5.24456	5.11797	5.16953	5.1275	5.18962
FMEP_CF (bar)	1.181	1.19098	1.21332	1.21748	1.18785	1.2755	1.27628	1.27627	1.28005	1.27894
CA50 (ATDC)	1.49893	0.75404	-1.22937	-1.62919	1.03514	1.2798	0.94752	1.12371	0.98458	1.03458
COV of IMEPg	2.9258	3.12583	2.95447	2.84677	3.15108	3.50926	3.74986	3.73936	3.46564	3.58353
COV of PPRR	8.04959	9.46803	8.27137	7.59432	9.61105	8.1352	8.30589	8.68555	8.62277	8.37426
EGR %	0	0	0	0	0	0	0	0	0	0
Fuel 1	E85	E85	E85	E85	E85	E85	E85	E85	E85	E85
Fuel 2	EHN + 91 Gasoline	EHN + 91 Gasoline	EHN + 91 Gasoline	EHN + 91 Gasoline	EHN + 91 Gasoline	EHN + 91 Gasoline	EHN + 91 Gasoline	EHN + 91 Gasoline	EHN + 91 Gasoline	EHN + 91 Gasoline
Fuel1 Flow (g/s)	0.76462	0.79753	0.77871	0.76943	0.85396	0.85821	0.83986	0.79364	0.77699	0.92604
Fuel2 Flow (g/s)	0.21132	0.17204	0.20492	0.20414	0.14513	0.20558	0.19819	0.23411	0.26101	0.14299
Fuel1 Fraction	0.78347	0.82256	0.79167	0.79032	0.85474	0.80675	0.80907	0.77221	0.74855	0.86624
Fuel2 Fraction	0.21653	0.17744	0.20833	0.20968	0.14526	0.19325	0.19093	0.22779	0.25145	0.13376
Fuel Energy (J/cyc)	2894.2488	2828.655	2907.128	2879.01303	2875.195	3124.254	3045.709	3062.144	3122.977	3061.315
Fuel H/C	2.50219	2.54447	2.51093	2.50949	2.58041	2.52719	2.52971	2.49029	2.46566	2.59352
Fuel O/C	0.2798	0.29835	0.28364	0.28301	0.31412	0.29077	0.29188	0.27458	0.26377	0.31988
Fuel MW/C	19.00908	19.34843	19.07924	19.06766	19.637	19.20971	19.22998	18.91353	18.71576	19.74228
RI (MW/m^2)	2.71911	2.69591	3.25616	3.61137	2.68809	2.94685	3.80303	4.06085	4.65231	3.44056
Peak HRR (J/deg)	333.13815	315.8232	285.0959	289.10555	323.972	352.5643	365.1644	386.8218	400.7858	356.9871
Peak PRR (bar/deg)	8.85969	8.86435	9.86657	10.39582	8.81211	9.99579	11.3331	11.71195	12.55603	10.78915
PP (bar)	127.13263	129.1286	133.5951	134.42795	128.5012	146.0327	146.1876	146.1853	146.9423	146.7191
LPP (ATDC)	4.7	4.2	2.6	2.1	4.6	4.4	4.1	3.9	3.7	4.1
P Intake (bar)	1.36537	1.36938	1.3661	1.36711	1.36561	1.67877	1.67815	1.67897	1.67646	1.67906
P Exhaust (bar)	1.46358	1.56194	1.44754	1.53366	1.52581	1.88562	1.88926	1.88697	1.88018	1.88792
T Intake (C)	22.67888	24.06476	22.91498	23.15414	22.11844	27.47713	31.69575	29.43618	31.86877	29.46739
T Exhaust Tank (C)	224.57083	219.7758	232.4541	237.67699	240.4163	234.9749	231.5015	229.3798	229.2547	230.6975
Gross Therm Eff	0.5615	0.57787	0.55755	0.56357	0.57042	0.55416	0.55891	0.56096	0.54635	0.56165
Net Therm Eff	0.52917	0.53653	0.52434	0.52199	0.53105	0.50939	0.51244	0.5138	0.50081	0.51576
Brake Therm Eff (CF)	0.42957	0.43376	0.42247	0.41877	0.43021	0.40974	0.41016	0.41207	0.40076	0.41378
Turbo Eff	0.51256	0.66931	0.89412	0.69389	0.701	0.71134	0.55464	0.71894	0.72204	0.55675
Vol Eff	0.94538	0.94231	0.93822	0.93025	0.93052	0.93618	0.93693	0.93061	0.93671	0.93091
comb loss	0.03827	0.03371	0.04519	0.03681	0.03924	0.06449	0.06112	0.06441	0.06368	0.05671
Comb Eff	0.96173	0.96629	0.95481	0.96319	0.96076	0.93551	0.93888	0.93559	0.93632	0.94329
Exhaust Loss	0.28163	0.27814	0.28867	0.29583	0.30212	0.3217	0.31404	0.3127	0.30207	0.31487
Pumping Loss	0.03233	0.04134	0.03321	0.04159	0.03938	0.04476	0.04647	0.04715	0.04554	0.04589
Heat Transfer Loss	0.1186	0.11027	0.10859	0.10378	0.08821	0.05966	0.06592	0.06193	0.0879	0.06677
HC (ppm)	449.1719	426.0598	1102.14	847.89744	793.9692	845.4178	818.0118	857.132	878.9322	782.9063
NOx (ppm)	41.33196	69.38948	138.696	154.58469	79.80926	16.44299	17.9867	14.70277	12.43756	16.26799
CO2ex (ppm)	34367.976	35182.19	35428.22	35810.50857	35519.84	29662.37	30121.99	29927.99	30070.31	30245.19
CO2in (ppm)	55.77395	78.33804	87.03495	93.37102	95.92657	153.4088	157.3818	150.8415	153.2637	149.5174
CO (ppm)	2080.0263	1806.99	1318.687	1179.64707	1495.615	2821.626	2676.47	2827.071	2734.987	2415.125
PM (mg/m^3)	0.76	1.12	1.11	1.06	1.1	1.31	0.57	0.5	0.96	0.98
HC (g/kg-fuel)	12.16705	11.38138	29.08099	22.38568	20.97863	25.34028	24.31012	25.47528	26.06693	23.38768
NOx (g/kg-fuel)	2.70929	4.40687	8.82334	9.84586	4.9398	1.18021	1.27867	1.06281	0.90661	1.13233
CO2ex (g/kg-fuel)	2155.3462	2137.73	2156.315	2182.18421	2103.394	2036.931	2048.726	2069.796	2097.086	2014.131
CO2in (g/kg-fuel)	3.4978	4.75995	5.29732	5.68975	5.68053	10.53467	10.70421	10.43208	10.68852	9.95688
CO (g/kg-fuel)	83.02208	69.87916	51.08179	45.75039	56.36783	123.3195	115.8575	124.4367	121.3935	102.3606
PM (g/kg-fuel)	0.01805	0.02538	0.02654	0.02478	0.02534	0.02983	0.01302	0.01151	0.02186	0.02174
HC (g/ikW-hr)	2.42808	2.24337	5.86455	4.46359	4.24677	5.17402	4.92624	5.06514	5.26979	4.83221
NOx (g/ikW-hr)	0.54067	0.86863	1.77934	1.96322	0.99998	0.24098	0.25911	0.21131	0.18328	0.23395
CO2ex (g/ikW-hr)	430.12546	421.365	434.8483	435.1166	425.7967	415.9037	415.1572	411.5285	423.9551	416.1466
CO2in (g/ikW-hr)	0.69803	0.93823	1.06827	1.13451	1.14993	2.15098	2.16912	2.07416	2.16083	2.05723
CO (g/ikW-hr)	16.56806	13.77378	10.30129	9.1224	11.41072	25.17956	23.47756	24.74121	24.54138	21.14908
PM (g/ikW-hr)	0.0036	0.005	0.00535	0.00494	0.00513	0.00609	0.00264	0.00229	0.00442	0.00449
Air Flow (kg/min)	2.41183	2.39981	2.39292	2.37244	2.37885	2.88969	2.85093	2.85424	2.84576	2.85504
AFR mass	41.1882	41.25225	40.54565	40.61401	39.68341	45.27378	45.77366	46.28629	45.69283	44.51111
AFR carbon	41.8671	40.59181	40.65103	40.72447	39.56158	45.68714	45.2682	46.01769	46.41001	44.33773
AFR Average	41.52765	40.92203	40.59834	40.66924	39.6225	45.48046	45.52093	46.15199	46.05142	44.42442
AFR Stoich	10.7773	10.5975	10.7396	10.7458	10.4495	10.67023	10.65954	10.82908	10.93796	10.39658
Phi mass	0.26166	0.2569	0.26488	0.26458	0.26332	0.23568	0.23287	0.23396	0.23938	0.23357
Phi carbon	0.25742	0.26107	0.26419	0.26387	0.26413	0.23355	0.23548	0.23532	0.23568	0.23449
Phi Lambda meter	0.26616	0.26938	0.26916	0.27157	0.27309	0.23636	0.23605	0.23725	0.23713	0.23804
GTE emisisons based	0.57075	0.56862	0.559	0.56511	0.56867	0.55921	0.55274	0.5577	0.55492	0.55946
EXH emissions based	0.27662	0.26758	0.2823	0.28838	0.29281	0.31692	0.30631	0.30555	0.2995	0.30715
HX emisisons based	0.12369	0.13284	0.11743	0.11556	0.10491	0.06328	0.07822	0.07276	0.08588	0.07874
charge based PHI	0.26175	0.26245	0.26608	0.26667	0.26685	0.2352	0.2348	0.23551	0.2374	0.23537
Emission charge based PHI	0.2595383	0.258985	0.264533	0.264224754	0.263727	0.234616	0.234175	0.234642	0.237531	0.234029

Table A. 11 0% EGR 22°C intake temperature Piston Oil Cooling Off

MATRIX POINT	29	30	31	32	33	34	35	36	37
RPM	1300	1300	1300	1300	1300	1300	1300	1300	1300
IMEPg (bar)	6.810542	6.783673	6.774159	6.792704111	6.727266	6.780038	6.756774	6.821648	6.725093
IMEPn (bar)	6.3186	6.282686	6.300648	6.347691365	6.278139	6.334091	6.288723	6.327203	6.239846
BMEP_CF (bar)	5.106854	5.065419	5.1039	5.174353335	5.112469	5.125268	5.092877	5.110758	5.043482
FMEP_CF (bar)	1.211746	1.217267	1.196748	1.17333803	1.16567	1.208823	1.195845	1.216445	1.196364
CA50 (ATDC)	0.845014	1.304987	0.642808	1.108945746	0.592138	-0.27772	0.602287	0.380566	1.470559
COV of IMEPg	3.313298	3.330337	2.879106	2.682356823	2.421359	2.776381	3.118773	3.042915	2.598296
COV of PPRR	9.801287	9.372062	8.081758	7.814770496	7.688142	7.406892	8.195364	7.961264	7.356843
EGR %	0	0	0	0	0	0	0	0	0
Fuel 1	E85	E85	E85	E85	E85	E85	E85	E85	E85
Fuel 2	EHN + 91 Gasoline	EHN + 91 Gasoline	EHN + 91 Gasoline	EHN + 91 Gasoline	EHN + 91 Gasoline	EHN + 91 Gasoline	EHN + 91 Gasoline	EHN + 91 Gasoline	EHN + 91 Gasoline
Fuel1 Flow (g/s)	0.799035	0.820935	0.777256	0.784231	0.76989	0.743056	0.760841	0.776674	0.797348
Fuel2 Flow (g/s)	0.194525	0.190096	0.211596	0.206412	0.206094	0.212243	0.205062	0.210994	0.188816
Fuel1 Fraction	0.804214	0.811978	0.786019	0.79163836	0.788835	0.777826	0.787699	0.786372	0.808535
Fuel2 Fraction	0.195786	0.188022	0.213981	0.20836164	0.211165	0.222174	0.212301	0.213628	0.191465
Fuel Energy (J/cyc)	2921.113	2962.808	2929.44	2927.88641	2887.933	2839.683	2859.454	2925.503	2894.119
Fuel H/C	2.524437	2.532871	2.504901	2.510900445	2.507903	2.496208	2.506692	2.505277	2.529123
Fuel O/C	0.289563	0.293264	0.280992	0.28362428	0.282309	0.277178	0.281778	0.281157	0.291619
Fuel MW/C	19.18765	19.25536	19.03081	19.07897612	19.05492	18.96103	19.04519	19.03383	19.22527
RI (MW/m^2)	2.615515	2.006829	3.217954	3.818055591	5.113848	3.473104	3.187311	2.997368	2.419823
Peak HRR (J/deg)	318.663	304.1322	334.105	370.2698684	387.6031	314.0712	332.6692	321.2036	323.2102
Peak PRR (bar/deg)	8.898355	7.889878	9.701636	10.30590416	11.74269	10.15197	9.648917	9.53918	8.47591
PP (bar)	133.2811	134.3853	130.2814	125.5994678	124.0659	132.6964	130.101	134.2209	130.2047
LPP (ATDC)	4.2	4.6	4	4.5	3.8	3.3	4.1	3.9	4.8
P Intake (bar)	1.429812	1.497342	1.367595	1.293640694	1.224903	1.367112	1.366194	1.429377	1.42643
P Exhaust (bar)	1.621964	1.697315	1.556907	1.453224264	1.401399	1.535216	1.59459	1.635099	1.622662
T Intake (C)	18.6241	20.12501	20.23905	21.485988	20.95998	19.77569	20.11698	21.03449	19.7428
T Exhaust Tank (C)	228.4405	226.1497	236.096	243.364979	249.8339	237.6352	240.4247	238.0565	237.6404
Gross Therm Eff	0.569087	0.558865	0.564438	0.566283165	0.568587	0.582784	0.576768	0.569159	0.567188
Net Therm Eff	0.52798	0.517591	0.524984	0.529184062	0.530627	0.544452	0.536815	0.527906	0.526263
Brake Therm Eff (CF)	0.426727	0.417308	0.425268	0.431367116	0.432105	0.440547	0.434736	0.426413	0.425363
Turbo Eff	0.673111	0.682431	0.653119	0.682837966	0.61914	0.683271	0.594943	0.64571	0.657268
Vol Eff	0.925899	0.932957	0.925906	0.926891701	0.918882	0.926894	0.926242	0.927745	0.925432
comb loss	0.049121	0.060567	0.043829	0.036698646	0.030837	0.031464	0.037798	0.045158	0.05131
Comb Eff	0.950879	0.939433	0.956171	0.963301354	0.969163	0.968536	0.962202	0.954842	0.94869
Exhaust Loss	0.299313	0.304202	0.292079	0.283242332	0.278548	0.30665	0.307182	0.309098	0.313529
Pumping Loss	0.041106	0.041273	0.039454	0.037099103	0.03796	0.038332	0.039954	0.041254	0.040925
Heat Transfer Loss	0.082479	0.076366	0.099654	0.113775858	0.122028	0.079102	0.078252	0.076585	0.067974
HC (ppm)	792.6437	835.1367	930.357	932.912978	935.6759	459.3221	642.468	766.208	785.7856
NOx (ppm)	43.01449	28.83664	58.5415	67.006957	104.0686	87.4838	64.34971	58.13773	38.68351
CO2ex (ppm)	33780.59	31654.85	35881.46	38412.68731	40963.95	35522.33	35272.81	33989.76	33283.15
CO2in (ppm)	34.90098	38.41493	33.82856	34.958556	34.626	21.84835	19.33515	16.58064	18.50301
CO (ppm)	2192.726	2821.329	1633.308	1202.358159	827.8635	1559.425	1683.649	1925.263	2342.556
PM (mg/m^3)	0.8	0.77	0.77	0.77	0.71	0	0.76	0.82	0.82
HC (g/kg-fuel)	21.53873	23.62728	24.17272	22.98174519	21.87383	12.22841	17.07419	20.8692	21.56043
NOx (g/kg-fuel)	2.802161	1.948979	3.676549	3.979830109	5.873135	5.650361	4.13055	3.826915	2.539596
CO2ex (g/kg-fuel)	2105.421	2046.898	2155.957	2182.794574	2211.799	2195.046	2166.182	2140.585	2090.532
CO2in (g/kg-fuel)	2.175251	2.484026	2.032607	1.986514136	1.869589	1.350084	1.187415	1.044204	1.162184
CO (g/kg-fuel)	86.97972	116.1105	62.45969	43.48442879	28.44882	61.32936	65.80638	77.16778	93.64489
PM (g/kg-fuel)	0.018385	0.017667	0.017605	0.017513622	0.015942	0	0.017677	0.019099	0.0192
HC (g/ikW-hr)	4.277872	4.794117	4.80393	4.563023444	4.320402	2.3457	3.322994	4.113605	4.304309
NOx (g/ikW-hr)	0.556546	0.395459	0.730653	0.790194911	1.16003	1.083874	0.803891	0.754338	0.507003
CO2ex (g/ikW-hr)	418.164	415.3279	428.4609	433.3936667	436.8626	421.0619	421.5841	421.9387	417.3523
CO2in (g/ikW-hr)	0.432033	0.504024	0.403947	0.394422203	0.369271	0.258978	0.231096	0.205827	0.232018
CO (g/ikW-hr)	17.2753	23.55952	12.41283	8.633829432	5.619058	11.76443	12.80729	15.21083	18.6952
PM (g/ikW-hr)	0.003652	0.003585	0.003499	0.003477328	0.003149	0	0.00344	0.003765	0.003833
Air Flow (kg/min)	2.507984	2.632913	2.385664	2.249499	2.115343	2.391145	2.385078	2.491637	2.491239
AFR mass	42.07067	43.4031	40.20932	37.8457729	36.12325	41.71722	41.15455	42.04579	42.10319
AFR carbon	41.57567	43.06253	40.13572	38.01889007	36.18123	41.29501	41.02194	42.02593	41.88303
AFR Average	41.82317	43.23282	40.17252	37.93233148	36.15224	41.50611	41.08824	42.03586	41.99311
AFR Stoich	10.68189	10.64618	10.76559	10.73973975	10.75264	10.80327	10.75786	10.76397	10.66202
Phi mass	0.253904	0.245286	0.267739	0.283776468	0.297665	0.258964	0.261401	0.256006	0.253235
Phi carbon	0.256927	0.247226	0.26823	0.282484305	0.297188	0.261612	0.262246	0.256127	0.254567
Phi Lambda meter	0.256174	0.242376	0.26725	0.284765	0.301262	0.266489	0.265711	0.25803	0.255017
GTE emisisons based	0.562391	0.554479	0.563405	0.568873502	0.569499	0.576885	0.57491	0.568891	0.564222
EXH emissions based	0.301125	0.305436	0.292377	0.282625729	0.278353	0.308249	0.307709	0.309202	0.314384
HX emisisons based	0.084015	0.077325	0.099873	0.113097291	0.121767	0.080453	0.078653	0.076615	0.068601
charge based PHI	0.253878	0.245262	0.267712	0.28374809	0.297635	0.258939	0.261375	0.25598	0.25321
Emission charge based PHI	0.256927	0.247226	0.26823	0.282484305	0.297188	0.261612	0.262246	0.256127	0.254567

Table A. 11 0% EGR 22°C intake temperature Piston Oil Cooling Off Continued

MATRIX POINT	38	39	40	41	42	43	44	45
RPM	1300	1300	1300	1300	1300	1300	1300	1300
IMEPg (bar)	6.857378	6.767361	6.748064	6.739403844	6.855726	6.702759	6.739183	6.744655
IMEPn (bar)	6.340741	6.310382	6.288344	6.270182197	6.361511	6.216524	6.296554	6.313389
BMEP_CF (bar)	5.115428	5.123405	5.119888	5.104954394	5.156977	5.028533	5.133464	5.161813
FMEP_CF (bar)	1.225313	1.186977	1.168456	1.165227803	1.204534	1.187991	1.16309	1.151576
CA50 (ATDC)	0.912866	0.062022	1.234778	0.56364935	1.229163	0.828352	0.815703	0.443415
COV of IMEPg	3.203729	2.585654	2.775044	2.357959605	2.967735	2.857084	2.415765	2.298877
COV of PPRR	8.806079	7.956757	7.998174	7.773175953	8.144314	7.484663	7.195517	7.166092
EGR %	0	0	0	0	0	0	0	0
Fuel 1	E85	E85	E85	E85	E85	E85	E85	E85
Fuel 2	EHN + 91 Gasoline	EHN + 91 Gasoline	EHN + 91 Gasoline	EHN + 91 Gasoline	EHN + 91 Gasoline	EHN + 91 Gasoline	EHN + 91 Gasoline	EHN + 91 Gasoline
Fuel1 Flow (g/s)	0.808864	0.754657	0.779686	0.769209	0.79432	0.757728	0.757281	0.783472
Fuel2 Flow (g/s)	0.202238	0.217858	0.19329	0.203409	0.198653	0.206614	0.19928	0.191319
Fuel1 Fraction	0.799983	0.775985	0.801341	0.79086445	0.799941	0.785746	0.79167	0.803733
Fuel2 Fraction	0.200017	0.224015	0.198659	0.20913555	0.200059	0.214254	0.20833	0.196267
Fuel Energy (J/cyc)	2977.959	2893.064	2864.039	2875.54017	2924.615	2857.153	2827.118	2866.509
Fuel H/C	2.519865	2.494264	2.521331	2.510072429	2.51982	2.504611	2.510935	2.523916
Fuel O/C	0.287557	0.276325	0.288201	0.283260989	0.287538	0.280865	0.283639	0.289335
Fuel MW/C	2977.959	2893.064	2864.039	2875.54017	2924.615	2857.153	2827.118	2866.509
RI (MW/m^2)	2.409387	4.581548	3.674479	5.457444969	2.827603	3.24001	5.058279	8.215959
Peak HRR (J/deg)	315.3277	354.33	368.0699	396.6868157	338.7581	338.2841	393.2781	446.3549
Peak PRR (bar/deg)	8.670563	11.37678	10.07563	12.10746077	9.168397	9.643659	11.63745	14.43073
PP (bar)	135.9945	128.3272	124.6232	123.9774224	131.8386	128.5301	123.5499	121.2471
LPP (ATDC)	4.4	3.5	4.6	3.8	4.6	4.1	4.1	3.5
P Intake (bar)	1.499515	1.291322	1.29224	1.223840446	1.429667	1.365325	1.237994	1.134284
P Exhaust (bar)	1.693662	1.467057	1.474217	1.433140525	1.59761	1.537619	1.387777	1.312833
T Intake (C)	18.82511	21.15751	21.13351	22.784519	20.91999	20.08635	22.67218	22.40856
T Exhaust Tank (C)	234.3506	245.8227	247.0392	254.86245	234.5835	236.1329	247.4747	255.8761
Gross Therm Eff	0.562062	0.570961	0.575103	0.572067426	0.572176	0.572618	0.581847	0.574317
Net Therm Eff	0.519716	0.532406	0.535923	0.532238025	0.530929	0.531079	0.543631	0.537594
Brake Therm Eff (CF)	0.419284	0.432261	0.436342	0.43332885	0.430399	0.429589	0.443212	0.439536
Turbo Eff	0.680091	0.646768	0.633436	0.541386714	0.698	0.680419	0.701561	0.557236
Vol Eff	0.921794	0.922424	0.923474	0.919866454	0.915671	0.908467	0.910269	0.897583
comb loss	0.056202	0.0339	0.037226	0.029800172	0.048729	0.044794	0.033797	0.026947
Comb Eff	0.943798	0.9661	0.962774	0.970199828	0.951271	0.955206	0.966203	0.973053
Exhaust Loss	0.316504	0.290469	0.29559	0.283818646	0.300642	0.295572	0.280068	0.25932
Pumping Loss	0.042346	0.038555	0.03918	0.039829401	0.041247	0.041539	0.038216	0.036723
Heat Transfer Loss	0.065231	0.10467	0.092082	0.114313756	0.078453	0.087015	0.104288	0.139416
HC (ppm)	817.5443	901.8584	910.6243	924.9245345	827.7923	909.9102	1035.505	1030.308
NOx (ppm)	38.27681	109.5923	72.89631	120.546886	41.66143	61.87919	113.3113	233.1945
CO2ex (ppm)	32221.81	38630.84	38022.43	41114.35654	34193.86	35664.31	40661.06	45982.08
CO2in (ppm)	17.80515	18.74198	17.58018	18.216742	17.87929	15.12609	14.35461	18.12476
CO (ppm)	2559.836	1024.125	1269.194	759.924348	2125.688	1745.374	874.6991	546.2715
PM (mg/m^3)	0.75	0.75	0.62	0.73	0.84	0.87	0.87	0.87
HC (g/kg-fuel)	22.94301	22.2128	22.6261	21.5864936	22.26199	23.71953	24.29355	21.63659
NOx (g/kg-fuel)	2.580136	6.553883	4.347873	6.785563292	2.691241	3.899472	6.40927	11.74277
CO2ex (g/kg-fuel)	2078.023	2210.274	2169.725	2214.200499	2113.295	2150.248	2200.43	2215.309
CO2in (g/kg-fuel)	1.148275	1.072328	1.003202	0.981056804	1.105	0.911971	0.776819	0.873209
CO (g/kg-fuel)	105.0689	37.29296	46.0951	26.04687023	83.61288	66.97381	30.12654	16.75005
PM (g/kg-fuel)	0.017406	0.017267	0.014287	0.016292664	0.019362	0.020143	0.019862	0.018486
HC (g/ikW-hr)	4.605561	4.345857	4.441482	4.241291694	4.389785	4.645995	4.694524	4.257315
NOx (g/ikW-hr)	0.517934	1.282245	0.853483	1.333220381	0.530679	0.763798	1.238538	2.310561
CO2ex (g/ikW-hr)	417.1405	432.4325	425.9149	435.0437991	416.7151	421.1737	425.2145	435.8945
CO2in (g/ikW-hr)	0.230504	0.209797	0.196927	0.192757015	0.217892	0.17863	0.150114	0.171817
CO (g/ikW-hr)	21.09144	7.296238	9.048423	5.117661831	16.48741	13.1183	5.821701	3.295817
PM (g/ikW-hr)	0.003494	0.003378	0.002804	0.003201166	0.003818	0.003945	0.003838	0.003637
Air Flow (kg/min)	2.616783	2.237139	2.241459	2.102727	2.460664	2.338063	2.10565	1.904064
AFR mass	43.13417	38.33941	38.39524	36.03208043	41.30129	40.40861	36.68785	32.55508
AFR carbon	42.97142	38.29155	38.17083	36.09342392	41.23583	40.26571	36.25238	32.36636
AFR Average	43.0528	38.31548	38.28304	36.06275218	41.26856	40.33716	36.47011	32.46072
AFR Stoich	10.70136	10.81174	10.69511	10.74329953	10.70155	10.76684	10.73959	10.68411
Phi mass	0.248095	0.282001	0.278553	0.29815929	0.259109	0.266449	0.292729	0.328186
Phi carbon	0.249034	0.282353	0.280191	0.297652546	0.259521	0.267395	0.296245	0.330099
Phi Lambda meter	0.24598	0.287262	0.284394	0.303748	0.258743	0.267337	0.299773	0.336923
GTE emisisons based	0.559942	0.570248	0.571741	0.573041353	0.57127	0.570593	0.57494	0.570988
EXH emissions based	0.317135	0.290679	0.296488	0.283605821	0.300911	0.296127	0.281779	0.260102
HX emisisons based	0.06566	0.104816	0.092864	0.114039618	0.078637	0.087473	0.106031	0.140299
charge based PHI	0.24807	0.281973	0.278525	0.298129474	0.259083	0.266423	0.2927	0.328153
Emission charge based PHI	0.249034	0.282353	0.280191	0.297652546	0.259521	0.267395	0.296245	0.330099

Table A. 12 40% EGR 43°C intake temperature Piston Oil Cooling On

MATRIX POINT	46	47	48	49	50	51	52	53	54	55
RPM	1300	1299	1300	1300	1300	1300	1300	1300	1300	1300
IMEPg (bar)	6.843898	6.833381	6.885806	6.849628898	6.801139	6.824037	7.320439	7.359463	6.63411	6.677682
IMEPn (bar)	6.367701	6.361945	6.416484	6.383287476	6.346512	6.363488	6.764181	6.816296	6.169673	6.210043
BMEP_CF (bar)	5.137401	5.132248	5.202901	5.193243906	5.175348	5.191303	5.479905	5.538129	5.023697	5.025661
FMEP_CF (bar)	1.2303	1.229697	1.213583	1.19004357	1.171164	1.172185	1.284276	1.278166	1.145976	1.184382
CA50 (ATDC)	0.326076	0.482434	0.66652	0.663872378	0.328873	0.322276	-0.06842	0.670946	2.602792	0.490026
COV of IMEPg	2.915323	2.911123	2.742869	2.419008169	2.21356	2.294269	2.741465	2.726606	2.873534	2.829492
COV of PPRR	8.050126	8.195907	7.698059	7.620214673	6.811112	7.509563	7.406815	7.088095	7.92697	7.462028
EGR %	32.91503	33.2792	34.72126	36.80097346	38.11317	38.51529	37.87978	36.15146	28.16833	28.02287
Fuel 1	E85	E85	E85	E85	E85	E85	E85	E85	E85	E85
Fuel 2	EHN + 91 Gasoline	EHN + 91 Gasoline	EHN + 91 Gasoline	EHN + 91 Gasoline	EHN + 91 Gasoline	EHN + 91 Gasoline	EHN + 91 Gasoline	EHN + 91 Gasoline	EHN + 91 Gasoline	EHN + 91 Gasoline
Fuel1 Flow (g/s)	0.824121	0.84146	0.848328	0.825937	0.801365	0.815177	0.891925	0.926589	0.777658	0.744446
Fuel2 Flow (g/s)	0.141776	0.143675	0.13997	0.170811	0.188401	0.173875	0.157388	0.147262	0.201046	0.217953
Fuel1 Fraction	0.853218	0.854157	0.858373	0.82863171	0.809651	0.8242	0.850009	0.862866	0.794579	0.773532
Fuel2 Fraction	0.146782	0.145843	0.141627	0.17136829	0.190349	0.1758	0.149991	0.137134	0.205421	0.226468
Fuel Energy (J/cyc)	2781.466	2837.909	2839.697	2900.50024	2903.329	2883.505	3025.826	3079.574	2889.054	2865.88
Fuel H/C	2.578689	2.579752	2.584538	2.551164724	2.530337	2.54627	2.57506	2.58966	2.514052	2.491678
Fuel O/C	0.313366	0.313833	0.315933	0.301290157	0.292152	0.299143	0.311774	0.31818	0.285007	0.27519
Fuel MW/C	19.62318	19.63171	19.67014	19.40221655	19.23501	19.36292	19.59405	19.71126	19.10428	18.92466
RI (MW/m^2)	4.165213	4.478008	5.141938	6.037075284	8.900998	9.002747	4.894274	4.832322	2.571832	4.22916
Peak HRR (J/deg)	368.4284	383.2884	416.3501	444.3278131	486.2812	490.3715	392.3146	418.7422	366.7757	375.1473
Peak PRR (bar/deg)	12.08855	12.51354	13.20473	13.98725501	16.47956	16.61041	13.7471	13.56646	8.831861	11.58691
PP (bar)	136.9918	136.9138	133.6485	128.9405757	125.1647	125.3689	147.7871	146.5652	120.1271	127.8083
LPP (ATDC)	3.4	3.5	3.8	3.6	3.1	2.8	3.1	3.6	5.6	3.6
P Intake (bar)	1.495989	1.49937	1.428652	1.340303032	1.233163	1.237897	1.611099	1.611775	1.36861	1.366871
P Exhaust (bar)	1.659177	1.663495	1.595922	1.514709641	1.407683	1.41606	1.849948	1.827851	1.522746	1.517989
T Intake (C)	38.04739	39.03368	41.97526	40.355945	41.25502	41.29432	35.90372	37.36192	33.4796	33.64251
T Exhaust Tank (C)	248.3309	249.886	255.9556	264.903544	272.6145	274.5113	249.2192	252.6327	254.8541	256.065
Gross Therm Eff	0.600586	0.587736	0.591872	0.576420362	0.571782	0.577651	0.590525	0.583312	0.560496	0.568739
Net Therm Eff	0.558797	0.547188	0.551531	0.537176091	0.533561	0.538666	0.545653	0.54026	0.521257	0.52891
Brake Therm Eff (CF)	0.450832	0.441422	0.447217	0.43702974	0.435099	0.439441	0.442053	0.438953	0.424437	0.428036
Turbo Eff	0.685902	0.683408	0.661872	0.625032691	0.589239	0.58005	0.637465	0.651467	0.686234	0.690232
Vol Eff	0.91743	0.90639	0.916561	0.900188741	0.879788	0.880726	0.90779	0.912385	0.904731	0.902385
comb loss	0.026863	0.024423	0.020755	0.018174569	0.015259	0.015462	0.024339	0.024305	0.038969	0.031911
Comb Eff	0.973137	0.975577	0.979245	0.981825431	0.984741	0.984538	0.975661	0.975695	0.961031	0.968089
Exhaust Loss	0.309916	0.300719	0.291332	0.276909702	0.255548	0.260589	0.30984	0.307563	0.287047	0.289462
Pumping Loss	0.041789	0.040548	0.040341	0.039244271	0.038221	0.038985	0.044872	0.043051	0.039239	0.039829
Heat Transfer Loss	0.062636	0.087123	0.09604	0.128495367	0.157411	0.146297	0.075296	0.08482	0.113489	0.109887
HC (ppm)	836.6577	824.1387	858.9324	925.677456	957.3589	983.4623	902.0071	880.0162	1326.538	1234.944
NOx (ppm)	43.19536	42.98223	54.06485	83.353236	150.37	138.7096	46.06866	38.4782	40.43252	71.49338
CO2ex (ppm)	53540.44	54294.56	59651.92	67199.52713	77656.32	78993.58	58547.32	56839.72	52267.31	53727.09
CO2in (ppm)	17883.14	18327.67	20965.18	24975.29237	29837.4	30663.16	22418.62	20796.12	15001.54	15335.15
CO (ppm)	1437.364	1195.907	902.7178	706.468877	544.38	569.5801	1248.423	1198.321	1804.821	1208.981
PM (mg/m^3)	0.82	0.97	1.08	1.09	1.31	1.71	0.8	1.23	0.89	0.97
HC (g/kg-fuel)	14.97428	14.6194	13.97086	13.43285642	12.07987	12.19482	14.84383	14.9197	23.90704	21.95277
NOx (g/kg-fuel)	1.812273	1.78656	2.056504	2.867725875	4.537473	4.086123	1.779817	1.522396	1.754544	3.08914
CO2ex (g/kg-fuel)	2149.127	2159.129	2170.863	2211.948055	2241.935	2226.333	2164.065	2151.584	2169.987	2221.051
CO2in (g/kg-fuel)	717.8339	728.8357	762.9685	822.0898531	861.4048	864.202	828.652	787.2068	622.8201	633.9473
CO (g/kg-fuel)	36.7205	30.26784	20.90845	14.80006017	10.00254	10.2168	29.36883	28.86963	47.68948	31.80875
PM (g/kg-fuel)	0.012958	0.014763	0.015892	0.014967073	0.016846	0.021968	0.010811	0.016946	0.01452	0.016122
HC (g/ikW-hr)	2.877189	2.871567	2.72993	2.661226994	2.393361	2.406293	2.896737	2.963829	4.801642	4.307388
NOx (g/ikW-hr)	0.348214	0.350919	0.401844	0.568134526	0.899001	0.806277	0.347327	0.302427	0.352394	0.606125
CO2ex (g/ikW-hr)	412.9377	424.0999	424.1904	438.2162431	444.1904	439.3019	422.312	427.4167	435.8338	435.796
CO2in (g/ikW-hr)	137.9261	143.1592	149.0853	162.8669019	170.6685	170.5251	161.7094	156.3803	125.0911	124.3878
CO (g/ikW-hr)	7.055554	5.945261	4.085546	2.932088189	1.981784	2.015988	5.731255	5.735013	9.578258	6.241245
PM (g/ikW-hr)	0.00249	0.0029	0.003105	0.002965176	0.003338	0.004335	0.00211	0.003366	0.002916	0.003163
Air Flow (kg/min)	1.635384	1.604242	1.499359	1.344405	1.18042	1.178359	1.624933	1.671414	1.603355	1.59955
AFR mass	28.21874	27.14081	25.2852	22.47985449	19.87709	19.85671	25.80947	25.94112	27.30405	27.70074
AFR carbon	27.04851	26.8132	24.60619	22.33674572	19.68904	19.23258	24.96901	25.55241	27.93186	27.84964
AFR Average	27.63363	26.97701	24.9457	22.4083001	19.78307	19.54464	25.38924	25.74677	27.61795	27.77519
AFR Stoich	10.45649	10.45217	10.43278	10.56958018	10.65689	10.58996	10.47125	10.41211	10.72621	10.82303
Phi mass	0.370551	0.385109	0.412604	0.470180098	0.536139	0.533319	0.405714	0.401375	0.392843	0.390712
Phi carbon	0.386583	0.389814	0.42399	0.473192484	0.54126	0.550626	0.41937	0.407481	0.384014	0.388624
Phi Lambda meter	0.405328	0.412472	0.444905	0.49671	0.568708	0.574291	0.436953	0.426154	0.395063	0.399496
GTE emisisons based	0.575679	0.580642	0.575978	0.572750819	0.566373	0.559495	0.571295	0.574571	0.573383	0.571796
EXH emissions based	0.31662	0.30256	0.29535	0.2778	0.25677	0.26482	0.31505	0.3099	0.28382	0.28869
HX emisisons based	0.06838	0.08883	0.09997	0.12944	0.1589	0.15115	0.0797	0.08685	0.11027	0.10913
charge based PHI	0.248584	0.256948	0.269343	0.297149245	0.3318	0.32791	0.25203	0.256272	0.282186	0.281224
Emission charge based PHI	0.259339	0.260087	0.276775	0.299053043	0.334969	0.338551	0.260514	0.26017	0.275843	0.27972

Table A. 12 40% EGR 43°C intake temperature Piston Oil Cooling On Continued

MATRIX POINT	56	57	58	59	60	61	62	63	64	65
RPM	1300	1300	1300	1300	1300	1300	1302	1300	1300	1300
IMEPg (bar)	6.639186	6.801008	6.654353	6.802855221	6.786958	6.779894	6.900676	6.83808	6.680284	6.706845
IMEPn (bar)	6.170636	6.327887	6.160885	6.306570009	6.271852	6.28839	6.347862	6.312934	6.222772	6.250412
BMEP_CF (bar)	5.006776	5.124208	4.965285	5.075327939	5.030967	5.06079	5.111542	5.092045	5.027976	5.047668
FMEP_CF (bar)	1.163861	1.203679	1.195599	1.231242069	1.240885	1.2276	1.236321	1.220889	1.194796	1.202743
CA50 (ATDC)	2.346384	0.53061	2.419732	0.805397379	0.98434	0.731108	-0.37724	0.634944	0.643765	0.283343
COV of IMEPg	2.952968	2.678287	3.624854	3.088693208	3.437196	3.236389	2.613396	2.844476	3.0308	3.146937
COV of PPRR	8.257436	7.118174	9.312436	7.933638616	8.289753	8.079346	7.349375	7.646344	8.420528	8.159362
EGR %	27.78538	28.13656	28.57587	26.48894141	42.09861	41.69983	38.81569	37.80902	31.09448	31.17594
Fuel 1	E85	E85	E85	E85	E85	E85	E85	E85	E85	E85
Fuel 2	EHN + 91 Gasoline	EHN + 91 Gasoline	EHN + 91 Gasoline	EHN + 91 Gasoline	EHN + 91 Gasoline	EHN + 91 Gasoline	EHN + 91 Gasoline	EHN + 91 Gasoline	EHN + 91 Gasoline	EHN + 91 Gasoline
Fuel1 Flow (g/s)	0.802057	0.77495	0.848666	0.819491	0.814063	0.801539	0.799774	0.813348	0.773257	0.770844
Fuel2 Flow (g/s)	0.186747	0.221679	0.15687	0.189395	0.196302	0.193857	0.219079	0.193613	0.185609	0.18465
Fuel1 Fraction	0.811139	0.777571	0.843994	0.812273141	0.805712	0.805246	0.784975	0.807725	0.806429	0.806749
Fuel2 Fraction	0.188861	0.222429	0.156006	0.187726859	0.194288	0.194754	0.215025	0.192275	0.193571	0.193251
Fuel Energy (J/cyc)	2898.695	2962.851	2907.041	2956.15519	2968.657	2925.245	3014.988	2944.367	2894.249	2828.655
Fuel H/C	2.531956	2.495939	2.568289	2.533192728	2.526059	2.525555	2.50379	2.528244	2.526836	2.527184
Fuel O/C	0.292862	0.27706	0.308803	0.293404977	0.290275	0.290054	0.280505	0.291234	0.290616	0.290769
Fuel MW/C	2865.88	2898.695	2962.851	2907.04141	2956.155	2968.657	2925.245	3014.988	2944.367	19.2097
RI (MW/m^2)	2.533355	4.259063	2.076782	2.980377742	2.640696	3.017698	4.502348	3.859398	2.509892	2.986869
Peak HRR (J/deg)	359.9229	380.7072	338.7504	344.7513153	342.7706	350.3648	365.7901	376.2542	321.1204	328.524
Peak PRR (bar/deg)	8.929308	11.84498	8.41972	10.24349333	10.04056	10.55442	12.73707	11.70448	9.184646	10.04814
PP (bar)	123.704	131.6677	130.0518	137.1802756	139.1089	136.4519	138.111	135.1096	129.891	131.4805
LPP (ATDC)	5.4	3.6	5.5	4.1	3.9	3.7	2.7	3.7	4.1	3.8
P Intake (bar)	1.420875	1.418267	1.553133	1.557819042	1.645057	1.577141	1.510963	1.516615	1.427107	1.427348
P Exhaust (bar)	1.571162	1.573159	1.718568	1.706130855	1.803709	1.728325	1.720045	1.705335	1.578143	1.567898
T Intake (C)	36.18356	36.01789	34.70229	34.972355	42.9523	42.39058	41.43299	40.672	30.14957	31.17862
T Exhaust Tank (C)	252.1261	253.984	245.1582	241.327402	237.6283	242.561	253.5006	252.3225	241.384	244.4467
Gross Therm Eff	0.559059	0.560284	0.558727	0.561706147	0.558034	0.565726	0.558665	0.564614	0.578937	0.583368
Net Therm Eff	0.519604	0.521308	0.517294	0.520728286	0.515681	0.524714	0.51391	0.521253	0.539287	0.543667
Brake Therm Eff (CF)	0.4216	0.422145	0.416906	0.419065644	0.413653	0.422281	0.41382	0.420446	0.435742	0.439051
Turbo Eff	0.701119	0.691774	0.706124	0.731648041	0.729654	0.723213	0.641144	0.664769	0.714074	0.726501
Vol Eff	0.917885	0.914522	0.932055	0.928597231	0.929416	0.922341	0.910932	0.913686	0.924186	0.922178
comb loss	0.038868	0.029657	0.049445	0.045837435	0.039546	0.033869	0.025633	0.028079	0.046731	0.036995
Comb Eff	0.961132	0.970343	0.950555	0.954162565	0.960454	0.966131	0.974367	0.971921	0.953269	0.963005
Exhaust Loss	0.291687	0.286572	0.316086	0.304388136	0.295595	0.293814	0.286321	0.294069	0.302379	0.304831
Pumping Loss	0.039455	0.038977	0.041434	0.040977861	0.042353	0.041012	0.044755	0.043361	0.03965	0.039701
Heat Transfer Loss	0.110387	0.123486	0.075742	0.088068282	0.106825	0.106592	0.129382	0.113238	0.071952	0.074806
HC (ppm)	1110.926	1041.097	1008.768	975.9687644	1087.03	1099.852	1077.654	1004.258	1513.045	1284.622
NOx (ppm)	33.36217	59.60518	17.3434	26.092376	26.69265	36.28338	70.02007	42.77203	60.95434	78.55787
CO2ex (ppm)	49323.71	52024.32	44293.28	43228.44995	54849.41	57702.52	60415.19	57430.68	50007.09	51484.03
CO2in (ppm)	13984.97	14916.68	12934.32	11735.98169	23315.5	24288.05	23687.97	21955.28	15816.8	16317.67
CO (ppm)	2009.995	1232.981	2989.464	2524.955978	2664.734	2084.966	1144.237	1468.842	2160.628	1574.818
PM (mg/m^3)	0.97	0.97	0.97	1.06	1.06	1.06	0.97	0.97	1.1	1.08
HC (g/kg-fuel)	21.15428	19.1495	20.8635	20.86099934	18.52524	18.03956	17.18216	16.74387	28.13479	23.60209
NOx (g/kg-fuel)	1.518237	2.660087	0.844443	1.332173741	1.089822	1.426042	2.699759	1.70693	2.714544	3.456225
CO2ex (g/kg-fuel)	2147.506	2221.323	2063.325	2111.594104	2142.542	2169.766	2228.651	2192.771	2130.676	2167.097
CO2in (g/kg-fuel)	608.8921	636.9092	602.5227	573.2713008	910.7561	913.2944	873.8238	838.2782	673.9138	686.8531
CO (g/kg-fuel)	55.69746	33.50607	88.63085	78.4975909	66.24805	49.89751	26.86419	35.69326	58.59054	42.18888
PM (g/kg-fuel)	0.01605	0.015811	0.016252	0.01813732	0.014085	0.014234	0.013003	0.013518	0.018045	0.017838
HC (g/ikW-hr)	4.289324	3.820435	4.292143	4.211930473	3.754588	3.605737	3.448461	3.356832	5.497965	4.577784
NOx (g/ikW-hr)	0.307844	0.530703	0.173723	0.268971926	0.220879	0.285037	0.541842	0.342207	0.530463	0.670358
CO2ex (g/ikW-hr)	435.4367	443.1667	424.4776	426.3404359	434.2379	433.6916	447.2905	439.6093	416.3664	420.3231
CO2in (g/ikW-hr)	123.4613	127.0671	123.954	115.7460782	184.5867	182.5488	175.3765	168.059	131.693	133.2198
CO (g/ikW-hr)	11.29343	6.684654	18.23358	15.84901997	13.42677	9.973488	5.391646	7.155827	11.44948	8.182818
PM (g/ikW-hr)	0.003254	0.003154	0.003343	0.003662007	0.002855	0.002845	0.00261	0.00271	0.003526	0.00346
Air Flow (kg/min)	1.682951	1.666459	1.856443	1.907668	1.548038	1.485612	1.481977	1.517907	1.656255	1.645398
AFR mass	28.36678	27.86826	30.77037	31.51442945	25.53595	24.87472	24.24257	25.12356	28.78843	28.70065
AFR carbon	29.25349	28.74761	31.199	32.71434555	26.29895	25.36387	24.93641	25.76872	28.61899	28.31632
AFR Average	28.81013	28.30794	30.98469	32.1143875	25.91745	25.1193	24.58949	25.44614	28.70371	28.50849
AFR Stoich	10.65004	10.80444	10.49892	10.64482525	10.67501	10.67715	10.77039	10.66574	10.67171	10.67023
Phi mass	0.375441	0.387697	0.341202	0.337776233	0.418038	0.429237	0.444276	0.424531	0.370694	0.371777
Phi carbon	0.364061	0.375838	0.336515	0.325387076	0.40591	0.420959	0.431914	0.413903	0.372889	0.376823
Phi Lambda meter	0.375846	0.388551	0.342775	0.338175	0.420466	0.437654	0.447091	0.430749	0.38809	0.394018
GTE emisisons based	0.576534	0.577964	0.56651	0.583093183	0.574707	0.57685	0.574654	0.579113	0.575529	0.575556
EXH emissions based	0.28727	0.28219	0.31391	0.29881	0.29131	0.29098	0.28234	0.29039	0.30327	0.3069
HX emisisons based	0.10607	0.11903	0.07402	0.08296	0.10278	0.10386	0.12537	0.10967	0.07276	0.07664
charge based PHI	0.271123	0.278613	0.243701	0.248302884	0.24205	0.250246	0.271827	0.26402	0.255429	0.255872
Emission charge based PHI	0.262905	0.27009	0.240353	0.239195484	0.235028	0.24542	0.264264	0.25741	0.256941	0.259345

Table A. 12 40% EGR 43°C intake temperature Piston Oil Cooling On Continued

MATRIX POINT	66	67	68	69	70	71	72
RPM	1300	1300	1300	1300	1300	1300	1300
IMEPg (bar)	6.70157	6.749105	6.729	6.749986717	6.694565	6.69681	6.719835
IMEPn (bar)	6.250235	6.263498	6.234291	6.26156005	6.220111	6.232323	6.259201
BMEP_CF (bar)	5.066406	5.059884	5.016249	5.05934136	5.040257	5.072724	5.105634
FMEP_CF (bar)	1.183828	1.203614	1.218043	1.20221869	1.179855	1.159599	1.153567
CA50 (ATDC)	1.586551	0.474962	0.679106	0.707956959	0.618246	0.623095	0.918301
COV of IMEPg	3.15326	2.854915	3.006982	2.692647063	2.55334	2.318486	2.276199
COV of PPRR	8.831149	8.263493	8.307197	7.884980756	7.667985	6.853852	7.160586
EGR %	31.43719	34.99549	34.38926	35.00480917	36.54596	37.97998	38.23027
Fuel 1	E85	E85	E85	E85	E85	E85	E85
Fuel 2	EHN + 91 Gasoline	EHN + 91 Gasoline	EHN + 91 Gasoline	EHN + 91 Gasoline	EHN + 91 Gasoline	EHN + 91 Gasoline	EHN + 91 Gasoline
Fuel1 Flow (g/s)	0.819351	0.827208	0.827678	0.816993	0.793423	0.823889	0.821286
Fuel2 Flow (g/s)	0.149854	0.143307	0.157981	0.159876	0.166136	0.180216	0.174439
Fuel1 Fraction	0.845385	0.852339	0.83972	0.836338342	0.826862	0.820521	0.824812
Fuel2 Fraction	0.154615	0.147661	0.16028	0.163661658	0.173138	0.179479	0.175188
Fuel Energy (J/cyc)	2907.128	2879.013	2875.195	3124.25407	3045.709	3062.144	3122.977
Fuel H/C	2.569851	2.577694	2.563501	2.559725097	2.549208	2.54222	2.546944
Fuel O/C	0.309489	0.31293	0.306703	0.305046004	0.300431	0.297366	0.299438
Fuel MW/C	19.55223	19.61519	19.50125	19.47093897	19.38651	19.33041	19.36834
RI (MW/m^2)	2.573303	3.895482	3.446415	4.000406499	4.840052	6.714708	6.518927
Peak HRR (J/deg)	2894.249	2828.655	2907.128	2879.01303	2875.195	3124.254	3045.709
Peak PRR (bar/deg)	9.227326	11.51305	11.00208	11.64526449	12.51249	14.31355	14.053
PP (bar)	127.6975	131.6547	134.5404	131.3755997	126.9028	122.8516	121.6453
LPP (ATDC)	4.9	3.7	3.9	3.9	3.8	3.1	3.8
P Intake (bar)	1.427396	1.428749	1.49396	1.428169267	1.336632	1.23611	1.236255
P Exhaust (bar)	1.567395	1.591765	1.665151	1.602237343	1.509969	1.414323	1.412829
T Intake (C)	32.25893	36.97882	37.22343	38.612637	39.22552	44.02428	42.06528
T Exhaust Tank (C)	246.7688	254.7592	250.7691	253.813159	261.9447	276.6797	280.5846
Gross Therm Eff	0.584131	0.589227	0.575341	0.581491842	0.584767	0.557516	0.565165
Net Therm Eff	0.544791	0.546832	0.533042	0.539415296	0.543324	0.518847	0.526424
Brake Therm Eff (CF)	0.441604	0.441751	0.428898	0.435847632	0.440264	0.42231	0.429404
Turbo Eff	0.724586	0.678661	0.683691	0.665685243	0.639624	0.585845	0.585773
Vol Eff	0.928111	0.922413	0.926244	0.922979989	0.915754	0.907401	0.900362
comb loss	0.033446	0.0248	0.028342	0.023852598	0.020571	0.016062	0.01573
Comb Eff	0.966554	0.9752	0.971658	0.976147402	0.979429	0.983938	0.98427
Exhaust Loss	0.308227	0.307452	0.309854	0.298462784	0.290199	0.260976	0.269667
Pumping Loss	0.03934	0.042396	0.042298	0.042076545	0.041443	0.038669	0.038741
Heat Transfer Loss	0.074197	0.078521	0.086463	0.096192777	0.104463	0.165446	0.149437
HC (ppm)	1005.891	937.066	898.1225	902.369968	983.2018	950.79	918.848
NOx (ppm)	64.66158	77.90187	63.27918	76.551737	105.6808	189.4682	179.6184
CO2ex (ppm)	51637.64	56805.92	52909.17	57030.49722	63404.77	74049.77	74211.39
CO2in (ppm)	16499.45	20131.73	18449.64	20215.59806	23418.09	28364.72	28610.88
CO (ppm)	1765.554	1135.651	1448.439	1096.953561	776.0379	571.7734	591.5912
PM (mg/m^3)	1.09	1.09	1.23	1.23	1.4	2.2	2.2
HC (g/kg-fuel)	18.46451	15.8965	16.23578	15.26947836	15.06962	12.56625	12.12057
NOx (g/kg-fuel)	2.792511	3.099165	2.698323	3.060310931	3.843386	5.959011	5.62724
CO2ex (g/kg-fuel)	2133.578	2162.14	2158.527	2181.278903	2206.142	2228.205	2224.379
CO2in (g/kg-fuel)	681.7287	766.2516	752.687	773.1978451	814.8224	853.5128	857.5697
CO (g/kg-fuel)	46.42852	27.51041	37.60872	26.7026291	17.18527	10.95008	11.28552
PM (g/kg-fuel)	0.017816	0.016622	0.018878	0.018431673	0.02034	0.028776	0.029081
HC (g/ikW-hr)	3.635566	3.112096	3.23776	3.008519478	2.940674	2.565147	2.445113
NOx (g/ikW-hr)	0.549831	0.606731	0.538103	0.602967883	0.749995	1.216412	1.135197
CO2ex (g/ikW-hr)	420.0905	423.2873	430.4561	429.7736905	430.5048	454.8431	448.7297
CO2in (g/ikW-hr)	134.2288	150.0109	150.1018	152.3418628	159.0038	174.2274	172.9997
CO (g/ikW-hr)	9.141534	5.385776	7.499977	5.261173819	3.353519	2.235237	2.276657
PM (g/ikW-hr)	0.003508	0.003254	0.003765	0.003631561	0.003969	0.005874	0.005867
Air Flow (kg/min)	1.643919	1.526903	1.616903	1.519001	1.374364	1.212326	1.205654
AFR mass	28.2692	26.22152	27.34047	25.91614979	23.87145	20.12283	20.1805
AFR carbon	27.80253	25.69208	27.48001	25.82170936	23.56598	20.48694	20.40936
AFR Average	28.03586	25.9568	27.41024	25.86892958	23.71872	20.30489	20.29493
AFR Stoich	10.49252	10.46053	10.51858	10.53413173	10.57772	10.60689	10.58715
Phi mass	0.371164	0.398929	0.384725	0.406469781	0.443112	0.527107	0.524623
Phi carbon	0.377395	0.40715	0.382772	0.407956405	0.448855	0.517739	0.51874
Phi Lambda meter	0.396019	0.428159	0.403332	0.430466	0.472428	0.546782	0.548522
GTE emisisons based	0.574488	0.57733	0.578277	0.579372841	0.577284	0.567604	0.571574
EXH emissions based	0.31081	0.31062	0.30907	0.29901	0.29208	0.25866	0.26816
HX emisisons based	0.07643	0.0813	0.08578	0.09671	0.10632	0.16272	0.14774
charge based PHI	0.254481	0.259322	0.252421	0.26418581	0.281172	0.326912	0.324058
Emission charge based PHI	0.258752	0.264666	0.251139	0.265152044	0.284817	0.321102	0.320424

Table A. 13 40% EGR 43°C intake temperature Piston Oil Cooling Off

MATRIX POINT	73	74	75	76	77	78	79	80	81	82
RPM	1300	1300	1300	1300	1300	1300	1299	1300	1300	1300
IMEPg (bar)	6.736915	6.759563	6.683316	6.798651603	6.281737	6.778127	6.775979	6.808042	6.801321	6.787679
IMEPn (bar)	6.276008	6.257785	6.233365	6.315553504	5.790666	6.256778	6.21675	6.277723	6.269369	6.271487
BMEP_CF (bar)	5.072443	5.031441	5.05588	5.091469905	4.580104	5.007018	4.993495	5.061095	5.048306	5.056421
FMEP_CF (bar)	1.203565	1.226344	1.177485	1.224083599	1.210563	1.24976	1.223256	1.216628	1.221063	1.215065
CA50 (ATDC)	0.687861	1.183629	0.878939	1.365147567	2.040693	0.980328	1.304926	0.89235	0.658344	0.645658
COV of IMEPg	2.981616	3.411206	2.525095	3.247103113	3.861322	3.273423	2.95593	2.760443	2.8064	2.746145
COV of PPRR	8.108081	8.846969	7.419072	8.757357152	8.591661	8.212419	7.488433	7.754298	7.967439	8.485948
EGR %	27.16228	27.73512	27.74705	26.75993487	33.18243	34.94906	40.73927	39.32327	39.34626	40.18238
Fuel 1	E85	E85	E85	E85	E85	E85	E85	E85	E85	E85
Fuel 2	EHN + 91 Gasoline	EHN + 91 Gasoline	EHN + 91 Gasoline	EHN + 91 Gasoline	EHN + 91 Gasoline	EHN + 91 Gasoline	EHN + 91 Gasoline	EHN + 91 Gasoline	EHN + 91 Gasoline	EHN + 91 Gasoline
Fuel1 Flow (g/s)	0.807351	0.846901	0.792319	0.853684	0.881254	0.822973	0.805133	0.796919	0.811324	0.852114
Fuel2 Flow (g/s)	0.177855	0.155484	0.190575	0.159958	0.082983	0.174768	0.189697	0.192873	0.183529	0.152066
Fuel1 Fraction	0.819474	0.844886	0.806108	0.842194779	0.913939	0.824836	0.809317	0.805138	0.815521	0.848567
Fuel2 Fraction	0.180526	0.155114	0.193892	0.157805221	0.086061	0.175164	0.190683	0.194862	0.184479	0.151433
Fuel Energy (J/cyc)	2878.029	2896.83	2887.461	2932.72271	2704.549	2908.055	2920.839	2908.909	2911.055	2897.463
Fuel H/C	2.541071	2.569291	2.526489	2.566270971	2.649427	2.546971	2.529974	2.525437	2.53674	2.573434
Fuel O/C	0.296862	0.309243	0.290464	0.307917994	0.344403	0.29945	0.291993	0.290002	0.294961	0.311061
Fuel MW/C	19.32119	19.54773	19.20412	19.52348905	20.19106	19.36855	19.2321	19.19568	19.28642	19.58099
RI (MW/m^2)	3.914979	2.846291	4.808479	3.101307973	3.161895	3.691599	3.582669	4.152776	4.252793	5.194597
Peak HRR (J/deg)	372.1943	349.2533	406.3042	366.3790425	361.0748	377.8357	392.9175	402.8661	388.9111	412.4674
Peak PRR (bar/deg)	11.38953	10.02658	12.26356	10.40502327	10.60274	11.79065	11.49743	12.18998	12.36244	13.46843
PP (bar)	131.6449	136.2008	126.4288	135.7485816	133.0444	140.8839	135.6255	134.2575	135.1445	133.9449
LPP (ATDC)	3.8	4.3	3.9	4.5	4.7	3.8	3.6	4.4	3.4	3.1
P Intake (bar)	1.420924	1.558157	1.333347	1.544873376	1.626025	1.644864	1.578252	1.517146	1.516953	1.44097
P Exhaust (bar)	1.566242	1.718681	1.477335	1.688660988	1.771399	1.817022	1.793366	1.711813	1.710807	1.635732
T Intake (C)	33.94398	34.25253	34.52184	34.691875	47.67668	40.35321	42.42756	40.62403	42.04063	42.58795
T Exhaust Tank (C)	250.7829	242.1099	254.4722	242.852603	235.3369	1272.863	246.435	250.8491	251.7134	257.5077
Gross Therm Eff	0.571362	0.569562	0.564964	0.565844322	0.566931	0.568921	0.566252	0.571265	0.57028	0.571806
Net Therm Eff	0.532272	0.527282	0.526928	0.525636596	0.522611	0.525162	0.519518	0.526765	0.525676	0.528321
Brake Therm Eff (CF)	0.430197	0.42395	0.427391	0.42375746	0.413357	0.420263	0.417294	0.424678	0.423292	0.425962
Turbo Eff	0.706529	0.712073	0.702232	0.730456005	0.745136	1.171295	0.657449	0.659016	0.658781	0.634159
Vol Eff	0.926427	0.933207	0.912841	0.933362728	0.93935	0.933489	0.932699	0.925509	0.930774	0.925761
comb loss	0.028411	0.041161	0.025594	0.040312	0.04259	0.039088	0.0336	0.028708	0.027663	0.022055
Comb Eff	0.971589	0.958839	0.974406	0.959688	0.95741	0.960912	0.9664	0.971292	0.972337	0.977945
Exhaust Loss	0.296614	0.311719	0.276757	0.30533935	0.30339	1.906446	0.299219	0.29702	0.296329	0.287823
Pumping Loss	0.03909	0.04228	0.038036	0.040207725	0.044319	0.043759	0.046733	0.044499	0.044603	0.043485
Heat Transfer Loss	0.103613	0.077558	0.132685	0.088504328	0.08709	-1.51445	0.100929	0.103008	0.105728	0.118317
HC (ppm)	875.4531	936.4032	1064.666	988.8915741	964.7236	1116.125	1117.463	1121.234	1097.626	994.4081
NOx (ppm)	57.15324	29.15046	77.78357	29.529788	10.70615	22.1329	28.99501	38.3951	53.25145	83.7267
CO2ex (ppm)	49790.78	44504.14	55074.31	44863.93012	44491.65	48342.09	56117.3	58366.37	58741	64365.3
CO2in (ppm)	13806.92	12623.66	15561.84	12289.72993	15022.66	17147.5	23091.71	23186.99	23347.72	26095.6
CO (ppm)	1302.454	2223.282	855.4	2042.39066	2326.612	1935.837	1883.196	1356.356	1287.12	1019.965
PM (mg/m^3)	1.02	0.9	0.9	0.9	0.9	0.49	0.51	0.51	0.46	0.46
HC (g/kg-fuel)	16.82761	19.6234	18.65577	20.62191313	20.16507	21.68743	18.87651	18.40273	17.93259	14.9619
NOx (g/kg-fuel)	2.615499	1.437535	3.264757	1.450911772	0.509834	1.021397	1.171502	1.510138	2.07504	2.959438
CO2ex (g/kg-fuel)	2179.998	2099.746	2211.595	2108.975466	2027.064	2134.396	2169.252	2196.326	2189.929	2176.66
CO2in (g/kg-fuel)	604.5109	595.5961	624.9099	577.7188676	684.4407	757.0951	892.6255	872.5264	870.4286	882.4825
CO (g/kg-fuel)	36.29371	66.76097	21.86188	61.10472136	67.46439	54.39765	46.33087	32.484	30.54002	21.95259
PM (g/kg-fuel)	0.017359	0.015304	0.014659	0.015379505	0.014334	0.022597	0.006931	0.007113	0.0064	0.006132
HC (g/ikW-hr)	3.3503	3.961736	3.735279	4.185872358	4.214042	4.346218	3.775964	3.642498	3.571116	3.013507
NOx (g/ikW-hr)	0.520734	0.290221	0.653673	0.294508635	0.106544	0.204691	0.234341	0.298905	0.413226	0.596067
CO2ex (g/ikW-hr)	434.0276	423.9142	442.8081	428.0835657	423.6104	427.7384	433.9265	434.7242	436.1048	438.4056
CO2in (g/ikW-hr)	120.3553	120.2439	125.1202	117.2663963	143.0326	151.7238	178.5564	172.7013	173.3381	177.7426
CO (g/ikW-hr)	7.225909	13.47826	4.377211	12.40314429	14.09853	10.90143	9.2678	6.429637	6.081773	4.421517
PM (g/ikW-hr)	0.003456	0.00309	0.002935	0.003121759	0.002996	0.004529	0.001386	0.001408	0.001274	0.001235
Air Flow (kg/min)	1.725822	1.889461	1.579921	1.89624	1.758344	1.761083	1.526769	1.500868	1.501861	1.396964
AFR mass	29.19562	31.41609	26.79029	31.17866071	30.39267	29.41784	25.57839	25.27245	25.16052	23.18582
AFR carbon	29.4522	31.62846	27.08531	31.5215672	30.53871	29.65357	26.0591	25.40701	25.17853	22.90962
AFR Average	29.32391	31.52227	26.9378	31.35011396	30.46569	29.5357	25.81874	25.33973	25.16953	23.04772
AFR Stoich	10.6117	10.49482	10.67318	10.50719368	10.17719	10.58704	10.65842	10.67765	10.62988	10.47788
Phi mass	0.363469	0.334059	0.398397	0.33699952	0.334857	0.359885	0.416696	0.422501	0.422483	0.451909
Phi carbon	0.360302	0.331816	0.394058	0.33333348	0.333255	0.357024	0.40901	0.420264	0.42218	0.457357
Phi Lambda meter	0.372048	0.33905	0.405127	0.340424	0.341346	0.366717	0.422418	0.434116	0.436721	0.472088
GTE emisisons based	0.576383	0.573412	0.571186	0.572067542	0.569655	0.57348	0.576894	0.574306	0.570688	0.564994
EXH emissions based	0.295322	0.310673	0.27525	0.303678537	0.302664	1.898868	0.296459	0.296233	0.296223	0.289558
HX emisisons based	0.102395	0.07668	0.131081	0.087053531	0.086453	-1.50916	0.098368	0.102274	0.10563	0.119987
charge based PHI	0.264743	0.241407	0.287854	0.246818668	0.223743	0.234109	0.246937	0.25636	0.256252	0.270321
Emission charge based PHI	0.263589	0.240597	0.286286	0.245476163	0.223208	0.233178	0.24466	0.255681	0.25616	0.271951

Table A. 13 40% EGR 43°C intake temperature Piston Oil Cooling Off Continued

MATRIX POINT	83	84	85	86	87	88	89	90	91	92
RPM	1300	1300	1300	1300	1300	1300	1300	1300	1300	1300
IMEPg (bar)	6.837014	6.838052	6.807925	6.801604787	6.782162	6.778732	6.77764	6.884828	7.010415	6.918471
IMEPn (bar)	6.350036	6.350796	6.332679	6.328529184	6.322825	6.329232	6.328504	6.358967	6.416525	6.38061
BMEP_CF (bar)	5.111387	5.111051	5.113968	5.110316508	5.125689	5.149062	5.144775	5.09952	5.124632	5.131845
FMEP_CF (bar)	1.23865	1.239744	1.218711	1.218212676	1.197135	1.18017	1.183729	1.259447	1.291893	1.248765
CA50 (ATDC)	0.452028	0.417818	0.541537	0.590251981	0.574317	0.461963	0.299643	1.862884	1.262019	1.264299
COV of IMEPg	2.998567	2.898842	2.868967	2.933309218	2.545039	2.530296	2.402278	3.363111	3.379098	3.064118
COV of PPRR	7.923424	7.441354	7.903238	8.331349063	7.292756	7.574097	7.110501	7.372888	7.21003	7.155689
EGR %	41.90999	42.05914	42.41496	42.48589947	43.07802	43.7806	43.76021	38.77231	43.07738	42.11375
Fuel 1	E85	E85	E85	E85	E85	E85	E85	E85	E85	E85
Fuel 2	EHN + 91 Gasoline	EHN + 91 Gasoline	EHN + 91 Gasoline	EHN + 91 Gasoline	EHN + 91 Gasoline	EHN + 91 Gasoline	EHN + 91 Gasoline	EHN + 91 Gasoline	EHN + 91 Gasoline	EHN + 91 Gasoline
Fuel1 Flow (g/s)	0.841255	0.83946	0.813266	0.823116	0.808251	0.793004	0.792599	0.926645	0.912707	0.850694
Fuel2 Flow (g/s)	0.149341	0.147153	0.162055	0.167959	0.161939	0.17489	0.179154	0.117622	0.146629	0.149576
Fuel1 Fraction	0.849241	0.85085	0.833844	0.830528467	0.833085	0.819309	0.815638	0.887364	0.861584	0.850464
Fuel2 Fraction	0.150759	0.14915	0.166156	0.169471533	0.166915	0.180691	0.184362	0.112636	0.138416	0.149536
Fuel Energy (J/cyc)	2857.445	2844	2831.885	2881.67596	2817.894	2827.654	2843.322	2944.367	2894.249	2828.655
Fuel H/C	2897.463	2857.445	2844	2831.88456	2881.676	2817.894	2827.654	2843.322	2944.367	2.575574
Fuel O/C	0.311394	0.312191	0.303828	0.302212084	0.303457	0.296782	0.295017	0.330601	0.317538	0.312
Fuel MW/C	19.58709	19.60168	19.44865	19.41908547	19.44187	19.31973	19.28744	19.93853	19.69951	19.59818
RI (MW/m^2)	3.468288	3.435958	3.524666	3.475147206	3.958544	4.79444	5.027103	3.557167	3.580006	3.907951
Peak HRR (J/deg)	354.3913	355.027	367.5364	367.2510458	385.9666	407.282	405.4772	399.3112	384.7294	400.0899
Peak PRR (bar/deg)	11.26848	11.22545	11.1461	11.07285393	11.55331	12.47364	12.79373	11.66292	12.06307	12.08158
PP (bar)	138.6618	138.8807	134.6741	134.574397	130.359	126.9658	127.6778	142.8212	149.3105	140.6849
LPP (ATDC)	3.7	3.7	3.9	4	4.1	3.9	3.7	4.6	3.9	4.2
P Intake (bar)	1.57801	1.57516	1.515697	1.515938838	1.439859	1.375565	1.373199	1.725968	1.809728	1.657182
P Exhaust (bar)	1.72464	1.723893	1.658267	1.65930649	1.5804	1.510959	1.509888	1.90606	2.036986	1.85529
T Intake (C)	43.0071	44.24527	42.4612	44.190083	43.28031	43.44824	45.06422	46.84309	44.71255	45.71319
T Exhaust Tank (C)	244.0878	247.2954	250.7495	252.343684	257.3063	262.7062	263.7698	243.8365	237.7929	243.0664
Gross Therm Eff	0.584028	0.586878	0.586792	0.576117977	0.587474	0.58515	0.581832	0.56712	0.56295	0.585577
Net Therm Eff	0.54243	0.545059	0.54583	0.536046939	0.547686	0.546349	0.543276	0.523804	0.515259	0.540052
Brake Therm Eff (CF)	0.436622	0.438658	0.440786	0.432860376	0.44399	0.444475	0.441657	0.42006	0.411518	0.434357
Turbo Eff	0.721315	0.714979	0.712693	0.709566456	0.702001	0.701745	0.698014	0.706792	0.696287	0.685301
Vol Eff	0.887079	0.891753	0.877007	0.883183639	0.870523	0.860849	0.864099	0.9068	0.89057	0.881851
comb loss	0.030059	0.029916	0.026169	0.026289211	0.022954	0.020309	0.020337	0.032333	0.04097	0.033281
Comb Eff	0.969941	0.970084	0.973831	0.973710789	0.977046	0.979691	0.979663	0.967667	0.95903	0.966719
Exhaust Loss	0.290235	0.294405	0.288373	0.283850313	0.280039	0.269878	0.267039	0.303363	0.300368	0.292501
Pumping Loss	0.041598	0.041819	0.040963	0.040071037	0.039788	0.038801	0.038556	0.043316	0.04769	0.045524
Heat Transfer Loss	0.095677	0.0888	0.098666	0.1137425	0.109532	0.124663	0.130792	0.097184	0.095713	0.088641
HC (ppm)	1059.49	1131.359	1074.158	1067.343955	1118.879	1129.223	1140.311	1034.618	1107.839	1207.618
NOx (ppm)	41.4307	43.1103	55.40325	51.933576	73.03611	94.90806	98.17145	18.71895	16.1976	24.10189
CO2ex (ppm)	58940.17	59672.11	62955.95	63100.72146	68492.7	74186.98	74224.48	53837.97	54292.17	58453.42
CO2in (ppm)	24927.21	25322.39	26926.18	27032.06379	29726.16	32697.63	32699	21111.79	23608.5	24841.53
CO (ppm)	1727.512	1596.993	1383.848	1425.641128	1095.037	909.9548	891.8993	1728.659	2767.481	1821.028
PM (mg/m^3)	0.91	1.01	0.86	0.86	0.86	0.86	0.86	1.35	0.74	0.99
HC (g/kg-fuel)	17.14143	18.10505	16.39901	16.25050611	15.80218	14.79333	14.93244	18.25518	19.01957	19.61234
NOx (g/kg-fuel)	1.574201	1.618993	2.000568	1.87300865	2.440571	2.960372	3.066026	0.761995	0.649347	0.918741
CO2ex (g/kg-fuel)	2142.609	2144.02	2174.946	2177.305736	2189.735	2213.933	2217.845	2096.78	2082.367	2131.795
CO2in (g/kg-fuel)	906.1608	909.834	930.2213	932.7479336	950.3554	975.7825	977.0541	822.2223	905.5	905.9701
CO (g/kg-fuel)	39.96819	36.51927	30.42717	31.3081242	22.28116	17.28297	16.9614	42.84846	67.5564	42.26821
PM (g/kg-fuel)	0.011801	0.013196	0.011088	0.01094596	0.010807	0.010486	0.010442	0.018126	0.008929	0.012493
HC (g/ikW-hr)	3.381211	3.55639	3.198495	3.223719425	3.07752	2.87568	2.914764	3.769639	3.912785	3.860396
NOx (g/ikW-hr)	0.310517	0.31802	0.390195	0.371561004	0.475308	0.575468	0.598478	0.15735	0.133586	0.18084
CO2ex (g/ikW-hr)	422.6377	421.1517	424.2057	431.926412	426.4572	430.367	432.9162	432.9787	428.3931	419.612
CO2in (g/ikW-hr)	178.7436	178.7195	181.4322	185.0353222	185.0844	189.6827	190.7178	169.7864	186.2832	178.3266
CO (g/ikW-hr)	7.883875	7.173511	5.934576	6.210797835	4.339319	3.359641	3.31081	8.848078	13.89798	8.319864
PM (g/ikW-hr)	0.002328	0.002592	0.002163	0.002171422	0.002105	0.002038	0.002038	0.003743	0.001837	0.002459
Air Flow (kg/min)	1.421673	1.417369	1.340608	1.341254	1.246324	1.162291	1.159177	1.655314	1.595349	1.466443
AFR mass	23.91949	23.94335	22.90883	22.55554154	21.41031	20.01409	19.8812	26.41907	25.09983	24.43412
AFR carbon	24.54533	24.26958	23.37765	23.35009133	21.69528	20.3085	20.33441	26.23474	25.81335	24.61253
AFR Average	24.23241	24.10646	23.14324	22.95281643	21.5528	20.16129	20.10781	26.32691	25.45659	24.52333
AFR Stoich	10.47478	10.46738	10.5456	10.56085561	10.54909	10.61246	10.62935	10.29943	10.41801	10.46916
Phi mass	0.437918	0.437173	0.460329	0.468215564	0.492711	0.53025	0.534643	0.389848	0.415063	0.428465
Phi carbon	0.426753	0.431296	0.451098	0.452283268	0.486239	0.522563	0.522727	0.392587	0.40359	0.425359
Phi Lambda meter	0.444603	0.447274	0.469248	0.469989	0.506071	0.544239	0.545417	0.390962	0.409943	0.433255
GTE emisisons based	0.599309	0.594875	0.598801	0.59641252	0.595293	0.593758	0.595095	0.563163	0.578953	0.589852
EXH emissions based	0.286535	0.292427	0.285481	0.279020927	0.2782	0.267922	0.264064	0.304429	0.296217	0.291441
HX emisisons based	0.091737	0.086781	0.095553	0.108424614	0.107462	0.122315	0.127136	0.098096	0.091862	0.087563
charge based PHI	0.254387	0.253302	0.265081	0.26928997	0.280461	0.298103	0.300682	0.238695	0.236265	0.248022
Emission charge based PHI	0.251144	0.251599	0.262423	0.264708312	0.278619	0.295942	0.297331	0.239534	0.232999	0.247123

Table A. 13 40% EGR 43°C intake temperature Piston Oil Cooling Off Continued

MATRIX POINT	93	94	95	96	97	98	99	100	101	102
RPM	1300	1300	1300	1300	1300	1300	1300	1300	1300	1300
IMEPg (bar)	6.889411	6.803593	6.841901	6.840555693	6.889639	6.829242	6.816434	6.841617	6.855651	6.835662
IMEPn (bar)	6.348128	6.284665	6.344311	6.357380079	6.390885	6.339218	6.330753	6.344023	6.364382	6.355122
BMEP_CF (bar)	5.106561	5.057921	5.104768	5.13641831	5.168121	5.138809	5.114807	5.154669	5.170949	5.208986
FMEP_CF (bar)	1.241568	1.226744	1.239543	1.220961769	1.222764	1.200409	1.215945	1.189354	1.193434	1.146136
CA50 (ATDC)	1.455599	1.180153	0.776182	0.854418773	0.461399	1.283451	0.547657	0.273084	0.338519	0.284036
COV of IMEPg	3.227925	2.907722	2.779716	2.786860477	2.745093	2.679863	2.694255	2.371144	2.296371	2.142279
COV of PPRR	7.173063	7.164443	6.893906	6.717658048	9.795381	6.906962	7.058494	6.563802	6.068004	6.181533
EGR %	42.18338	42.62636	39.23024	40.02206129	40.02114	41.01564	39.99813	43.63234	43.58871	45.441
Fuel 1	E85	E85	E85	E85	E85	E85	E85	E85	E85	E85
Fuel 2	EHN + 91 Gasoline	EHN + 91 Gasoline	EHN + 91 Gasoline	EHN + 91 Gasoline	EHN + 91 Gasoline	EHN + 91 Gasoline	EHN + 91 Gasoline	EHN + 91 Gasoline	EHN + 91 Gasoline	EHN + 91 Gasoline
Fuel1 Flow (g/s)	0.848636	0.822452	0.811972	0.793901	0.804224	0.807079	0.819676	0.78541	0.802572	0.711531
Fuel2 Flow (g/s)	0.138816	0.158263	0.17612	0.20669	0.201917	0.171367	0.176468	0.211696	0.193128	0.269554
Fuel1 Fraction	0.85942	0.838625	0.821757	0.793432082	0.799315	0.824858	0.822849	0.78769	0.806038	0.725249
Fuel2 Fraction	0.14058	0.161375	0.178243	0.206567918	0.200685	0.175142	0.177151	0.21231	0.193962	0.274751
Fuel Energy (J/cyc)	2907.128	2879.013	2875.195	3124.25407	3045.709	3062.144	3122.977	3061.315	2925.168	2979.886
Fuel H/C	2.58573	2.562277	2.54358	2.512821793	2.519146	2.546995	2.544781	2.506682	2.526413	2.441908
Fuel O/C	2894.249	2828.655	2907.128	2879.01303	2875.195	3124.254	3045.709	3062.144	3122.977	3061.315
Fuel MW/C	19.67971	19.49142	19.34133	19.09440064	19.14517	19.36874	19.35097	19.04511	19.20351	18.5251
RI (MW/m^2)	3.544123	4.180077	4.651165	4.384027927	4.08174	5.137456	5.99553	8.202309	8.781549	8.366831
Peak HRR (J/deg)	394.3699	400.9282	402.1626	404.7772155	386.3342	438.5006	426.8114	470.4865	485.3186	483.3785
Peak PRR (bar/deg)	11.4695	12.2227	12.98639	12.39059796	11.97736	13.15029	14.28687	16.17663	16.73196	15.65104
PP (bar)	139.2454	136.2806	138.8404	135.1242155	135.4846	131.0137	134.1209	128.8026	129.6186	120.159
LPP (ATDC)	4.4	4.1	3.7	3.9	3.8	4.5	3.6	3.4	3.5	3.4
P Intake (bar)	1.66008	1.576803	1.573808	1.517001527	1.51763	1.442419	1.440584	1.307504	1.304654	1.199495
P Exhaust (bar)	1.854592	1.763817	1.723243	1.674081197	1.670103	1.598195	1.588469	1.465352	1.463648	1.372987
T Intake (C)	44.56839	43.88068	45.57585	42.560219	44.10322	42.92678	43.2062	46.2834	43.19561	44.05886
T Exhaust Tank (C)	243.1477	246.9266	247.2518	250.286621	251.9186	256.5764	256.2589	268.0507	270.0176	284.3466
Gross Therm Eff	0.592956	0.584379	0.579128	0.56502515	0.567333	0.584521	0.572573	0.565733	0.572062	0.55992
Net Therm Eff	0.546369	0.539807	0.53701	0.525115179	0.526262	0.542579	0.531776	0.524587	0.531069	0.520558
Brake Therm Eff (CF)	0.43951	0.434439	0.43209	0.424264585	0.425573	0.439835	0.429638	0.426239	0.431484	0.426677
Turbo Eff	0.688719	0.676548	0.715074	0.696741379	0.699809	0.682301	0.69404	0.647864	0.642745	0.569287
Vol Eff	0.878019	0.866584	0.896934	0.874931166	0.884055	0.879304	0.87622	0.858962	0.846964	0.826141
comb loss	0.033994	0.029852	0.030319	0.026490467	0.023303	0.021975	0.023324	0.016004	0.015829	0.022191
Comb Eff	0.966006	0.970148	0.969681	0.973509533	0.976697	0.978025	0.976676	0.983996	0.984171	0.977809
Exhaust Loss	0.299439	0.286909	0.288759	0.275122065	0.276155	0.279795	0.272309	0.24597	0.251913	0.234183
Pumping Loss	0.046587	0.044572	0.042118	0.03990997	0.04107	0.041942	0.040797	0.041146	0.040993	0.039362
Heat Transfer Loss	0.073611	0.098861	0.101794	0.133362318	0.133209	0.113709	0.131795	0.172294	0.160195	0.183706
HC (ppm)	1213.049	1221.397	1190.141	1159.31798	1158.82	1064.257	1230.969	1000.861	993.9832	1116.678
NOx (ppm)	23.39602	32.94178	33.25365	42.621476	120.7845	80.37434	115.8522	170.5624	165.3339	148.8752
CO2ex (ppm)	58200.5	62517.56	58354.11	62223.62125	64403.71	67092.85	66225.06	83005.39	83025.13	96144.35
CO2in (ppm)	24775.27	26871.57	23128.24	25135.89024	26007.81	27747.43	26721.59	36435.9	36408.46	43900.64
CO (ppm)	1891.899	1582.106	1429.266	1195.979357	844.2807	988.4687	784.8725	772.0542	755.2891	2363.774
PM (mg/m^3)	0.93	0.62	0.62	0.62	0.52	0.67	0.67	0.67	0.67	0.98
HC (g/kg-fuel)	19.75707	18.67004	19.4904	17.92655624	17.42549	15.37118	18.01104	11.79107	11.71057	11.19392
NOx (g/kg-fuel)	0.890688	1.188365	1.295189	1.58772244	4.363939	2.756985	4.029501	4.853303	4.665932	3.705732
CO2ex (g/kg-fuel)	2119.843	2157.737	2174.498	2217.659762	2226.241	2201.845	2203.752	2259.717	2241.71	2289.649
CO2in (g/kg-fuel)	902.3921	927.4479	861.847	895.8471277	899.0111	910.6118	889.2068	991.9212	983.0422	1045.481
CO (g/kg-fuel)	43.85677	34.75311	33.89709	27.12845484	18.57419	20.64597	16.62269	13.37695	12.97911	35.82719
PM (g/kg-fuel)	0.01189	0.00774	0.008491	0.008046	0.006782	0.008692	0.008663	0.007688	0.007687	0.010516
HC (g/ikW-hr)	3.855242	3.663912	3.832098	3.569910221	3.464516	2.998243	3.58343	2.339543	2.315545	2.187276
NOx (g/ikW-hr)	0.173802	0.233211	0.254653	0.316180447	0.867634	0.537767	0.801699	0.962975	0.9226	0.724095
CO2ex (g/ikW-hr)	413.6498	423.4462	427.5381	441.626721	442.6186	429.4834	438.4528	448.365	443.2559	447.394
CO2in (g/ikW-hr)	176.0858	182.0075	169.4517	178.3997871	178.7404	177.6204	176.9143	196.8135	194.378	204.2854
CO (g/ikW-hr)	8.557871	6.820143	6.664665	5.402384423	3.692899	4.027122	3.307207	2.654208	2.566374	7.00058
PM (g/ikW-hr)	0.00232	0.001519	0.001669	0.001602287	0.001348	0.001695	0.001724	0.001525	0.00152	0.002055
Air Flow (kg/min)	1.466129	1.366872	1.487686	1.393772	1.402058	1.308289	1.323332	1.095458	1.089165	0.942112
AFR mass	24.746	23.22917	25.09358	23.21581279	23.22501	22.28515	22.14091	18.31062	18.23114	16.00459
AFR carbon	24.57632	23.34205	25.15627	24.10954051	23.41545	22.25918	22.56086	18.60707	18.45572	16.34883
AFR Average	24.66116	23.28561	25.12493	23.66267665	23.32023	22.27217	22.35088	18.45885	18.34343	16.17671
AFR Stoich	10.42796	10.52361	10.6012	10.73148911	10.70443	10.58694	10.59618	10.7579	10.67351	11.04511
Phi mass	0.4214	0.453034	0.422467	0.462249123	0.460901	0.475067	0.478579	0.587522	0.585455	0.690121
Phi carbon	0.424309	0.450844	0.421414	0.445113796	0.457152	0.475621	0.469671	0.578162	0.57833	0.67559
Phi Lambda meter	0.432569	0.460994	0.426432	0.455799	0.469046	0.48798	0.480184	0.597872	0.600392	0.699632
GTE emisisons based	0.58889	0.587219	0.580575	0.586776645	0.571985	0.58384	0.583433	0.574892	0.579109	0.571963
EXH emissions based	0.300473	0.286215	0.288399	0.270022752	0.275032	0.279958	0.269775	0.24401	0.250381	0.231717
HX emisisons based	0.074611	0.098135	0.10143	0.127585884	0.132006	0.113886	0.128899	0.169673	0.158204	0.18015
charge based PHI	0.243639	0.259922	0.256732	0.277247496	0.276443	0.280215	0.287156	0.331173	0.330262	0.376523
Emission charge based PHI	0.24448	0.259294	0.256412	0.272108788	0.275319	0.280379	0.284484	0.328535	0.328253	0.372559

Appendix B - Impingement

A.B.1 GTE and Losses of Tested E85 Fuels

This appendix section investigates the influence of the direct injected fuel properties on efficiency. The engine was operated in the Φ-T matrix, as described shown in Figure 44 with conditions in Table 16. The engine was fueled with a E85 PFI and ULSD DI strategy, or a E85 PFI and 3% EHN + 91 PON Gasoline DI strategy. The GTE results from the matrix of test conditions are plotted below in Figure A. 3 for EHN gasoline/E85 at left and ULSD/E85 at right.

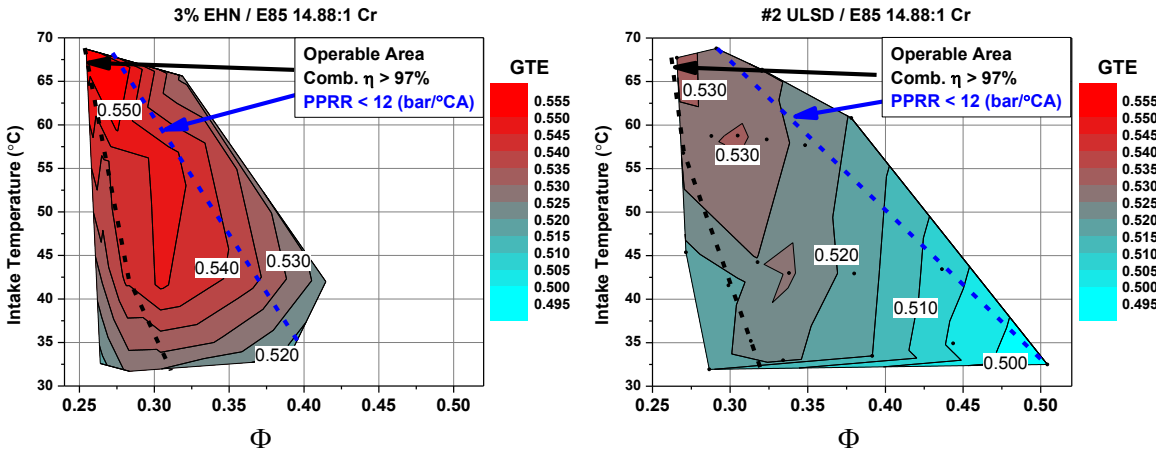

Figure A. 3 GTE contours from direct measured mass flow rates. Left, EHN gasoline displays ~2 GTE point improvement compared to ULSD operation.

The results demonstrate that there is an approximate 2% point difference in thermal efficiency from the two cases. Initially combustion efficiency was investigated as a potential source of difference between the two cases. However, as seen in Figure A. 4 it was found that the combustion efficiencies are generally the same between the two cases, with a slight advantage observed with EHN

gasoline of approximately 0.5% point higher combustion efficiency (0.5% lower incomplete combustion).

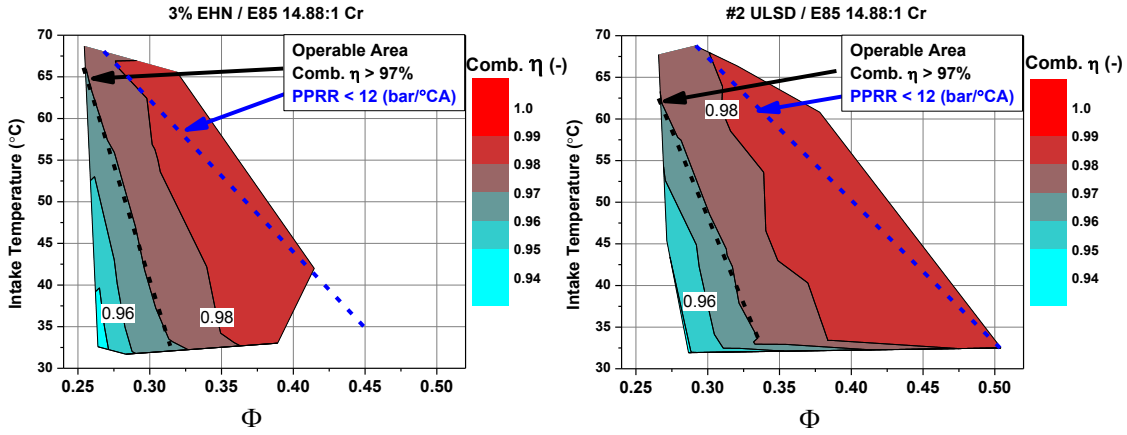

Figure A. 4 Contours of combustion efficiency from the two E85 fueled strategies, ULSD (right) EHN gas (left). It is observed that only a fraction of the GTE difference observed results from combustion efficiency.

The results show that the combustion efficiency are similar and therefore only heat transfer and exhaust losses are possible sources to account for efficiency differences. The exhaust losses are plotted in Figure A. 5.

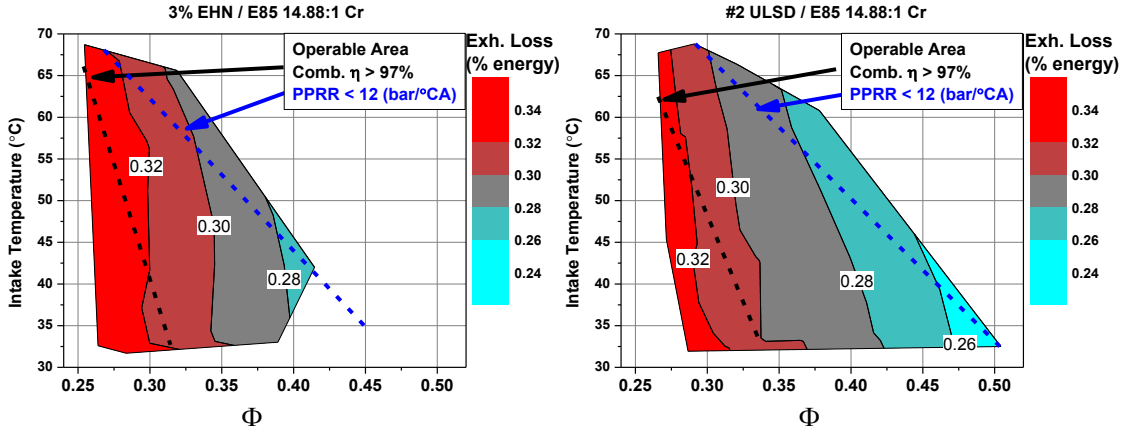

Figure A. 5 Contours of exhaust loss for E85 fueling strategies, ULSD (right) EHN gas (left). The results demonstrate that for a given Φ-T condition, the exhaust losses are generally similar.

It is observed that the exhaust losses are almost identical. For instance the 0.30 Φ contour is essentially identical for both E85 strategies, with the overall values and trends being similar across the comparable Φ-T space. Although not plotted for the sake of brevity, the exhaust temperature and volumetric efficiency (VE) of the two cases are nearly identical, thus the exhaust losses are the same due to similar temperature exhaust and mass flow rates (see Appendix A, Table A. 1 and Table A. 2 for details)

The last source that loss is due to is heat transfer. Heat transfer is not directly solved for as shown in Chapter 4, but is calculated as the unaccounted for loss (see Equation 40). The results of Chapter 5 demonstrated that HX was strongly tied to trapped mass. In the present study this was also observed where the trends in HX are plotted in Figure A. 6.

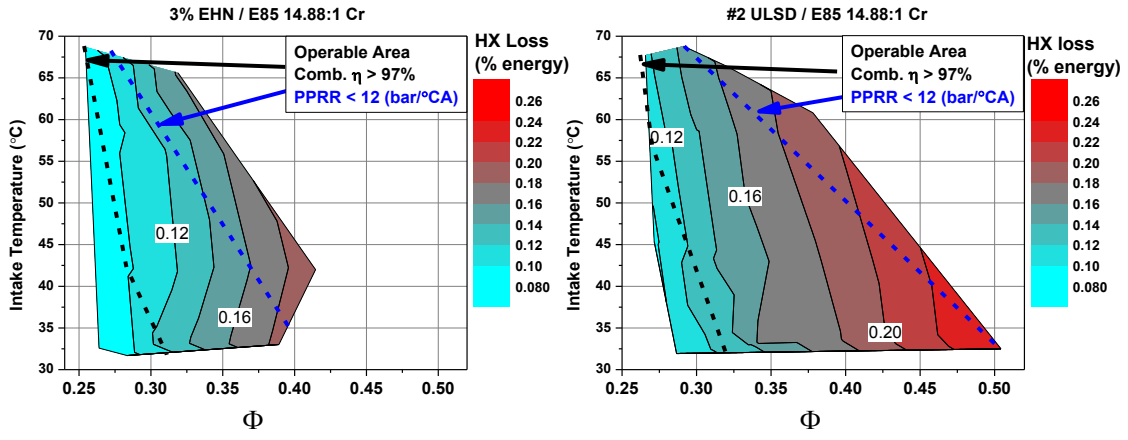

Figure A. 6 HX losses for the tested E85 fueling strategies, ULSD (right) EHN gas (left). Notice that the HX values of ULSD operation are significantly higher than those of EHN operation, ~1.5-2 points HX for a given Φ-T condition.

The results illustrate that the higher efficiency results with EHN gasoline vs. ULSD are from HX differences. This could be a result of in-cylinder mixing

differences as gasoline vaporizes at lower temperatures More plausible is that the higher HX is a result of the definition of HX, and that outside losses are being interpreted as heat transfer. For example, in the present analysis GTE is calculated from the direct measured fuel and mass flow rates (not from an average of AFR determined mass rates as in Chapters 5 and 6). As previously stated, this approach affords the potential for discrepancies, as it combines independent measurements from emissions (combustion efficiency) and mass (GTE, EXH. Loss) to calculate HX.

The results Figure A. 6 show that losses contributing to GTE are strongly coupled to trapped mass (Φ at fixed load and combustion phasing), and less to intake temperature. For a given Φ, only incomplete combustion was observed to decrease as temperature was increased, which only had a slight fuel dependence. Additionally, the HX and Exhaust losses of the ULSD/E85 case are observed to have a weak temperature dependency, particularly at the lowest trapped masses and temperatures.

A.B.2 Effects of Volatility for Direct Injected Fuel

To determine the validity of the GTE and HX trends in Figure A. 3 and Figure A. 6 respectively, a carbon balance was performed using Equation 42. Figure A. 7 shows the results as functions of reactive fuel fraction, for reference CDC operation from Table 22 in section 5.2.2 are also plotted as control conditions.

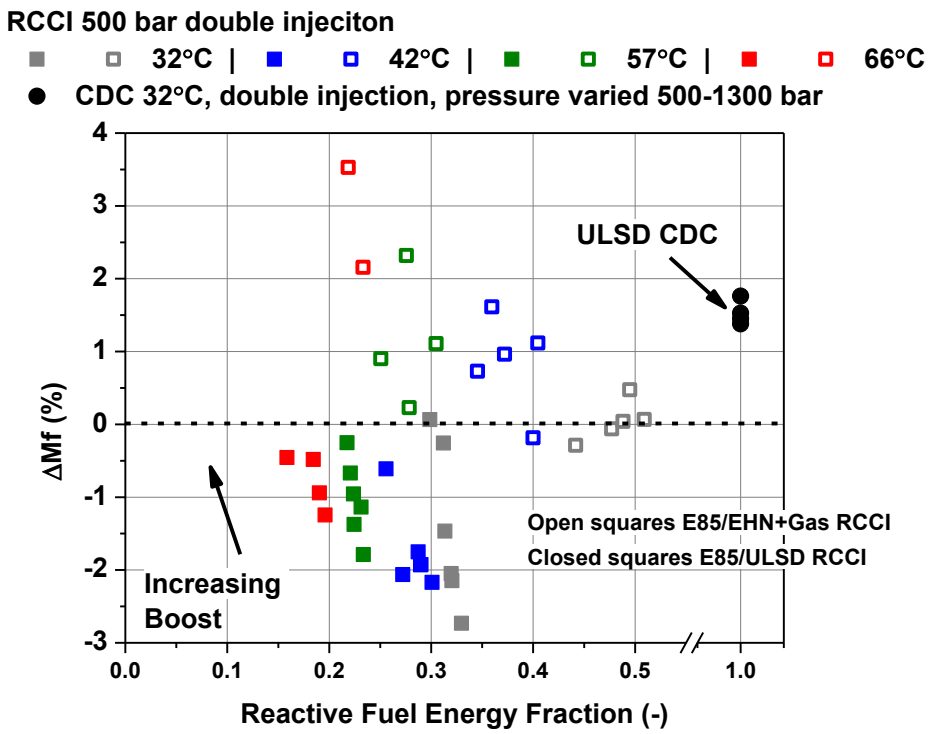

Figure A. 7 Carbon balance of Φ-T matrix RCCI operation Figure 44 with ULSD (solid markers) and EHN gasoline (open markers). The results are color coded to intake temperature, where the highest and lowest ΔM_f values, respectively, correspond to the highest and lowest boot conditions. CDC with ULSD is plotted for reference, as it is assumed that minimal fuel impingement exists at the near TDC timings required for mixing controlled combustion.

The figure illustrates several trends that are key in understanding the GTE and corresponding HX differences from the results with EHN gasoline and ULSD. The a differences in the measured and calculated fuel masse are generally within the accepted error range, but the errors span the limits of acceptability, with each fueling strategy being clumped at ~1-2% high or low of zero difference in AFR. This results in a ~2% point difference in fuel flow rates from the two studies. As will be shown, this can stem from charge preparation and fuel property sources.

In the presented contour plots of GTE and HX, the fuel flow was determined only from the direct mass flow measurements. A more detailed comparison of these results is presented in Figure A. 8, where results are at a

constant temperature of 57°C while sweeping Φ (boost) (corresponding to Φ-T conditions).

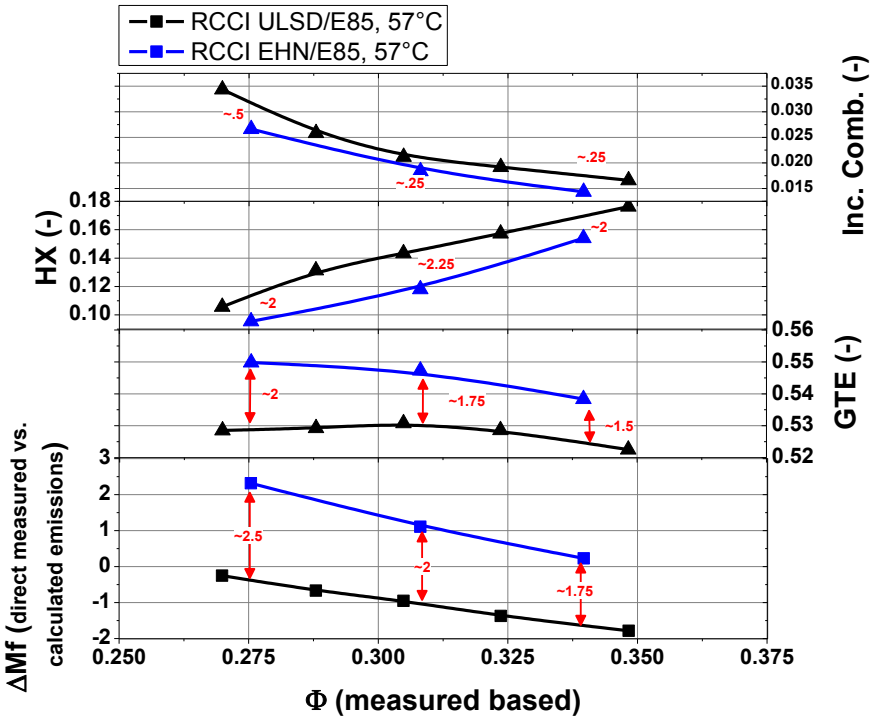

Figure A. 8 Losses and performance of fixed temperature varied Φ (analogous to boost at constant phasing and load). The trends demonstrate that the carbon difference between the two fuels is directly captured in HX, and corresponding the HX and incomplete combustion differences is accounted for in GTE. This demonstrates that differences in HX and correspondingly GTE are likely to be real and from impingement.

From the figure it is clear that corresponding difference in GTE and HX are likely to be a result of different fuel flow measurements, and not from actual HX differences. If the GTE is determined from the emissions bench, the performance of the cases are very similar, with EHN gasoline operation being slightly improved due only to reduced incomplete combustion. Figure A. 9 illustrates this where contours of GTE calculated from AFR_c are plotted in Φ-T space.

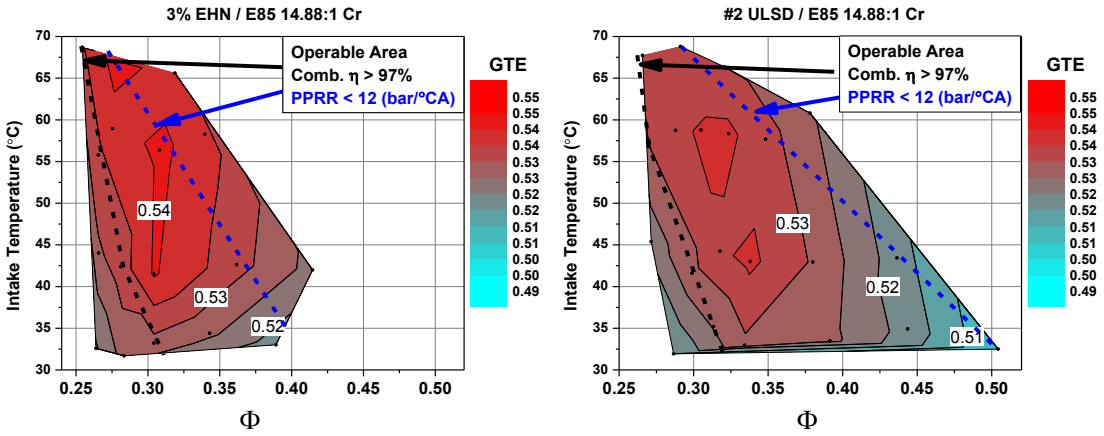

Figure A. 9 GTE contours determined from AFR_c based fuel flow. This approach demonstrates that the differences in GTE are likely to be from fuel impingement which is metered in the mass based AFR but not captured in the emissions based AFR.

The results show that when operated with ULSD at injection timings of -60 and -35°CA ATDC there is a discrepancy in the AFR measurements. To investigate the sources of this, injection timings were swept. The sweep was performed with the high compression ratio piston, see Figure 34. In the study, single injection timings were swept from -60 to -85 °CA ATDC, and a double injection -60 and -35 °CA ATDC as a baseline, (injection timing of both Φ-T and Oil Matrices). The operating conditions were similar to that of the earlier study, but load was fixed at 6.4 bar IMEPn due to higher in-cylinder pressure with 18.7:1 Cr. Fuel combinations of ULSD/E100, ULSD/E85, and 3% EHN + 91 PON gasoline/E85 were tested. The results are presented in Figure A. 10.

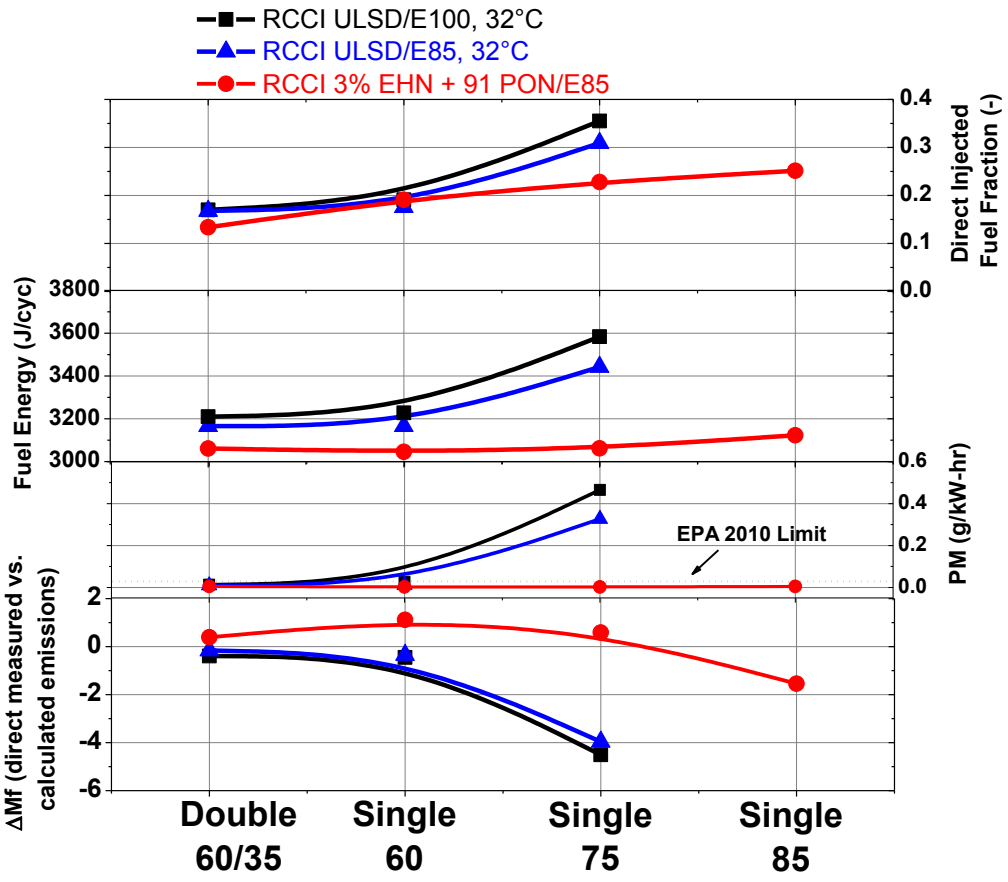

Figure A. 10 Fueling rate, energy, PM, and carbon balance of different early injection strategies for ULSD and EHN gasoline direct injections with ethanol based port fuels. Note that EHN gasoline does not exhibit injection timing sensitivity as dramatically as lower volatility ULSD. The x-axis label denotes the DI strategy and the numbers denote the injection timing used in CA BTDC.

From the results it is seen that as injection timings are advanced, operation with ULSD requires higher fuel flow rates to maintain load. This was the most prevalent at the single injection at -75 °CA ATDC (-85 not tested with ULSD). The results show that with ULSD, fuel is being lost within the engine, that is, metered fuel is unaccounted for in the exhaust emissions determined fuel flow rate. The tendency was not observed with EHN gasoline, where even earlier injection timings resulted in only slight decreases in the mass flow rate of carbon, suggesting that at the baseline condition of 60/35 ULSD may be impinging (as

shown in Figure A. 6). The increase in fueling rate was only required to the reactive fuel as seen by the corresponding reactive fuel flow rate (g/sec) values in Table A. 14.

Table A. 14 direct injection fueling requirements for respective early injection strategies with ethanol based fuels

Fuel	Injection Strategy							
	-60/-35		-60		-75		-85	
	DI (g/s)	PFI (g/s)	DI (g/s)	PFI (g/s)	DI (g/s)	PFI (g/s)	DI (g/s)	PFI (g/s)
ULSD/E100	0.200	0.976	0.223	0.946	0.424	0.77	N/A	N/A
ULSD/E85	0.182	0.832	0.190	0.824	0.344	0.691	N/A	N/A
EHN Gas/E85	0.143	0.926	0.198	0.840	0.234	0.794	0.261	0.777

From the Table A. 14 it is seen that regardless of the fuels, as the injections are advanced higher fueling is required. This demonstrates that there are changes in the reactivity gradient, and in the case of very early injection timings, the dramatic increase in reactive fuel required could be from spray-liner impingement. Figure A. 11 shows the spray targeting of injections at -60 and -35°CA ATDC.

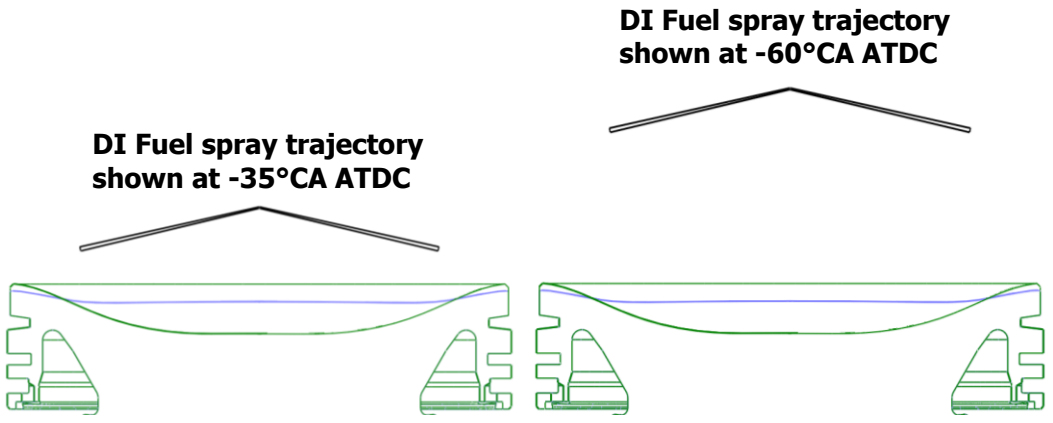

Figure A. 11 Spray targeting for operation with -60/-35 CA ATDC injector timings with the DI injector described in Table 9, and pistons described in Figure 34. Green outline is of the 14.88:1 bathtub piston, blue outline is of the 18.7:1 Cr pancake piston.

The targeting images show that at the early injection timings, fuel-liner impingement is possible, as the spray is directed at the liner.

In similar early injection strategies like LTC, increased PM emissions have been observed with simultaneous linear impingement as demonstrated with detailed PM emissions measurements by Kolozdiej et al. [146]. Likewise, Figure A. 10 demonstrates that there is a marked increase in PM emissions with advanced injections of ULSD, suggesting that fuel-liner impingement is occurring at the early timings. Conversely, with EHN gasoline there was not an observed increase in PM. The results show that fuel volatility may be important if efficiency and the operable window of RCCI are to be maximized.

Appendix C – Combustion Phasing Effects

A.C.1 GTE and Losses of Tested E85 Fuels

This appendix section investigates the influence of combustion phasing on efficiency and operating conditions. Although later combustion phasing does not offer the highest gross efficiency it often does have increased brake efficiency due to reduced peak cylinder pressure and reduced pumping losses. Thus, it is of merit to investigate the relation on EGR and CA50 on the operable window. The engine was operated in the Φ-T matrix, as described shown in Figure 44 with conditions in Table 16, but the combustion phasing (CA50) was retarded to 5.0°CA ATDC and 45% EGR was used. The engine was fueled with a 91 PON gasoline PFI and ULSD DI strategy. Select AHRR and cylinder pressure traces are seen in Figure A. 12, where 0% EGR cases are plotted for reference.

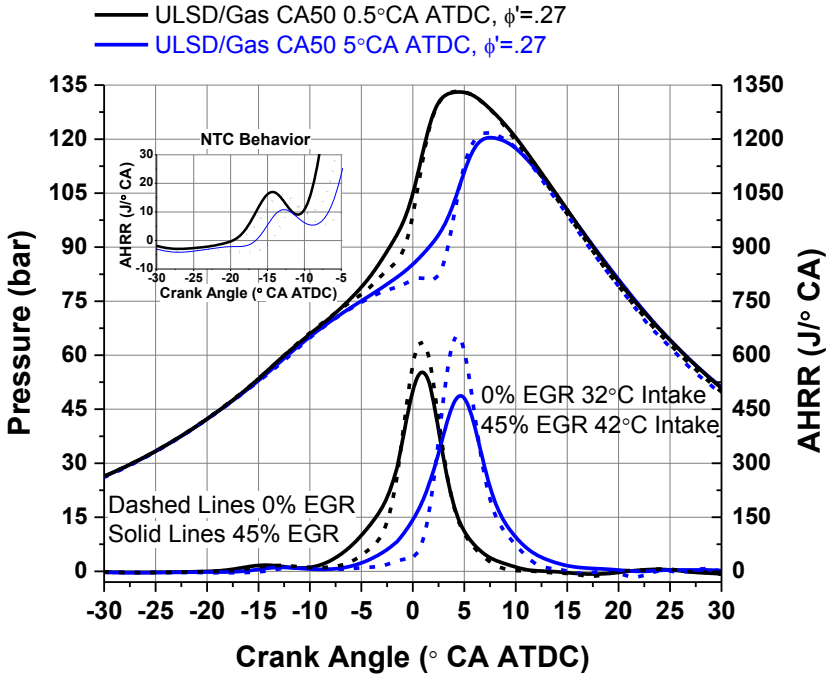

Figure A. 12 Dilute RCCI operation at TDC and 5°CA ATDC CA50 combustion phasing both with (solid) and without EGR(dashed). The trends support the previous equivalence ratio results above, where EGR offers a significantly higher diluent effect than air alone.

The results of the operable area are presented in Figure A. 13 where it was seen that the operable window was significantly increased. The same color coding of Table 23 are used.

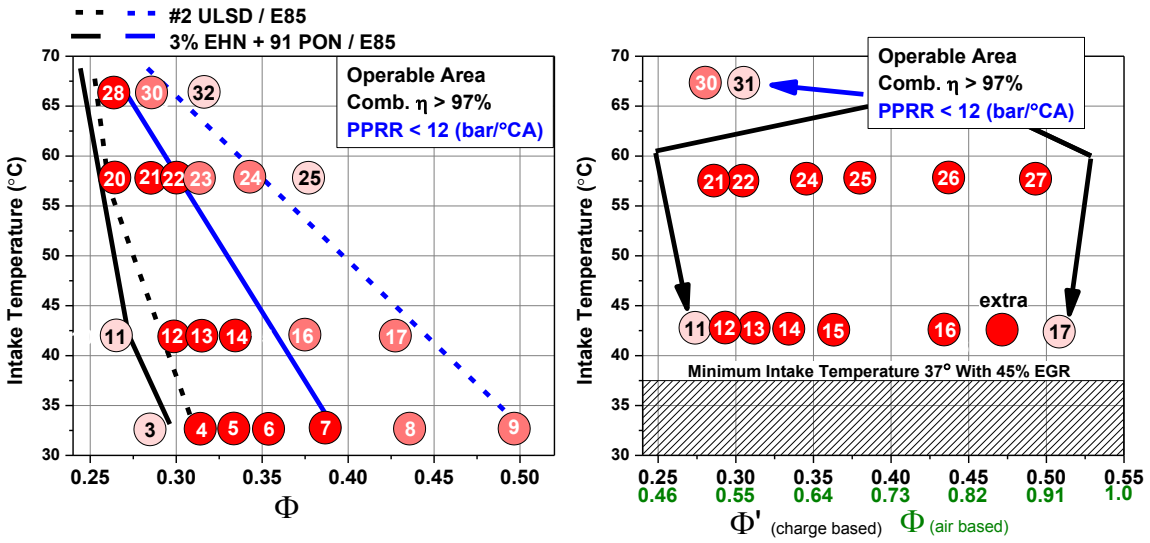

Figure A. 13 Effect of combustion phasing on the Φ-T operable window of gasoline/ULSD RCCI at 8.45 bar IMEPg. With later combustion phasing, the operable window dramatically expands with only HCCI conditions exhibiting PPRR constraints issues

From the figure it is seen that the entire Φ-T matrix could be operated, provided that HCCI was not encountered (66°C, see section 5.2.8). Additionally, only at the conditions of HCCI were maximum PPRR encountered (+12 bar/°CA). Thus, at the later combustion phasing with EGR, the only Φ-T operable window limiting factors of RCCI are increased incomplete combustion at locally lean and rich conditions (as demonstrated in Figure 46 of Chapter 5 where CO emissions with EGR were discussed).

The present results demonstrate that if the majority of HTHR occurs after TDC, the combustion event is similar, but the process it is confined to is expanding. This is a key point, as the later combustion phasing are actually quite similar in charge preparation and combustion behavior, as indicated in Figure A. 14.

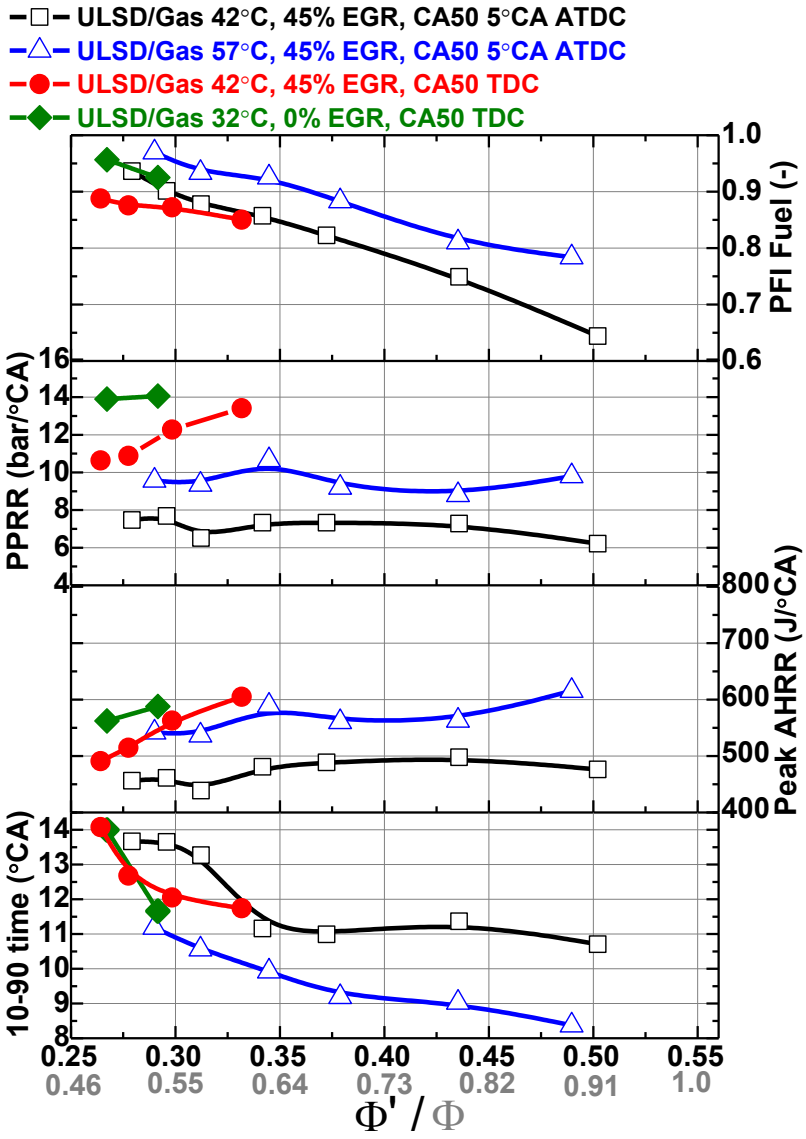

Figure A. 14 Combustion process behavior and fuel requirements for gasoline/ULSD operation at TDC without EGR (green, diamonds), at TDC with 45% EGR (red, circles), at 5°CA ATDC phasing with EGR (black squares) and at 5°CA ATDC phasing and higher intake temperature (blue triangles).It is observed that the major difference in operation is PPRR.

These presented relations demonstrate that the dynamic pressure and temperature combination with the expanding volume after TDC lends itself to reduce PPRR, even though the combustion event and fueling requirements are only marginally different. First this shows the power that fuel reactivity has on combustion phasing, where only small incremental changes are required to phase combustion. Secondly, this shows that the Φ-T matrix TDC tests of Chapter 5 are relatable to multiple combustion phasings, as the cycle denominates the PPRR more than the phasing. Similar results have been demonstrated by Dec and Yang [21] where later combustion phasing enables higher load knock free HCCI.

As shown in Chapter 5, later combustion phasings offer the potential for increased brake efficiencies, even though their gross efficiencies are often lower. These trends are demonstrated in Figure A. 15 below where BTE was computed using the approach described in Splitter et al. [37].

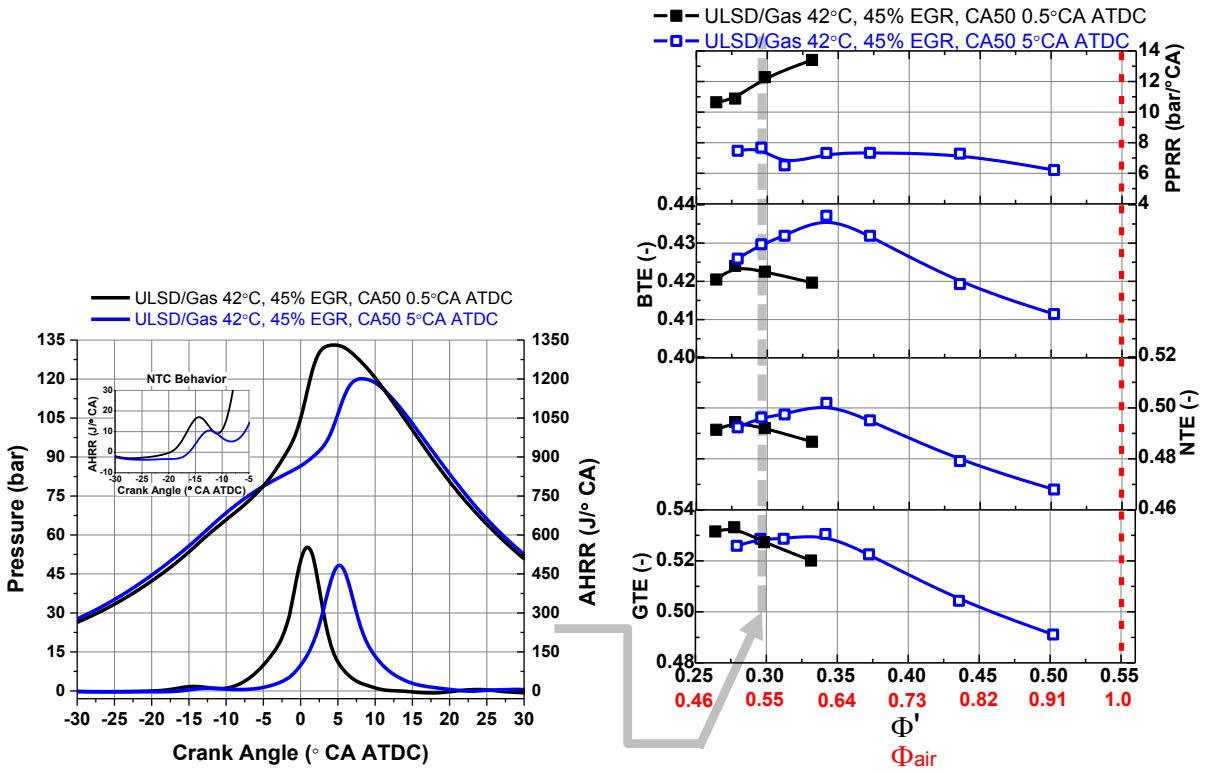

Figure A. 15 If the heat release event is retarded, even 5 CAD, then the operation window is expanded, and BTE can actually increase. This shows that the dynamic effect of pressure and temperature has a profound effect on heat release.

The present section has demonstrated that combustion phasing can be manipulated to offer reduced PPRR results. This affords the opportunity to increase the operable window of RCCI. Figure A. 16 graphically depicts these observations.

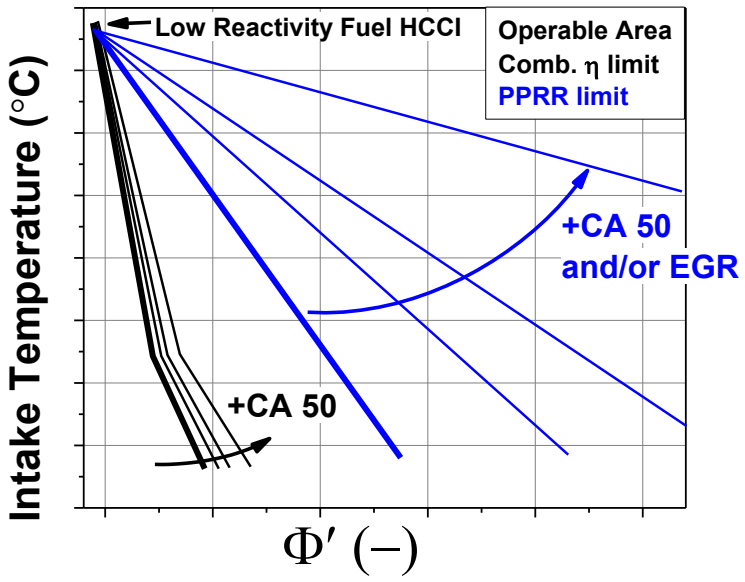

Figure A. 16 Generalization of the operable window findings of operation with EGR and retarded combustion phasing

It was also shown that at the later phasings the combustion event was relatively similar, and the expanded window was related more to the process of expansion during heat release than the existence of actually longer or less abrupt heat release rate.

Appendix D – Codes

A.D.1 AFR Calculation

The following MATLAB script outlines the procedure used to calculate AFRc for oxygenated and wet (hydrous) fuels. The code and calculations were developed by Wissink [122]

```
% Calculates emissions balances and AFRs

function [AFR,phi,emissions,EGR,fuel] =
emission_calc(emissions,phi,geom,mdot,temp,pressure,Pn,Pg,Pb,P_FMEP,Eta
s_mode)

omega = 0;      % mass specific humidity of air


% EGR% based on CO2 at intake and exhaust
EGR = max(100*(emissions.CO2in.ppm - 388)/(emissions.CO2ex.ppm -
388),0);

% calculate fuel mixture properties on molar basis
y_DI = geom.HtoC_DI;
y_PFI = geom.HtoC_PFI;
z_DI = geom.OtoC_DI;
z_PFI = geom.OtoC_PFI;
H2Ofrac_DI = geom.H2Ofrac_DI;           % mass fraction of H2O in DI
H2Ofrac_PFI = geom.H2Ofrac_PFI;         % mass fraction of H2O in PFI
MW_DI = 12.01 + 1.008*y_DI+z_DI*16;     %g/mol
MW_PFI = 12.01 + 1.008*y_PFI+z_PFI*16;  %g/mol
ndot.DI = (1-H2Ofrac_DI)*mdot.DI/MW_DI;     % molar flowrate of DI fuel
ndot.PFI = (1-H2Ofrac_PFI)*mdot.PFI/MW_PFI; % molar flowrate of PFI
fuel
y = (ndot.DI*y_DI+ndot.PFI*y_PFI)/(ndot.DI+ndot.PFI);    %H/C ratio
z = (ndot.DI*z_DI+ndot.PFI*z_PFI)/(ndot.DI+ndot.PFI);    %O/C ratio
MW_fuel = 12.01 + 1.008*y+z*16; %g/mol
MW_H2O = 18.01528;              %g/mol
ndot.H2O.DI = H2Ofrac_DI*mdot.DI/MW_H2O;    % molar flowrate of H2O in
DI
ndot.H2O.PFI = H2Ofrac_PFI*mdot.PFI/MW_H2O; % molar flowrate of H2O in
PFI
n_H2O_f = (ndot.H2O.DI + ndot.H2O.PFI)/(ndot.DI+ndot.PFI); % moles H2O
per mole carbon
fuel.MW = MW_fuel;
fuel.HtoC = y;
fuel.OtoC = z;
fuel.mfH2O = (H2Ofrac_DI*mdot.DI +
H2Ofrac_PFI*mdot.PFI)/(mdot.DI+mdot.PFI);
```

```
% Gas properties
MW_air = 28.97;     %g/mol
R_air = 8.314/MW_air*1000;   %J/kg-K
MW_CO2 = 44.01;     %g/mol
MW_CO = 28.01;      %g/mol
MW_NO2 = 46;        %g/mol
MW_HC = 83.25/2;    %g/mol (from GM test code)

% calculation of rho for use in specific PM calc
T = temp.extank + 273.15;   %K
P = pressure.exhaust*6894.75729+101325; %Pa
rho = P/(R_air*T); %kg/m^3

% total fueling rate
mdot.fuel = (1-H2Ofrac_DI)*mdot.DI + (1-H2Ofrac_PFI)*mdot.PFI;

% indicated specific fuel consumption
[ISFCn,ISFCg,BSFC,ISFC_FMEP] = ISFC_calc(mdot,Pn,Pg,Pb,P_FMEP);

Carr_Chen=(1-((1-.74)*(0.608*(z/.5)^2)+ (0.092*(z/.5))));%correct for
FID response using the CARR and CHEN correlation alpha term in
correklation is taken to be .74
emissions.HC.ppm = emissions.HC.ppm/Carr_Chen;

% measured concentrations
HCwet = emissions.HC.ppm/1e6; % wet basis
COdry = emissions.CO.ppm/1e6;
CO2exdry = emissions.CO2ex.ppm/1e6;
CO2indry = emissions.CO2in.ppm/1e6;
NOdry = emissions.NOx.ppm/1e6;

% compute dry moles of exhaust per mole of fuel based on carbon
balance,
% hydrogen balance, and CO/H2 relation
beta = 7.65*omega/(2*4.76+7.65*omega);
% n_exh_dry = (1/HCwet - (y/2)/(1+(y/2)*HCwet))/...
%     ((1-(y/4)*COdry)/(1+(y/2)*HCwet) + (COdry + CO2exdry)/HCwet);
n_exh_dry = (1/HCwet - (y/2+n_H2O_f*(1-beta)-
beta*z)/(1+(y/2)*HCwet+beta*(2*HCwet-1)))/...
    ((1-(y/4)*COdry+beta*(1-
(2+y)*COdry/2))/(1+(y/2)*HCwet+beta*(2*HCwet-1)) + (COdry +
CO2exdry)/HCwet);

% dry to wet conversion (based on hydrogen balance and CO/H2 relation)
n_exh_wet = (1-n_exh_dry*(COdry+CO2exdry))/HCwet;

% number of moles
n_HC = HCwet*n_exh_wet; % wet basis
n_CO = COdry*n_exh_dry;
n_CO2ex = CO2exdry*n_exh_dry;
n_CO2in = CO2indry*n_exh_dry;
n_NO = NOdry*n_exh_dry;
```

```
% CO/H2 relation
n_H2 = 0.25*y*n_CO;
% Moles of water
n_H2O = n_exh_wet - n_exh_dry;
% Moles of air, carbon-based
n_air_carbon = (2*n_exh_wet - 2*n_HC - 2*n_H2 - n_CO - n_H2O - z -
n_H2O_f)/...
    (2*4.76 + 7.65*omega);

%Air/Fuel Ratios
% AFR.carbon = (MW_air/MW_fuel)*(n_exh_wet - 0.5*(n_CO + n_H2O + n_H2)
- n_HC);
% AFR.carbon = (MW_air/MW_fuel)*(n_exh_wet - 0.5*(n_CO + n_H2O + z) -
n_H2 - n_HC);
AFR.carbon = (MW_air/MW_fuel)*4.76*n_air_carbon;
AFR.mass = mdot.air*(1000/60)/mdot.fuel;
alpha = (2+y/2-z)/2;
AFR.stoich = alpha*4.76*MW_air/MW_fuel;
phi.carbon = AFR.stoich/AFR.carbon;
phi.mass = AFR.stoich/AFR.mass;

%Oxygen balance
if isfield(emissions,'O2ex')
    n_O2 = emissions.O2ex.ppm*n_exh_dry/1e6;
    n_air_oxygen = (2*n_CO2ex+ n_CO + n_H2O + 2*n_O2 + n_NO - z -
n_H2O_f)/...
        (2 + 7.65*omega);
    AFR.oxygen = (MW_air/MW_fuel)*4.76*n_air_oxygen;
    phi.oxygen = AFR.stoich/AFR.oxygen;
end

% Check lambda meter mode
if Etas_mode % 0 = Lambda mode, 1 = O2% mode
    phi.meter = AFR.stoich/AFR.oxygen;
else
    if exist('phi.meter','var')
        AFR.meter = AFR.stoich/phi.meter;
    end
end

AFR_fields = fields(AFR);
AFR_sum = 0;
for i=1:length(AFR_fields)
    if ~strcmpi(AFR_fields(i),'stoich')
        AFR_sum = AFR_sum + AFR.(AFR_fields{i});
    end
end
AFR.mean = AFR_sum/sum(~strcmpi(AFR_fields,'stoich'));
clear AFR_sum

phi.mean = AFR.stoich/AFR.mean;

% Fuel Specific Emissions Index Equations
emissions.NOx.g_kgfuel =
(MW_NO2/MW_fuel)*(emissions.NOx.ppm/1e6)*n_exh_dry*1000;
```

```
emissions.CO.g_kgfuel =
(MW_CO/MW_fuel)*(emissions.CO.ppm/1e6)*n_exh_dry*1000;
emissions.CO2ex.g_kgfuel =
(MW_CO2/MW_fuel)*(emissions.CO2ex.ppm/1e6)*n_exh_dry*1000;
emissions.CO2in.g_kgfuel =
(MW_CO2/MW_fuel)*(emissions.CO2in.ppm/1e6)*n_exh_dry*1000;
emissions.HC.g_kgfuel =
(MW_fuel/MW_fuel)*(emissions.HC.ppm/1e6)*n_exh_dry*1000;
if isfield(emissions,'PM')
    if isfield(emissions.PM,'g_kgfuel')
        emissions.PM.g_kgfuel =
emissions.PM.mg_m3*mdot.air/60/rho/mdot.fuel;
    end
end

% Power Specific Emissions Index Equations
emissions.NOx.g_kWhr = emissions.NOx.g_kgfuel*ISFCg/1000;
emissions.CO.g_kWhr = emissions.CO.g_kgfuel*ISFCg/1000;
emissions.CO2ex.g_kWhr = emissions.CO2ex.g_kgfuel*ISFCg/1000;
emissions.CO2in.g_kWhr = emissions.CO2in.g_kgfuel*ISFCg/1000;
emissions.HC.g_kWhr = emissions.HC.g_kgfuel*ISFCg/1000;
if isfield(emissions,'PM')
if isfield(emissions.PM,'g_kgfuel')
    emissions.PM.g_kWhr = emissions.PM.g_kgfuel*ISFCg/1000;
end
end
end
```

A.D.2 AFR, GTE, and Efficiency Uncertainty Calculation

This EES script is used to determine the uncertainty of lab measurements and calculated efficiency and losses (see Chapter 4, section 4.8.3).

```
"!THIS CODE DETERMINES THE UNCERTAINTY OF GTE AND LOSSES FOR THE SCOTE LAB"
"========================================================================="

"!AIR"
OrfAirFlow = (UpstOrfPress*convert(bar,kpa))/sqrt(converttemp(C,K,UpstOrfTemp))    "kPa/K^0.5"
"this line determines the airflow rate through the orifice rack through calibrated flow"
IntAirFlowRate = ((0.00264+0.01867*OrfAirFlow)*Orf1) + ((0.00470+0.02805*OrfAirFlow)*Orf2)
+((0.00465+0.04455*OrfAirFlow)*Orf3) +((0.02481+0.05629*OrfAirFlow)*Orf4)
+((0.06549+0.06898*OrfAirFlow)*Orf5) +((0.12142+0.06948*OrfAirFlow)*Orf6)

"finds the mass flow rate of air into the engine"
M_dot_air=IntAirFlowRate-M_dot_bench
M_dot_bench=Bench_suction*rho_intake
Bench_suction=30[l/min]                                  "this is the reading from the bench rotameter"
rho_intake=Density(Air,T=T_intake,P=P_intake)*convert(kg/m^3,kg/l)"intake surge tank conditions"
P_intake=P_bar*convert(bar,kpa)                          "intake surge tank conditions"

"========================================================================="

"!Fuel"
speed=1300[rev/min]
Cyc_sec=speed*convert(rev/min,rev/sec)/2{[rev/cyc]}
y_DI = HtoC_DI
y_PFI = HtoC_PFI
z_DI = OtoC_DI
z_PFI = OtoC_PFI
H2Ofrac_DI =0 {H2Ofrac_DI}                               " mass fraction of H2O in DI"
H2Ofrac_PFI = 0{H2Ofrac_PFI}                             "mass fraction of H2O in PFI"
MW_DI = 12.01[g/mol]   + 1.008[g/mol]  *y_DI+z_DI*16[g/mol]   "g/mol"
MW_PFI = 12.01[g/mol]   + 1.008[g/mol]  *y_PFI+z_PFI*16[g/mol] "g/mol"
n_dot_DI = (1-H2Ofrac_DI)*m_dot_DI/MW_DI                 "molar flowrate of DI fuel"
n_dot_PFI = (1-H2Ofrac_PFI)*m_dot_PFI/MW_PFI             " molar flowrate of PFI fuel"
y = (n_dot_DI*y_DI+n_dot_PFI*y_PFI)/(n_dot_DI+n_dot_PFI)   "H/C ratio"
z = (n_dot_DI*z_DI+n_dot_PFI*z_PFI)/(n_dot_DI+n_dot_PFI)   "O/C ratio"

"input fuel energy"
E_fuel=((m_dot_DI*LHV_DI*convert(MJ/kg,J/g))+(m_dot_PFI*LHV_PFI*convert(MJ/kg,J/g)))/Cyc_sec
LHV_fuel=E_fuel/M_fuel
m_dot_fuel=m_dot_DI+m_dot_PFI
M_fuel=(m_dot_fuel)*convert(g/sec,mg/sec)/Cyc_sec
```

```
$CHECKUNITS Off

"=========================================================================="

"! Emissions Bench Uncertainties"
DELTACO2_exh=(.005*span_CO2_EXH)
DELTACO2_int=(.005*span_CO2_INT)
DELTACO=(.005*span_CO)
DELTAHC=(.005*span_HC)
DELTANOX=(.005*span_NOX)

"these are the span values used for the emissions analyzers, and the ranges)"
span_CO2_EXH=1000000*.1996/2                    "range 3 % by 2 is for range 3"
span_CO2_INT=1000000*.08/2                      "range 3 % by 2 is for range 3"
span_CO=3000                                    "range 4"
span_HC=4545                                    "range 4"
span_NOX=100                                    "range 4"


"!Molecular Weights"
MW_air = MOLARMASS(AIR)
MW_CO2 = MOLARMASS(CO2)
MW_CO = MOLARMASS(CO)
MW_NO2 = MOLARMASS(NO2)
MW_HC = 83.25/2                                 "Per GM Test code"
MW_fuel = 12.01 + 1.008*y+z*16


"!measured concentrations"
HCwet = emissions_HC_ppm/1e6                     " wet basis"
COdry = emission_CO_ppm/1e6
CO2exdry = emissions_CO2ex_ppm/1e6
CO2indry = emissions_CO2in_ppm/1e6
NOdry = emissions_NOx_ppm/1e6

beta = 7.65*omega/(2*4.76+7.65*omega)           "omega is the air humidity ratio"
omega=0                                         "assume dry, but can be changed"
n_H2O_f=0                                       "assume no water in the fuel"
"!compute dry moles of exhaust per mole of fuel based on carbon balance,  hydrogen balance,
and CO/H2 relation"
n_exh_dry = (1/HCwet - (y/2+n_H2O_f*(1-beta)-beta*z)/(1+(y/2)*HCwet+beta*(2*HCwet-1)))/((1-
(y/4)*COdry+beta*(1-(2+y)*COdry/2))/(1+(y/2)*HCwet+beta*(2*HCwet-1)) + (COdry +
CO2exdry)/HCwet)

"!dry to wet conversion (based on hydrogen balance and CO/H2 relation)"
n_exh_wet = (1-n_exh_dry*(COdry+CO2exdry))/HCwet


"!number of moles"
n_HC = HCwet*n_exh_wet                          "wet basis"
n_CO = COdry*n_exh_dry
n_CO2ex = CO2exdry*n_exh_dry
n_CO2in = CO2indry*n_exh_dry
n_NO = NOdry*n_exh_dry
```

```
"!CO/H2 relation"
n_H2 = 0.25*y*n_CO
"! Moles of water"
n_H2O = n_exh_wet - n_exh_dry
"!Moles of air, carbon-based"
n_air_carbon = (2*n_exh_wet - 2*n_HC - 2*n_H2 - n_CO - n_H2O - z - n_H2O_f)/(2*4.76 +
7.65*omega)

"!Find the EGR rate"
EGR = max(100*(emissions_CO2in_ppm - 388)/(emissions_CO2ex_ppm - 388),0)

"!Air-fuel ratio calculations"
AFR_carbon = (MW_air/MW_fuel)*4.76*n_air_carbon
AFR_mass = m_dot_air*convert(kg/min,g/s)/m_dot_fuel
alpha = (2+y/2-z)/2
AFR_stoich = alpha*4.76*MW_air/MW_fuel


"!PHI calculations, prime are charge based"
phi_carbon = AFR_stoich/AFR_carbon
phi_prime_carbon = phi_carbon*(1-(EGR/100))

phi_mass = AFR_stoich/AFR_mass
phi_prime_mass = phi_mass*(1-(EGR/100))

phi_lambda=AFR_stoich/AFR_lambda
phi_prime_lambda = phi_lambda*(1-(EGR/100))


DELTAAFR_C = UncertaintyOf(AFR_carbon)
DELTAPHI_C = UncertaintyOf(phi_carbon)
DELTAPHI_prime_C = UncertaintyOf(phi_prime_carbon)

DELTAAFR_mass = UncertaintyOf(AFR_mass)
DELTAPHI_mass= UncertaintyOf(phi_mass)
DELTAPHI_prime_mass = UncertaintyOf(phi_prime_mass)
DELTAAFR_lambda = UncertaintyOf(AFR_lambda)
DELTAPHI_lambda= UncertaintyOf(phi_lambda)
DELTAPHI_prime_lambda = UncertaintyOf(phi_prime_lambda)
$CHECKUNITS On

"========================================================================="

"!Efficiencies"
GTE_mass=Work_gross/(M_fuel_AFR_mass*LHV_fuel*convert(Mj/kg,j/kg))
GTE_carbon=Work_gross/(M_fuel_AFR_carbon*LHV_fuel*convert(Mj/kg,j/kg))
GTE_lambda=Work_gross/(M_fuel_AFR_lambda*LHV_fuel*convert(Mj/kg,j/kg))

GTE_ave=(GTE_mass+GTE_carbon)/2

Work_gross=IMEP_g*convert(bar,pa)*V_d
V_d=2.44[l]*convert(l,m^3)
M_fuel_AFR_mass=(m_dot_air/AFR_mass)*convert(kg/min,kg/s)/(cyc_sec*1[rev])
M_fuel_AFR_carbon=(m_dot_air/AFR_carbon)*convert(kg/min,kg/s)/(cyc_sec*1[rev])
M_fuel_AFR_lambda=(m_dot_air/AFR_lambda)*convert(kg/min,kg/s)/(cyc_sec*1[rev])
```

```
DELTAGTE_mass = UncertaintyOf(GTE_mass)
DELTAGTE_C = UncertaintyOf(GTE_carbon)
DELTAGTE_ave = UncertaintyOf(GTE_ave)
DELTAGTE_lambda = UncertaintyOf(GTE_lambda)

"============================================================================="

"!Combustion"
LHV_CO = 10100              " J/g"
LHV_PM = 32800              " J/g"
LHV_HC = 43800              " J/g (propane)"


"finds the average of AFRc and AFRmass fuel flows"
M_DOT_FUEL_AVE=(m_dot_fuel+(m_dot_air*convert(kg/min,g/s)/AFR_carbon))/2

 " finds the fuel energy from the average fuel flow J/g"
Qhfv = (((1-
H2Ofrac_PFI)*m_dot_PFI*(m_dot_fuel_AVE/M_DOT_FUEL)*LHV_PFI*convert(mj/kg,j/g))+((1-
H2Ofrac_DI)*m_dot_DI*(m_dot_fuel_AVE/M_DOT_FUEL)*LHV_DI*convert(mj/kg,j/g)))/m_dot_fu
el_AVE

" finds mass fraction CO from the average fuel flow J/g"
y_CO =
(emissions_CO_g_kgfuel*m_dot_fuel_ave/1000)/(m_dot_air*convert(kg/min,g/s)+m_dot_fuel_ave
)

" finds mass fraction HC from the average fuel flow J/g"
y_HC =
(emissions_HC_g_kgfuel*m_dot_fuel_ave/1000)/(m_dot_air*convert(kg/min,g/s)+m_dot_fuel_ave
)


emissions_HC_g_kgfuel = (MW_fuel/MW_fuel)*(n_hc)*1000
emissions_CO_g_kgfuel = (MW_CO/MW_fuel)*(n_co)*1000
top = (y_CO*LHV_CO) + (y_HC*Qhfv)
bot = (Qhfv*m_dot_fuel_ave)/((m_dot_air*convert(kg/min,g/s))+m_dot_fuel_ave)
eta_c = 1 - (top/bot)"combustion efficiency"

Loss_comb=1-eta_c
DELTAloss_comb = UncertaintyOf(Loss_comb)

"============================================================================="

"!Exhaust Losses"
cp_ex = 1.080[j/g-k]"CP OF GAS OUT OF THE ENGINE"
cp_air = 1.006[j/g-k]"CP OF GAS INTO THE ENGINE"

E_ex = (((m_dot_air*convert(kg/min,g/s)/(1-
(EGR/100))))+m_dot_fuel_ave)*cp_ex*CONVERTTEMP(c,k,T_EXHAUST);
E_air = ((m_dot_air*convert(kg/min,g/s)/(1-(EGR/100))))*cp_ex*converttemp(c,k,T_intake);
{E_fuel = m_dot_fuel*Qhfv;}

Loss_EXH= (E_ex-E_air)/(m_dot_fuel_AVE*Qhfv)
DELTAloss_EHX = UncertaintyOf(Loss_EXH)
```

"=="

"!HX loss"
1=GTE_ave+Loss_HX+Loss_comb+Loss_EXH

DELTAloss_HX = UncertaintyOf(Loss_HX)

Appendix F – Fuel Properties

A.E.1 Fuel Lubricity Additive

Infineum R655

Description

Infineum R655 is an additive designed to improve distillate fuel lubricity, thus reducing wear of moving parts in contact with the fuel (particularly fuel injector pumps).

Normal treat rates are 50-200 ppm.

Typical Inspections

Property:	Value	Unit:	Method
Appearance	Yellow Clear Liquid		Visual
Density at 15°C	960	Kg/m³	ASTM D 4052
Flash Point (PMCC)	>210	°C	ASTM D 93
Pour Point	-15	°C	ASTM D 97
Viscosity at 20°C	192	cSt	ASTM D 445
Viscosity at 40°C	65	cSt	ASTM D 445
Viscosity at 60°C	29	cSt	ASTM D 445
Viscosity at 100°C	9	cSt	ASTM D 445
Total Acid Number	<1	mg KOH/g	ASTM D 974
Coefficient of Thermal Expansion	0.00080	1/°C	ITM 50-020

Handling / Precautions

Infineum R655 requires no special handling above that which is normal for petroleum products.

The recommended additive storage temperature range is from 20°C to 40°C.

Where LP steam coils are used for heating purposes, agitation is recommended to prevent excessive local skin temperatures.

Note that the product has a Pour Point of -15°C, but that under prolonged unheated storage, the product may solidify at temperatures up to +10°C.

Further Information

For further information please contact your local Infineum affiliate or representative.

Version: 4th February 2004 (4.1)

A.E.2 Gasoline Fuel Properties

Southwest Research Institute
Test Summary Report
for
University of Wisconsin - Madison
May 4, 2012

ASTM Test Method	*Test Property*	*Sample Code: Gasoline*
D240 GROSS	Heat of Combustion by Bomb Calorimeter	
	BTU/lb	20426
	MJ/kg	47.512
	cal/g	11348
D240 NET	Heat of Combustion by Bomb Calorimeter	
	BTU/lb	19046
	MJ/kg	44.301
	cal/g	10581.2
D2699	Research Octane Number	94.7
D2700	Motor Octane Number	87
D4052	API Gravity at 60°F	70.4
	Specific Gravity at60°F	0.7009
	Density at 15°C (grams/L)	700.7
D5291	Instrumental Determination of C, H	
	Carbon (Weight %)	84.78
	Hydrogen (Weight %)	15.13
D5453	Sulfur by Ultraviolet Fluorescence (ppm)	22.3
D86	Distillation (°F)	
	IBP	78
	5%	94
	10%	106
	15%	117
	20%	131
	30%	163
	40%	191
	50%	209
	60%	223
	70%	236
	80%	257
	90%	315
	95%	375
	FBP	416
	Recovered (mL)	97.3
	Residue (mL)	0.7
	Loss (mL)	2.0

A.E.3 ULSD Fuel Properties

DATA SUMMARY			
University of Wisconsin			
SWRI Work Order # 60533			
	ProjSeq		2894
	SmplCode		JET A
D240G	BTUHeat	BTU/lb	19489
	MJHeat	MJ/kg	45.332
	CALHeat	cal/g	10827.3
D240N	BTUHeat	BTU/lb	18319
	MJHeat	MJ/kg	42.609
	CALHeat	cal/g	10177
D4052s	API@60F		33.1
	SPGr@60F		0.8595
	Dens@15C	grams/L	859.1
D445 40c	Viscosty	cSt	2.705
D5291 CH	Carbon	wt%	86.97
	Hydrogen	wt%	12.83
D5453	Sulfur	ppm	10.1
D613	CetaneNo		42
D86	IBP	deg F	344.5
	Evap_5	degF	389.3
	Evap_10	degF	411.2
	Evap_15	degF	427.3
	Evap_20	degF	439.1
	Evap_30	degF	463
	Evap_40	degF	484.6
	Evap_50	degF	504.4
	Evap_60	degF	524.5
	Evap_70	degF	547.8
	Evap_80	degF	572.9
	Evap_90	degF	608.5
	Evap_95	degF	637
	FBP	degF	661.9
	Recoverd	mL	98
	Residue	mL	1.2
	Loss	mL	0.8
D1331A	SurfTension	dynes/cm	IC
	TestTemp	deg C	IC

A.E.4 Ethanol Fuel Properties

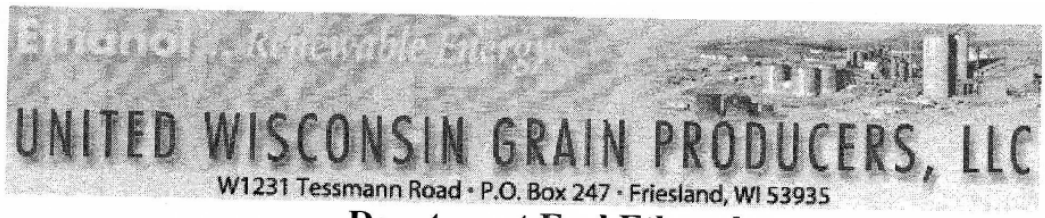

Denaturant Fuel Ethanol
Certificate of Analysis

Date of Shipment: _____

Bill of Lading No.: _____

Storage Tank Sample Number 8308

Test Procedures	Results	Limit	Method
Apparent Proof	200.05	Report [1]	Hydrometer
Karl Fischer Moisture, vol %	0.782	1.0 % Max [2]	ASTM E1064
Acidity, wt %	0.006	0.007 Max	ASTM D1613
pHe	7.50	6.5 - 9.0	ASTM D6423
GC Composition Results			
Ethanol, wt %	96.67	93.5 % Min	ASTM D5501
Methanol, wt%	0.06	0.50 % Max	ASTM D5501
Denaturant, wt%	2	1.96 - 2 %	Calculated
IC Composition Results			
Chloride, ppm	<0.1	10 ppm Max	ASTM D7319
Sulfate, ppm	<0.1	4 ppm Max	ASTM D7319
Appearance	Clear & Bright	Clear & Bright	Visual Examination
Total Sulfur	1.2	10 ppm Max	ASTM D5453 [3]
Copper, mg/L	<0.02	0.08 mg/L Max	ASTM D1688 [4]
Solvent-unwashed Gum, mg/100mL	<0.5	5 mg/100mL Max	ASTM D381 [4]
Benzene, wt %	0.026	0.06 % Max	ASTM D5580 [5]
Olefins, wt %	< 0.001	0.50 % Max	ASTM D6550 [5]
Aromatics, wt %	0.068	1.70 % Max	ASTM D5580 [5]